DEEP SPIKING NEURAL NETWORK ARCHITECTURE FOR THE CLASSIFICATION OF SPATIO-TEMPORAL DATA

A THESIS SUBMITTED TO AUCKLAND UNIVERSITY OF TECHNOLOGY
IN FULFILMENT OF THE REQUIREMENTS OF THE DEGREE OF
DOCTOR OF PHILOSOPHY

By

Dhvani Shah

School of Engineering, Computer and Mathematical Sciences /

Department of Computer Science and Software Engineering

August 2022

Abstract

This thesis aims to build a deep spiking neural network (SNN) using spike-based filters for temporal feature extraction to produce distinguishing spiking activity while classifying spatiotemporal data. Existing deep learning (DL) architectures such as convolutional neural networks (CNNs) combined with long short-term memory (LSTM) neural networks have demonstrated their ability to classify this type of data. The neurons employed in these DL architectures do not include a time component in their operation modules resulting in loss of possibly important temporal information. The spiking neurons of third-generation neural networks (NNs), i.e., SNNs, produce discrete event-based output incorporating time dimension in their computational model. However, the application of SNNs to produce temporal-based feature extraction and classification is still not well understood.

Current DL architectures, such as CNNs, use hierarchical feature representation to achieve high classification accuracy. Recent studies have adopted a similar design approach to implement variations of deep SNNs. These artificial neural networks (ANN) to SNN conversions are challenging as they use approximation techniques for producing spikes in SNNs that may result in the loss of temporal feature information. In short, it is not currently known how to build SNN architectures that combine the advantages of both CNNs and SNNs such that temporal features can be extracted layer by layer within a spiking neural framework.

To address the above-mentioned limitations, this thesis proposes a novel temporal-based SNN architecture that is shown to be effective when applied to spatiotemporal datasets, i.e., electroencephalogram (EEG) and music signals. In addition, a method for hand-engineered spike-based filters for use in deep SNNs to extract spatiotemporal information from the output of spiking neurons is proposed.

The first contribution of this thesis is the applicability of utilising the neuron's voltage and spike timings as classification criteria. Next, spike train analysis methods reveal the value of information hidden in the temporal coding neural scheme. The final contribution of this research is building a deep SNN framework with hierarchical feature representation, using rate and temporal neural coding techniques. Furthermore, the proposed end-to-end SNN design presented in this research is optimised to be applied in clinical management.

Contents

List of Tables

List of Figures

List of Abbreviations

ML	Machine Learning
AI	Artificial Intelligence
SNN	Spiking Neural Network
DNN	Deep Neural Network
ANN	Artificial Neural Network
MLP	Multilayer Perceptron
DL	Deep Learning
ReLu	Rectified Linear Unit
BP	Backpropagation
LIF	Leaky Integrate Fire
STDP	Spike Time Dependent Plasticity
CV	Cross Validation
RNN	Recurrent Neural Network
CNN	Convolutional Neural Network
LSTM	Long-Short Term Memory
MDD	Major Depressive Disorder
BDI	Beck Depression Index
LLM	Large Language Models
EEG	Electroencephalogram
MP	Membrane Potential
RMSE	Root Mean Squared Error
SNR	Signal-to-Noise Ratio
SVM	Support Vector Machine
DT	Decision Tree
EO	Eyes-open
EC	Eyes-closed
DE	Differential Evolution
GA	Genetic Algorithm
KNN	K-Nearest Neighbor
TBR	Threshold-based Representation
BSA	Ben's Spike Algorithm
deSNN	Dynamic Evolving Spiking Neural Network
RO	Rank Oder
ISI	Inter-spike Interval
ms	milliseconds
s, sec	seconds

Attestation of Authorship

I hereby declare that this submission is my own work and that, to the best of my knowledge and belief, it contains no material previously published or written by another person nor material which to a substantial extent has been accepted for the qualification of any other degree or diploma of a university or other institution of higher learning.

Signature of candidate

Publications

Shah, D., Wang, G. Y., Doborjeh, M., Doborjeh, Z., & Kasabov, N. (2019, December). Deep learning of EEG data in the Neucube brain-inspired spiking neural network architecture for a better understanding of depression. In International Conference on Neural Information Processing (pp. 195-206). Springer, Cham.

Author Contributions – Conceptualisation, Shah, D.; Formal Analysis, Shah, D.; Investigation, Shah, D.; Methodology, Shah, D and Kasabov, N.; Supervision, Kasabov, N., Wang, G., Doborjeh, M., Doborjeh Z.; Validation, Shah, D.; Writing– original draft, Shah, D.; Writing– review and editing, Kasabov, N. and Wang, G.

Part of the Sections – Abstract, Introduction, Methods, and Experiments and Results of Chapter 3 are drawn from this paper (Shah, Wang, Doborjeh, Doborjeh & Kasabov, 2019).

D. Shah, A. Narayanan and J. I. Espinosa-Ramos, Utilizing the Neuronal Behavior of Spiking Neurons to Recognize Music Signals Based on Time Coding Features, in IEEE Access, vol. 10, pp. 37317-37329, 2022, doi: 10.1109/ACCESS.2022.3164440.

Author Contributions – Conceptualisation, D. Shah and A. Narayanan; Formal Analysis, D. Shah; Investigation, D. Shah; Methodology, Shah, D, and J.I. E.Ramos; Supervision, A. Narayanan; Validation, D. Shah; Writing– original draft, D. Shah; Writing– review and editing, A. Narayanan.

Sections – Methods, Experiments and Results, and Conclusion of Chapter 4 are drawn from this paper (Shah, Narayanan & Espinosa-Ramos, 2022).

Acknowledgements

I would like to express my deepest gratitude to everyone who supported me throughout my Ph.D. journey. Their assistance and dedicated involvement have helped to accomplish this thesis.

Professor Ajit Narayanan - for being incredibly supportive, encouraging, empathetic, optimistic, systematic, and an amazing problem solver. Your observation and assessment of my work and your suggestion of writing reports before every meeting has extensively improved the overall quality of my thesis. From the day I started my Ph.D. journey until my thesis submission, I couldn't visit my family. But your counsel and moral support helped to reach get to where I am now. Thank you so much for always encouraging and sharing your strength with me.

Professor Grace Wang - for your encouragement and for stepping in whenever I needed you. Your advice and suggestions influenced the direction of my work. Thank you once again for walking with me patiently throughout this journey.

Ms. Joyce D'mello - for your tremendous kindness, compassion, and sympathetic ear. Your support, strength, and positive spirit always gave me the courage to fight and stand up gain.

Dr. Josafath Israel Espinosa Ramos - Thank you for taking me through the Java implementation of the NeuCube framework.

I would further like to thank Professor Nikola Kasabov for giving me this opportunity and for guiding me during the initial months of my journey.

My awesome friends, Gaurav Pathak, and Helena Bahrami - thank you for providing me a comfort zone through your sweet friendships. You both gave me a home away from home. I am forever grateful to have met you both.

I am grateful for my parents and my family, whose constant love and support kept me motivated. Thank you for your kind support through the good times and bad decisions.

Finally, I owe my deepest gratitude to the AUT administration, especially Karishma Bhat for their great support throughout the entire thesis process.

Chapter 1

Introduction

The first part of this chapter discusses the information processing principles of the human brain and the fundamentals of SNN. The second part presents the research background of this study and the motivation for developing brain-inspired SNN architecture for the spatiotemporal processing of event-based data. The structural connectivity of spiking neurons inspired by the deep learning design principles, the selection of depression detection and music instrument recognition as case study problems, and finally, the inspiration for the development of spike-based binary filters are discussed in this chapter.

1.1 Introduction

1.1.1 Human Brain

The human brain is the most complex organ that controls all the important functions in the human body – movement, memory, learning, feeling, hunger, vision, breathing, etc. The human brain and the spinal cord make up the central nervous system. The major functions of the brain include the integration of information that it receives from the sensory organs, processing them, distributing them across different brain regions,

and coordinating and sending instructions to other parts of the body. The basic unit of processing information in the human brain is the neuron. The human brain comprises approximately 100 billion neurons.

From a high-level view, the brain can be segmented into three major parts – cerebrum, brainstem, and cerebellum.

The cerebrum is located at the front of the brain and contains the cerebral cortex at its centre. Regulating high-level functions such as vision, hearing, speech, reasoning, emotions, learning, and the fine control of movement falls under the responsibility of the cerebrum. The cerebral cortex is further divided into two halves – right and left hemispheres. The left hemisphere governs the right side of the human body, whereas the right hemisphere controls the left side.

The cerebrum and the spinal cord are connected through the brainstem located at the centre of the human brain. The brainstem functions include the regulation of heart rate, breathing, sleeping, and eating. It acts as a hub relaying information from the body to the cerebrum and cerebellum, and vice versa.

The cerebellum which is also called as "little brain" because of its small size, is located at the back of the head, below the temporal and occipital lobes. Although it is small in size (10 percent of the brain), over 50 percent of the total neurons in the brain are located here. New studies (Ferrari, Ciricugno & Cattaneo, 2022; Pierce, Thomasson, Voruz, Selosse & Péron, 2022) are exploring the cerebellum's involvement in the thought process, the processing of feelings and emotions, and the social behaviour of an individual.

Further, each brain hemisphere consists of four lobes: frontal, parietal, temporal, and occipital. Each lobe has a specific role to play in the overall functioning of the human brain.

1. Frontal lobe: Situated in the front, it covers the largest section of the brain. The

frontal lobe is responsible for the decision-making process of an individual, bodily movements, and personality characteristics. Stress, anxiety, and depression affect the thinking and decision-making process of an individual.

2. Parietal lobe: Situated in the middle section of the brain, the parietal lobe helps humans in the identification of objects and their spatial orientation relative to the body. The responsibility of this lobe includes the perception of pain and touch in the body and helping the brain understand any spoken language.

3. Occipital lobe: Situated at the back of the brain, this lobe is significantly involved with vision.

4. Temporal lobe: Situated at the sides of the brain, this lobe is involved in speech, short-term memory, and musical rhythms.

A few of the key components within the deeper structures of the brain that play an important role in the process of depression detection are the hypothalamus, amygdala, and hippocampus. They are involved in processing emotions, memory learning, and the reward system at different levels.

Brain disorders like depression affect the overall brain structure and its functioning. It may cause shrinkage of some structures, inhibition of the development of neurons, alterations in the functional connectivity of different brain regions, etc. (Palmer, Crewther, Carey et al., 2015; Pandya, Altinay, Malone & Anand, 2012).

As mentioned earlier, neurons are the elementary processing units in the brain with different sizes and shapes. As described in Figure 1.1, each neuron consists of a cell body, axon, and dendrites. Dendrites and axons connect different neurons to each other. The connecting link between two neurons is called a synapse, and the connection is termed a synaptic connection. Information is transmitted between the neurons through these synapses. The neuron sending the information is called the pre-synaptic neuron,

whereas the neuron receiving this information is called the post-synaptic neuron. The dendrites receive information from the other neurons, the cell body processes this information, and the axon transmits it to the connecting neurons. The information is transmitted through the axons to other neurons when the total input received by the neuron crosses a threshold leading to an action potential.

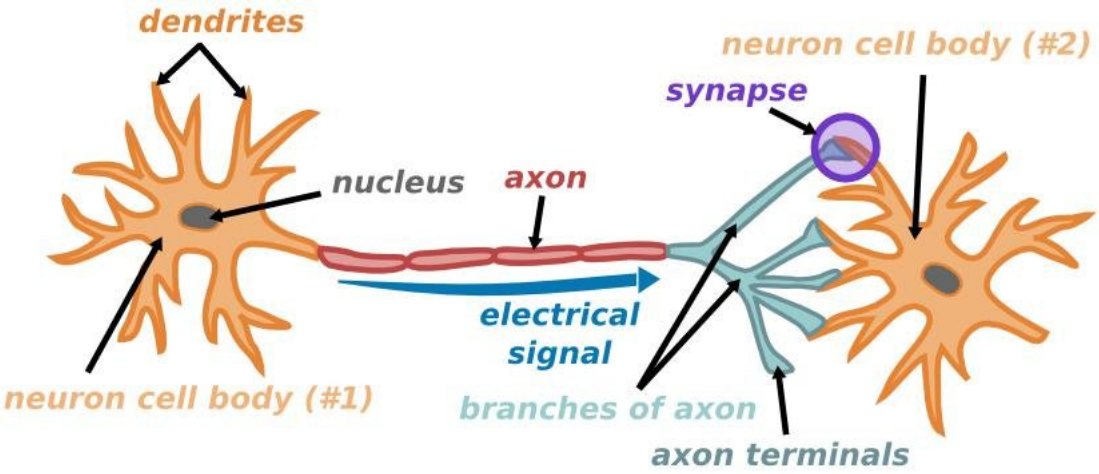

Figure 1.1: *Illustration of Biological Neurons from (Tamaazousti, 2018)*

All the information the human brain perceives through the sensory organs (i.e., information about stimulus through light, sound, taste, smell, and touch) is encoded in a temporal pattern of electrical pulses, and through the synaptic connections, these pulses are transmitted to other neurons.

At a lower level, two types of synapses are found in the brain: chemical and electrical. Electric signals are transmitted through ions in electrical synapses, whereas chemical synapses use chemical messengers called neurotransmitters. Pre-synaptic neurons release a neurotransmitter on the rise of an action potential. This neurotransmitter then dispenses through the synapse into the receptors of the post-synaptic neurons. The transmission speed of signals using electrical synapses is greater than that of chemical synapses. The brain consists more of chemical synapses and releases different types

of neurotransmitters. Neurotransmitters can be inhibitory or excitatory in nature. Excitatory neurotransmitters tend to increase the possibility of an action potential, whereas inhibitory neurotransmitters decrease the possibility of an action potential. Different neurotransmitters like glutamate are responsible for cognitive functions like memory and learning, while others like gamma-aminobutyric acid (GABA) cause inhibition in the nervous system. The development of these neurotransmitters in the human depends on various factors; this is how the human brain goes through many physical changes throughout its lifetime. This is the basis of learning, memory, and adaption in the human brain, which is extremely complicated as we further drill down into the brain's inner workings. Learning and memory are impacted by small-scale changes occurring every minute between the neuronal connections, i.e., synaptic plasticity (Ramirez & Arbuckle, 2016).

The inspiration from the principles of information processing, learning, memory, the reward system, and other functionalities in the human brain led to the development of computational methodologies and architectures for different tasks, like classification and prediction.

1.1.2 Generations of Artificial Neuron

Figure 1.2 illustrates an artificial neuron designed based on a biological neuron. Input channels represented by $\mathrm{x}_1, \mathrm{x}_2, ..., \mathrm{x}_\mathrm{n}$ in the artificial neuron are related to the dendrites in the biological neuron. Neurons transmit signals to each other through synapses (synaptic connections). The output of each neuron is computed by some non-linear function (activation function) of the sum of its inputs. Threshold-based neurons are such that the signal is transmitted only if the aggregate signal crosses this threshold. Synaptic connections have weights $\mathrm{w}_{1\mathrm{j}}, \mathrm{w}_{2\mathrm{j}}, ..., \mathrm{w}_{\mathrm{nj}}$ that are adjusted as learning takes place. Synaptic plasticity is a process where these weights are either strengthened or

weakened through backpropagation, evolutionary algorithms, Synaptic Time Dependent Plasticity, etc. (Storn & Price, 1997; LeCun, Bengio, Hinton et al., 2015). These learning algorithms, during supervised classification, adjust the weights of the network to improve the accuracy of the result by mapping the input to an output y. The following section briefly introduces the properties of artificial neurons that evolved over time (Ghosh-Dastidar & Adeli, 2009; Maass, 1997a).

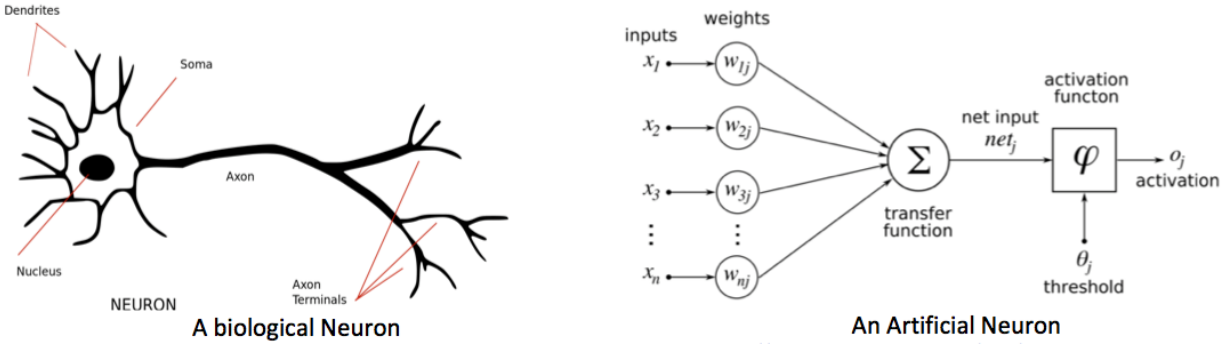

Figure 1.2: *Illustration of Artificial Neuron with Biological Neuron apdated from (Kapoor, 2019)*

First Generation Neurons

The perceptron model marked the beginning of artificial neurons. The inputs (real values) are summed together to produce an activation value. If this activation value is greater than the threshold, the neuron fires. Thus, the output from the perceptron is not a real value, i.e., they are binary outputs. These neurons cannot handle spatiotemporal inputs.

Second Generation Neurons

In 1960, second-generation neurons, also called rate-coded neurons, were implemented. Neurons with different activation functions producing real-valued outputs have shown breakthroughs in diverse applications like computer vision, speech recognition, medical, etc. Neurons with sigmoid activation function produce an output within the range of

0, 1, and the Tanh function produces an output within the range of -1, 1, and so on. A more detailed description can be found in (LeCun et al., 2015). These neurons were very effective and powerful as compared to the first-generation neurons because of incorporating continuous non-linear activation functions to classify complex datasets. However, these neurons could not represent temporal information in their computation module.

Third Generation Neurons

Third-generation neurons were designed to overcome the limitations of the neurons of previous generations. Thus, neurons capable of communicating via precise timings of spikes or a sequence of spikes have been developed. These neurons capable of processing temporal information are called third-generation neurons or spiking neurons (Maass & Bishop, 2001). Similar to the first-generation neurons, the input information is summed by the neuron, and if the activation value crosses the threshold, the neuron fires. However, the internal state of a perceptron model and spiking neurons' internal states are quite different. The internal state of a spiking neuron changes with time, and when the internal state of the neuron crosses the threshold, the spiking neuron emits an action potential at that time instance. Similar to biological neurons, all the information is encoded in the temporal pattern of action potentials or in the timing of spikes. In other words, temporal codes are of high importance in biology where even a single spike or small temporal variations of single neuron firing may trigger different reactions (Gerstner, Ritz & Van Hemmen, 1993; Aldworth, Dimitrov, Cummins, Gedeon & Miller, 2011).

1.1.3 Spiking Neuron Models

The internal state of a biological neuron (post-synaptic) changes when it receives input signals, i.e., electrical impulses from its pre-synaptic neurons. This input causes a potential difference in the intrinsic environment of the post-synaptic neuron, which is called the membrane potential $\mathrm{u(t)}$. A pre-synaptic neuron can be either excitatory or inhibitory in nature. When the pre-synaptic neuron causes a positive change in the post-synaptic membrane potential, the pre-synaptic is called excitatory. And if the change in the post-synaptic membrane potential is negative, the pre-synaptic is called inhibitory. The post-synaptic neuron is at rest with a membrane potential $\mathrm{u_{rest}}$, when no information (i.e., no spike) is received from the pre-synaptic neurons.

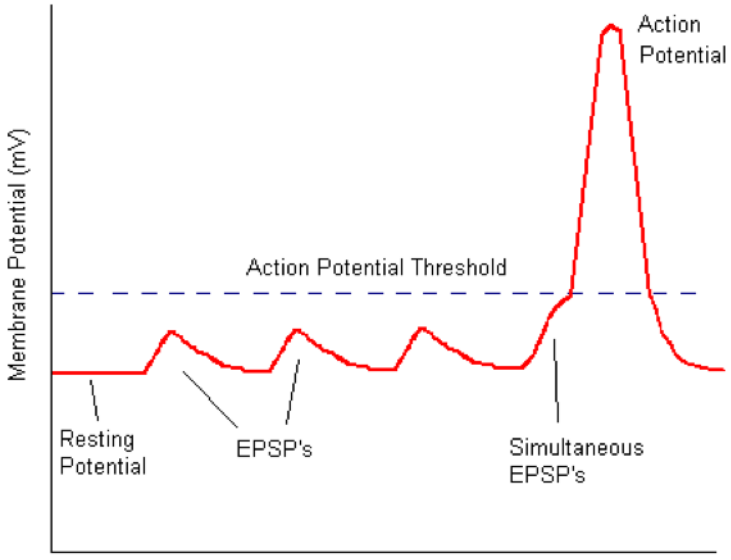

Figure 1.3: *Shape of Post-Synaptic Potential from (Gerstner & Kistler, 2002)*

As the pre-synaptic neurons cause a potential difference (positive or negative), the membrane potential of the post-synaptic neuron changes accordingly. The total of the post-synaptic potential (PSP) of a neuron before it crosses the threshold can be formalised as follows:

$$u_i(t) = \sum_j \sum_f \epsilon_{ij}(t - t_j^{(f)}) + u_{rest} \tag{1.1}$$

In Eq. 1.1, $\mathrm{u_{rest}}$ represents the resting membrane potential of a post-synaptic neuron i at time t. The pre-synaptic connections to this neuron are represented by neurons $\mathrm{j} = 1, 2, ..., \mathrm{n}$. The membrane potential of the post-synaptic neuron caused due to input spikes from pre-synaptic neurons is represented by ϵ_{ij}. $\epsilon_{\mathrm{ij}}(\mathrm{t} - \mathrm{t_j^{(f)}})$ represents the time duration of PSP receiving input spikes from pre-synaptic neurons. Figure 1.3 illustrates the neuronal behaviour of a spiking neuron. When PSP surpasses the action potential threshold value, it evokes a spike and goes into a refractory state. The neuron cannot emit a spike during this time even if it reaches the threshold. The refractory time usually lasts for one millisecond.

Figure 1.4 shows the behaviour of a post-synaptic neuron i receiving spikes from pre-synaptic neurons $\mathrm{j} = 1$ and $\mathrm{j} = 1, 2, ..., \mathrm{n}$. When the membrane potential of neuron i crosses the firing threshold ϑ, it fires. The firing times of neuron i is represented by $\mathrm{t_j^{(f)}}$ and $(\mathrm{f} = 1, 2, ...)$. The sequence of firing times caused by the stimulating current from pre-synaptic neurons is represented by a spike train as shown:

$$S_i(t) = \sum_f \delta(t - t_i^{(f)}) \tag{1.2}$$

where $\delta(\mathrm{x})$ represents Dirac function. $\delta(\mathrm{x}) = 1$ indicates the occurrence of a spike and $\delta(\mathrm{x}) = 0$ means no spike.

In response to stimulating current, biological neurons can show four different types of behaviour (Gerstner & Kistler, 2002) as shown in Figure 1.5. The details of these neuron dynamics are described in Gerstner and Kistler (2002) (Gerstner & Kistler, 2002). Simplified computational spiking neuron models have been introduced to model the neuronal dynamics of biological neurons.

There are trade-offs between biological accuracy and computational viability in

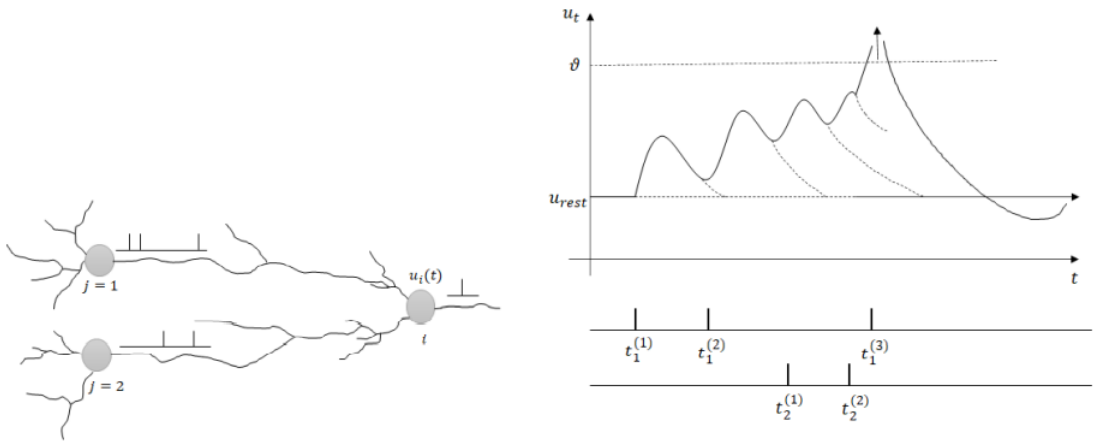

Figure 1.4: *Interaction between Pre and Post-Synaptic Neuron from (Gerstner & Kistler, 2002): the firing pattern of a post-synaptic neuron (right side of the image) when it receives input (spikes) from its pre-synaptic inputs (first two neurons of the left side of the image)*

the various spiking neuron models that have been developed as shown in Figure 1.6 and reviewed in detail in Gerstner and Kistler (Gerstner & Kistler, 2002). Choosing an appropriate model depends on the goal, as argued by Izhikevich (Izhikevich, 2003). This thesis employs the Leaky-Integrate-Fire (LIF) neuron model as it is necessary to model an SNN architecture with a large number of interacting neurons. Also, the implementation of LIF neurons is more flexible and readily adaptable, plus they rely on fewer meta parameters, which makes them generally easier to use.

1.1.4 Leaky-Integrate-Fire Neuron Model

The LIF neuron model is a one-dimensional (one differential equation for modeling) spiking neuron model with low computational cost (Gerstner & Kistler, 2002). The working of a LIF neuron model could be modeled as a parallel Resistor R - Capacitor C circuit. The stimulating current $I(t)$ charges the RC circuit. This causes an increase in the membrane potential $u_{(t)}$ and finally beyond the capacitor voltage. When at time $t_i^{(f)}$, $u_{(t)}$ crosses the firing threshold ϑ, i.e., $u_{(t)} = \vartheta$, a spike is released which is represented

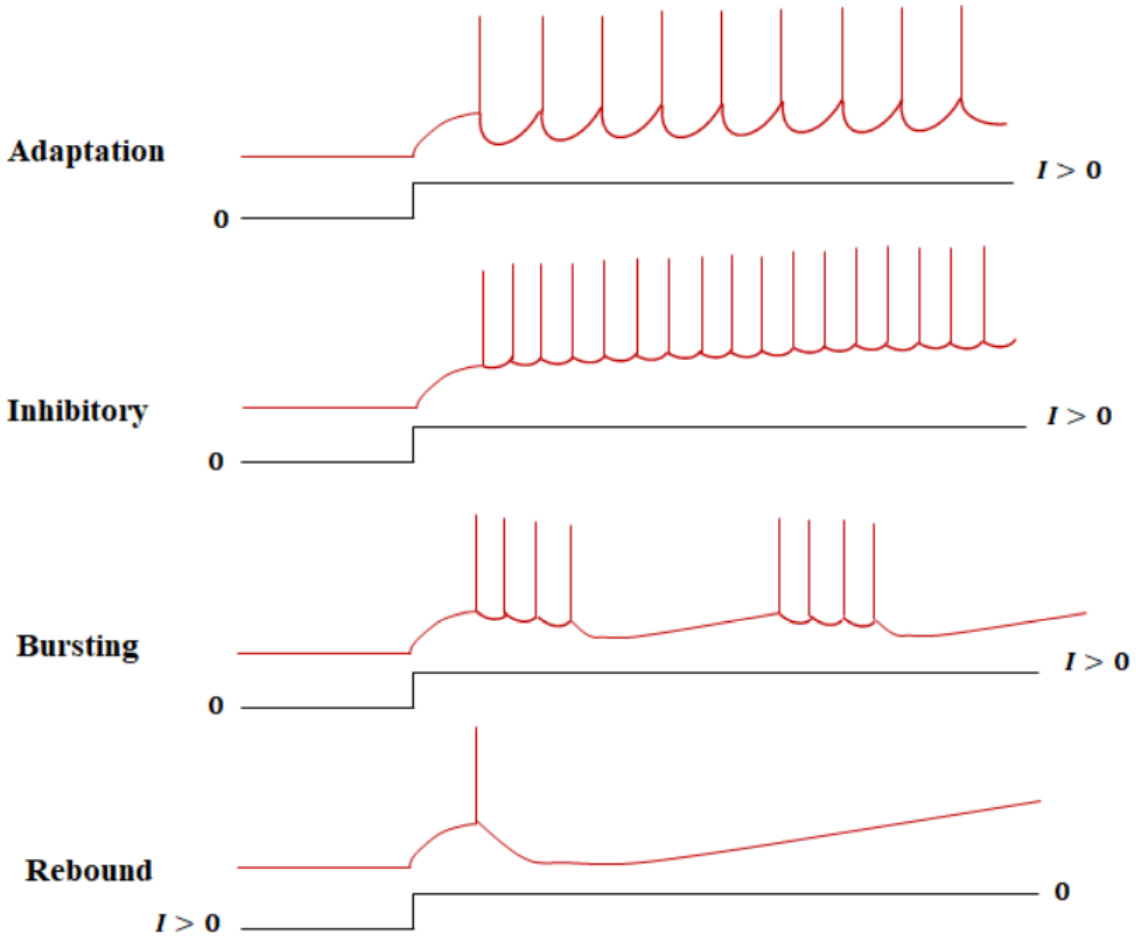

Figure 1.5: *Neuron dynamics to a stimulating current I from (Gerstner & Kistler, 2002)*

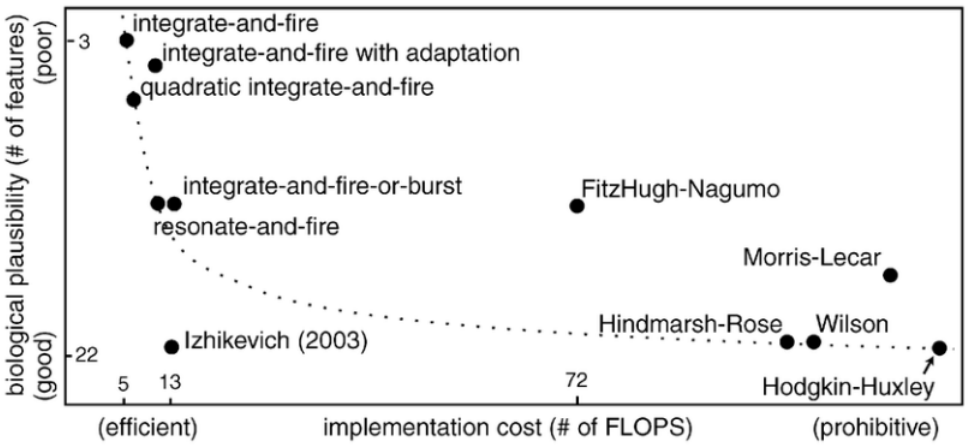

Figure 1.6: *Comparisons of Spiking Neuron Models from (Gerstner & Kistler, 2002)*

by $\delta(\mathrm{t} - \mathrm{t}_{\mathrm{i}}^{(\mathrm{f})})$. After the emission of an output pulse, the neuron leaks to its resting potential, i.e., $u_{(t)} < \vartheta$, and emits no spike during the refractory period. This leakage, called the membrane time constant, is indicated by the τ_{m} factor.

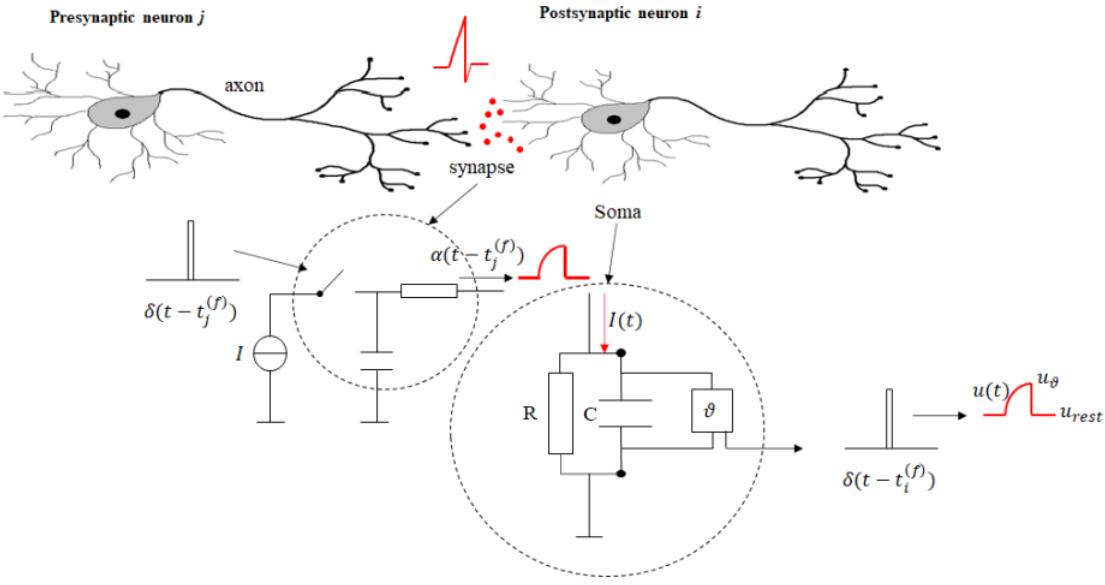

Figure 1.7: *LIF Neuron Model from (Gerstner & Kistler, 2002)*

The dynamics of LIF neuron models are defined by the following equation:

$$\tau_m \frac{du}{dt} = u_{rest} - u(t) + RI(t) \tag{1.3}$$

where $\frac{du}{dt}$ represents the change in membrane potential, $u(t)$ is the neuronal membrane potential at time t, τ_m is the membrane time constant, R is the membrane resistance and $I(t)$ is the sum of current supplied by the input synapses (connection from the input layer to the hidden layer).

In a network of spiking neurons where there are multiple pre-synaptic connections to a post-synaptic neuron i, the total stimulating current $I(t)$ is computed using the following equation:

$$I_i(t) = \sum_j W_{ij} \sum_f \delta(t - t_i^{(f)}) \tag{1.4}$$

where $W = w_1, w_2, ..., w_n$ is the weight vector representing the measure of the efficacy of the synaptic connection between neurons j and i. $\delta(t - t_i^{(f)})$ is the time duration for which neuron i receives pre-synaptic spikes. $\delta(t - t_i^{(f)})$ is the spatiotemporal input spike pattern containing N input spike trains, $s_i(t)$ for $i = 1, 2, ..., N$. Spike trains contain binary events with one as a spike and 0 as no spike.

1.1.5 Spike Time Dependent Plasticity: Unsupervised Learning in SNN

Synaptic plasticity, i.e., change in the strength of the synapses, is the biological basis of learning and memory. This study adopts the unsupervised learning inspired by the Hebb Rule (Hebb, 1949b), where weight changes during the learning process are dependent on the time dimension. Spike Time Dependent Plasticity (STDP) (Song, Miller & Abbott, 2000) is a variant of the Hebbian unsupervised learning algorithm where the

weights are adapted based on the relative timing of pre-and post-synaptic spikes. The dynamics of the STDP algorithm can be represented by Equations (1.5) and (1.6):

$$W(x) = A_+ \exp \frac{-x}{\tau_+} \qquad for\ t_i < t_j \tag{1.5}$$

$$W(x) = -A_- \exp \frac{x}{\tau_-} \qquad for\ t_i > t_j \tag{1.6}$$

The synaptic weight $W(x)$ will be potentiated if the pre-synaptic neuron t_i fires before the post-synaptic neuron, t_j. The potentiation is a function of t which decays exponentially with a time constant τ_+ and can be calculated by $A_+ \exp \frac{-x}{\tau_+}$, where A_+ is the maximum synaptic change. On the other hand, if the post-synaptic neuron fires before the pre-synaptic neuron, the weight of the synapse between these two neurons is decreased by a magnitude of $-A_- \exp \frac{x}{\tau_-}$, where A_- indicates the maximum negative change and τ_- is the time constant. Time constant variables for potentiation and depression are set to 10ms. Only the last (most recent) firing time of the pre-synaptic neuron is considered for this STDP implementation.

SNNs with biologically plausible neuron models and unsupervised learning are efficient in analysing spatiotemporal data.

1.2 Research Background

The human brain is an extraordinarily complex dynamical system processing information and performing critical operations over various timescales (from milliseconds to years). Various multi-neuronal activation patterns are formed in the brain in response to what humans see, hear, think and feel (King & Dehaene, 2014). These mental representations captured across multiple brain areas through neuroimaging tools like EEG are spatiotemporal in nature (Drevets, 2000).

Biological neurons interact with each other by sending sparse spiking signals,

whereas neurons in deep learning networks output real continuous values. Inspired by the biological neurons, SNN, a computational model, uses information processing principles similar to the human brain. SNN computation relies on the spike carrying space (which neuron fires) and time (when a neuron fires) information and can provide a larger solution space than ANN (Maass, 1997a; Rubin, Monasson & Sompolinsky, 2010). In other words, information is represented in the temporal sequences of binary signals (spikes) that are transferred between spatially located neurons.

Spatiotemporal data like EEG signals store valuable information capable of achieving high classification performance and psychological understanding, i.e., emotional processing in the brain (J. Li, Duan, Cui, Chen & Liao, 2019; Waugh, Shing & Avery, 2015). EEGs can help researchers understand brain activities over time and elucidate interactions between abnormalities of brain structure and functions in a given mental disorder (Drevets, 2000; Kadipasaoglu et al., 2015). Hence, EEG data being spatiotemporal in nature, if analysed considering both the aspects – spatial and temporal – could be used as an additional tool for detecting a brain disorder. Hence, the spatiotemporal nature of EEG signals and SNNs' capability to process such data inspired the use of SNNs for spatiotemporal data classification, such as EEG signals.

This study employs different SNN architectures, from a 3D reservoir (a 3D network of recurrent spiking neurons) brain-inspired SNN framework to a deep temporal-based SNN design for analysing and treating spatiotemporal datasets. The proposed framework is then utilised to design an AI framework for use in clinical management.

1.3 Rationale and Significance

1.3.1 SNNs as the Computational Model

SNNs are capable of processing event-driven data and, by design, are the potential approach for processing spatiotemporal EEG signals. For classifying EEG signals, the state-of-the-art studies had implemented various ML and DL architectures (Książek, Abdar, Acharya & Pławiak, 2019; Bashivan, Rish, Yeasin & Codella, 2015; Yıldırım, Pławiak, Tan & Acharya, 2018; Yildirim, San Tan & Acharya, 2018). Extensive feature extraction using signal processing techniques is applied to improve the discriminative performance in traditional machine learning (ML) methods. This process is made more efficient by automatic feature extractions using CNN (Convolutional Neural Networks) and CNN-LSTM (Long Short-Term Memory) based architectures. These architectures require high training samples and extensive hyperparameter tuning for high model performance. Although DL architectures produce high accuracy in EEG classification tasks, there exists a gap concerning the capture of the spatial-temporal dynamics hidden in the data that can be used to distinguish both groups. DL architectures do not employ individual pulses, but the output signals lie between 0 and 1. This is known as the rate coding scheme (Maass, 1997b). However, information processing in the human brain is event-driven in the form of spikes. On the other hand, SNN increases biological realism by individual spikes, i.e., neuronal information contains the precise timing of spikes (Maass, 1997a; Vreeken, 2003). Also, in most existing studies, the sequential temporal information is lost as the EEG signals are compressed for feature extraction (Wan et al., 2020). Further, to handle time-series data, LSTM networks have incorporated feedback loops at the cost of increased time complexity and experience vanishing gradients (Pfeiffer & Pfeil, 2018). There still exists a need for a computational model which incorporates the dynamic aspects of EEGs (temporal relations). The membrane potential

computation of spiking neurons acts as an implicit recurrence since it integrates inputs and passes them on to the next time step. This implicit recurrency allows the SNN to handle sequential temporal data better than non-sequential neural nets.

Spiking neurons send signals as a short and sudden voltage to propagate information to the other neurons. This information is relative to the timing and frequency of spikes. The voltage accumulation due to incoming signals causes an impulse at the receiving neuron when it crosses the threshold. Thus, neural computation is believed to rely on the spikes' firing frequency, the spikes' timing, and the spikes' temporal coordination (Waugh et al., 2015). Spiking neurons employed in SNNs enable incorporating spatiotemporal information in communication and computation (Maass, 1997a).

EEG data represents data across various brain areas (EEG channels) collected over time (seconds or minutes of recording). The nature of EEG signals is compatible with the spatiotemporal information processing capability of an SNN (Capecci, Kasabov & Wang, 2015). In other words, an SNN allows spatial and temporal neuroinformatic data to be encoded with synapses and neuron locations and the timing of the spiking activities. The SNN considers the sequence order of the EEG data, which can greatly help the recognition results. Thus, we have employed SNNs to model EEG signals.

On the other hand, there is no doubt that SNNs are still behind ANNs in performance. Two possible reasons behind this may be the under-utilisation of the properties of the spiking neurons or the less efficient learning algorithms (or lack of them altogether) learning algorithms (Pfeiffer & Pfeil, 2018). The conversion of deep ANNs into SNNs (J. H. Lee, Delbruck & Pfeiffer, 2016), deep spiking networks (Venna et al., 2018), spiking variants of backpropagation (J. H. Lee et al., 2016), biological variants of STDP (Tavanaei & Maida, 2019) and hybrid CNN-SNN models (Tavanaei & Maida, 2016) are some of the recent methods implemented in SNN to achieve high classification accuracy. Among these studies, ANN to SNN conversion has proven to be a good approach to achieving better classification accuracy for deep SNN architectures. Most

of the approaches based on mathematical analysis are inspired by the concept of gradient descent (LeCun et al., 2015). Whether the human brain utilises the theory of backpropagation employed in ANNs to learn something new is still an ongoing debate (Illing, Gerstner & Brea, 2019). Also, all of these architectures use a rate coding scheme or develop an approximation between the activations of CNNs and the spike rate of SNNs. In other approaches, the input data is convolved with multiple convolutional and pooling layers, and finally, the output is provided to the SNN for classification. Additionally, most of the deep SNNs built using convolutional and pooling layers have been implemented on static data, i.e., images. Thus, deploying deep SNN models is still an open research area.

1.3.2 Deep SNN as a CNN Design

Learning in the cerebral cortex involves information processing at multiple levels of neurons (Yamins & DiCarlo, 2016), and this layered structural organisation is responsible for the high classification accuracies of DL architectures. To model an SNN as a layered architecture, recent studies have combined the convolution kernels and pooling operation of CNNs to extract the features from the data and propagate them to the fully connected layer or recurrent reservoir of spiking neurons, forming a deep SNN. Spike-based feature extraction for use in deep SNNs is still under-explored. This research aims to apply hand-crafted filters for extracting spatial and temporal features from the binary spike train (data from spiking neurons), proposing a methodology to build a deep SNN framework. The proposed idea is inspired by the filters designed to extract shapes from the digits, the first breakthrough in the deep learning era which led to the development of CNN (LeCun et al., 2010). A detailed description is provided in Chapter 6. The significance of this study includes extracting high-level features from raw EEG signals encoded in spike trains through multiple layers of spiking neurons. The

proposed filters at different levels will produce unique patterns bringing separability to the two groups. Identifying spatiotemporal patterns in the spiking activities of neurons in hidden and output layers will help design binary filters to build a deep feed-forward SNN model.

Studies suggest that most of the information about the stimulus is encoded in the spatiotemporal pattern of neurons, which may not be associated with the rate-code (mean firing rate) encoding mechanism (Gerstner et al., 1993) (Grossberg, 1987) (Crick et al., 1989). However, most traditional SNN architectures employ a firing rate for classification purposes. In this thesis, with one aim to achieve better classification performance, metrics derived from temporal patterns of firing of neurons and neuronal membrane potential have been utilised in the model. Thus, temporal coding is used for classification decisions in the proposed architecture. Classification is carried out by considering the root mean square error between the predicted and the actual signal of the membrane potential of the output neuron and the gamma distance between the predicted and the actual spike train (firing times) of the output neuron.

1.3.3 Depression as a Case Study

In our modern society, depression has become a huge challenge amongst various age groups (S. Z. Williams, Chung & Muennig, 2017). By 2030, depression may affect around 300 million people worldwide as reported by the World Health Organization, and approximately 800,000 people among them may lose their lives (Mathers & Loncar, 2006; Whiteford et al., 2013). A study of meta-analysis of 50,371 patients from 118 studies found that the correct recognition rate for depression was only 47.3% (Mitchell, Vaze & Rao, 2009). So, with the high incidence and low recognition rate of depression, exploring simple, objective, accurate evaluation methods or biomarkers for depression detection is a major public health challenge (Sartorius, 2001).

Depression is usually diagnosed subjectively based on a standardised set of questions using frameworks like the Diagnostic and Statistical Manual of Mental Disorders (Fourth Edition) (DSM-IV) (DSM-IV., 1993), Beck depression inventory (BDI) (Ghassemzadeh, Mojtabai, Karamghadiri & Ebrahimkhani, 2005) and Hamilton Depression Rating Scale (HDRS) (J. B. Williams, 1988). These screening tools determine how many symptoms the subject is experiencing and the time duration, analyse the responses to specific questions, and, more specifically, seek to understand a person's emotional state. The physicians decide the course of treatment after examining their responses. These screening surveys are utilised to give emotional evaluations of a patient's conduct, either from a self-report viewpoint or from the point of view of the clinician or parental figure. For instance, a patient may vary in how they talk about or depict their manifestations or distress level depending on their social foundation. Choosing the alternative 'much of the time' to describe how frequently one experiences sadness may have different meanings for different people. Although this concern is addressed to some extent in the most recent DSM-5 guide (Cooper, 2018), it features one hindrance of depending on absolutely subjective measures (Newson, 2018). Therefore, there is a need for a new computational model that can be used as an additional tool to aid clinicians in their decision-making process.

1.3.4 Depression from a Musical Perspective

The rhythmic patterns in the brain waves caused by the activity of neurons can be captured as oscillations in membrane potential or as rhythmic patterns of action potentials. On the other hand, EEG records voltage fluctuations due to the electrical activity in the brain's neurons, indicating rhythmic behaviour. EEG signals that capture the brain dynamics over periods of time being a complex time-series data; a comparable approach was wanted to understand the behaviour better and firing patterns of spiking neurons.

Hence, music signals were considered for this preliminary analysis.

Music represents various sequences of sounds playing at different frequencies over time. Music signals are periodic in nature, whereas EEG signals are chaotic or non-periodic (Chemin, Huang, Mulders & Mouraux, 2018), but both signals have waveforms and the time dimension in common. Apart from this, music therapy is found to be an effective treatment for reducing anxiety and depression (Maratos, Gold, Wang & Crawford, 2008). It uplifts the mood and emotions of people, improves sleep quality, and has many other psychological benefits. The right brain hemisphere is preferentially activated when listening to music in relation to the emotional experience (Trimble & Hesdorffer, 2017). Thus, considering the rhythmic natures of these signals and the benefits of music therapy for depression treatment, this research study proposes a deep SNN-based architecture for the study of depression incorporating a musical perspective. The proposed SNN framework is applied to two spatiotemporal datasets – music and EEG signals.

1.3.5 Application of SNNs – Clinical Management

Mental illness could be detected by the effectiveness of different brain regions in communicating with each other (J. Wang et al., 2020; Al Zoubi et al., 2019; Kragel, Hariri & LaBar, 2022; Shim, Im, Kim & Lee, 2018; M. L. Elliott, Romer, Knodt & Hariri, 2018), or through brain activity patterns (Stevens et al., 2021) captured in non-invasive neuroimaging tools like EEG. Structural connectivity refers to the anatomical organisation of different brain regions, and functional connectivity is defined as the relationships developed between brain regions over time. The configuration of structural connections formulates the functional connectivity within the brain (Stevens et al., 2021).

The magnitude and direction of information flow between two or more connected

brain regions (Ewald, Avarvand & Nolte, 2013; Nolte et al., 2008) lead to pattern development over time which is the basis for understanding functional behaviours in the brain. These patterns and alterations are visible in structural and/or functional connectivities within and between the brain regions of affected individuals (de Kwaasteniet et al., 2013; Du et al., 2018). Irregularities in information processing disrupt cognitive functioning (Warren, Pringle & Harmer, 2015; Roiser & Sahakian, 2017; R. Elliott, Zahn, Deakin & Anderson, 2011) and alterations in the functional connectivity (Thibodeau, Jorgensen & Kim, 2006; Ahmadlou, Adeli & Adeli, 2012) are reported as prominent symptoms of any brain disorder. Analysis of information flow through inter- and intra-hemispheric connections and long- and short-range communications in significant brain regions are of great significance in psychology for the clinical diagnosis and treatments (Thibodeau et al., 2006; Güntürkün, Ströckens & Ocklenburg, 2020).

SNNs to produce temporal-based feature extraction are still under exploration for the classification of EEG signals (Khosla, Khandnor & Chand, 2021). There is no efficient design of an SNN framework that has explored these traditional approaches of information flow through inter- and intra-hemispheric connections and long- and short-range communications from raw EEG signals. This integration of AI, neuroscience, and psychology can provide a way to identify biomarkers that can be used in clinical settings for the purposes of screening, diagnosis, treatment selection, and monitoring.

In this thesis, a novel deep SNN architecture for the classification of spatiotemporal data is proposed. This research evolved through various phases of testing and validating the architectures. First, the capability of spiking neurons and STDP with supervised learning for depression detection was explored. Next, a 2-layered temporal-based architecture applied to music EEG signals was proposed. After the successful validation of the model, the focus was to apply this novel architecture to design an efficient SNN framework for EEG classification. So, the best way of enabling the flow of input from EEG signals into the SNN model was identified, and potential brain regions indicative

of depression were detected. Finally, a deep SNN framework with hierarchical feature extraction using hand-crafted spike-based binary filters is proposed.

1.4 Research Questions

We hypothesise that the input patterns in the spatiotemporal data will be learned effectively if analysed using an SNN framework that is capable of capturing spatiotemporal relationships through spiking neurons. Taking this hypothesis as a frame of reference, the following research questions are formulated to support the hypothesis.

RQ 1. How can brain-based sequential EEG signals be classified using a brain-inspired computational model?

(i) How can unsupervised learning in SNNs be combined with supervised learning to classify spatiotemporal brain data?

(ii) How capable are spiking neurons of identifying unique patterns to distinguish healthy and depressed people?

To answer this research question, brain-inspired SNN Neucube architecture was utilised to discriminate between healthy and depressed people. This computational model was trained using unsupervised and supervised learning algorithms. The study was further extended to visualise the functional connectivity between different brain regions to identify depression biomarkers, i.e., the unique patterns. SNN outperformed MLP (Multilayer Perceptron Model) and LSTM networks; hence, the results obtained from answering this research question became this research study's foundation (benchmark). In the following research questions, this thesis aimed at improving SNNs' performance for depression detection.

RQ 2. Will spiking neurons encode enough rhythmical features in the spike train from EEG signals to categorise different groups of subjects?

(i) How to recognise spike patterns in the spike train from music signals to categorise different groups?

(ii) How can the rate and temporal coding techniques be leveraged to build a computationally efficient SNN in classifying and recognising musical instruments?

A novel 2-layered deep spiking neural network was proposed and trained using an unsupervised learning algorithm to answer this research question. Two temporal metrics were derived from the spiking information and used as classification criteria. Further, the spiking information obtained from the neurons was analysed to observe the temporal patterns hidden in the rhythmical nature of spiking neurons. This research question was answered in two parts: first, the architecture was applied and tested on music signals, and later on, EEG signals.

RQ 3. How to design an SNN framework to produce temporal-based feature extraction for classifying spatiotemporal data such as EEG signals?

(i) Can the temporal neural coding techniques applied in SNN architecture classify complex EEG datasets?

(ii) How effectively can the temporal-based SNN architecture classify EEG signals when combined with the traditional methods of psychology?

To answer this research question, the proposed SNN architecture was applied to different datasets for EEG classification – Figshare and PREDICT. The traditional methods for depression detection in psychology were studied. The best strategy of information flow from EEG signals into SNN was examined by studying the

various functional connectivity patterns between brain regions. This best strategy is chosen by comparing the classification results from four input configurations – brain asymmetry, grouped clusters of EEG channels, and short- and long-distant communications. After identifying the input strategy, different brain regions were investigated to recognise potential brain areas of depression. The main objective here is to see if SNNs can be combined with the traditional methods of psychology by understanding which EEG channels (or brain regions) are more indicative of depression. Concluding about the feature engineering process involving transformation, combination, or compression is not the primary objective.

RQ 4. How far can we go in building deep SNN so that sufficient information is transmitted to make the neurons fire in the next layer?

(i) What filters can be applied on the spike train to build another layer of spiking neurons by extracting spike-based features?

Our objective was to build a deep SNN using filters for extracting spike-based features from the spike trains. So, for this question, we were looking for a methodology/concept to build this deep architecture, and hence we have used the word "How". To answer this research question, spike-based filters have been proposed using the hybrid mechanisms of neural coding schemes – rate and temporal coding. A novel deep SNN framework with hierarchical feature representation has been presented. The convolution and pooling operations at each layer resulted in unique patterns which might aid the classification performance. Also, all the processes designed in this architecture aimed to exploit the capability of spiking neurons.

1.5 Hypotheses

H 1. Depression is a system-level disease related to the dysfunction of neuronal network activity across multiple brain areas. Having seen the spatiotemporal properties of both – EEG and SNN, it was decided to employ SNN to perform EEG-based classification tasks for distinguishing depression. It is hypothesised that EEG data being spatial-temporal in nature, if analysed considering both spatial and temporal aspects using an SNN, healthy and depressed individuals could be separated and provide better interpretability of EEG signals (brain activity). This hypothesis relates to the first research question. This hypothesis is tested, and the results are presented in Chapter 3.

H 2. Spiking neurons containing valuable temporal data can encode the rhythmic behaviour of EEG signals. To test this hypothesis, it was decided to conduct preliminary experiments with a simple dataset – music signals, i.e., violin and piano instrument recognition. The neuronal firing in the hidden layer was analysed to detect rhythmic patterns in response to different stimuli – musical instruments. The firing times and the membrane potential leading to an action potential in a spiking neuron contain a hidden temporal pattern which may boost the classification performance. This study has implemented similarity metrics based on the properties of the output neuron for making classification decisions. If the proposed SNN architecture can encode the rhythmic nature of music signals, it will perform well for EEG classification as well. The second research question is related to this hypothesis. The experiments and results to support this hypothesis are described in Chapters 4 and 5.

H 3. Changes in the brain are expected to be reflected in bioelectrical activity. Mining the EEG signals would extract the variations in the physiology of the brain. To

this end, the functional abnormalities in the frontal-limbic network, the inter-hemispheric difference of EEG channels, and short- and long-distance communications between brain regions could, it is believed, display different states and behaviours. Utilising the EEG signals in an efficient way could produce distinguishing temporal patterns separating both groups. This hypothesis was explored to answer the third research in Chapter 5.

H 4. Neural networks learn features from the input data. Applying filters at different layers in SNN will produce better feature representations of the input data. With this end in mind, we have proposed spike-based binary filters convolved with spike trains have been proposed. This hypothesis is related to the fourth research question. A novel deep, pure SNN-based architectural framework with convolution and pooling operations is proposed in Chapter 6.

1.6 Design of the Research

Since the focus is on developing a novel SNN architecture, this research incorporated the 'Design Science' research methodology (Carstensen & Bernhard, 2019).

This research was designed in the following phases as summarised below and further distributed across different chapters described in detail in Section 1.7:

1. **Phase 1**: The NeuCube (N. K. Kasabov, 2014) architecture was compared with MLP and LSTM for classifying the EEG signals. Further, this architecture was employed to extract patterns from SNN for depression detection as described in Chapter 3. The extracted patterns helped develop a deeper understanding of depression using EEG signals.

2. **Phase 2**: Based on the results and patterns in the first phase, a two-layer SNN

feedforward architecture was further developed to analyse the effect and importance of using temporal information of spiking neurons in classification decisions. A novel temporal-based SNN architecture for music instrument recognition is proposed in Chapter 4.

3. **Phase 3**: After the successful implementation and better classification performance of the proposed architecture in phase 2, the next phase was to test its effectiveness on complex EEG signals. In this phase, two different public datasets for depression detection were used. An end-to-end AI framework that can be applied in clinical management is also proposed in Chapter 5.

4. **Phase 4**: Based on the findings of these earlier phases, a methodology to design filters to build a deep SNN by extracting spike-based features from the spiking information is finally proposed in Chapter 6.

1.7 Thesis Outline

NeuCube, a brain-inspired framework, is the main foundation for the developed methods in this thesis. This section provides the entire thesis structure.

Chapter 1 discusses some fundamental background, motivation, research questions, hypothesis, and contributions of this Ph.D. study.

Chapter 2 briefly reviews various machine and deep learning techniques employed for depression detection, different learning techniques and neuron models for SNN, the significance of rate- and temporal-based metrics, and the design of the binary spike-based filters. This chapter discusses the background of various fundamental elements of this research.

Chapter 3 introduces the NeuCube (N. K. Kasabov, 2014) computational architecture and introduces the methodology of integrating it with EEG data for depression

detection. The NeuCube framework enabled a better understanding of depression than existing DL techniques through the temporal patterns developed by unsupervised and supervised learning techniques. This chapter covers hypothesis H1 and research question RQ1.

Chapter 4 investigates the rate- and temporal-based coding techniques for information representation in SNN. A novel temporal-based SNN architecture is proposed here for recognising event-based data: musical instrument recognition. This chapter covers hypothesis H2 and research question RQ2.

Chapter 5 validates the effectiveness of the proposed architecture on EEG datasets for depression detection. An end-to-end SNN design is proposed for depression detection by exploring different information flow strategies from EEG signals into the proposed SNN architecture and identifying prominent brain regions. This chapter covers hypotheses H2 and H3 and research question RQ3.

Chapter 6 gives an overview of CNNs and existing spiking-based convolutional NNs. This chapter presents a new architectural model to build a deep spiking neural-based architecture inspired by CNN-SNN architecture. Hand-crafted filters are proposed for spike-based feature extraction. This chapter covers hypothesis H4 and research question RQ4.

Chapter 7 summarises the thesis achievements, key findings, and contributions. Future directions are also suggested.

Chapter 2

Literature Review

This chapter presents a review of the existing literature in the following order:

1. The first section discusses the different architectures and methods applied to build a deep SNN along with their applications, particularly deep spiking convolutional neural networks.

2. The second section discusses the various ML and DL architectures and the prominent brain regions and features identified for depression detection using EEG signals.

2.1 Introduction

The brain processes information at various layers, i.e., it has a layered organisation. This can be explained through the following concept of visual recognition. The visual image processing steps conducted by the brain explain this layered functionality of the brain (Hubel & Wiesel, 1959, 1962). The receptive field of each vision cell gets turned on when light hits the retina. Through the cornea and the lens, the vision becomes clearer as the light passes by, and this information is passed to the primary visual cortex.

The interpretation of the stimuli (the image we see through our eyes) begins when we understand the shape, colour, structure, orientation, etc. of the object. In other words, visual signals are the inputs to three fundamental information processing systems. The first system recognises the shape, the second system identifies the colour, and the third one processes movement, location, and structural organisation. The brain processes these pieces of information at different layers at high speed in a unified manner to enable human perception and object recognition.

Based on this understanding, artificial neural networks profoundly inspired by the organisation of the human brain's networks have various layers to extract features from the input (stimuli), process them, and finally use them to recognise the input (K. Fukushima & Miyake, 1982; GI, 1989; LeCun et al., 1989; Riesenhuber & Poggio, 1999; Cao, Grossberg & Markowitz, 2011; Grossberg, Markowitz & Cao, 2011). In other words, a huge network of rate-coded neurons is stacked with full connectivity to create very deep structures called deep neural networks (DNNs). A neural network is said to be a DNN if it consists of atleast two hidden layers. One variant of DNNs is the convolutional neural network. Their architectural design is inspired by the object recognition principles in the human brain. Leveraging the convolutional and pooling layers into their architectures, CNNs have proved their potential largely in vision-based models.

Although DNNs have achieved great success in various domains in the past decade, they are resource intensive in terms of immense computational cost, huge data requirements, and high energy consumption. Additionally, they still lag behind the biological neural networks in terms of information processing capability and energy efficiency.

One promising solution to these challenges is the use of SNNs. SNNs were developed with the aim of integrating the principles of neuroscience and machine learning. They are computationally efficient and biologically modeled as compared to deep neural network architectures. The information processing is faster because the spiking neurons

perform event-driven (spike-based) computations, i.e., they can adopt the sparsity found in biological neural networks as well as being compatible with temporal information. This makes them more like the real neurons in the human brain (Maass, 1997b).

2.2 Deep Spiking Neural Networks

The neural computations, learning rules, and the capability to embrace sparsity and process temporal information make SNNs an effective solution to overcome the bottlenecks of ANNs and also process spatiotemporal data. However, training SNNs is difficult because of the complex dynamics of spiking neuron models and as the neuronal activation function is non-differentiable. For these reasons, SNNs are behind ANNs in terms of performance. A comparison of the properties of biological neural networks, ANNs, and SNNs is presented in Table 2.1 (Yamazaki et al., 2022).

Table 2.1: Comparison between biological neural networks, ANNs, and SNNs (Yamazaki et al., 2022)

Properties	**Biological NNs**	**ANNs**	**SNNs**
Information Representation and Processing	Spikes	Scalars	Spikes
Learning Mechanism	Synaptic Plasticity	Backpropagation	Synaptic Plasticity and Backpropagation

ANNs have witnessed great success in classification performance as they can use stochastic gradient descent and backpropagation techniques to train the neural nets. Since the information processed in SNNs is discrete in nature, SNNs do not have efficient training methods to achieve high classification performance. The prominent learning mechanisms in SNN could be categorised into three categories, as discussed below.

2.2.1 Spike-based Backpropagation

Supervised learning using gradient descent and backpropagation (Bohte, Kok & La Poutré, 2000; J. H. Lee et al., 2016, 2016; Stromatias, Soto, Serrano-Gotarredona & Linares-Barranco, 2017; Neftci, Augustine, Paul & Detorakis, 2017; Wu, Deng, Li, Zhu & Shi, 2018; Jin, Zhang & Li, 2018) have been used to increase the performance of SNNs. These methods usually work around the firing times (Bohte et al., 2000; Sporea & Grüning, 2013) and membrane potential (Zenke & Ganguli, 2018; O'Connor, Neil, Liu, Delbruck & Pfeiffer, 2013) to derive the derivatives for computing error functions.

2.2.2 STDP-based Learning

STDP and variants of STDP like reward-based STDP, STDP with backpropagation, and anti-Hebbian STDP are widely used to train SNNs based on the temporal order of pre-and post-synaptic neurons (Tavanaei & Maida, 2017; Tavanaei, Kirby & Maida, 2018; Tavanaei & Maida, 2019; Kheradpisheh, Ganjtabesh, Thorpe & Masquelier, 2018; Thiele, Bichler & Dupret, 2018; Howard, Gale, Bull, de Lacy Costello & Adamatzky, 2012).

2.2.3 ANN-SNN Conversion

CNN-SNN conversion or ANN-SNN conversion (Cao & Grossberg, 2012) techniques have attracted much research. The real-valued activities from ANNs are transmitted to SNNs as binary-valued spikes through various approximation and conversion techniques. Alternatively, transferring the learned weights and biases from ANNs to SNNs produces comparable performance in SNNs.

A detailed review of the different architectures employing one or more of the above methods to increase the classification performance of SNNs performance is presented below.

2.2.4 Review of Deep SNN architectures

Pérez-Carrasco et al. (2013) in (Pérez-Carrasco et al., 2013) came up with early work of conversion from a trained neural network to an event-based characterisation. This paper describes the mathematical process of converting an analog calculation to an event-driven neuron. Taking inspiration from this study, Cao, Chen, and Khosla (2015) in (Cao, Chen & Khosla, 2015) proposed the unique approach of using the learned weights from the CNN model in the SNN network. The SNN and CNN structure (10 layers deep) were organised in a similar fashion. Rectified linear unit (ReLu) activation function was used to train the CNN, whereas the LIF neuron was used in the SNN. This architecture achieved high accuracy on CIFAR-10 and Defense Advanced Research Projects Agency (DARPA) Neovision Tower datasets. One of the key findings of this research was to remove all the negative values in the inputs and between layers and also remove the biases from all layers of the CNN. Although there has been success with advances in the CNN-SNN conversion, CNNs are still unbeatable due to the error approximation step in the conversion process. This approximation is introduced as spiking neurons process discrete values, whereas the analog neurons process continuous values. The main motivation behind all the studies related to ANN-SNN conversion is to develop techniques for the reduction of approximation error.

Sparse firing in SNN can lead to performance loss as there is less information in the network to distinguish inputs. Hence, (Diehl et al., 2015) presented optimisation techniques to maximise the performance in the conversion process. This study thoroughly analyzed the network for different settings of the firing rate and threshold during the conversion. They proposed a weight normalisation technique where the weights are normalised based on the maximum possible activation and the maximum input to produce a single spike. This architecture could stabilise the behaviour of spiking neurons, reducing the approximation error on the Modified National Institute of Standards and

Technology (MNIST) dataset (Deng, 2012).

(Rueckauer, Lungu, Hu, Pfeiffer & Liu, 2017) proposed a deep CNN equivalent deep SNN by extending deep SNN to incorporate the implementation of max-pooling layers, softmax optimisation, neuron biases, and batch normalisation. The equation of the spiking neuron model was modified to develop a direct relationship between the artificial neuron's activation function and the spiking neuron's firing rate. They have described a methodology for converting the Inception-V3 network to a precise SNN implementation, improvised the weight normalisation technique, and finally built an open-source ANN-SNN conversion tool.

In the previous studies, the threshold of spiking neurons was adapted based on the maximum activation of CNN. However, (Sengupta, Ye, Wang, Liu & Roy, 2019) proposed a novel algorithm, SPIKE-NORM, in which the threshold is related to the maximum input of each layer in the converted SNN. This architecture was thoroughly tested on ImageNet and CIFAR-10 datasets and was successful in reducing the classification accuracy loss.

With an objective of utilising rich temporal information classifying a visual scene, (Sironi, Brambilla, Bourdis, Lagorce & Benosman, 2018; Lagorce, Orchard, Galluppi, Shi & Benosman, 2016) proposed a unique event-driven hierarchical architecture. Spatiotemporal features are extracted from the event-based data to build an event-based context, and then exponential kernels are applied to them. This creates time surfaces, i.e., the first layer is derived from the group of pixels and then constitutes the input to the next layer. The central theme of this study was to utilise temporal information to understand the temporal activity within the local spatial region.

Utilising the learned synaptic weights from ANN to SNN conversion has proven to be a good approach to achieving better classification accuracy for deep SNN architectures. However, all the state-of-the-art architectures use a rate coding scheme, i.e., Poisson distributed rate, to produce the spikes within a certain limit. With the aim

of producing more information, the classification latency of the network increases as the architecture goes deeper. Thus, (Kim, Kim, Huh, Lee & Choi, 2018) proposed a novel algorithm with weighted spikes (SNN-WS) for image classification. The weights here do not represent the synaptic weights. Instead of rate coding, the authors have employed a phase coding scheme in which spikes are attached to different weights based on the phases. The inclusion of the weight factor on the spikes added more information to the network, which overall increased neuronal activity. However, phase coding produced more noise in the network, and also the conventional spiking neuron model was modified to incorporate this design.

Most of the CNN-SNN conversion techniques have used rate coding to develop an approximate relation between the activations of CNN and the spike rate of SNN. However, to reduce the approximation error, either the firing rate of the neuron or the stimulation duration of SNN should be increased to a level enough to excite the neurons of all the layers. Hence, the computational cost of SNN increases. To overcome this issue and the issue of noise caused by phase coding, (Rueckauer & Liu, 2018) exploited the concept of temporal coding in the brain. They devised the architecture in such a way that each neuron fires only once by developing a time inverse relation with the activation of the CNN. Here, the output time spikes were computed as the inverse of the activations of the CNN. This implementation was successful in increasing the computational efficiency with decreased classification accuracy on the MNIST dataset.

The time-to-first spike coding decreased the computational cost as well as the overall accuracy of the SNN. (R. Chen et al., 2018) introduced the concept of pruning to maintain high computational efficiency with increased spatial information. The output of the spiking neuron model was not just restricted to 0 or 1, but the LIF neuron was formulated to output 1.5 or 2. Neurons with less membrane potential were pruned in the first two phases as they could not produce sufficient spikes. Weak synaptic connections were removed in the third phase as they cannot stimulate the neurons. This

SNN implementation effectively reduced the computational cost and achieved high classification accuracy.

This (S. Park, Kim, Choe & Yoon, 2019) is the first study to embed phase and burst coding in the input and hidden layer. Motivated by the impact of burst spikes on information transmission, the authors have analysed different spike patterns in the spike trains and proposed a hybrid neural coding scheme. The threshold of spiking neurons was dynamically adapted to produce sufficient firing in the higher layers of the SNN. This architecture presented a successful proof-of-concept for incorporating hybrid neural coding mechanisms to maintain accuracy, speed, and energy efficiency on image classification tasks.

The information transfer in SNN occurs through the spikes. Over time, neurons accumulate the membrane potential, and a spike is generated when the membrane potential crosses the threshold. Neurons are stimulated by the input, which either increases or decreases the membrane potential. In other words, membrane potential and threshold evoke a neuron's impulse. Membrane potential largely depends on the weights of the network. Hence, when the input stimulation stops or when the weights are very small, the accumulation of membrane potentials will stop or may tend to decrease. As a result, there will no spikes, as the membrane potential will not cross the threshold. This entire process will result in reduced neuron activities, leading to the loss of information. To overcome this issue, (Y. Chen, Mai, Feng & Xiao, 2022) proposed an adaptive threshold mechanism with 19 layers (CNN and CNN-SNN) to maintain a balance between the network weights and the neurons' threshold. The output (spike rate) from the RELU activation function in CNN is provided as input to the LIF neuron in SNN. The threshold of spiking neurons is dynamically adapted to the input data, and the reason is to produce sufficient firing in the network. And this threshold adjustment strategy generated enormous firing to excite the higher layers, achieving an accuracy of 93.93% on the CIFAR-10 dataset.

The studies described so far imported the weights from CNN to SNN, or they developed a relation between the analog signal of CNN and the firing rate of spiking neurons. The architecture described in (Turkson, Qu, Mawuli & Eghan, 2021) performs a classification of Alzheimer's disease (AD) using a deep convolutional SNN. The MRI scans are provided as input to an unsupervised SNN, and the output is then fed into a supervised CNN model for predictions. Time-to-first coding is implemented in the SNN to encode the MRI pixels into spike times. The synapses connecting the neurons of SNN with excitatory and inhibitory neurons are adapted using STDP. Competitive inhibition is enabled between the second and fourth layer allowing the network to learn AD features from the scans. The output (spike trains) from the fourth layer is fed into deep CNN for supervised classification.

Deep SNN with multiple convolutional and pooling layers, along with a temporal coding scheme for object recognition, was proposed in this study (Kheradpisheh et al., 2018). A Difference-of-Gaussians (DoG) filter was used to extract features from the images in the MNIST database in the initial layers, the convolutional layers were trained by STDP, and finally, only information related to time-to-first spike was fed to a support vector machine (SVM) classifier securing 98.4% accuracy on MNIST. To investigate how deep SNN can go for better performance, (Illing et al., 2019) implemented SNN with one single hidden layer and a readout layer achieving 98.6% test accuracy. Localized Gabor filters were used to assign weights (fixed) between the input layer and the hidden layer. They used STDP and then applied the delta learning rule to update the output layer weights.

This study (C. Lee, Srinivasan, Panda & Roy, 2018) proposed a hierarchical deep convolution NN with unsupervised learning. The input layer was followed by a stack of convolutional and spatial-pooling layers for feature extraction. The convolutional kernels were trained layer-by-layer using STDP, which led the network to learn features from the input. Thus, different patterns were developed for the samples of different

groups. Furthermore, the feature maps produced after the pooling technique were fully connected to the output layer. Competitive inhibition was incorporated at the output layer to predict the pattern. A positive STDP rule is implemented at the final layer for supervised learning. The output neuron rendered for a particular category is made to fire by keeping its threshold at zero. The threshold is increased by a small amount every time the neuron fires; this is how a pattern is produced for each input class. This architecture was capable of achieving a classification accuracy of 91.1% on the MNIST dataset with 25488 trainable parameters. Also, on the CALTECH dataset, an accuracy of 97.6% was attained with the same number of training parameters. This study successfully proved the capability of STDP learning and competitive inhibition for classification tasks on static datasets.

The study (Ke, Xing, Di Caterina, Petropoulakis & Soraghan, 2020) performed hand gesture recognition using convolutional spiking neural networks. However, here the convolutional kernels were applied on spike trains. The first layer consists of LIF neurons which encode the input, followed by convolutional and pooling layers. Finally, the output layer again consists of fully connected LIF neurons. Two datasets (Strathclyde and CapgMyo) are used for experimentation, achieving a classification accuracy of 98.76% and 98.21%, respectively. Additionally, this approach reduced data processing time and training time.

Another application that exploited the capabilities of SNN is the field of video analytics (Berlin & John, 2020). Spatial and temporal features are captured from pre-trained models MobileNet (Ullah, Muhammad, Del Ser, Baik & de Albuquerque, 2018) and PWC-NET (Sun, Yang, Liu & Kautz, 2018), respectively. The features are then fed to SNN for classification purposes. Threshold adaption and lateral inhibition are employed in SNN for the generation of unique patterns belonging to each input class. The SNN classifier is trained using BP-based stochastic gradient descent (J. H. Lee et al., 2016) on MDB51 and UCF101 datasets.

Most of the studies described above used an average or cumulative number of spikes as the output of the max-pooling method. Nevertheless, this particular research (D.-A. Nguyen, Tran, Dang & Iacopi, 2020) proposed a novel max-pooling mechanism using the neuronal membrane potential. The neurons with maximum membrane potential in the pooling layer are allowed to propagate spikes to the next convolutional layer. The threshold value determines the maximum membrane potential. The trained weights from VGG16 nets were normalised using the approach mentioned earlier (Rueckauer & Liu, 2018). These weights were later incorporated into SNN with the same implementation as described in (Rueckauer & Liu, 2018). This architecture was tested and validated on MNIST and CIFAR10 datasets, reaching a classification accuracy of 99.38% and 92.1%, respectively.

The following limitations have been identified in deep SNN architectures:

1. Spike-based supervised learning and rate-based learning with gradient descent and BP methods either ignore the temporal effect of the spike sequences or train the model without taking the occurrences of spikes into account.

2. Gradient descent and BP methods are suitable for processing real-valued numbers and are not biologically plausible.

3. ANN-SNN conversion techniques involve high computational costs by converting and transmitting real-valued data in the form of spikes. Also, information is lost using this conversion which results in sparse firing.

In summary, most deep SNNs have been implemented on static data, i.e., images. Previous work has implemented the backpropagation technique by computing spike-based or membrane potential based derivatives to build a deep SNN aiming for better classification accuracy. STDP and the unsupervised learning rule have shown promising results in early spatiotemporal pattern recognition and classification problems. The last

three years have witnessed a huge growth in combining CNN with SNN and STDP for classification tasks. The potential of spiking neurons, dynamic threshold adaption, temporal coding, filters, STDP, and layered architecture have been the key components in these existing studies and in driving the foundation and innovation of this thesis.

2.3 Depression Detection

This section provides a detailed overview of existing ML and DL architectures using EEG datasets for depression recognition.

Firstly, there is a review of the clinical-based depression diagnosis followed by ML-based techniques, which involve the application of different pre-processing techniques to remove artifacts from the EEG signals before performing the classification task. Next, the focus turns to the advantages of applying DL architectures for automatic feature extraction. The main reason behind reviewing these articles was to develop an understanding of the prominent brain regions and EEG channels for depression recognition. Finally, the reasons for applying SNN to EEG-based classification tasks are described.

2.3.1 Depression Detection using ML techniques

The diagnosis of depression is based mainly on an evaluation of the intensity of subjective symptoms using clinical interviewing and psychiatric questionnaires. Detection of a decline in brain physiology before the subjective symptoms appear is crucial for the early detection of depression, enabling treatment that is more effective and improving the quality of mental health. Any decline in the brain's neuronal activity and in the mental state is expected to be reflected in the brain's bio-electrical activity. EEG is an easily available, cost-effective technique, providing high temporal resolution for the evaluation of the dynamics of the bio-electrical activity of the brain. It is a medical test used to

measure the brain's electrical activities and evaluate brain disorders. EEG features have been successfully applied to the investigation of brain behaviour in various mental diseases (Abásolo, Escudero, Hornero, Gómez & Espino, 2008; Fingelkurts & Fingelkurts, 2015; Hinrikus et al., 2010; Knott, Mahoney, Kennedy & Evans, 2001; Leuchter, Cook, Hunter, Cai & Horvath, 2012; Henriques & Davidson, 1991; Omel'Chenko & Zaika, 2002).

In (Mohammadi et al., 2015), electroencephalogram (EEG) signals are analysed at the group and individual levels to differentiate patients with major depressive disorder (MDD) and non-depressive healthy volunteers (HVs). The data was collected during the eyes-open (EO) and eyes-closed (EC) states, and potential features were obtained. Linear discriminant analysis (LDA) was used for feature reduction, a genetic algorithm (GA) was applied for feature selection, a decision tree was implemented for classification rules, and hidden patterns were derived. The authors extracted the various frequency bands from the raw signals. The classification accuracy was examined when all the frequency bands were used collectively with an ML classifier and also when individual bands were fed into the classifier. With all frequency bands analysed together, the model showed average classification accuracy (MDD vs. HV) of 80%. A sample of 53 adults with a primary diagnosis of MDD and 43 age-matched HV adults participated in this study. MDD diagnoses were psychiatrist-confirmed using the Structured Clinical Interview for DSM. The Montgomery-Asberg Depression Rating Scale (MADRS) was used to assess symptom severity, and patients with scores greater or equal to 22 were considered as moderately depressed.

EEG recordings were obtained during three min vigilance-controlled EC and 3 min EO resting conditions (counter-balanced). EEG was recorded (sampling rate 500 Hz) with reference to the activity from electronically linked mastoids and using a cap system with 28 Ag/AgCl scalp electrodes (EasyCap, Herrsching-Breitbrunn, Germany) positioned on the scalp according to the 10–10 system. EEG data were processed

offline using BrainVision Analyzer Software (BrainVision, Richardson, TX, USA). Signals were referenced with electronically linked mastoid electrodes (TP9/10) or a scalp vertex (Cz) electrode to yield two data sets for each of the EC and EO recordings (Mohammadi et al., 2015). For both referenced recordings, signals were filtered (0.1–30 Hz), ocular corrected, and segmented into 2s epochs (50% overlap). A fast Fourier transform (FFT) algorithm (Hanning window with 5% cosine taper) for computation (μV2) of both absolute and log-transformed power in delta (1–4 Hz), theta (4–8 Hz), alpha-lower (8–10.5 Hz), alpha-band (10.5–13 Hz), alpha total (8–13 Hz) and beta (13–30 Hz) frequency bands were applied to the raw EEG signals. Frequency bands for each of the 28 electrodes were obtained – Fp1, Fp2, F3, F4, C3, C4, P3, P4, O1, O2, F7, F8, T7, T8, P7, P8, Fz, Cz, Pz, Oz, Fc1, Fc2, Cp1, Cp2, Fc5, Fc6, Cp5, Cp6. Accuracy was between 40-66%, and specificity ranged between 0-54% for all individual frequency bands except the delta band. The accuracies were increased when LDA and GA were used for feature reduction and selection, respectively. Accuracy was as high as 88% for the delta band when used with GA and LDA. Delta was the exceptional individual band classifier when analysed during EO. Modest accuracy and sensitivity rates (64 %) were observed with EC and EO alpha band analysis using all candidate features. However, GA and LDA feature extraction processes increased the EC alpha classifier's sensitivity, positive predictive values (PPV), negative predictive values (NPV), and accuracy rates to 94, 83, 90, and 86%, respectively. For the test set, the accuracy of the model fluctuated between 70% and 80%. Individual bands resulted in relatively high classification errors, regardless of whether or not the complexity and redundancy of signal features were reduced by the genetic algorithm. Group-level comparison studies showed activity of alpha and, to a lesser extent, delta oscillations to distinguish depressed and HV samples. Given the questionable reliability of diagnoses based on clinical symptoms, this quantitative methodology may be a useful adjunctive clinical decision support for identifying depression, and it supports independent studies

confirming the potential clinical utility of the computer-aided diagnosis of depression using EEG signals.

Studies showed that patients with depression have hemispheric asymmetry in their brain signals compared to non-depressed subjects (Davidson, 1998; Gotlib, 1998; Henriques & Davidson, 1991). A preliminary study by Nandrino and team (Nandrino et al., 1994) shows that the decrease in complexity of brain functioning in patients with depression is a sign of a lower level of interaction with the environment. Pezard and team (Pezard et al., 1996) confirmed and extended the conclusion presented in (Nandrino et al., 1994). Their study showed that patients differ significantly in their dynamic response to therapeutic interventions during first and recurrent episodes.

In (Deslandes et al., 2008), the authors assessed the differences in EEG signal asymmetry of depressed and normal elderly subjects and observed the connections between depressive symptom measures and quality of life. They reported that the EEG signal asymmetry at the alpha band in clinically depressed elderly adults is similar to that of younger depressed subjects compared to normal subjects.

The resting frontal EEG alpha asymmetry is reliably assessed in clinically depressed patients; thus, it serves as a trait marker of risk for depression and other emotion-related psychopathologies (Allen, Urry, Hitt & Coan, 2004). This study (Debener et al., 2000) explained the relationship between alpha EEG asymmetry and depression in patients on two separate occasions between two and four weeks apart. Their results show that the increased variability of anterior EEG asymmetry can be used as a characteristic feature or marker for depression detection from EEG signals. Authors (Stewart, Bismark, Towers, Coan & Allen, 2010) used resting frontal EEG asymmetry as a marker of depression and showed that it is predominant in women.

A study (Davidson, 1992) suggested that pronounced corresponding right anterior EEG activity acted as an indicator for the evolution of depression and anxiety problems. It was investigated and proved by experimental results that anterior and posterior EEG

asymmetry patterns predicted the future occurrence of depression symptoms (Blackhart, Minnix & Kline, 2006). The study predicted that those with comparatively lower right posterior EEG activity might complain about higher depressive symptoms after a year (Blackhart et al., 2006). In contrast, particularly the frontal asymmetry of EEG alpha power indicated the risk for depression (Smit, Posthuma, Boomsma & De Geus, 2007). The complex, nonlinear, and non-stationary EEG signals are very tedious to interpret visually, and it is difficult to extract their significant features. The linear and nonlinear methods effectively identify the changes in EEG signals to detect depression.

A number of EEG studies based on linear methods found frontal asymmetry (Fingelkurts et al., 2006; Iosifescu et al., 2009; Salustri et al., 2007; Stewart, Towers, Coan & Allen, 2011) but reported different results in depressed patients. A bilateral increase in the frontal lobe alpha band activity (Grin-Yatsenko, Baas, Ponomarev & Kropotov, 2010), an increase in the frontal beta band activity, and a reduction in the slow wave activity during sleep (Nissen et al., 2001, 2006) are results observed by different researchers. Knott et al. (Knott et al., 2001) suggested the EEG power as a useful tool for investigating brain regional mechanisms in depressed patients. They reported that EEG measurements (amplitude, frequency, and power) obtained using linear methods in depressed patients appeared to describe a pattern of aberrant inter-hemispheric asymmetry and a profile of frontal activation.

Linear methods do not exhibit complex dynamical variations in the EEG signals. Hence, chaos theory and nonlinear dynamic methods are widely used in extracting the EEG signal features for computer-aided diagnosis (CAD) of depression. The section below presents the recent efforts on the computer-aided diagnosis of depression using EEG signals, focusing on nonlinear methods. In other words, during past years, theoretical and experimental studies of the brain have shown that nonlinear dynamical processes best characterise this system. The brain's nonlinearity limits linear analysis's ability to fully describe the underlying brain dynamics for studying mental disorders

(Stam, 2005).

In (Faust, Ang, Puthankattil & Joseph, 2014), the authors examined EEG indicating discriminant features that represent the mental state of patients with depression by combining a feature extraction process, i.e., wavelet packet decomposition (WPD) and non-linear algorithms. WPD (linear method) was used to select appropriate EEG frequency bands. The resulting signals were processed with the non-linear measures of approximate entropy (ApEn), sample entropy (SampEn), renyi entropy (REN), and bispectral phase entropy (Ph). The features were selected using the t-test, and only discriminative features were fed to various classifiers, namely a probabilistic neural network (PNN), support vector machine (SVM), decision tree (DT), k-nearest neighbor algorithm (KNN), naive bayes classification (NBC), Gaussian mixture model (GMM) and Fuzzy Sugeno Classifier (FSC). Their classification results show that, with a classification accuracy of 99.5%, the PNN classifier performed better than the rest of the classifiers in discriminating between normal and depressed EEG signals. Bipolar EEG recordings were done from locations FP1-T3 (left half) and FP2-T4 (right half) of the brain in a resting state. Each recording lasted five minutes with a sampling rate of 256 Hz. The resulting signals were notch filtered at 50 Hz to remove the power line interference. An expert removed eye and muscle movement artifacts during visual inspection. First, WPD was carried out to extract an appropriate sub-band from the EEG signal. In the second step, the resulting sub-band signals were used as input for non-linear feature extraction algorithms (various entropies).

It was found that right-side EEG signals give a low p-value for the AA2 band. Similarly, low p-values were achieved with ApEn on both AA2 and DD2 bands. The DD2 band was also used to extract a feature value with the REN method. For the left side, it was found that SampEn on AA2, REN on DA2 and DD2, and ApEn on DD2 give low p-values. This result supports the hypothesis that EEG signals from the right and left sides of the brain are not the same. Further analysis of the measurements revealed

that the information content, as measured by Ph, ApEn, and SampEn, in the EEG signals from clinically depressed patients, is significantly lower compared to the normal control group. Signals from the right part of the human brain discriminate the depressed from the normal subjects much more efficiently. The fact that the information in the EEG signals is reduced for depressed subjects aligns with general diagnostic practices. The ability of a depressed subject to master tasks that require a high information content of the EEG signals is reduced. This shows diminished cognitive functioning.

Authors (Hosseinifard, Moradi & Rostami, 2013) have studied nonlinear analysis of EEG signals for discriminating depression patients and normal controls. For diagnosing depression symptoms and illness severity, two criteria were considered: a DSM-IV interview resulting in a diagnosis of depression and a Beck Depression Inventory (BDI) score greater than or equal to 10. Forty-five unmedicated depressed patients and 45 normal subjects participated in this study. The power of four EEG bands – delta, theta, alpha, and beta (frequency and linear features) – and four nonlinear features, namely detrended fluctuation analysis (DFA), Higuchi fractal, correlation dimension, and Lyapunov exponent, were extracted from the EEG signal (13 channels). KNN, linear discriminant analysis, and logistic regression as the classifiers were used to discriminate the two groups. A classification accuracy of 90% was achieved by all nonlinear features and a logistic regression (LR) classifier. A genetic algorithm was employed in all experiments to select the most important features. This study shows that a nonlinear analysis of EEG can be a useful method for discriminating between depressed patients and normal subjects. It is suggested that this analysis may be a complementary tool to help psychiatrists diagnose depressed patients. The data cleaning process is followed by a feature extraction step using linear/non-linear methods, a feature selection using a genetic method, and the classification step using LDA, LR, KNN, SVM with the non-linear kernel, and naive Bayes. LDA, LR, and KNN performed better. The highest accuracy, 73.3%, was achieved when alpha power was applied to the classifiers as the

input. The alpha power band of five electrodes in the left hemisphere (C3, P3, O1, F7, T3) and one electrode in the right hemisphere (O2) differ significantly between depressed patients and normal controls. Individual non-linear features show that the correlation dimension has achieved the highest accuracy among all features, 83.3% when used as the input for the LR classifier. Finally, about nine features are selected by GA in each classifier when 19 features are used as input. Accuracy has the lowest value when the Lyapunov exponent is used as the input to the classifiers. LDA and LR classifiers have better accuracy in all features than the KNN classifier. The best accuracy, 90%, is achieved when all nonlinear features are used as input to the LR classifier. The best accuracy is obtained by LR and LDA classifiers and all power bands as the input of classifiers. The highest accuracy of all power bands is 76.6% in LR and LDA classifiers. The accuracy of the three classifiers is higher for all nonlinear features as the input compared to power band features.

In this study (Henriques & Davidson, 1991), Henriques and Davidson reported that the left hemisphere of depressed patients had higher alpha power than the left hemisphere of normal subjects. Also, this study showed alpha power was higher in the left hemisphere of depressed patients than in the right hemisphere of this group. Knott et al. (Knott et al., 2001) reported an accuracy of 91.3% in classifying 70 depressed patients and 23 normal subjects using linear features such as relative power and absolute power.

Spyrou, Frantzidis, Bratsas, Antoniou, and Bamidis (2016) used Random Forest (RF), random tree, multilayer perceptron (MPL Network), and SVM (Spyrou, Frantzidis, Bratsas, Antoniou & Bamidis, 2016) to identify 34 participants suffering from both cognitive impairment and geriatric depression (mean age 69.81) and 32 control subjects (mean age 70.33) using synchronisation and oscillatory features. Results indicated that RF gained the highest accuracy (95.5%). X. Li, Hu, Sun, and Cai (2016) (X. Li, Hu, Sun & Cai, 2016) sought the prominent frequency band and brain regions that are

most related to mild depression, as well as an optimal combination of classification algorithms and feature selection methods that can be used in future mild depression detection.

An experiment based on a facial expression viewing task (Emo_block and Neu_block) was conducted, and EEG data of 37 university students were collected using a 128-channel HydroCel Geodesic Sensor Net (HCGSN). Emo_block is a process where brain data is recorded when subjects are presented with pictures with facial expressions such as sadness, fear, anger, and happiness, while Neu_block process presents pictures with neural face images. For discriminating mild depressive patients and normal controls, BayesNet (BN), SVM, LR, KNN, and RF classifiers were used. BestFirst (BF), GreedyStepwise (GSW), GeneticSearch (GS), LinearForwordSelection (LFS), and RankSearch (RS) based on Correlation Features Selection (CFS) were applied for linear and non-linear EEG features selection. Independent samples t-test with Bonferroni correction was used to find the significantly discriminant electrodes and features. Accuracies were 92% and 98%, and AUC achieved 0.957 and 0.997 for the Emo_block and Neu_block beta band data, respectively, using GSW based on CFS and KNN for the beta frequency band. A simplified EEG system with only FP1, FP2, F3, O2, and T3 electrodes was also explored with linear features, which yielded accuracies of 91.70% and 96.00%, AUC of 0.952 and 0.972, for Emo_block and Neu_block respectively. In the spatial distribution of features, it was found that the left parietal-temporal lobe in the beta EEG frequency band has a greater effect on mild depression detection. Also, fewer EEG channels (FP1, FP2, F3, O2, and T3) combined with linear features may be good candidates for using portable systems for mild depression detection. The BDI scores ranging from 0 to 13 and 14 to 28 corresponded to healthy and mildly depressed individuals. The total number of subjects was 20 (balanced classes). The stimuli consisted of 60 facial expression images selected from the Chinese Facial Affective Picture System

(CFAPS), which in total has 870 representative facial expression pictures of seven emotion types, including 74 anger faces, 47 disgust faces, 64 fear faces, 95 sadness faces, 120 surprise faces, 248 happiness faces, and 222 neutral facial expressions. So, the 15 negative pictures used were randomly selected from anger, disgust, fear, and sadness. 16 electrodes (Fp1, Fp2, F3, F4, F7, F8, C3, C4, T3, T4, P3, P4, T5, T6, O1, O2) were chosen in reference to Cz, according to the standard international 10/20 system. Linear features and non-linear features were extracted from the raw EEG signals. In all, there were 17 EEG features for 16 electrodes for three frequency bands (alpha, theta, beta). SVM with linear kernel outperformed SVM with RBF kernel and polynomial kernel. Statistical tests showed the linear features had a greater effect in discriminating between mild depressive and normal groups than the non-linear features. This has also been confirmed in previous studies. On statistical analysis, it was observed that Emo_block showed the left frontal lobe (FP1, F3), left temporal lobe (T3), right frontal lobe (FP2), and right occipital lobe (O2) as the prominent brain regions. For Neu_block, significant brain regions are the left frontal lobe (FP1, F3), left parietal-temporal lobe (P3, T3), right frontal lobe (FP2), right occipital lobe (O2), and right temporal lobe (T4). Li et al. (X. Li, Hu, Xu, Shen & Ratcliffe, 2015) have demonstrated that a mildly depressed group exhibited higher activation in the temporal lobe of the beta band. Koo et al. (Koo, Berger, Bartz, Wybitul & Höppner, 2015) indicated that, compared to the healthy controls, depressive patients had increased beta band power mainly in frontal, central, and centroparietal regions, often found to have symptoms like trouble falling asleep and inner restlessness in MDD patients. To have fewer electrodes to ease the process of data collection from large populations, in the next experiment, these authors chose five common electrodes from Emo_block and Neu_block – FP1, FP2, FP3, O2, and T3. Extracting linear features and using the KNN classifier, they achieved an accuracy of 91.70% and 96.00%, respectively.

Authors (Bachmann et al., 2018) compared various single-channel EEG signals

against each other for the detection of depression using linear and non-linear analysis – spectral asymmetry index, alpha power variability, and relative gamma power and nonlinear methods such as Higuchi's fractal dimension, detrended fluctuation analysis and Lempel-Ziv complexity and LR with leave-one-out cross-validation (LOOCV). Maximal testing accuracy using a single measure was 81% for linear and 77% for nonlinear measures. A combination of two linear measures provided the accuracy of 88% and two nonlinear measures of 85%. Maximal classification accuracy of 92% was indicated using a mixed combination of three linear and three nonlinear measures. The results of the preliminary study confirmed that single-channel EEG analysis, employing the combination of measures, can provide the accuracy for the discrimination of depression not lower than reported in other studies where multichannel EEG signals were analysed. The study showed that there is no single superior measure for the detection of depression. The experimental results presented above show that the features related to depression are evident in all EEG channels. Higher discrimination ability between control and depressive subjects occurs in central, temporal, and parietal regions for linear measures and in frontal, central, and temporal brain areas for nonlinear measures. Beta, gamma, and alpha power showed a discriminating ability between control and depressive subjects. The study's results demonstrated that linear EEG methods provided comparable or even better classification accuracies compared to non-linear EEG measures for the discrimination of depression.

The authors (Puthankattil & Joseph, 2012) used signal processing techniques involving relative wavelet energy (RWE) to analyse the EEG signals and an artificial feed-forward neural network to classify them for the detection of depression. The performance of the artificial neural network was evaluated using the classification accuracy, and its value of 98.11% indicates a great potential for classifying normal and depression signals. In (M. Sharma, Achuth, Deb, Puthankattil & Acharya, 2018), authors applied signal processing methods to derive features from the EEG signals and classified the

control and depressed subjects using SVM. They designed a bandwidth-duration localised (BDL) three-channel orthogonal wavelet filter bank (TCOWFB) to decompose the signals into seven wavelet sub-bands. Using ten-fold cross-validation, they achieved a classification accuracy of 99.58%.

The authors (Kaur, Bisht, Singh & Joshi, 2021) focused on noise-reducing techniques to increase the EEG classification accuracy of identifying depressed and healthy individuals. They have implemented signal processing techniques like discrete wavelet transform (DWT) and wavelet packet transform (WPT) combined with variational mode decomposition (VMD) and detrended fluctuation analysis (DFA) for signal denoising and analysing EEG signals. After artifact removal, features like Mean, Hjorth parameter, and Shannon entropy were extracted. Further, ML models like RF and SVM were used to make classification decisions and achieved an accuracy of 98.51% and 98.07%.

This study by (Shen et al., 2020) illustrated a strategy for EEG channel selection to detect depression. The authors used kernel-based methods for channel selection and particle swarm optimisation (PSO) to find an optimal EEG channel. Classification accuracy of 80%, 74.29%, 71.43% was achieved using SVM, KNN, and DT, respectively. The bilateral and left temporal regions played a significant role in depression detection.

Akbari et al. (2021) proposed a (Akbari et al., 2021) proposed strategy for depression detection by extracting 26 geometrical features (time, frequency, and time-frequency domain) from EEG signals (left and right hemisphere separately) using the second-order differential plot (SODP) method. Later, they used PSO to select the features and fed them to SVM and KNN for classification purposes. The average classification accuracy of SVM and k-NN was 97.625% and 98.315%, respectively.

Various signal processing methods were applied to the EEG signals for feature extraction, which required domain-specific knowledge and manual feature extraction steps. With the advancement of deep learning techniques, the focus has shifted to automatic feature extraction from the manual process.

2.3.2 Depression Detection using Deep Neural Networks

Jirayucharoensak, Pan-Ngum, and Israsena (Jirayucharoensak, Pan-Ngum & Israsena, 2014) introduced a deep learning approach that performed better than SVM and naive Bayes classifiers. CNN-based models have been exploited extensively in recent years for depression detection, described in detail in this section.

To the best of my knowledge, the first application was proposed by Acharya et al. for depression classification using CNN (Acharya et al., 2018). Later, hybrid CNNs (Ay et al., 2019) with long short-term memory (CNN-LSTM) developed for depression detection achieved a classification accuracy of 97.66% (EEG electrodes positioned on left hemisphere) and 99.12% (EEG electrodes position on the right hemisphere).

A CNN-based hybrid was proposed by Wan et al. (Wan et al., 2020) to study the synchronous and regional attributes of EEG signals. This architecture was evaluated to classify three categories of subjects (medicated depressive, unmedicated depressive, and healthy), achieving a classification accuracy of 79.08%. Decreased alpha power or impaired alpha oscillations were found to be one of the bio-markers for depression detection.

Advanced architecture comprising multi-kernel CNN and LSTM2D was proposed by Fan, Yu, Li, Zhu, and Li (Fan, Yu, Li, Zhu & Li, 2020). Unlike previous studies, the internal state of LSTM was modified to capture spatiotemporal features instead of temporal features alone. Also, three different convolution kernels were used for EEG signals with alpha, delta, and theta bands. This architecture attained an accuracy of 83.47% with eight-fold cross-validation.

The authors (X. Zhang et al., 2020) extracted features from EEG data using CNN and combined these features with demographic factors like gender and age via attention mechanism. The feature matrix and demographic vector were integrated through mathematical addition and provided to the $\tanh$ function. This research showed the

importance of demographic information in detecting depression.

The authors in this study (D. Li, Tang, Deng & Yang, 2021) combined CNN via a statistical trough number method for depression detection on EEG data (resting state, 14 subjects). The fusion of these methods yielded 86.66% accuracy.

The study (Seal et al., 2021) introduced a CNN-based model achieving an average accuracy and AUC of 95.385% and 0.944, respectively. This architecture consisted of five convolutional, five pooling layers, two fully connected layers, and one dense output layer. The trainable parameters summed up to 343,082. Further, analysis of the convolutional layers revealed that right electrodes played a major role in the depressed subjects, whereas it was different for the healthy subjects.

Authors (G. Sharma, Parashar & Joshi, 2021) demonstrated the success of applying deep learning techniques, i.e., hybrid integration of CNN for temporal learning and LSTM for sequential learning. This model achieved a classification accuracy of 99.01%. The model consisted of one convolutional layer, one LSTM layer, two fully connected dense layers, and one output layer with 46,658 trainable parameters.

It is clear from the literature that manual and automatic feature extraction techniques have been explored for depression detection using EEG signals. However, in most previous studies, the sequential temporal information is lost as the EEG signals are compressed for feature extraction. DL architectures using CNN and CNN-LSTM models involve extensive hyperparameter tuning. ANNs have been successful in detecting depression with high classification accuracies. They have been modeled and inspired by the principles of the human brain but only from the topology of a neural network. The neuron model implemented in ANNs is not biologically plausible; hence, the information processing differs from the one in a biological neural network. Additionally, there is an ongoing controversy regarding the learning rules in the brain, stating that they are quite different from the gradient-based backpropagation algorithms (Marblestone, Wayne & Kording, 2016; Whittington & Bogacz, 2019). In summary, ANNs suffer

from the following limitations:

1. With a small amount of data, ANNs have poor generalisation ability and low accuracy (A. Nguyen, Yosinski & Clune, 2015)

2. ANNs are less energy efficient and require a high amount of computational time when dealing with a large amount of data

2.3.3 SNNs for Spatial and Temporal Datasets

SNNs introduced in section 1.1.3 implement neuron models generating spike trains. Spike trains represent sequences of spiking signals depending on the firing of neurons. These spike trains represent the temporal component; hence, SNNs can process information having spatial and temporal associations. Also, the information transmission between the neurons is biologically plausible and only active neurons are considered in the training process. This asynchronous processing capability of SNNs makes them energy efficient, unlike ANNs, where all the neurons are involved in the information transmission process. Also, like the biological neural network, SNNs can incorporate both excitatory and inhibitory neurons. The SNN stands out as a potential approach in processing EEG signals as EEG signals represent electric activity in the brain comprising both spatial and temporal components.

The understanding, limitations, and inspirations arising from this existing research are summarised studies below:

The conversion of deep ANNs into SNNs, spiking variants of BP, biological variants of STDP, and hybrid CNN-SNN models are some of the recent methods implemented with the aim of building a deep SNN architecture. The conversion methods still suffer from poor performance due to issues related to the sparse coding of spiking neurons. Most of the approaches based on mathematical analysis are inspired by the concept of gradient descent and BP. Whether the human brain utilises the theory of backpropagation

employed in the ANN to learn something new is still an ongoing debate (Bengio, Lee, Bornschein, Mesnard & Lin, 2015; Crick et al., 1989; Grossberg, 1987; Illing et al., 2019). A lot of complexity is introduced in implementing different methods to match the performance of the SNN with the ANN. Also, most deep SNNs have been implemented on static data, i.e., images. Deploying a deep SNN model is still an open research area.

Recent breakthroughs have explored the potential of unsupervised learning for classification tasks (Illing et al., 2019). Also, STDP has successfully learned spatiotemporal structure even from small training sets and achieved better performance in classifying unseen patterns (Tavanaei & Maida, 2016; Rekabdar, Nicolescu, Nicolescu & Louis, 2017; Rekabdar, Fraser, Nicolescu & Nicolescu, 2018).

Inspired by these studies, the main focus of this research is to build an SNN architecture using unsupervised learning. The spatiotemporal information of spiking neurons has been leveraged to make classification decisions, i.e., spike times and membrane potential, to build a robust pure SNN-based architecture. Instead of applying filters from CNN to the raw EEG signals, handcrafted binary filters have been applied on the spike trains. Binary filters for use in CNN have previously been proposed and implemented in (Yang et al., 2020; Tseng et al., 2018). Using the design principles of CNN, the firing dynamics of spiking neurons have been leveraged for spike-based feature extraction to build the next layer of neurons.

This approach can deal with sequential temporal information and spatial information in EEG signals. Also, to build a deep SNN with high classification performance, the complexity of the ANN-SNN conversion would be reduced as the aim is to utilise all the available neuronal information.

2.4 Chapter Summary

This chapter has provided an overview of existing literature in two broad research areas related to this thesis: depression detection using ML and DL techniques and deep SNNs for spatiotemporal classification. The manual feature extraction process applied in ML techniques was replaced with automatic feature generation with the advent of DL architectures and powerful computing resources. However, with increased time complexity to handle spatiotemporal inputs, this chapter described the feasibility of using SNNs to classify spatiotemporal datasets. The following chapters test the hypotheses and answer the research questions presented in sections 1.5 and 1.4, respectively. Further, each of the following chapters discusses the literature review specific to the research questions and contributions under consideration in each chapter.

Chapter 3

Deep learning of EEG data in the NeuCube brain-inspired Spiking Neural Network architecture for a better understanding of depression

This chapter introduces the building blocks of brain-inspired SNN-based NeuCube architecture and its components for encoding, structural connectivity, and unsupervised and supervised learning algorithms. Later in the chapter, we explore spiking neurons and STDP's capability to distinguish between healthy and depressed groups and interpret brain activities using the NeuCube model. Further, a comparative analysis of SNN with MLP and LSTM models is performed. This is the first study where SNN is applied for depression detection.

3.1 Abstract

In recent years, machine learning and deep learning techniques have been applied to brain data to study mental health. The activation of neurons in these models is static and continuous-valued. However, a biological neuron processes the information in the form of discrete spikes based on the spike time and the firing rate. Understanding brain activities is vital to understand the mechanisms underlying mental health. Spiking Neural Networks offers a computational modelling solution to understand complex dynamic brain processes related to mental disorders, including depression. This research aims to model and visualise the brain activity of people experiencing symptoms of depression using the SNN NeuCube architecture. Resting EEG data were collected from 22 participants and further divided into groups as healthy and mild-depressed. NeuCube models have been developed along with the connections across different brain regions using the Synaptic Time Dependent Plasticity (STDP) learning rule for healthy and depressed individuals. This unsupervised learning revealed some distinguishable patterns in the models related to the frontal, central, and parietal areas of the depressed versus the control subjects that suggest potential markers for early depression prediction. Traditional machine learning techniques, including MLP and LSTM networks, have also been employed for classification and prediction tasks on the same data, but with lower accuracy and less new information gained.

This chapter addresses the following research questions:

1. How to classify brain-based sequential EEG signals using a brain-inspired computational model?

    (i) How can unsupervised learning in SNN be combined with supervised learning to classify spatiotemporal brain data?

(ii) How capable are spiking neurons in identifying unique patterns to distinguish healthy and depressed people?

These research questions are explored based on hypothesis H1: EEG data being spatial-temporal in nature if analysed considering both the aspects – spatial and temporal using SNN could be able to separate healthy and depressed individuals and provide better interpretability of brain activity.

3.2 Introduction

3.2.1 Computational Models for EEG classification

In recent years, deep learning models have been successful in achieving high accuracy in various applications like speech recognition (Hinton et al., 2012), image recognition (Krizhevsky, Sutskever & Hinton, 2012), biomedicine and bioinformatics (Mamoshina, Vieira, Putin & Zhavoronkov, 2016), (Min, Lee & Yoon, 2017), temporal data processing, etc. (Venna et al., 2018), assisting humans and challenging the other traditional machine learning models. In all the standard deep neural architectures (supervised learning), the input data in the form of vectors are passed into multiple hidden layers with numerous neurons in each layer (depending on the input data size), and activation functions are applied to produce an outcome. The actual aim is to minimize the error by hyperparameter optimisation methods. All these methods used a scalar, vector-based information representation.

In the human brain, spikes (represented by the spiking neurons – spiking neural network (SNN) models as binary units) are generated when a neuron's activation crosses a threshold value during changes in the membrane potential based on the stimulation. Here, the time of spiking, the neuron's location, the firing rate of neurons, and the temporal patterns carry information about external stimuli and the various internal

calculations. Extracting knowledge and learning patterns from them helps understand the various brain states and processes modeled using brain data. SNNs are more biologically inspired (Maass, 1997b) as compared to deep neural networks (DNNs). Spiking neurons work with spatial-temporal data using pulse coding strategies to send information to many other neurons and receive the same from others. Based on the membrane potentials, these neurons can be excitatory or inhibitory. In this research, the NeuCube SNN architecture (N. K. Kasabov, 2014) is employed on depression case study data for extracting knowledge from the EEG signals to understand the brain processes in healthy and depressed individuals. By 2030, the World Health Organization reported that around 322 million people worldwide would be affected by depression, leading to other physiological issues in the near future (K. Smith, 2014). Depression is a major contributor to the overall global burden of disease, wherein it is more prevalent in females than males. Depression affects a person's physical and mental well-being in various aspects, such as lack of memory power, heart attacks, suicidal thoughts, lack of motivation and interest, high fatigue, erratic sleep patterns, etc. It is very important to identify and treat depression before depression is manifested for a better treatment outcome. There are many techniques to detect depression, like laboratory methods, non-laboratory methods, genomics, etc. (K. M. Smith, Renshaw & Bilello, 2013). One of them is using EEG data recordings. After capturing EEG data, processes like Pearson correlation coefficient (PCC), phase locking value (PLV) and phase lag index (Moon, Jang & Lee, 2018), detrended fluctuation analysis and power spectral analysis (Abásolo, Hornero, Escudero & Espino, 2008), (Hinrikus et al., 2009), etc. can be applied to the EEG data for identifying the detectors of the underlying brain condition. Deep learning architectures (Yıldırım et al., 2018), (Bairy et al., 2017), (Acharya et al., 2018), (Martinez-Murcia, Górriz, Ramírez & Ortiz, 2018), (Yildirim et al., 2018), (Antoniades et al., 2018), (Książek et al., 2019) have been recently applied in addition to the classical machine learning models (Abdar et al., 2020), (Abdar, 2015), (Bairy et

al., 2017), (Bachmann et al., 2018), (Puthankattil & Joseph, 2012). Some researchers first acquire features from the raw data and then feed them into machine learning (ML) and artificial neural networks (ANN) for classifying the depressed individuals from the healthy ones using various algorithms, such as logistic regression (Puthankattil & Joseph, 2012); artificial feedforward network (Hosseinifard et al., 2013); support vector machine (SVM) (Acharya et al., 2015). CNNs have been used extensively for classifying raw EEG signals (Schirrmeister et al., 2017). In (Jirayucharoensak et al., 2014), the authors implemented a deep learning approach varying the number of hidden units (100 and 50), outperforming SVM and naïve Bayes classifiers. In (Oh, Ng, San Tan & Acharya, 2018) and (Yildirim, 2018), the authors used a hybrid model of CNN and LSTM for categorizing EEG signals. In recent studies of depression detection, Acharya and team (Acharya et al., 2018) developed a 13-layer CNN achieving an accuracy of 93.54 % and 95.96 % from EEG signals of the left and right hemisphere, respectively. To overcome the drawback of CNN (poor sequential learning) in (Ay et al., 2019), authors employed a hybrid CNN-LSTM model for depression detection, reaching classification accuracy of 97.66 % (L.H.) and 99.12 % (R.H.). Despite the high accuracy of classification results of EEG data, none of the papers reviewed above reported the actual brain patterns that can be used to distinguish the groups. There are gaps related to the application of brain features underlying depression detection into ML. Brain-inspired SNN has been used in various applications like forecasting (Mohanty, Priyadarshini, Desai & Sirisha, 2018), modelling the effect of mindfulness on depressed individuals (Z. Doborjeh et al., 2019), real-world data classification, image recognition, odour recognition, motor control, and trajectory tracking, etc. SNN aid in providing unique brain patterns and also models brain functions and brain connectivity computationally. An SNN NeuCube model (M. G. Doborjeh, Wang, Kasabov, Kydd & Russell, 2015) reached 90.91 % accuracy, whereas traditional methods achieved just 50.55 % accuracy in classifying opiate addicts from the healthy controls. This results from a deeper modeling insight

into neural circuitry, information processing, and plasticity in the brain areas to build a relation between the depressive symptoms at the neural level and the resulting mental disorders of a subject. Following the successful usage of the NeuCube SNN architecture for EEG data modelling and understanding, here we apply this architecture to EEG data related to depressed and controlled individuals in an attempt to understand better and predict depression.

3.3 Methods

3.3.1 Dataset Description

Ethics: Auckland University of Technology (AUT) Ethics Committee (AUTEC), New Zealand granted ethics approval (15/45).

The EEG data were collected under strict monitoring with 2 min eyes opening and 2-minute eyes closing states. Recordings were carried out using a SynAmps amplifier and 61-channels (FP1, FPZ, FP2, AF3, AF4, F7, F5, F3, F1, FZ, F2, F4, F6, F8, FT7, FC5, FC3, FC1, FCZ, FC2, FC4, FC6, FT8, T7, C5, C3, C1, CZ, C2, C4, C6, T8, TP7, CP5, CP3, CP1, CPZ, CP2, CP4, CP6, TP8, P7, P5, P3, P1, PZ, P2, P4, P6, P8, PO7, PO3, POZ, PO4, PO8, O1, OZ, O2, PO1, PO2, OI1) with electrode placements based on standard 10–20 international system. The data were recorded at a sampling rate of 1000 Hz. After EEG recording, a 2 seconds epoch was extracted. Off-line ICA computerised artifact correction was used to remove detectable eye movement or muscle potentials. The dataset consists of participants with BDI scores ranging from 0 to 30. Participants having BDI scores 0-10 are considered healthy subjects (12), and those having BDI scores> 10 are considered mild-depressed subjects (10) for this experiment. After data pre-processing techniques, each data sample (subject) consists of 16,383 time points (number of rows).

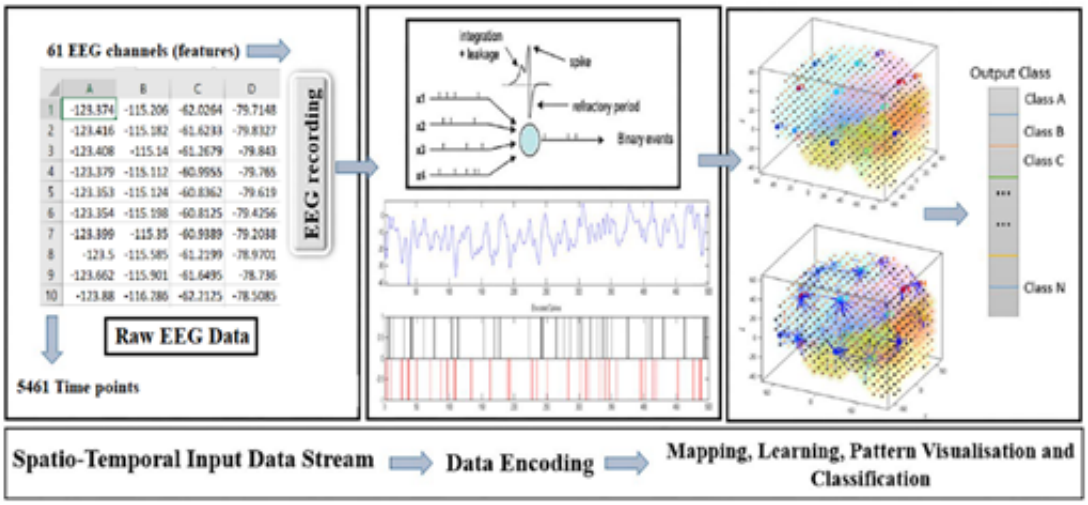

Figure 3.1: *NeuCube Computational Model (N. K. Kasabov, 2014)*

3.3.2 Proposed NeuCube Model for classifying and analyzing the brain regions using EEG data of healthy and depressed individuals

The NeuCube is a unified computational model based on spiking neural networks to model, analyse, learn, and visualise spatiotemporal data. This model was designed by Professor Nikola Kasabov in 2014. As shown in Figure 3.1, it consists of various algorithms for encoding input data into spike trains, for unsupervised and supervised learning, and optimisation (N. K. Kasabov, 2014). Since this research is built upon the principles of NeuCube, a brief overview of this methodology is provided below.

The following procedures are applied in the modelling part:

Data Encoding

SNNs process binary temporal events, i.e., they have the capability to learn from the spatiotemporal data represented in the form of spike trains. The input spatiotemporal data generally comprises continuous real values. Hence, it is important to convert them into sequences of spike trains. NeuCube consists of a range of encoding algorithms such as

Ben's Spiker Algorithm, Threshold-based Representation (TBR) or Temporal Contrast Algorithm, Step-Forward (SF) Spike Encoding Algorithm, and Moving-Window Spike Encoding Algorithm (MV) (Chan, Liu & van Schaik, 2007; Petro, Kasabov & Kiss, 2019; N. K. Kasabov, 2014). For our first experiment, we selected TBR as the encoding algorithm because of its simplicity. Also, it is capable of capturing the changes in the data based on the threshold value. We have optimised the threshold parameter using the Grid search algorithm.

From a high-level view, spikes are generated based on the threshold from the EEG spatiotemporal data (continuous real values) using the Threshold-based Representation algorithm described below. If the signal changes above the spike threshold, then a positive spike is generated; if the signal changes below the threshold value, a negative spike is generated, or else no spikes are generated.

Threshold-based Representation encoding algorithm encodes a signal into a spike train given a threshold value. The absolute difference between the consecutive signal values is calculated. The mean and standard deviation of the differences are calculated. A threshold is computed using these two measures. Now, the difference and the threshold are compared. If the difference is greater than the threshold, a positive spike (1) is emitted; else if the difference is smaller than the threshold, then a negative spike (-1) is emitted, and no difference is represented as 0.

The encoding process is explained below using the following steps:

Algorithm 1 TBR Encoding Algorithm

1: **procedure** TBR ENCODING ALGORITHM($ssignal, ffactor$)
2: startpoint = s(1)
3: diff = zeros(length(s))
4: **for** t = 1: (length(s)-1) **do**
5: diff(t) = s(t+1) - s(t)

Calculates the derivative of the signal, i.e., the differences between each

consecutive pair of temporal points.

6: **end for**

7: threshold = mean(diff) + f * std(diff)

Calculates the mean of the differences.Calculates the standard deviation of the differences. Calculates the real threshold value.

8: out = zeros(length(s))

9: **for** t = 1: (length(s)-1) **do**

10: **if** diff(t) > threshold

11: out(t) = 1

12: **elseif** diff(t) < -threshold

13: out(t) = -1

14: **end for**

15: **end procedure**

To select the optimal threshold, the reconstruction error i.e. the root mean square error between the spike trains and original signals, should be minimum. The TBR decoding algorithm to generate the original signal values from the spike trains is described below:

Algorithm 2 TBR Decoding Algorithm

1: **procedure** TBR DECODING ALGORITHM($spikes, threshold, startpoint$)

2: recon = zeros(length (spikes))

3: recon(1) = startpoint

4: **for** t = 2: (length(s)-1) **do**

5: **if** spikes(t) == 1:

6: recon(t) = recon(t-1) + threshold

7: **elseif** spikes(t) == -1:

8: recon(t) = recon(t-1) - threshold

9: **else**:

recon(t) = recon(t-1)

end for

end procedure

3D SNN Reservoir (SNNr) Module

The connectivity between the neurons in the SNN network is inspired by the connections between the different brain areas. The SNNr is a 3D structure consisting of clusters of neurons that are organised using the standard brain atlas coordinate system such as the Talairach Atlas (Dervin, 1990). Hence, SNNr can provide an approximate map of spatially located brain regions through the Talairach brain template. After this, the input EEG channels are mapped to the SNNr module using the mapping rules mentioned in Appendix (Koessler et al., 2009) This physical organisation of neurons and mapping of EEG channels into the network of neurons make NeuCube effective in interpreting the patterns developed between the neurons during the learning phase.

The connectivity in the SNN reservoir, the spiking neuron model, and the unsupervised learning algorithm governing the synaptic changes are explained below.

Small World Connectivity Algorithm

The initial structural connections between the neurons in the network and the initial weights to the synapses (neuronal connections) play an important role during the learning phase in NN architecture. Small-world connectivity model developed by Watts and Strogatz (Watts & Strogatz, 1998) is inspired by the structural connections among the neurons in the human brain.

Important small-world properties are described below. A network is said to have small property if it has a high clustering coefficient and a small characteristic path length. Hence, a graph $G = (V, E)$ with small-world property is termed as a small-world graph or small-world network (Mehlhorn & Schreiber, 2013). A high clustering coefficient

denotes that almost all nodes in the subnetwork (cluster) are connected to each other. This means that the network comprises dense local connections (high local connectivity). The average number of edges in the shortest paths between all the network node pairs is termed characteristic path length. So, a small characteristic path length makes it possible to reach all nodes in the network efficiently (global reachability). The human brain is believed to exhibit these properties and show small-world organisation (Bullmore & Sporns, 2009).

Based on the principle of small-world model, in the SNNr model, the probability of connecting two neurons in this graph is proportional to the distance between these neurons. The closer the brain regions, the higher the probability of connections between the neurons located in these brain areas. After establishing the connection matrix, the neuronal connections are instantiated with initial weights following a random uniform distribution between (0,1).

Spiking Neuron Models

The SNNr module consists of 1471 spiking neurons having coordinates mapped from the Talairach template. In this thesis, the current implementation of SNNr is comprised of LIF-spiking neurons with recurrent connections. The inner working principle of LIF neurons has been explained in Section 1.1.4. This network of LIF neurons is stimulated with the input data producing sequences of spike trains.

Unsupervised Learning in the NeuCube SNNr module

Once the structural connections between the input and the SNNr, and among the neurons in the SNNr are established, the initial synaptic weights are set up; the LIF neurons are configured, then these synaptic weights are modified to learn the input representations using a learning rule.

The STDP (Song et al., 2000) learning method, as explained in Section 1.1.5, is used for adapting the neuronal connections i.e., synaptic weights. SNNr employs STDP to learn spike sequences from the input data. During the learning phase, the SNNr accumulates temporal information from these spike sequences and produces responses for different classes of inputs. Thus, unique patterns are generated in the SNNr reservoir over time, representing spatiotemporal interactions between the input variables that can be classified further.

Evolving Output Classification Module

The NeuCube architecture implements the Dynamic Evolving Spiking Neural Network method (deSNN) (N. Kasabov, Dhoble, Nuntalid & Indiveri, 2013) as one of its classification modules. DeSNN learns from the association of the input samples and their labels during the training phase and trains the output neurons to classify spatiotemporal data. Once the SNNr is trained using the unsupervised STDP learning rule, the input data is propagated to the output layer. The output neurons then learn the behaviour of the input using the deSNN algorithm along with unsupervised learning and assign it to an output class neuron. All the neurons in the SNNr are connected to the output neurons.

The deSNN supervised learning algorithm in NeuCube and unsupervised learning are described below in more detail.

DeSNN supervised learning algorithm

The deSNN algorithm (N. Kasabov et al., 2013) uses the rank-order (RO) (S. Thorpe & Gautrais, 1998) learning and Spike Driven Synaptic Plasticity (SDSP) learning rule (Fusi, Annunziato, Badoni, Salamon & Amit, 2000) for training the output neurons to recognise the Spatio-temporal pattern. In the RO coding principle, importance is given to the spikes arriving early on the synapses from the input neurons. The firing of LIF

depends on the strength of the input, and thus, LIF neurons are capable of capturing the input patterns. The spikes from the input LIF neurons from the SNNr to the synapses connected to the output neuron are given a rank, and initial weights are set up according to the RO rule. The output that received the first spike becomes the winning neuron and is assigned a class label of the input sample. Later, these initial weights are modified using SDSP (or STDP) learning. According to the SDSP learning rule, the weight of a synapse is increased at the arrival of a spike else; it is decreased. The mathematical equations based on principles are explained below in the training phase.

In the deSNN training phase, for each M-dimensional training input pattern $\mathrm{P_i}$, a new output neuron i is created and connected to each neuron in the trained SNNr module. The synaptic weights $\mathrm{w_{ij}(j = 1, 2, ..., M)}$ between the input neuron j in the reservoir and the newly created output neuron i are calculated based on the order of the incoming spikes on the corresponding synapses using the RO learning rule:

$$w_{ji} = \alpha.mod^{(order(j,i))} \tag{3.1}$$

where α is a learning parameter that ranges between 0 and 1, the mod a modulation factor which indicates the importance of the order of the first spike that lies between 0 and 1, $\mathrm{w_{j,i}}$ is the synaptic weight between a pre-synaptic neuron j and the postsynaptic neuron i and $\mathrm{order(j, i)}$ the order of the first spike arriving through synapse ji among all spikes arriving from all other synapses to the neuron i. For the first spike to neuron i, the $\mathrm{order(j, i)}$ is 0 and increases according to the input spike order at other synapses.

After initializing the synaptic weight $\mathrm{w_{j,i}}$ according to the first spike at the synapse j, this synaptic weight is adjusted using the SDSP (or STDP) learning rule. According to the SDSP rule, if there is a spike at synapse j at time t, the synaptic weight $\mathrm{w_{j,i}}$ increases with a small positive value called the positive drift parameter. On the other hand, if there is no spike at synapse j at time t the synaptic weight $\mathrm{w_{j,i}}$ creases with a small

negative value called the negative drift parameter.

$$\triangle w_{j,i} = e_j(t).D \tag{3.2}$$

In Eq.3.2 while presenting the learnt input pattern $\mathrm{P_i}$ to the output neuron i if at time t there is a successive spike at synapse j, $\mathrm{e_j(t)} = 1$ and if at time t there is no spike at synapse j, $\mathrm{e_j(t)} = -1$. Under the influence of synaptic dynamism denoted by $\mathrm{e_j(t)}$ parameter, the parameter D can have positive or negative values for up and down synaptic drifts. This behaviour helps the output neurons capture the temporal relationship of spike timing across the learned pattern $\mathrm{P_i}$ at time t.

While presenting the input training pattern to the output neurons, a spiking threshold $\mathrm{Th_i}$ is assigned to the output neuron $\mathrm{Th_i}$. The firing threshold $\mathrm{Th_i}$ is calculated as a fraction (C) of the total (called $\mathrm{PSP_{imax}}$) of neuron i accumulated during the presentation of the input pattern in a time-window T. During the recall phase, this firing threshold makes the output neuron release a spike in the presence of patterns similar to the learned ones during training.

$$PSP_{imax} = \sum_{t=0}^{T} \sum_{j=1}^{M} f_j(t).w_{j,i}(t) \tag{3.3}$$

$$Th_i = C.PSP_{imax} \tag{3.4}$$

In Eq. 3.3, T represents the time units in which the input pattern is presented to the output neuron, M is the number of the input synapses to the neuron i, $\mathrm{f_j(t)}$ shows the firing dynamics of synapse j at time t (i.e. $\mathrm{f_j(t)} = 1$ if there is a spike at synapse jfor this learnt input pattern at time t and $\mathrm{f_j(t)} = 0$ if otherwise), and $\mathrm{w_{ji}(t)}$ the efficacy of the synapse ji calculated at time t using of Eq. 3.2. The parameter C that is used for calculating the threshold $\mathrm{Th_i}$ (Eq. 3.4) enables neuron i to emit a spike (recognise the

input pattern) before the whole learned pattern is presented.

During the recall phase, for each input pattern, a new output neuron is created in the way that is created in the training phase, then the synaptic weight vector of the newly created output neuron is compared to the existing output neurons using Euclidean distance. The closest output neuron in terms of synaptic connection weights to the new neuron is the 'winner' output class. Inspired by transductive reasoning principles, this method uses nearest neighbour classification in the synaptic weight space to capture or match a new pattern to an existing one. The pseudo-code described below is adapted from (N. Kasabov et al., 2013).

Algorithm 3 deSNN Algorithm

procedure DESNN ALGORITHM
    Initialise deSNN parameters: $\mathrm{mod}, \mathrm{D}, \mathrm{C}, \alpha, \mathrm{sim}(\mathrm{similaritythreshold})$
    for each input pattern $\mathrm{P_i}$ **do**
        create a new output neuron i
        initialise synaptic weights $\mathrm{w_i}(0)$ using RO learning rule denoted in Eq. 3.1
        modify the synaptic weights $\mathrm{w_i}$ for successive spikes on the corresponding synapses using SDSP rule denoted in 3.2
        calculate $\mathrm{PSP_{imax}}$ using Eq. 3.3
        calculate the firing threshold $\mathrm{Th_i}$ of each neuron i using 3.4.
        if the new weight vector $\mathrm{w_i}$ is similar to an existing output neuron using Euclidean distance similarity measure and sim threshold
            merge the two neurons by averaging their threshold and synaptic weights
        else:
            add new output neuron to the network
            end if
    end for

15: **end procedure**

This implementation uses deSNN and STDP unsupervised learning in the output classification module.

Visualisation of learned patterns

The visualisation module shows distinct patterns formed between the neurons in the SNNr during the learning phase. The patterns represent the associations between neuronal connections developed due to the adaption of weights using STDP learning.

3.3.3 Recurrent Neural Networks for Depression Detection

In traditional ML (first-generation) methods and also in MLP, we provide data and labels, define a model architecture, and the model learns the rules that fit the data to the labels. The model generates rules which are then utilised for future data prediction. However, there are no efforts to understand the sequence in which data occurs (LeCun et al., 2015). The human brain learns from previous contexts and applies them to understand future events. For example, imagine if we want to classify what kind of event is happening at every point in a movie. It is unambiguous how a traditional neural network like MLP could use its reasoning about past events in the movie to characterise later ones. Recurrent Neural Networks (RNN) are designed to address this issue.

In RNNs, the information persists as they incorporate the concept of recurrence, i.e., these networks have loops in them, as shown in Figure 3.2. From a high-level overview, an input value is labeled as x_t, which is fed at a time step t into a function F and produces an output value y_t at that time step. The arrow from F indicates a value that is fed forward to the next step. In Figure 3.2, A function F is applied to an input x_0 to produce y_0 at time step t_0 and a value that's passed forward. At the next step receives that value and x_1 and produces y_1 and a value that's passed forward and so on down the line. In other words, the loop allows the information to be passed from one

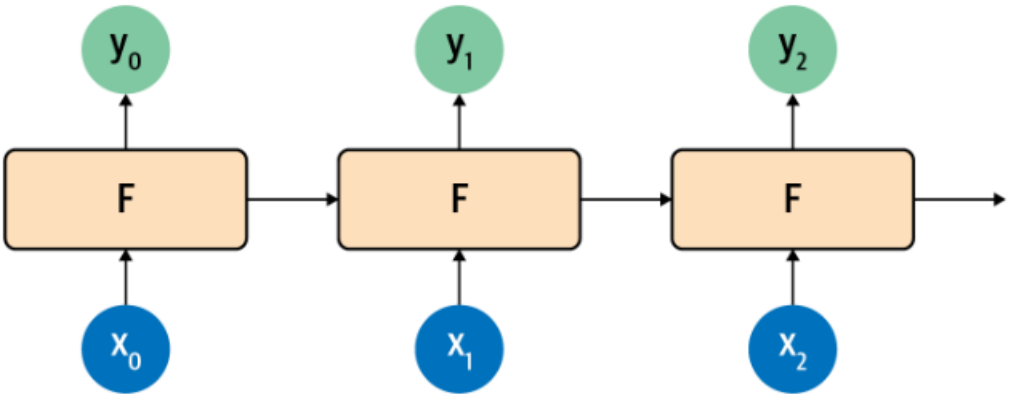

Figure 3.2: *Recurrent neurons in time from (Moroney, 2020)*

step to the next step of the network. This is how RNNs maintain the contexts across a sequence over several time steps. However, the effect of the output of the first neuron is huge at step 2, small at step 3, and smaller at step 4, and it gets diminished further over time. Thus, there was a need to remember these contexts over a longer distance, as in the human brain. To address the issue of short-term memory in RNNs, LSTM (long short-term memory) networks were developed (Hochreiter & Schmidhuber, 1997). The LSTM architecture includes a cell state that enables context to persist across the entire long sequences of steps. The important information in the context is learned and maintained over extended time intervals.

Long Short-Term Memory Networks

LSTMs were designed to overcome the problem of short-term memory in RNNs. They remember information for long periods due to adding a "cell state" module in their architecture. LSTMS have a chain-like structure where four neural networks within a single block interact with each other in a unique way, as shown in Figure 3.3. Each of these neural networks consists of input and output layers. In each of these neural networks, input neurons are connected to all output neurons. As a result, the LSTM unit

has four fully connected layers.

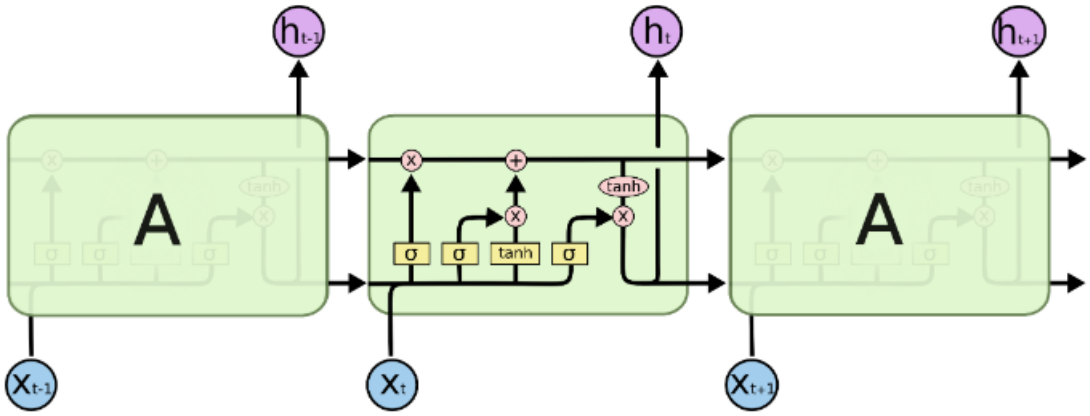

Figure 3.3: *LSTM module with its four interacting layers from (Olah, 2015)*

In this figure, the yellow block represents neural nets with $sigmoid$ and $tanh$ activation functions; the pink circles represent pointwise operations, merging lines denote concatenation and branching lines show that the content is being copied and the copies stay at different locations. The top horizontal line is the cell state. LSTM adds or removes information to the cell, carefully controlled by four feedforward networks called gates, as depicted in Figure 3.4.

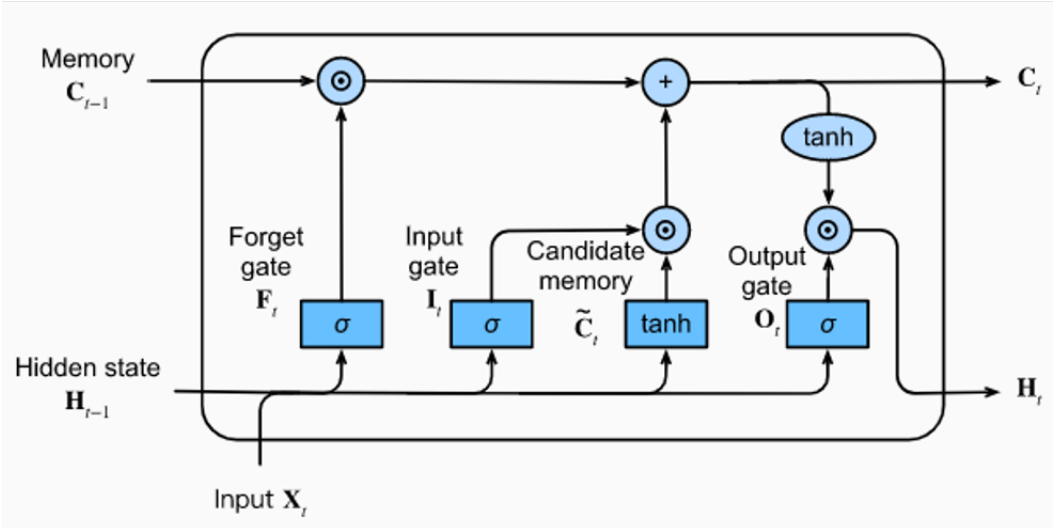

Figure 3.4: *Architecture of a LSTM unit from (A. Zhang et al., 2021)*

Three of the four feedforward networks are responsible for selecting the information,

i.e., composed of a sigmoid neural net layer; and a pointwise multiplication operation; they perform memory management tasks: the deletion of information from memory (the forget gate), the insertion of new information in memory (the input gate), and the use of information present in memory (the output gate). The fourth neural network, the candidate memory, is used to create new candidate information to be inserted into the memory. The cell and hidden states are represented as C and H, respectively. LSTM uses the recent past information, i.e., the short-term memory (H), the new information, i.e., the current input (X), and then updates the long-term memory, i.e., the cell state (C). Finally, the short-term memory (H) is updated using the long-term memory (C). Let us now describe the computation of each gate.

The forget gate decides the amount of information to be discarded from the previous state. At any time, t, it takes information from the previous state, H_{t-1}, the current input X_t, producing a value between 0 and 1 (using the sigmoid activation function) for each number in the cell state, C_{t-1}. A 1 means "completely keep this," while 0 means "completely discard this." Forget gate is computed using Equation 3.5:

$$F_t = \sigma(X_t W_{xf} + H_{t-1} W_{hf} + B_f) \tag{3.5}$$

The next step is to decide what new information will be stored in the cell state. This step is performed by two neural networks: the input gate (X_t) and the candidate memory ($\tilde{C}_t$). The input gate layer, called the sigmoid layer, decides which values are to be updated as shown in Equation 3.6, and the candidate memory, called the tanh layer, creates a new vector that is added to the cell vector as shown in Equation 3.7. This ensures that all the values are within the range (-1,1).

$$I_t = \sigma(X_t W_{xi} + H_{t-1} W_{hi} + B_i) \tag{3.6}$$

$$\tilde{C}_t = \tanh(X_t W_{xc} + H_{t-1} W_{hc} + B_f) \tag{3.7}$$

Now, we have to update the previous cell state to a new state, C_t, as shown in Equation 3.8. During the element-wise multiplication of the forget gate (sigmoid layer) and the previous cell state, C_{t-1}, it is decided which parts of the cell state are eliminated (multiplication with 0 gives 0). Then, the new candidate values are added ($I_t \odot \tilde{C}_t$) which scales up each cell state value.

$$C_t = F_t \odot C_{t-1} + I_t \odot \tilde{C}_t \tag{3.8}$$

Finally, we decide what we are going to output. First, we run a sigmoid layer which decides what parts of the cell state we're going to output, as shown in Equation 3.9. Later, the cell state is pushed through the $\tanh$ layer ($\tilde{C}_t$) and multiplied by the output of the sigmoid gate (I_t) so that it output only the required parts as shown in Equation 3.10.

$$O_t = \sigma(X_t W_{xo} + H_{t-1} W_{ho} + B_o) \tag{3.9}$$

$$H_t = O_t * \tanh(C_t) \tag{3.10}$$

The variables used in the above equations are described as follows:

$X_t \in \mathbb{R}^d$	= input vector to the LSTM unit
$F_t \in (0,1)^h$	= forget gate's activation vector
$I_t \in (0,1)^h$	= input/update gate's activation vector
$O_t \in (0,1)^h$	= output gate's activation vector
$H_t \in (-1,1)^h$	= hidden state vector also known as output vector of the LSTM unit
$O_t \in (0,1)^h$	= output gate's activation vector
$\tilde{C_t} \in (-1,1)^h$	= cell input activation vector
$C_t \in \mathbb{R}^h$	= cell state vector
$W_{xf}, W_{xi}, W_{xc}, W_{xo} \in \mathbb{R}^{h*d}$	= weight matrices
$W_{hf}, W_{hi}, W_{hc}, W_{ho} \in \mathbb{R}^{h*h}$	= weight matrices
$B_t \in \mathbb{R}^h$	= bias vector parameters

The initial values are $C_0 = 0$ and $H_0 = 0$, and the operator $\odot$ denotes the element-wise product. The subscript t denotes the time step. The superscripts d and h refer to the number of input features and hidden units. The weight and bias vectors must be learned during training using an optimisation algorithm like gradient descent combined with Backpropagation Through Time (BPTT).

The output Y of a neural network depends on the flow of information that passes through multiple LSTM units placed in a chain. A small increase in the output of any of these units affects the output (decrease or increase) value of all the subsequent units until the output layer. The error minimisation is done by calculating the ratio between the increase in the output value of a particular unit and the increase in the network error. In LSTM, the flow of information does not occur only through elements of the neural network. It also happens over time. The error committed by the network at the time t also depends on the information received from previous times and processed in these instants of time. In any RRN, therefore, backpropagation also considers the chain of

dependencies between instants of time. For this reason, it is called BPTT.

3.4 Experiments and Results

The NeuCube architecture utilised for depression detection in the first phase of this research study is structured in a two-step analysis as follows:

1. NeuCube SNN model learning and visualization of the EEG data to investigate brain connectivity of depressed and healthy individuals for both the Eyes Closed and the Eyes Opened states.

2. Using MLP and LSTM techniques for comparative analysis.

3.4.1 Experiment Design

The original dataset consists of 16,383 rows (temporal features) with 61 columns (spatial features) for each participant (10 depressed, 12 healthy). But for experimentation purposes, we formulated the dataset to suit our requirements according to the architecture:

1. NeuCube: Each participant is a 'sample' with a spatiotemporal dataset ('.csv'). Each sample is a matrix consisting of 16,383 rows and 61 columns. In machine and deep learning, the model learns to build relationships between the inputs and the output. This means that should be enough data to capture these relationships between the input features and the output. DL architectures require massive amounts of training samples for classification tasks (Alzubaidi et al., 2021). For depression detection using MLP and LSTM, it was necessary to have more training samples and hence each subject was divided into three subsets of data (randomly chosen). Thus, we constructed three subsets of samples from each

sample, i.e., generating 66 samples altogether (30 depressed, 36 healthy) from 22 samples. In this dataset, each sample has 5,461 time points (rows), and the number of columns is 61. At this point, care is taken that if the subject belongs to the training set, its subsets are also placed in it. Hence, there was no overlap between the train and test samples.

2. MLP and machine learning algorithms: MLP cannot process temporal inputs. Hence, while using MLP, we performed temporal averaging on each sample (5,461 rows) to obtain one input representation (row) for each participant, keeping the columns consistent (61).

3. LSTM and NeuCube: We compared the NeuCube-based SNN architecture with LSTM architecture on the EC state of EEG signals in this experimental setting. This comparison is conducted in two categories: the first experiment considers EEG inputs with 5,461 time points (66 samples), and the second one takes EEG signals with 16,383 time points (22 samples) as inputs.

3.4.2 Results

NeuCube, being a stochastic model, classification accuracy depends on the parameters' settings (Petro et al., 2019; Goulden et al., 2012) as described below:

1. Spike threshold was set to 0.5 for converting the input data to sequences of spikes. The spike rate depends on this threshold value.

2. The threshold of firing, the refractory time, and the potential leak rate were set to 0.5, 6ms, and 0.002, respectively, after optimisation.

3. The STPD learning rate parameter was set to 0.01, which causes changes in the connection weights (increase or decrease) of two connected neurons depending on the firing order.

4. For unsupervised learning, the training iteration was set to one which is considered optimal for incremental, online adaptive learning.

5. For supervised learning, the parameters 'mod' and 'drift' of the deSNN classifier were set to 0.4 and 0.25, respectively. Also, we set k=3 in the K-NN classifier for mapping the input data to the labeled outcome in the training procedure.

Comparative Analysis - SNN and MLP

For a comparative analysis, we implemented a 2-layer MLP network after using grid search optimization with 100 - neurons in each layer. 'Relu' was used as an activation function for hidden layers, 'softmax' was used for output layer activation, 'adam' was used for weight optimization, the learning rate was set to 0.001, and alpha was set to 0.001 (L2 regularization parameter).

After applying five fold cross-validating technique (Schaffer, 1993) during the optimisation process, the accuracy of the NeuCube model for classifying depressed versus healthy subjects EEG data was 68.18% (eyes closed (EC) state) and 72.13% (eyes open (EO) state). The MLP NN models for both eyes opened and eyes closed EEG data achieved slightly higher than 50% accuracy, which was inferior to the NeuCube model classification.

The reason for reporting only the MLP results and parameters is that all other traditional machine learning algorithms, such as SVM, decision tree, and logistic regression, obtained worse results than MLP. The NeuCube models obtained much higher classification accuracy and have been used here to reveal brain activity patterns related to each of the two subjects, facilitating a better interpretation and understanding of the depression phenomenon, as explained in the following section.

Comparative Analysis - SNN and LSTM

A comparison between LSTM and NeuCube-based SNN models with 66 and 22 samples for depression detection is described in this section. Keras Tuner, a TensorFlow library (O'Malley et al., 2019), is used for hyper tuning the LSTM network. Adam as the optimiser (Kingma & Ba, 2014) and the "SparseCategoricalCrossentropy" as the loss function (Pang, Nijkamp & Wu, 2020) are used for training these LSTM models. Hyperparameters include the number of LSTM units, the number of neurons in each LSTM unit and the denser layer, the dropout percentage, and the learning rate of the Adam optimiser. Tables 3.1 and 3.3 represent the search space of hyper-parameters to optimize and the values they can take for 66 and 22 samples, respectively. The number of epochs is set to 100, and early stopping is used to interrupt training if there is no performance gained after 30 epochs. The Hyperband technique (L. Li, Jamieson, DeSalvo, Rostamizadeh & Talwalkar, 2017) within the TensorFlow implementation of the Keras tuner is used as the search algorithm. The validation split is set to 20% of the train samples.

Table 3.1: Search space for tuning LSTM with 66 samples

Layer	**Min**	**Max**
Input layer	32	512
Number of LSTM units	1	4
Neurons in LSTM units	32	312
Dropout	0	0.5
Dense	10	100
Learning Rate	[0.01, 0.001, or 0.0001]	

The hyperparameter search for 66 samples is as follows 3.1: the optimal learning rate for the optimizer is 0.01, the number of LSTM layers is five, the dropout rate (no node activation and weight updates) is 0.2, the LSTM input layer has 288 neurons, LSTM layer one has 160 hidden units; LSTM layer two has 160 hidden units; LSTM layer three has 224 hidden units; LSTM layer four has 128 layer hidden units; and

LSTM layer five have 96 hidden units. The optimal number of neurons in the densely-connected layer is 69. The output layer consists of two neurons since this is a binary classification problem. "5460" represents the number of time points.

Table 3.2: Model Summary with 66 samples

Layer	**Output Shape**	**Number of Parameters**
Input layer	(None, 5460, 288)	403200
LSTM unit 1	(None, 5460, 160)	287360
LSTM unit 2	(None, 5460, 160)	205440
LSTM unit 3	(None, 5460, 224)	344960
LSTM unit 4	(None, 5460, 128)	180736
LSTM unit 5	(None, 96)	86400
Dropout	(None, 96)	0
Flatten	(None, 96)	0
Dense	(None, 69)	6693
Output Layer	(None, 2)	140
		Total params: 1,514,929
		Trainable params: 1,514,929

Table 3.3: Search space for tuning LSTM with 22 samples

Layer	**Min**	**Max**
Input layer	100	850
Number of LSTM units	1	4
Neurons in LSTM units	32	512
Dropout	0	0.5
Dense	10	200
Learning Rate	[0.01, 0.001, or 0.0001]	

The hyperparameter search for 22 samples is as follows - the optimal learning rate for the optimizer is 0.0001, the number of LSTM units is two; the LSTM input layer has 400 neurons; Layer 1 has 416 hidden units; and Layer 2 LSTM has 192. The optimal number of units in the densely connected layer is 101. The dropout rate is 0.1.

The number of training parameters in LSTM is calculated as $4 * ((x + h) * h + h)$. x represents the number of features (columns) in the previous layer, h represents the number of hidden units in the LSTM layer, and since each LSTM block has four gates,

the output is multiplied by four. For example, Table 3.2 has $403,200$ parameters as the output from the input layer. This is achieved by computing $4 * ((61 + 288) * 288 + 288)$. Here, the previous layer is the input data which has 61 features. The number of trainable parameters for the next layer is $4 * ((288 + 160) * 160 + 160)$, where the number of features in the previous layer is 288, and the number of hidden units in the current layer is 160. This is how the number of training parameters is calculated in the LSTM TensorFlow implementation.

Table 3.4: Model Summary with 22 samples

Layer	**Output Shape**	**Number of Parameters**
Input layer	(None, 5460, 400)	739200
LSTM unit 1	(None, 5460, 416)	1359488
LSTM unit 2	(None, 5460, 192)	467712
Dropout	(None, 192)	0
Flatten	(None, 192)	0
Dense	(None, 101)	6693
Output Layer	(None, 2)	19493
		Total params: 2,586,097
		Trainable params: 2,586,097

Table 3.5: Classification Accuracy of LSTM and SNN with 66 samples

Classifier	**66 samples**	**20 samples**
LSTM	53.33%	50%
SNN	68.18%	54.36%

The LSTM models were built using hyperparameters for better model performance. The comparative analysis between the SNN and the LSTM modes is shown in Table 3.5. As shown in this table in Table 3.5, the NeuCube SNN framework achieved a classification accuracy of 68.18% and 54.36% with 66 and 22 samples, respectively. LSTM produced a classification accuracy of 53.33% and 50% with 66 and 22 samples, respectively. The difference between the performance of SNN(54.36%) and LSTM(50%) on 20 samples shows that both architectures performed poorly on the provided data. However, with 66 samples, the performance of SNN (68.18%) is better than LSTM

(54.36%), which shows that SNNs are capable of better learning with a lower number of samples than LSTM in this case.

In summary, through these experiments, we can conclude that the LSTM networks can process temporal data, but they couldn't perform well with fewer training samples when compared to SNN. This demonstrates the advantage of using the SNN approach of time-space brain data modeling for spatiotemporal data classification.

Visualisation - Pattern discovery of dynamic brain activities of depressed versus healthy individuals

This section discusses the functional connectivity inside the brain by analyzing the learned NeuCube models using visualization of the feature interaction network (FIN) (N. K. Kasabov, 2014; N. Kasabov, 2018) graphs and the SNN connectivity graphs.

This section explains the similarities and differences in the eyes closed state by looking at FIN and SNNr connectivity models, as presented in Figure (3.5) and Figure (3.6) across 61 EEG channels (features).

1. Eyes Closed State In terms of similarity between groups, there are feature input interactions in the frontal, parietal, and temporal regions, suggested by a great number of lines observed in these areas. Also, the interactions are stronger in the frontal and lower part of the brain as these areas have thick black lines like channels F8, F6, FC6, FT8, T8, TP8, PO3, and PO7. Interaction between PO7 and FT8 is evident in both groups.

   Some noticeable differences between groups include interaction between channels F5, FT8, and CP5. In contrast to the healthy group, the depressed group failed to exhibit any interaction between F5 and FT8 channels. The lack of connection between frontal and frontotemporal regions may reflect dysfunction within corticolimbic connections in individuals vulnerable to depression (Goulden et

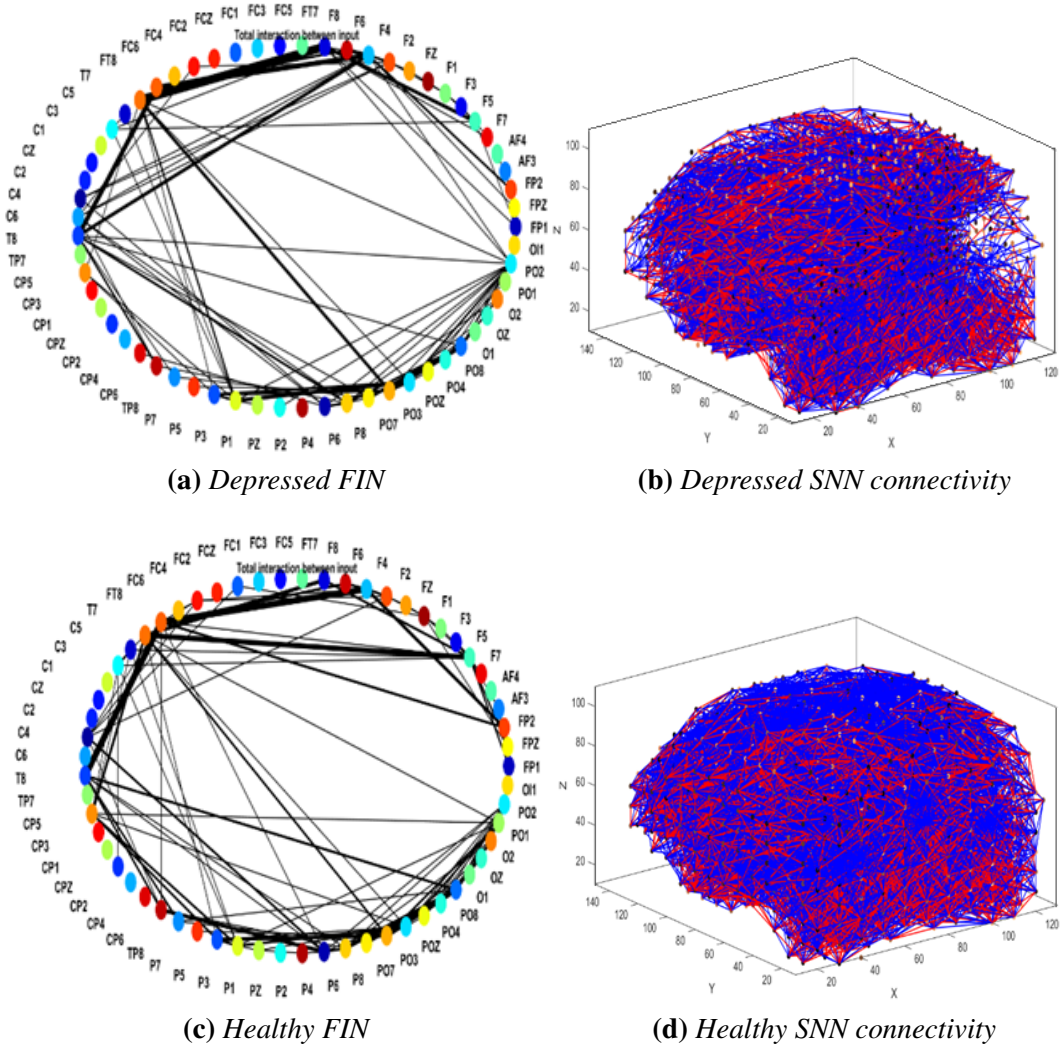

(a) *Depressed FIN* **(b)** *Depressed SNN connectivity*

(c) *Healthy FIN* **(d)** *Healthy SNN connectivity*

Figure 3.5: *Visualization for eyes closed state of an individual*

al., 2012). Continuous long-range communication between F4 and T8 indicates cross-hemispheric communication in the depressed group. By analyzing the SNN connectivity network (Figure 3.5 (3.5b and 3.5d), there is a complete absence of interaction in the parietal region in the depressed group. By observing the FIN of the depressed group, it is seen that P4 plays no role in the network change. It may be speculated that the relative reduction in right parietal activity may reflect a reduction in arousal in those at risk of depression. Previous research has demonstrated the decreased right parietal activity in resting state EEG data in

those with major depressive disorder in females (Stewart et al., 2011) and within males (Flor-Henry, Lind & Koles, 2004). More positive connections (blue color) are seen in the healthy group. In contrast, there is a lot of saturation of positive (excitatory) and negative (inhibitory) connections in the depressed group across the scalp. Both groups have a combination of positive and negative connections in the lower occipital region.

2. Eyes Open State

   Both groups have strong connections in the frontal, parietal-occipital, and parietal brain regions of the Functional Interaction Networks (FIN) models (PO3, PO7, PO8, PO4, F4, FP2, T8). Still, the interaction in the parietal region of the depressed group is greater than those in the healthy group, as shown in Figure 3.5.

   The evident difference is the strong triangular connection between F4-T8-PO8 across the right hemisphere in the healthy group, which is completely absent in the depressed group (less interaction between PO8 and T8). There are greater connections in the right frontal regions, including the F4, F6, F8, FC4, FC6, and FC8, compared to the healthy group. FC4 is totally inactive in the healthy group. Long-range interaction between FT8-PO7 and F8-P1 in the depressed group is another noticeable difference. In the depressed group, there is more information exchange and communication between the frontal-parietal and parietal-occipital regions.

   A meta-analysis (Kaiser, Andrews-Hanna, Wager & Pizzagalli, 2015) suggests that depressive disorders can be characterized by hypoconnectivity within fronto-parietal networks, which are often reported to be involved with attention, emotion regulation, and cognitive control systems. This abnormal connectivity across these resting states may also suggest atypical internal and self-referential thought.

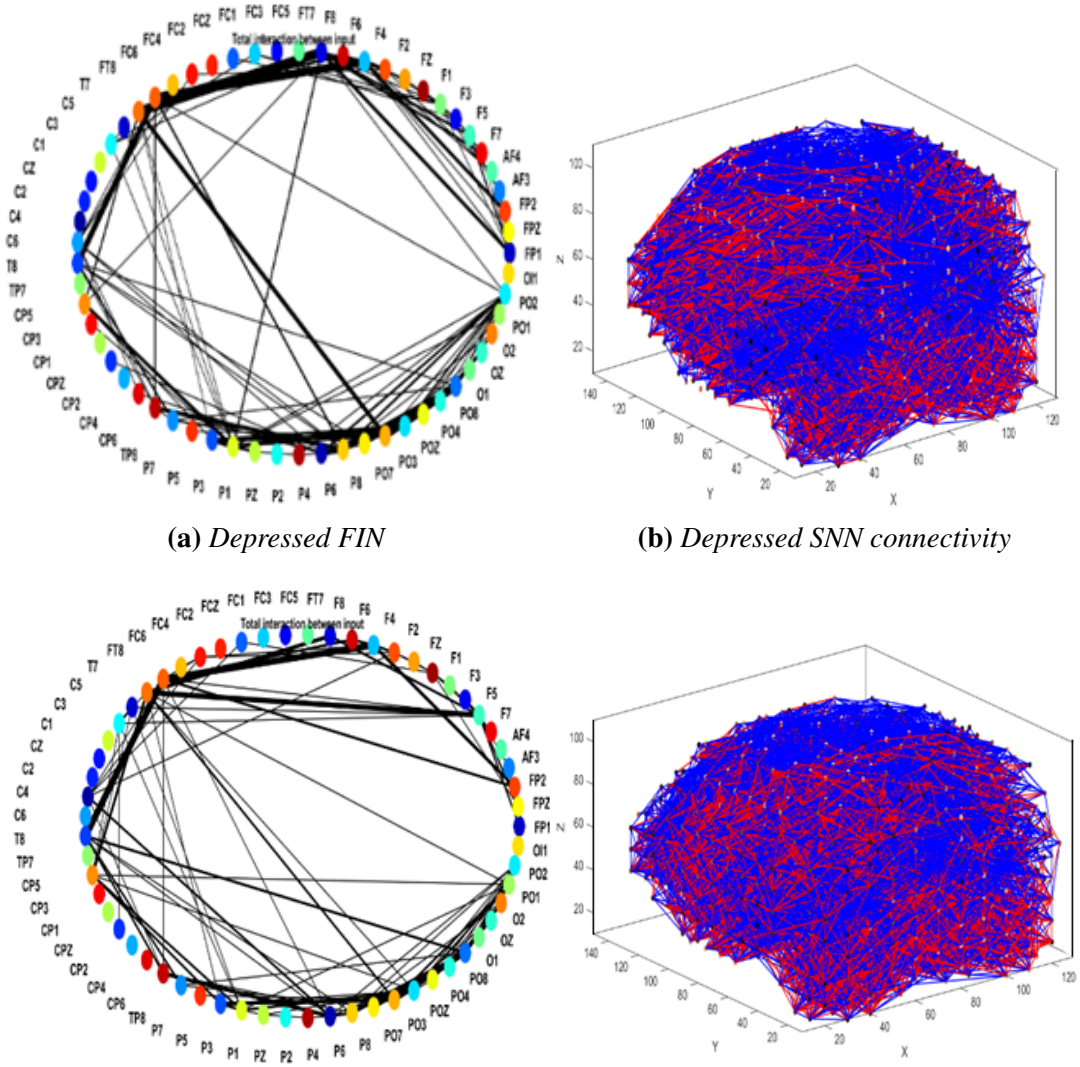

(a) *Depressed FIN* **(b)** *Depressed SNN connectivity*

(c) *Healthy FIN* **(d)** *Healthy SNN connectivity*

Figure 3.6: *Visualization for eyes-open state of an individual*

This dysfunctional processing of internal and external attention could reflect the depressive thought patterns and biases experienced by those with depression or those that may be at risk.

3.5 Conclusion and Discussion

The experiments in this chapter showed that the NeuCube SNN framework achieved a classification accuracy of 68.18% (EC) and 72.13% (EO) for classifying spatiotemporal data such as EEG signals for depression detection. Also, significant patterns were discovered in frontal, parietal, and temporal brain areas that can potentially be used as markers for an early prediction and possible prevention of depression. In addition, this experimental study also performed a comparative analysis using other machine and DL learning techniques, such as MLP and LSTM. Though LSTM networks can process temporal data, they couldn't perform well with fewer training samples. This demonstrates the advantage of using the SNN approach of time-space brain data modeling for spatiotemporal data classification. The results that we achieved in this chapter proved the small-sample learning capability of SNNs.

This chapter proved the feasibility of SNNs in classifying depressed and healthy subjects and revealed informative patterns of neuronal activities that can be further interpreted to understand depression better. Thus, the results from this chapter proved that SNNs are effective in analysing, processing, learning, and understanding spatiotemporal data, and hence, our first hypothesis that EEG data is spatial-temporal in nature if analysed considering both the aspects – spatial and temporal using SNN could be separate healthy and depressed individuals and provide better interpretability of brain activity is validated and accepted.

However, the classification accuracy achieved by the NeuCube SNN architecture was less, i.e., between 65% and 75% because the difference between depression scores of healthy and mildly depressed people was less. This research further improves the classification accuracy of SNN models and studies the biomarkers of depression in Chapter 5.

NeuCube is a complex SNN-based architecture for knowledge extraction and pattern recognition from spatiotemporal brain data. The deSNN algorithm of NeuCube considers the arrival of the first spikes on the input synapses (the neuron is allowed only to fire once) to learn the input pattern and assigns a class label to it. However, it neglects the rest of the firing pattern of the output neuron. Thus, to further increase the performance of the SNN model, we propose a novel SNN architecture that utilises complete temporal patterns.

3.6 Chapter Summary

A 3D reservoir-based Neucube architecture (the first phase of our research study) was presented in detail, forming the baseline and inspiration for developing novel SNN frameworks in this study. This chapter showed the capability of spiking neurons and the feasibility of employing SNNs for depression detection. Comparative analysis of SNN with MLP and LSTM models and better interpretation of brain activities through SNN and unsupervised learning demonstrated that SNNs effectively analyse, process, learn and understand spatiotemporal data. Further, the unsupervised STDP learning algorithm with the supervised deSNN algorithm led to the creation of unique patterns. These unique, distinguishable patterns in healthy and depressed groups projected over the 3D brain-like structure of SNNr provided a better interpretation of the results.

These patterns described in the visualisation module developed over time inspired us to investigate the temporal patterns hidden in spiking neurons. Thus, to increase the performance of the SNN model, we started working on the second phase of our research to propose a novel temporal-based SNN architecture, as described in the next chapter.

Chapter 4

Utilizing the Neuronal Behaviour of Spiking Neurons to Recognise Music Signals based on Time Coding Features

In the first phase of this research study, we used SNN-based NeuCube architecture to classify spatiotemporal data such as EEG signals. To simplify the understanding of hidden temporal patterns in spiking neurons, we have utilised music signals similar to EEG (temporal nature).

In this chapter, the physical organisation of neurons and the classification module from the existing 3D NeuCube architecture are modified to enhance the performance of SNN. The supervised deSNN algorithm from the NeuCube framework considers only the order of the first spike of the output neurons. On the other hand, the proposed 2-layered novel SNN architecture utilises the complete temporal pattern of the output neurons for the classification of music signals. Furthermore, this chapter presents a comparative analysis of rate and temporal coding techniques to understand the neural mechanisms of information processing in spiking neurons.

This chapter addresses the following research questions:

1. Will spiking neurons encode enough rhythmical features in the spike train from EEG signals to categorize different groups of subjects?

   (i) How to recognise spike patterns in the spike train from music and EEG signals to categorise different groups?

   (ii) How can the rate and temporal coding techniques be leveraged to build a computationally efficient SNN in classifying and recognising musical instruments and depression?

These research questions are explored based on hypothesis H2: Spiking neurons containing valuable temporal data can encode the rhythmic behaviour of EEG signals. If the proposed SNN architecture can encode the rhythmic nature of music signals, it will perform well for EEG classification as well.

We wanted to test the proposed architecture and the capability of spiking neurons to learn the input representation for classification purposes. Hence, we initiated the second phase of this research from a musical perspective which has been the most exciting part of this research. This chapter provides details of our proposed SNN architecture, and the architecture is applied to music signals. Further, the proposed architecture is applied to EEG signals for depression detection, described in the next chapter.

4.1 Introduction

4.1.1 EEG and Music Signals

The rhythmic nature of EEG and music signals are illustrated in Figures 4.1 and 4.2, respectively.

The x-axis is time, and the y-axis is the voltage potential measured by an electrode placed on the scalp. The dynamical nature of EEG signals with temporal fluctuations

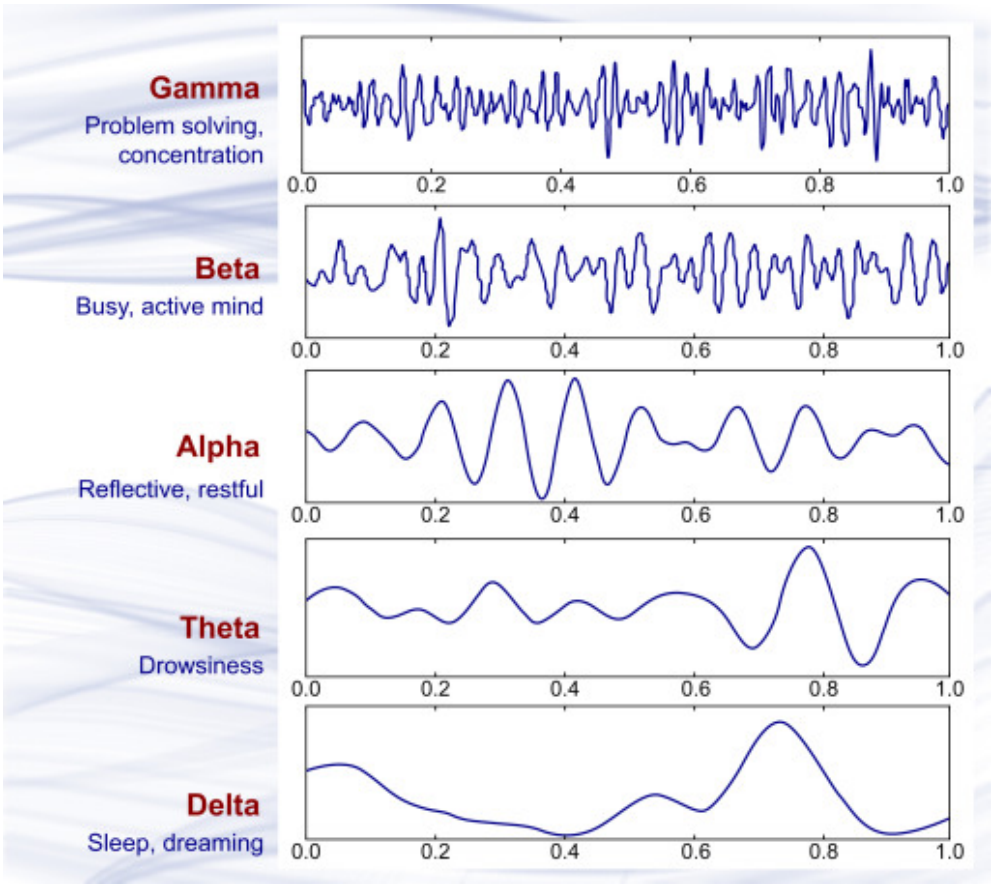

Figure 4.1: *Distinctive Rhythms in EEG signals from (Abhang et al., 2016)*

at different frequencies is observed during sleep, rest, analytical mind, and busy mind states. EEG signals contain bands like gamma, beta, alpha, theta, and delta, with frequencies ranging from 0.1 Hz to more than 100 Hz.

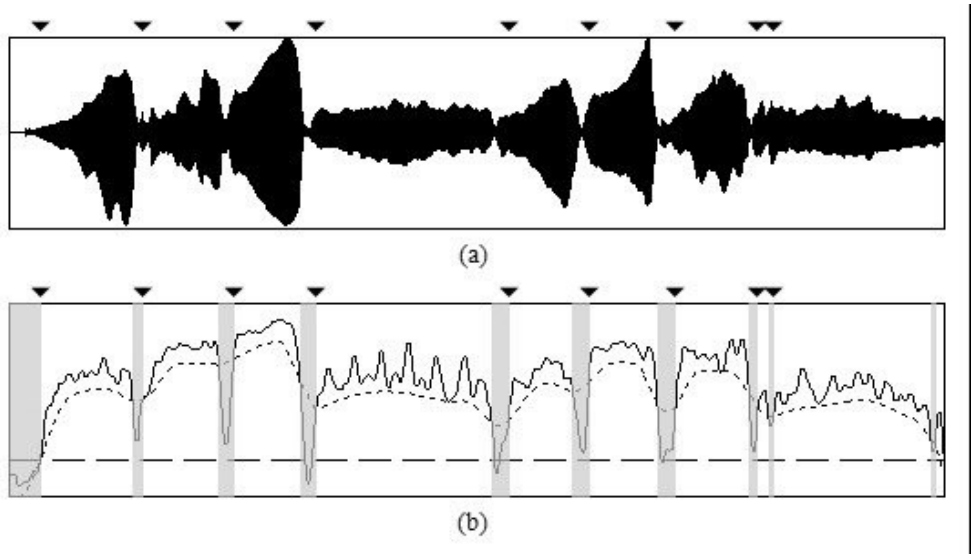

Figure 4.2: *Rhythmic Nature of Music Signals: (a) raw signal (b) Smooth waveform from (Heo et al., 2013)*

Figure 4.2 shows the dynamical aspects and temporal changes in music signals. The x-axis in the music signals represents time, and the y-axis represents different frequencies. In other words, music signals have frequency and time domain characteristics that make them two-dimensional data, i.e., spatiotemporal in nature.

The music and EEG signals are temporal in nature; however, EEG signals are more chaotic and complex. On the other hand, music plays a vital role in our lives. Music can inspire us, make us feel our emotions, heal us, and make us sleep. Psychologists and Neuroscientists use music therapy for patients suffering from Parkinson, depression, and other mental disorders (Z. Doborjeh et al., 2019).

Thus, considering their similarities in terms of temporal nature, we validated and evaluated our proposed dataset on simple music signals. Additionally, the fact that music therapy is used to treat depression further motivated us to approach our research problem of depression detection through a novel SNN-based architecture from a musical

perspective.

4.1.2 Neural Coding

The deSNN architecture in the NeuCube framework used the time-to-first spike coding scheme of the output neurons to infer the class of the samples. To improvise the SNN performance, we wanted to use the metrics derived from the properties of spiking neurons by exploiting all the neuronal information.

Understanding how a neuron perceives and processes information that it receives is referred to as neural coding (Gollisch & Meister, 2008). Interpreting the nature of neural code will help to exploit the neuronal information extensively. In the presence of a stimulus, the internal state of a neuron is affected, and spikes are released. Based on the effect of stimulus or pre-synaptic inputs on neurons, neural codes can be broadly divided into rate-code and temporal code (Hubel & Wiesel, 1959, 1962; Brette, 2015).

When the number of spikes is directly proportional to the intensity of the stimulus, it is termed a rate-coding scheme. Poisson's model is the mathematical framework used to generate spikes where the intensity (real value) of the stimulus is considered as the firing rate or frequency of spikes. When the information about the stimulus is identified in the timing of spikes, the nature of neural coding is termed temporal code. The time of the first spike, the time interval between two spikes (inter-spike interval), the time difference between a pre-synaptic spike and post-synaptic spike, and spike bursting are different types of temporal coding schemes (Guo, Fouda, Eltawil & Salama, 2021).

Rate coding is the average of spikes over time, whereas temporal code is the timing of spikes. The major difference between them is the timescale. The primary visual cells need to operate within ten milliseconds (ms) of resolution (S. J. Thorpe & Imbert, 1989). Additionally, the bits of information transferred using the rate coding scheme within ten (ms) is $log_2(n+1)$ whereas using the temporal coding schemes, neurons can

transmit $log_2(n!)$ bits of information (S. Thorpe & Gautrais, 1998). Thus, rate coding schemes or the firing rate of spiking neurons are considered inefficient for information processing. On the other hand, there is an ongoing debate over rate coding versus temporal coding. In other words, is the information encoded in the rate of firing or in the timing of spikes? (Brette, 2015).

Thus, with our proposed architecture and by analysing the neuronal behaviour using different temporal coding schemes, a comparative analysis between these coding schemes is conducted in our research.

4.1.3 Spike Train Analysis

Spike trains represent the sequences of firing times of neurons. Spike trains are analysed to understand the temporal characteristics of neural information processing. Measuring the discrepancy between pairs of spike trains (called spike train distance) has been the prominent approach to analyse spike trains. This dissimilarity measure between spike trains can be useful in classification and recognition problems. The nature of neural information processing, i.e., rate coding, temporal coding, or both, can be indicated by the measurement of spike train distances, and several methods have been developed to measure this metric (Sihn & Kim, 2019; Satuvuori & Kreuz, 2018; Satuvuori et al., 2017; Victor & Purpura, 1996; van Rossum, 2001).

Spike train distance metric designed to represent a rate-coding scheme considers the number of spikes over a timescale divided by the time length. On the other hand, the temporal coding inspired spike train distance metric considers the distribution of spike times between pairs of spike trains. In other words, the former approach is rate-sensitive, and the latter is time-sensitive and focuses on temporal patterns. Studies have stated the importance of information encoded in temporal patterns and that they explain various brain functions (Tabuchi et al., 2018; Logiaco, Quilodran, Procyk &

Arleo, 2015; M. Fukushima, Rauske & Margoliash, 2015; Mechler, Victor, Purpura & Shapley, 1998; Narayan, Grana & Sen, 2006; Machens, Prinz, Stemmler, Ronacher & Herz, 2001). It has been suggested that precise spike timing plays a crucial role in neural information processing (Gollisch & Meister, 2008; Butts et al., 2007; Johansson & Flanagan, 2009).

For example, a spike train with spike timings at (1, 4, 10, 50) has a temporal pattern similar to another train (1, 4.1, 10, 50.1, 0.9, 10, 50, 50.1) while their overall firing rates are different. Temporal coding spike train distance can assess the divergence of temporal patterns of neural spike trains, which may not be described by rate coding alone. Firing rates over a temporal scale may vary. Hence, there lies ambiguity in whether the spike train reflects temporal changes or firing rate changes, or a combination of both (Sihn & Kim, 2019).

Precise spike timings in neural information processing play an important role, as most studies mentioned above. Inspired by these findings, this research has implemented a temporal coding spike distance metric for classification purposes.

4.1.4 Neuronal Membrane Potential

Most studies use spike timings or spike trains to analyse neuronal behaviour. Spikes are generated when the membrane potential of a neuron crosses the threshold. Spikes have constant magnitude, whereas the membrane potential keeps fluctuating until it reaches the threshold, as shown in Figure 1.3. Approaches driven by spike timings consider the magnitude of action potentials constant over time, and the variance is ignored (Sarangdhar & Kambhampati, 2008). Very few studies (Xu, Zeng & Zhong, 2013; M. Zhang, Qu, Belatreche, Chen & Yi, 2018) have incorporated membrane potential in training the spiking neural networks using a supervised learning algorithm.

This research has incorporated membrane potential for making classification decisions with an assumption that important information (information helps distinguish two groups better) is hidden not only in the spike trains but also in the fluctuating membrane potentials.

Thus, our proposed architecture presented in this chapter aims to achieve the following objectives:

1. To explore the capability of a two-layer feedforward SNN in recognising the music samples
2. To compare the rate-coding and temporal coding mechanisms using traditional ML classifiers to make classification decisions
3. To analyse the behaviour of spike train to detect the spiking patterns
4. To identify the potential of neuronal membrane potential
5. To evaluate our proposed time coding features for spatiotemporal classification

4.2 Methods

This section details each step of our proposed 2-layer temporal-based SNN architecture.

4.2.1 Dataset Description

The piano and violin music files were downloaded from an online website (Home, 2016). Each group consists of 5 samples, and the time duration is 61 seconds. The music signals were loaded using the Librosa python library at the sampling frequency of $22050Hz$ as illustrated in Fig. 4.3. and Fig. 4.4.

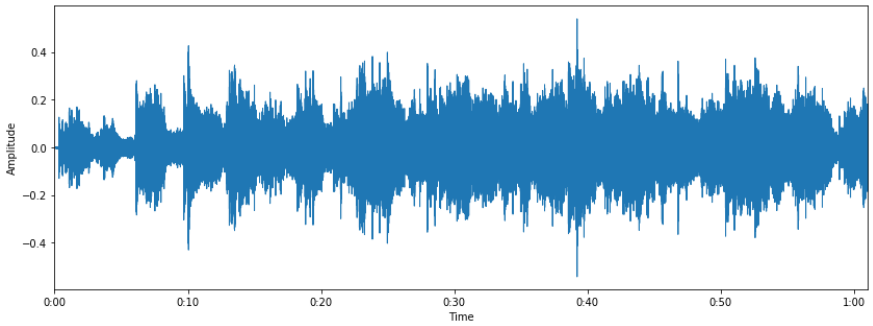

Figure 4.3: *Piano Signal.*

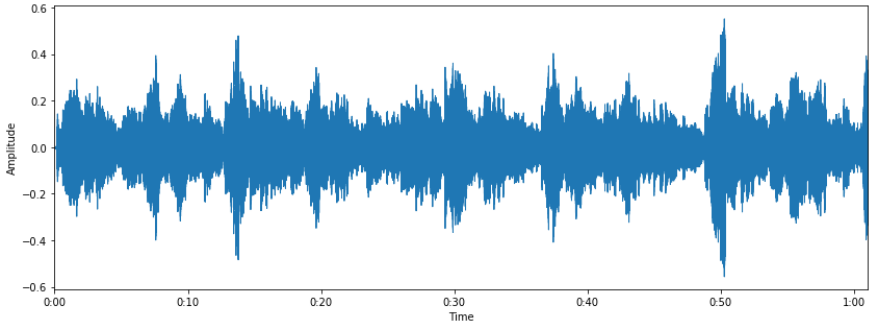

Figure 4.4: *Violin Signal.*

4.2.2 Proposed 2-layered SNN architecture

This section introduces the proposed SNN architecture and explains the various methods used. First, the data is prepared in a format that can be readily used by SNN, i.e., music signals are encoded into 2D binary spike trains. Spike trains are propagated into the network of spiking neurons. STDP learning is applied between the inputs and spiking neurons in the hidden layer, from the hidden layer to the output layer, which consists of one LIF neuron. MP and spike timings are recorded for classification and further analysis.

Fig.4.5 describes the SNN aspects of the proposed architecture.

- **Encoding**

  For encoding, we used spike encoding algorithms: Ben's Spiker algorithm (BSA)

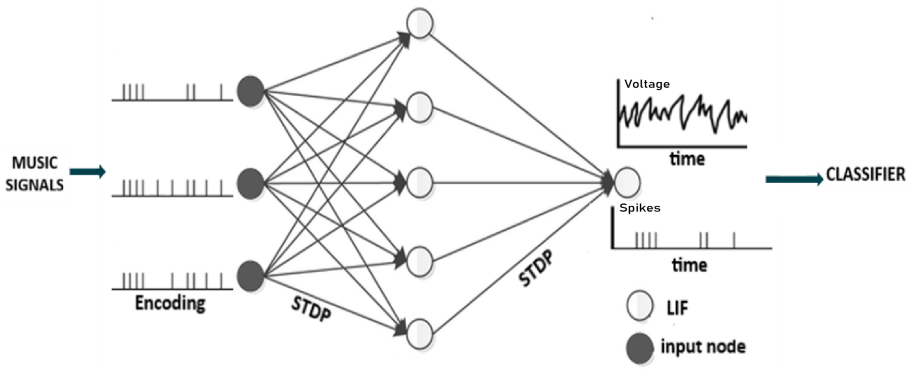

Figure 4.5: *Novel 2-layer temporal-based SNN.*

(Schrauwen & Van Campenhout, 2003a). Each music sample (frequency components) is a 2D matrix representing the frequency value at an instant of time. The output from the encoding algorithm is also a 2D matrix of spike trains for each sample.

BSA is less adaptable to any alterations in the filter and threshold. Due to the use of optimal threshold value, which smoothens the amplitude and frequency characteristics of the signals, we have selected for encoding the analog signals of the music dataset into sequences of binary events. In BSA encoding, the input signals are convolved with the filter coefficients. The process of creating filter weights (LLC, 2010) is described in Algorithms 4 and 5.

Algorithm 4 Create Filters for BSA Encoding

1: **procedure** CREATEFILTER(M, f_c, f_s)
2: Compute normalized transition frequency, $f_t = \frac{f_c}{f_s}$
3: Compute $length\_of\_filter$, $fir = M + 1$
4: $half$ = M/2
5: **for** x=0 to : fir **do**
6: **if** (x ≠ half):
7: $fir[x] = \frac{\sin(2*\pi*f_t*(x-half))}{\pi*(x-half)}$

8: **else**:

9: $fir[x] = 2 * f_t$

10: **end for**

11: return fir

12: **end procedure**

In Algorithm 4, f_s is the sampling frequency, f_c is the cut-off frequency, and f_t is the normalised transition frequency. We have created low-pass FIR filters. The length of the filter is equal to the number of features in the input dataset. x is the input signal. If the number of filters is equal to 1, then all the features of the sample will be encoded using the same filter; otherwise, if the number of filters is greater than 1, then the number of filters must be the same as the number of features of the data. The filter length equals the number of rows (input samples) in the input dataset. M is the number of taps minus 1, where the number of taps is the same as the filter length, fir. Now, for each input signal, at every time instant, the FIR filters allow us to generate the responses using the $sinc$ function as described by the variable $fir[x]$.

This process generates the $sinc$ function weights, and a windowing technique is applied that provides extra control over the characteristics of the filters (LLC, 2010). The window weights are calculated, in this case, a Hamming Window has been used, and the equation is described by the variable $fir(x)$. The two sets of weights are multiplied together to create the final set of filter weights which are then utilised in the BSA encoding. The FIR design is a standard implementation described in (LLC, 2010).

The pseudocode for the BSA algorithm is explained in Algorithm 6. BSA uses the aforementioned filter weights for converting analog waveforms to spike trains. To convert the continuous-valued data to spike train using BSA, two error measures

are calculated for each input analog signal s at every timestamp τ as shown in equations 4.1 and 4.2.

$$e_1 = \sum_{k=0}^{M-1} abs(s(k+\tau) - h(k)) \tag{4.1}$$

$$e_2 = \sum_{k=0}^{M-1} abs(s(k+\tau)) \tag{4.2}$$

where M, s, and $h(k)$ represents the number of filter taps, input analog signal, and impulse response of a filter at tap k, respectively, error e_1 is yielded by subtracting the filter coefficients from the subsequent signal values at each time point, and error e_2 is the signal value without changing at each time point. A spike is released if e_1 is smaller than e_2 minus threshold and $h(k)$ (filter coefficients) is deducted from the input. The optimal value for the threshold is 0.9550 according to (Schrauwen & Van Campenhout, 2003b).

The construction of spikes from analog signals and reconstruction of signals from spikes is carried out using a finite impulse response (FIR) filter. Using the Differential Evolution (DE) algorithm, this encoding and decoding process yields more accurate spike trains. The number of filters, size, and threshold value are optimized using the DE algorithm. The optimisation is performed for each channel in every sample. Since we have 20 channels in the input, every sample will have $20 * 3 = 60$ parameters to be optimised. The range of values for these parameter are: $th = [0.0, 2.0], FIRsize = [3, 50], FIRcut - off = [0.0, 0.5]$.

Algorithm 5 Window Hamming Technique for BSA Encoding

1: **procedure** WINDOWHAMMING(fir)

2: $m = fir\_length - 1$:

for x = 0 to fir_length **do**:

$fir(x) * = 0.54 - 0.46 * \cos\left(\frac{2\pi x}{m}\right)$

return fir

end for

end procedure

Algorithm 6 BSA Encoding Technique

procedure BSAENCODING($input, filter$)

for i = 1 to $size(input)$ **do**:

$error1 = 0$:

$error2 = 0$:

for j = 1 to size(fir) **do**:

if $(i + j - 1 \leqslant size(input)$:

$error1 += |input(i + j - 1) - filter(j)|$

$error2 += |(input(i + j - 1))|$

end if

end for

if $error1 \leqslant (error2 - threshold)$:

$output(i) = 1$

for j = 1 $\leqslant$=size(filter) **do**:

if $(i + j - 1 \leqslant size(input)$:

$input(i + j - 1) -= filter(j)$

end if

end for

else:

$output(i) = 0$

end if

end for

22: **end procedure**

- **Connectivity and Unsupervised learning in proposed SNN architecture**

  The number of nodes in the input layer equals the number of columns in the sample. The hidden layer consists of spiking neurons, and all the input nodes are connected to all the spiking neurons.

  The music recognition system implements the LIF neuron model as described in Section 1.7. Standard or simple IF represents membrane potential as a function for integrating temporally stochastic synaptic inputs or currents until a threshold is exceeded. At this point, a spike is produced, and the membrane potential returns to its resting potential for the next cycle. The membrane potential in IF is, therefore, a 'passive' integrative component and may fire continuously in the presence of signals. LIF, or 'forgetful' IF, allows for membrane potential to rise in response to input but also to reduce (leak). The amount of membrane potential leakage over time, in conjunction with refractory effects during which the neuron is inactive, allows for the emergence of spiking rates and interspike intervals.

  The sum of weighted inputs to each spiking neuron is calculated using Eq.1.4. The membrane potential difference of spiking neurons is measured using Eq.1.1. The dynamics of LIF neurons are modelled using Eq.1.3. The spikes of neurons from this layer are propagated to the succeeding layer in the next timestamp, $t + 1$.

  Detection of a spike in the hidden layer instantiates the STDP learning rule. Synaptic weights are initialized randomly, including positive (80%) and negative connections (20%). Based on the timings of spikes of the input nodes (pre-synaptic neurons) and the spike timings of spiking neurons in the hidden layer (post-synaptic neurons), synaptic potentiation (Eq.1.5.) or depression (Eq.1.6.) takes place, and the synaptic weights are updated accordingly as explained in Section 1.1.5.

- **Novel Classification Module**

  This layer consists of only one spiking neuron that performs the classification task. All the spiking neurons in the hidden layer are connected to this neuron. The synaptic connections are adapted using the STDP rule as discussed in Section 1.1.5. For each sample, the membrane potential (voltage at each time point) and the spike train (spike/no spike event at each time point) of the output neuron are extracted. From this information, five metrics are computed for the next stage of classification:

  1. Firing Rate: It is calculated by dividing the total number of spikes of the output neuron by the total stimulation time.
  2. Total Membrane Potential: This is the sum of the membrane potential of the output neuron.
  3. Signal-to-Noise ratio (SNR): SNR is calculated from the membrane potential signal as the mean of the signal divided by its standard deviation.
  4. Gamma Factor: This metric which is also called the coincidence factor (Jolivet, Rauch, Lüscher & Gerstner, 2006) considers the number of coincidences of spikes with a given time window, further sliding the window for the length of the spike train i.e. the temporal information is given preference over the overall firing rate of the neuron.

     At the end of each training step, the firing times and membrane potential of the output neuron are extracted for classification. Using the spike time, firing rate and Gamma factor are calculated.

     The coincidence factor (Jolivet et al., 2006; Kistler, Gerstner & Hemmen, 1997) defined between two spike trains is described as:

$$\Gamma = \frac{N_{coinc} - \left\langle N_{coinc} \right\rangle}{\frac{1}{2} * (N_{data} + N_{SRM}) * N}$$

where N_{data} is the number of spikes in the actual (training sample) spike train, N_{SRM} is the number of spikes in the predicted (test/validation sample) spike train, N_{coinc} is the number of coincidences between the two spike trains with precision Δ (time window), and $\left\langle N_{coinc} \right\rangle = 2v\Delta N_{data}$ is the number of expected coincidences generated with same rate v as the predicted spike train. The coincidence factor can range between 0 and 1 (both inclusive), where 0 means the least coincident between the two spike trains and 1 denotes the maximum value when both spike trains are identical to each other.

This factor is calculated between the spike train of the output neuron of the test sample with all the spike trains of the output neuron of the training samples. In other words, the gamma factor is calculated between each pair of the test sample and all the training samples. The label of the training sample, which has the highest gamma factor among all the pairs is assigned as the label to the test sample and denotes the prediction.

5. Root Mean Square Error (RMSE): The RMSE value is calculated between the membrane potential signal of the output neuron of the test sample and all the membrane potential of the output neuron of the training samples. The label of the training sample, which has the least RMSE value among all the pairs, is assigned as the label to the test label.

Out of these classification metrics, firing rate, total membrane potential, and SNR fall under the category of rate-coded metrics, whereas gamma factor and RMSE are classified as temporal metrics.

- **Evaluation and Optimisation**

The metrics from the output layer are used for the classification of music signals.

A feedback cycle checks the accuracy of test results, with optimization then used to fine-tune the SNN parameters using differential evolution. The DE algorithm is employed for optimizing various parameters in the encoding algorithm, LIF neuron model, STDP learning rule, number of neurons in the hidden layer, and range of synaptic weights. This approach analyses various parameters in the given search space and provides the best possible solution (the best set of parameters) through the processes of recombination, mutation, and selection to maximise the overall classification accuracy.

In analogy with natural selection, DE generates a child population by recombining the randomly chosen parent vectors from the initial population. After the recombination of parents, each of their children is mutated by adding a random deviation, i.e., Gaussian white noise. All the children are evaluated on the fitness function, and DE selects the best children to be the parents of the next generation. These recombination, mutation, and selection steps continue iteratively until convergence is met [terminating condition].

We have implemented Differential Evolution (DE) (Storn & Price, 1997) from the various existing nature-inspired optimization techniques under evolutionary computation. DE is a stochastic, population-based optimization technique based on finding differences between candidate solutions in a population of solutions to guide the direction and length of search steps. Each solution is called an agent. Each agent undergoes mutation followed by the recombination operation. The target vector is the solution undergoing evolution [initial parameters], and the target vector is used in mutation to generate the donor vector. Finally, the donor vector undergoes recombination to obtain the trial vector. The selection operation chooses the best solutions only after generating all the trial Vectors. The target and trial vectors choose the best solutions for the next generation. DE

strategies for optimizing SNN parameters have been previously shown to improve accuracy on classification and prediction problems (Schliebs & Kasabov, 2013). The pseudo-code for the DE algorithm is explained in the Algorithm 7.

Algorithm 7 DE algorithm

procedure DE(Fitness function, lower bound $(l_b$ and upper bound (u_b) of each parameter (decision variables), the population size $(N_p$, termination criteria (T), the scaling factor $(0 < F \leqslant 2)$ to be used in mutation and cross-over probability $(p_c = 0.1))$
  Initialize a random population (P)
  Evaluate fitness (f) of (P)
  for $i = 1$ to T
    for $i = 1$ to N_p
      Generate the donor vector (V_i) using mutation
      Perform crossover to generate offspring (U_i)
    end for
    for $i = 1$ to N_p
      Bound (U_i)
      Evaluate the fitness (f_{U_i}) of (U_i)
      Perform selection using (f_{U_i}) and (f_i) to update (P)
    end for
  end for
end procedure

4.3 Experiments and Results

This section details the experiment design as illustrated in Figure 4.6, starting from the dataset to the classification decision and results to validate and evaluate our proposed architecture.

4.3.1 Experiment Design

Z-Score Normalisation is used as part of the pre-processing method. No other pre-filtering techniques such as representing recording intervals and window size, or applying noise reduction techniques, were used. The aim is to test the capability of spiking neurons to distinguish musical instruments without such data cleansing steps, as would be usual with other techniques.

The following pseudo-code enclosed in frame boxes represents the dataset configuration, the algorithmic step for calculating the neuron's membrane potential, propagation of spikes, and the computation of synaptic weights. These steps can be defined into the following implementation phases, as described below.

Input to Network of Spiking Neurons

- Initialization: This step initialises the number of spiking neurons in the hidden layer, connects the input layer to the hidden layer with full connectivity, and randomly assigns weights to these synaptic connections. The input nodes act are pre-synaptic inputs to the post-synaptic neurons in the hidden layer. Also, all the spiking neurons in the hidden layer are connected to the output neuron. The encoded data is divided into a training set (80%) and a testing set (20%). k defines the number of splits based on the cross-validation technique selected.

```
Initialization:
1: data = read(data)
2: initializeNetwork()
3: train, test= split(data)
4: k= 1,2..,n
```

- Propagation: After the network initialisation, the training set is divided into the

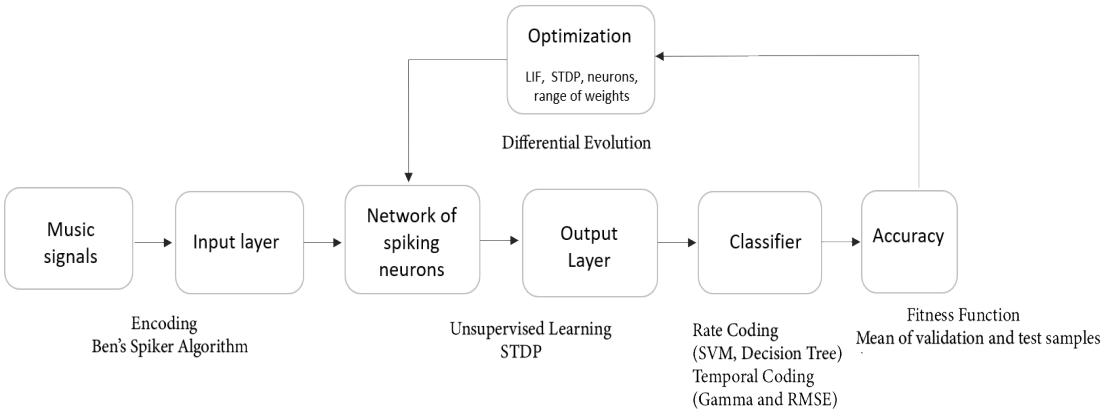

Figure 4.6: *Experimental Setup.*

train and validation sets. To avoid overfitting, the test set is not introduced during the cross-validation step of the training process. We have implemented the Leave-One-Out cross-validation (LOOCV) technique (Hastie, Tibshirani, Friedman & Friedman, 2009) is used as we have used only ten samples in all. Pre-synaptic spikes, i.e., the encoded data using the BSA process, are then propagated into the network of spiking neurons. The active neurons, i.e., neurons in the hidden layer that released spikes, are considered for propagating these spikes to the output layer. This further makes our architecture energy efficient. The efficacy of the synaptic connections from the input layer to the hidden layer and from the hidden layer to the output layer is updated when the neuron's membrane potential crosses the threshold using the STDP rule.

```
Propagate:
1: for each neuron
        computeMembranePotential()
        detectFiredNeurons()
end for
2: for each firedNeuron:
        propagateSpike()
end for
3: for each timestep:
        update_status_inputnodes()
        call Propagate
        update_Weights()
end for
```

- Train and Test Processes: 80% of the training samples are divided into trainData and validationData.During the SNN training, spikes are propagated throughout, the membrane potential is computed and synaptic weights are updated using the STDP rule. For each validation sample, the accuracy of the model is evaluated, and the trained weights are stored. During the testing process, the unseen 20% of the dataset, i.e., the test set, is propagated throughout the network. For each test sample, the accuracy of the model is evaluated. Finally, the performance of the model is evaluated by averaging the accuracies of the cross-validation and testing processes.

```
Train and Test Processes:
5: validation_accuracy = list()
6: for i in k:
        trainData, validationData = cv_spilt(I, k, train)
        model = fit(trainData)
        accuracy_train = evaluate(model, validationData)
        validation_accuracy.append(accuracy_train)
end for
7: model = fit(train)
8: accuracy_test = evaluate(model, test)
```

Output layer and Classifier: Evaluation Module

The music instrument recognition is a binary classification problem; hence, the output layer consists of only one LIF neuron model. The firing activity and the membrane potential of the output neuron are recorded during the training and testing phase. As mentioned earlier, five different temporal metrics are used for the classification decisions. For rate coding metrics, traditional ML classifiers using the Weka library (Garner et al., 1995) are implemented, and temporal metrics are derived using Gamma and RMSE factors. The labels to the validation and test samples are decided on the basis of similar temporal patterns observed among them and training samples, as discussed in the proposed architecture above. The label of the training sample, which is the closest of all pairs, is assigned as the label of the current sample.

To summarise, the dataset is split into train (80%) and test (20%) sets. The network is initialized with input nodes equal to the number of columns, i.e., 40 in the encoded data, and the simulation time 1000 is equal to the number of rows. The hidden layer and the output layer are implemented using LIF neurons. Within the 80% training set, we have applied the leave-one-out cross-validation technique (Hastie et al., 2009)

for evaluating the performance of the network. BSA encoded data is then propagated throughout the network of spiking neurons. As the neuronal membrane potential crosses the threshold, a spike is emitted, and spike time is recorded. For each fired post-synaptic neuron, the synapses are strengthened if the pre-synaptic neuron is fired before the post-synaptic neuron and vice versa. Thus, the spiking neurons, along with STDP, produce spatiotemporal patterns.

Accuracy: Optimisation Process

We used DE optimization during the cross-validation process to best optimize the SNN parameters. For the music recognition problem, the total number of evaluations is shown below in the frame box:

The number of evaluations for optimising various SNN parameters in our proposed 2-layer temporal-based SNN architecture:

- 7 SNN parameters: Threshold and refractory time of LIF neuron model, maximum potentiation (A_+) and depression (A_-) in STDP learning rule, the number of spiking neurons in the hidden layer, the range of synaptic weights (minimum and maximum value)
- Differential evolution: 70 candidate solutions (number of parameters $*10$), 100 iterations
- Every candidate solution: 30 models
- Total number of evaluations = $70 * 100 * 30 = 210,000$

4.3.2 Results

Dataset

Short-time Fourier transforms (STFT)(McFee et al., 2015) was applied to extract frequency components from the music signals. Fig. 4.7 and Fig. 4.8 show the frequency spectrum of the respective signals. In a spectrum representation plot, the x-axis represents time; the y-axis represents frequencies, and colours represent the magnitude (amplitude) of the observed frequency at a particular time. STFT converts signals in a manner that the amplitude of a given frequency at a given time is known, and, in this case, the STFT function returns data in the time-frequency domain with dimensions of

1025 rows and 2628 columns. For the experimental demonstration, only 20 columns (center) have been selected to explore the capability of SNN with less computational cost. For the proper brain circuity to be developed, the neurons produce negative and positive feedback signals during the generation and flow of neurotransmitters. (Takano, Funahashi & Kaibuchi, 2019). To incorporate this concept, we have 20 positive and 20 negative connections from the input to the hidden layer in the proposed SNN architecture.

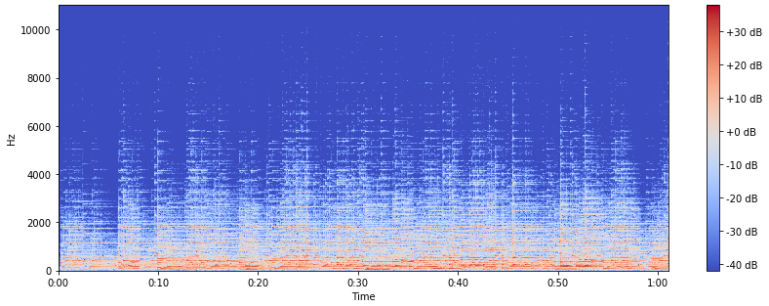

Figure 4.7: *Spectrum for Piano Signal.*

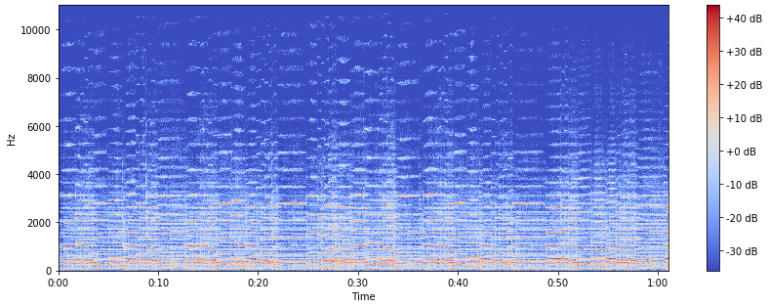

Figure 4.8: *Spectrum for Violin Signal.*

Data Encoding

For music instrument recognition, the BSA encoding (Schrauwen & Van Campenhout, 2003b), which is a part of NeuCube's framework, is used to convert the music signals (real number) into spike train (binary data).

Figures 4.9a and 4.9b represent a violin signal and its corresponding spike encoding. The x-axis shows the time duration, and the y-axis represents the amplitude in Fig. 4.9a. The blue color in Fig.4.9b indicates the occurrence of the spike at that time instant on crossing the threshold value.

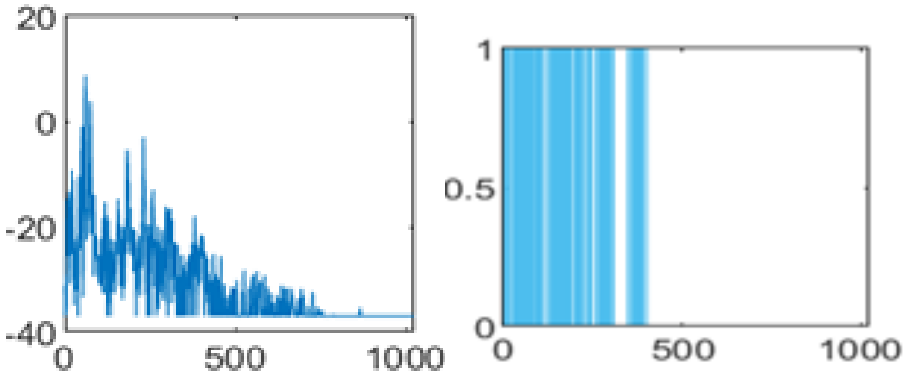

(a) *Input Analog Violin Signal* **(b)** *Spike representation for violin sample*

Figure 4.9: *Data Encoding: (a) x-axis represents time, and the y-axis represents the amplitude.(b): x-axis represents time, and the y-axis indicates a spike where 0.5 is the spike threshold. The absence of blue lines indicates no spike.*

Performance Evaluation

Our main focus at every point in this research was the maximum utilisation of all information obtained from the spiking neurons. Averaging the number of spikes over the entire time length, i.e., FR, calculating the sum and SNR from the membrane potential resulted in the loss of temporal data. Fig. 4.14., Fig. 4.15., Fig. 4.16. and Fig. 4.17. clearly illustrate the rhythmic behaviour hidden in the spike train. Thus, we realized the need to incorporate a metric that processes the temporal information and can aid in classification performance. Hence, we decided to incorporate a coincidence factor called Gamma (Γ) factor (Jolivet et al., 2006) as the criteria to classify the samples.

The gamma factor considers the temporal information (spike times), which produced a classification accuracy of 92.38% with optimal parameter setting as shown below in Table 4.2. Further, the membrane potential signal contains the value of the voltage at

Table 4.1: Performance Evaluation of ML Classifiers

Sr No.	***Classifier***	***Metric***	***Threshold***	***No. of neurons***	***Weights(min,max)***	***Mean Acc. (%)***
1	SVM	FR	0.542374	74	$0.01, 0.366542$	75.5
		SNR	0.031405	49	$0.01, 0.109176$	59.34
		MP_SUM	0.32567	67	$0.03, 0.565800$	72.87
2	Decision Tree	FR	0.089848	43	$-0.26654, 1.15908$	79.50
		SNR	0.282274	75	$-0.17485, 0.638234$	78.55
		MP_SUM	0.276826	77	$-0.62101, 0.880077$	78.87

Table 4.2: Performance Evaluation of temporal metrics: Gamma and RMSE

Sr No.	***Metric***	***Threshold***	***No. of neurons***	***Weights(min, max)***	***Mean Acc. (%)***
1	Gamma	0.311189	54	$-0.508710, 0.880842$	92.38
2	RMSE	0.3964	67	$-0.288482, 0.9027$	93.19

each time step. Hence, the root mean square error was calculated at each time step from the signal.

As in previous experiments, in the above-mentioned Gamma and RMSE experiment setting, the network was trained using STDP, and the firing times (spike train) and membrane potential was extracted from the output neuron. The coincidence factor and RMSE were calculated between the test/validation sample and all the training samples. The label of the closest training sample was assigned as the label to the test/validation sample, and classification accuracy was recorded as shown in Table 4.2.

We also performed classification using rate coding mechanisms by computing the following properties from the output neurons: firing rate (FR), the sum of voltages (MP_SUM), and signal-to-noise ratio computed using membrane potential (SNR). These features were used in different combinations to support vector machine and decision tree classifiers. Top accuracies have been recorded as shown in Table 4.1

To compare the performances of all models, we performed the paired t-test statistical analysis. The significance value, p, was set to 0.05, and the null hypothesis (H0) was, "There is statistically no significant difference between the accuracy of each paired model."

We have implemented the SNN model with nine different classification criteria; hence, we have 36 pairs of models (considering only the top left of the symmetric t-test matrix). For all the combinations, the significance value was far less than 0.05 except for SNR_Weights-MP_SUM, where the p-value was 0.013. Thus, we rejected the null hypothesis except for this pair and concluded that the performances of the other models were significantly different.

Further, we performed the Friedman test (Friedman, 1937) as shown in Table 4.3 to test and rank all the implemented models. After analysing the mean rankings, the model with RMSE as a classification criterion achieved a mean rank value of 8.69, the highest amongst all models, followed by the model implemented with the gamma factor. We could thereby infer that the temporal coding mechanisms carry more information relatively.

Table 4.3: Friedman Test

Sr No.	***Classification Criteria***	***Mean Rank***
1	RMSE	8.69
2	Gamma	8.26
3	FR	7.01
4	MP_SUM	4.64
5	SNR	4.43

For the posthoc analysis, we used the Wilcoxon signed-rank (Wilcoxon, 1992) test, a non-parametric statistical hypothesis test used to compare two related samples. Here, we compared the accuracies of gamma and RMSE factors with all the other criteria. We discovered that in all 70 runs, the score of the gamma factor was higher than FR, MP_SUM, and SNR. The performance of gamma and RMSE factors had 32 ties, six negative rankings (RMSE<gamma), and 32 positive rankings (RMSE>gamma). When analysing the performance of RMSE with other models, it was a win situation for RMSE. The conclusion after this analysis proves that temporal coding outperforms rate-coding mechanisms. Comparative analysis with traditional ML implies that SNN

can process spatiotemporal data with acceptable performance.

Thus, the overall accuracy experimentally recorded in Table 4.1 and Table 4.2 along with the statistical results, Table 4.3 concludes that the temporal dynamics of the neurons captured in its firing activity and membrane potential signal producing rhythmic patterns play an essential role in the classification task.

The spike trains and the membrane potential thus carry useful information for discriminating samples from different groups. As we observed in the spike train analysis, gamma, and RMSE criteria, this initial SNN architecture performs accurately when the classification criterion includes the temporal dimension of the spiking neuron for distinguishing violin and piano signals.

Visualisation: Neuronal Behaviour

This section discusses results and different spike train analysis techniques showing the rhythmic behaviour of spiking neurons, thus distinguishing the piano and violin signals. This nature of spiking neurons is evident because of their capability to process spatiotemporal information. The spike train analysis reflects aspects of neural functioning that affect learning.

Fig. 4.10. and Fig. 4.11. shows the firing rate of all the neurons in the network. We have 40 input nodes, 60 hidden neurons, and 1 output neuron. The firing rate of the hidden and output neuron in the piano class lies within the range of 0.02 and 0.03, whereas for the violin class, it lies between 0.06 and 0.07. The initial exploration of the rate coding scheme led to further analysis considering the temporal dimension.

In Fig. 4.12. and Fig. 4.13., the x-axis represents the time component, and the y-axis represents the neurons. The blue dot symbolizes a spiking event i.e.; the neuron has emitted a spike at the given time. Violin samples excite the network much greater than the piano class. This firing activity reveals the temporal pattern hidden in the spiking behaviour of neurons and proves to encode more rich information than the

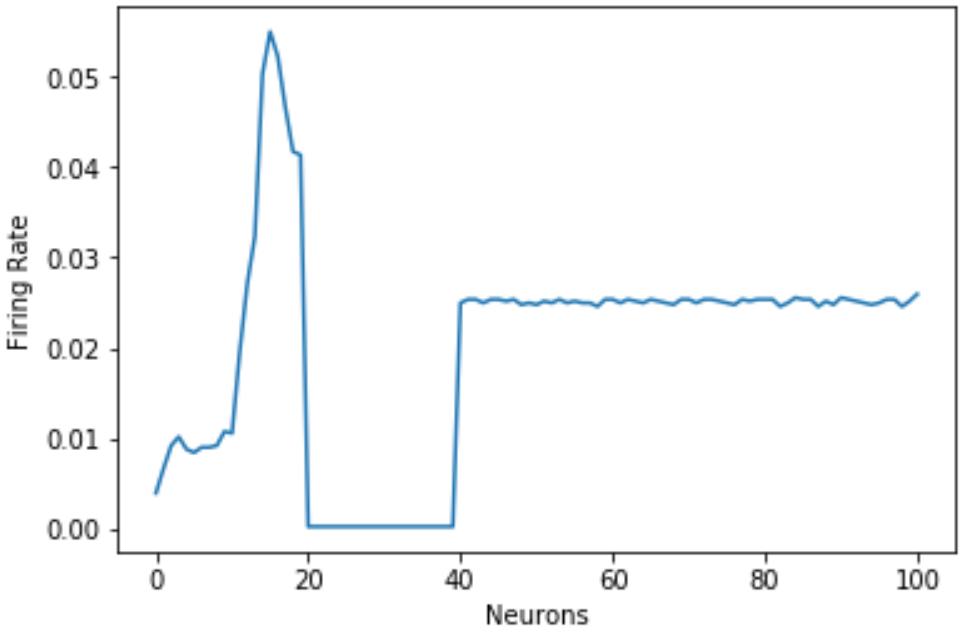

Figure 4.10: *Firing rate for piano class.*

rate-encoding mechanisms.

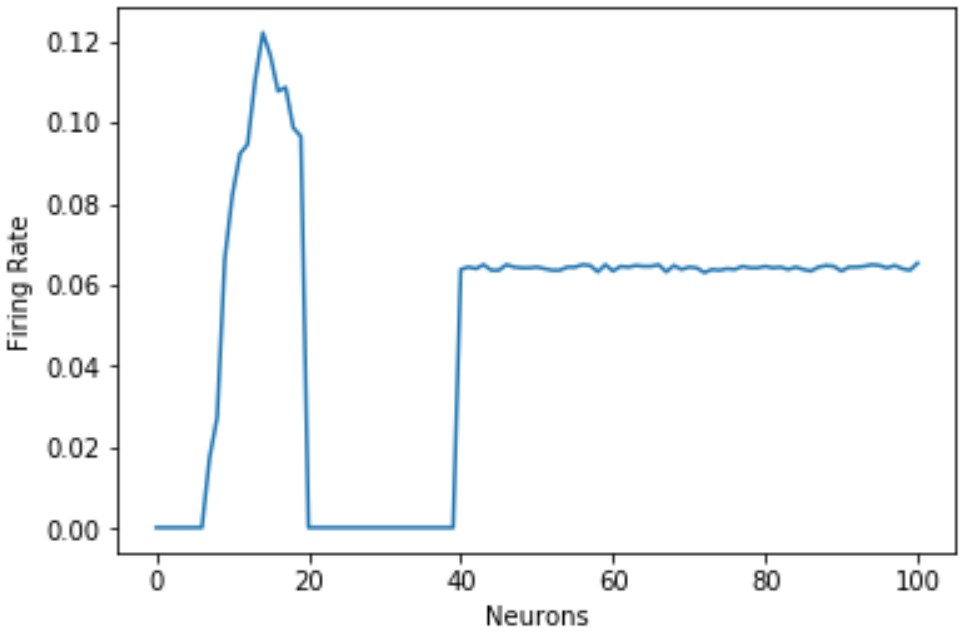

Figure 4.11: *Firing rate for the violin class.*

Inter Spike Interval (ISI) is the time difference between each two successive spike

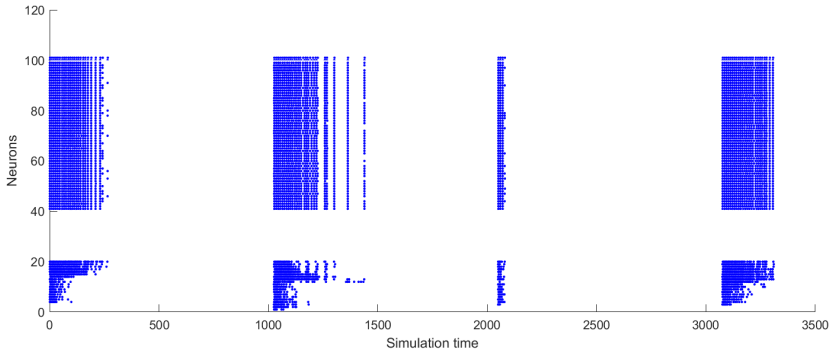

Figure 4.12: *Raster plot for piano class*

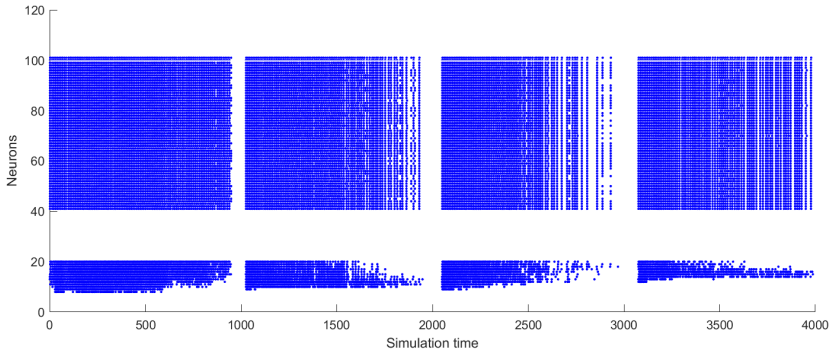

Figure 4.13: *Raster plot for violin class*

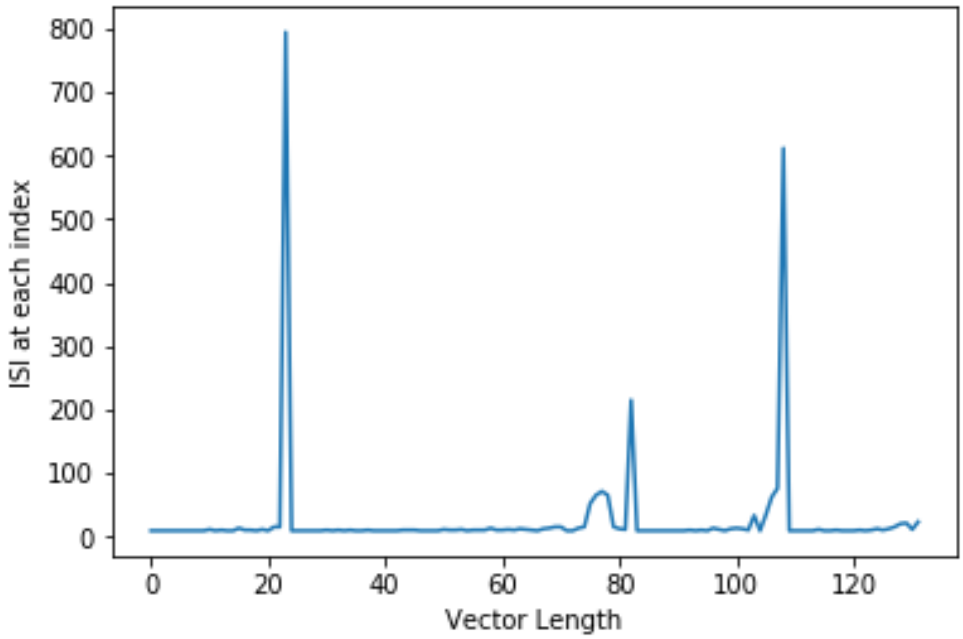

Figure 4.14: *Inter Spike Interval of the output neuron in the piano class.*

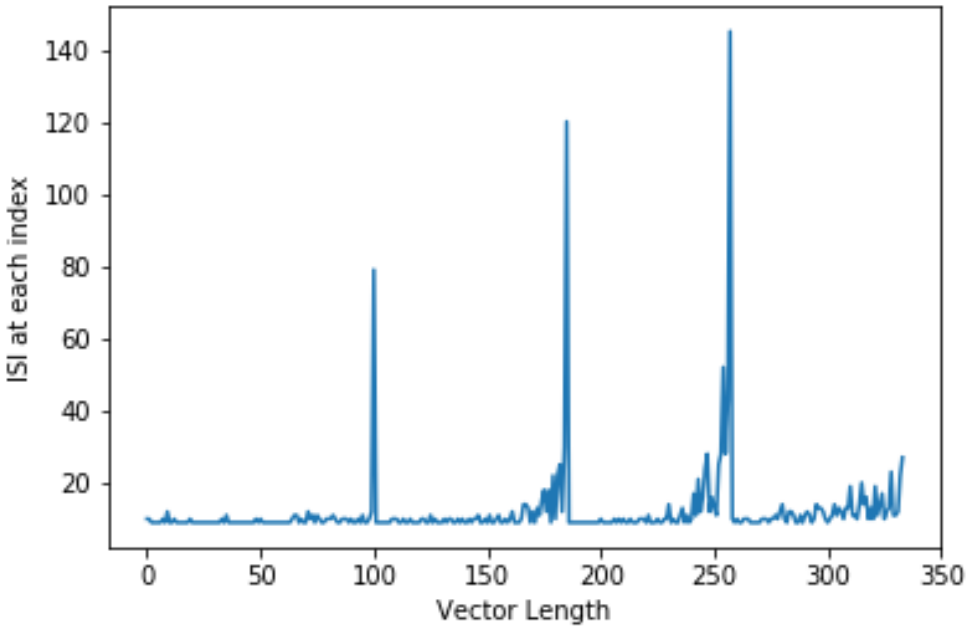

Figure 4.15: *Inter Spike Interval of the output neuron in the violin class.*

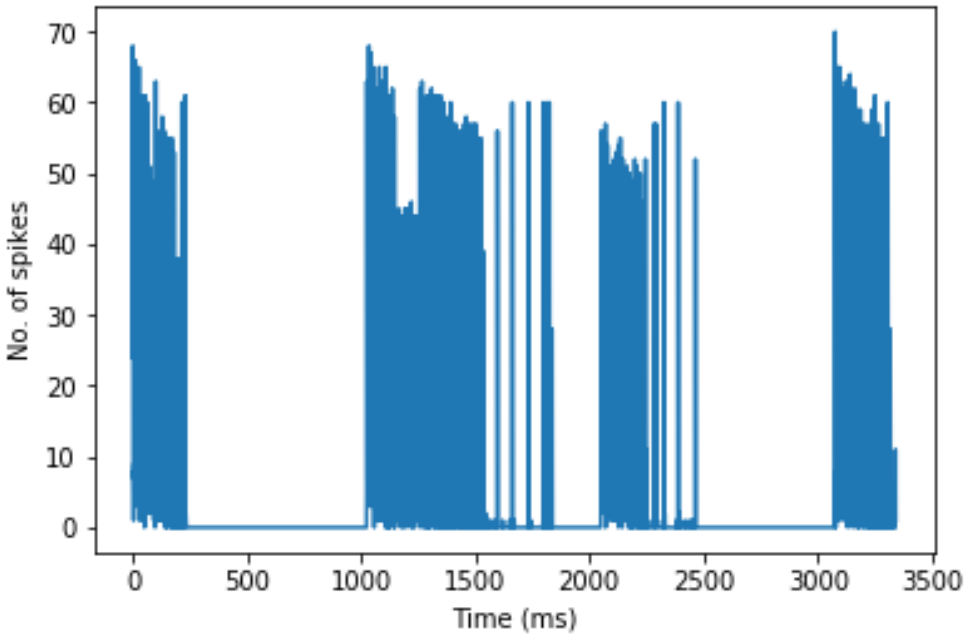

Figure 4.16: *Number of spikes in the piano class.*

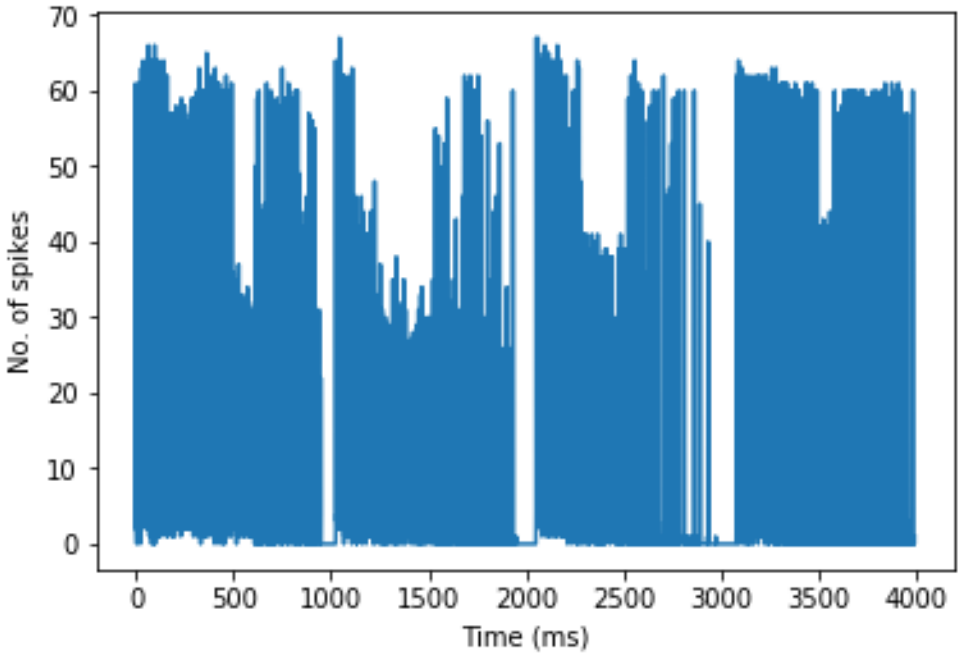

Figure 4.17: *Number of spikes in the violin class.*

arrival times at the output neuron as illustrated in Fig. 4.14 and Fig. 4.15. The x-axis shows the number of times the neuron is fired, and the y-axis shows the difference between the spike arriving at time $t, t + 1, t + 2$ and so on. There is a noticeable difference in the pattern of ISI for both classes. Extracting information from temporal encoding shows the power to be useful for classification purposes.

4.4 Conclusion and Discussion

The proposed 2-layered temporal-based SNN with Gamma and RMSE as the classification criteria successfully distinguished two musical instruments with a classification accuracy of 92.38% and 93.19%, respectively.

The findings of this chapter are a) highlight the importance of temporal-based spiking features for time-series classification, b) the strength of SNN with less number of neurons (less than 70) and few training samples (10 samples in total) achieving

higher accuracy, c) the application and relevance of coincidence factor and RMSE computed from spike timings and neuronal membrane potential respectively to estimate the category of the input d) demonstrate structurally optimised networks for producing distinguishable spiking activity using DE, a derivative-free optimisation strategy, and e) demonstrate the crucial role of analysing neural firing patterns which can potentially contribute in feature binding process.

Understanding the rhythmic nature of these neurons through analysing neural activity gave insights into the behaviour of two different musical instruments. The attributes derived from voltage and spiking timings of the output neuron proved our second hypothesis that temporal patterns in neuronal information could boost classification performance.

The future work of this research includes a) the SNN model is yet to be tested on a benchmark dataset, b) hybrid computation of weighted Gamma and RMSE as classification criteria as shown in Equation 4.3. RMSE is weighted more than Gamma as it produced better results, c) evaluates the proposed deep SNN on polyphonic music signals and d) this research opened a research avenue in the music domain as well by implementing a layered SNN, which can be further extended to study the impact of music on the brains of these patients (Z. Doborjeh et al., 2019) (Shah et al., 2019).

$$GammaRMSE = [0.6(RMSE) * 0.4(Gamma)]/2 \tag{4.3}$$

4.5 Chapter Summary

This chapter discussed the importance of a layered organisation in ANNs, the common nature of EEG and music signals, the significance of rate and temporal coding techniques, the introduction to spike-train distance, and the relevance of under-utlilised

neuronal membrane potential. We presented our 2-layered temporal-based SNN architecture, outperforming ML models with rate coding techniques for recognizing piano and violin signals. The results showed that the temporal coding techniques outperform the rate coding techniques, thus, demonstrating the significance of temporal information encoded by spiking neurons from the input representations.

This architecture validated our hypothesis and proved a breakthrough in Automatic musical instrument recognition (AMIR) using SNNs. This research contributes to the music domain and has been published as a journal (Shah et al., 2022).

The second phase of this research is completed with Chapter 4. In the next chapter, the performance and effectiveness of our proposed architecture are demonstrated on another spatiotemporal dataset - EEG signals.

Chapter 5

SNN Opportunities for EEG Classification: Strategic Information Flow and Identification of Biomarkers

This chapter provides a methodology for applying SNNs to produce temporal-based feature extraction and classification of EEG signals.

Chapter 3 explored the capability of spiking neurons and STDP in distinguishing healthy and depressed groups using the NeuCube model. The overall accuracy of the NeuCube model for classifying depressed versus healthy subjects was 68.18% (EC) and 72.13% (EO). In Chapter 4, the proposed temporal architecture with the RMSE metric as the classification criterion performed well amongst the other rate coding and Gamma metrics for musical instrument recognition.

In this chapter, we apply the earlier proposed architecture of chapter 4 to EEG signals for depression detection. To test the robustness of this architecture, it is applied to two different public datasets - Figshare and PREDICT. After EEG classification, the traditional methods of psychology using EEG are studied to design and optimise the SNN framework for clinical management. The efficient way for information to

flow from EEG signals to the SNN model and prominent brain regions for depression detection is identified using these methods.

This chapter addresses the third research question, RQ3 as mentioned in Section 1.7:

1. How to design an SNN framework to produce temporal-based feature extraction for classifying spatiotemporal data such as EEG signals?

   (i) Can the temporal neural coding techniques applied in SNN architecture classify complex EEG datasets?

   (ii) How effectively can the temporal-based SNN architecture classify EEG signals when combined with the traditional methods of psychology?

The first research question is answered by applying the proposed 2-layered architecture to the Figshare public dataset. The second research question is answered by studying the role of functional connectivity between different brain regions of healthy and depressed subjects using the PREDICT dataset.

The research questions addressed in this chapter are related to hypothesis H2: Spiking neurons containing valuable temporal data can encode the rhythmic behaviour of EEG signals and perform well for EEG classification.

5.1 Introduction

Classification using EEG signals faces many challenges that may be detrimental to the classification tasks: (a) EEG signals have low signal-to-noise (SNR) ratio because of the environmental and physiological conditions under which they are recorded, containing many artifacts. Artifact reduction may remove useful information and is also time-consuming. (b) Generalisation across various subjects is challenging due to

the physiological differences between individuals. To resolve these challenges, several researchers have developed an EEG processing pipeline for cleaning, extracting relevant features, and applying classification/regression models to transform the low-level (raw data) features into high-level features (after feature extraction processes like the use of a filter, signal magnitude, correlation score, etc.). However, AI techniques have revolutionised the handling of EEG data because of their ability to learn raw data features automatically.

Studies from a review of 154 papers about the application of DL to EEG signals showed that using raw EEG signals directly as input to the network yields better classification performance (Roy et al., 2019) as compared to the models with a feature extraction module (using traditional ML techniques). CNN achieved a classification accuracy of 87% with raw EEG signals, whereas it reached only 84% accuracy when calculated features were used as inputs (A. Craik, He & Contreras-Vidal, 2019) for emotion recognition. Authors in (Antelis, Falcón et al., 2020) carried out experiments for the recognition of motor imagery tasks from EEG signals using SNN in two different settings: in Stage 1, the authors performed the classification task after the feature extraction methods of PSD and Wavelet Decomposition (static features) with a classification accuracy of 90%; in Stage 2, implementation with raw EEG signals (time-space property of EEG signals) achieved a classification accuracy of 97.22%. The classification performance was increased in stage 2 due to the capability of spiking neurons for analysing data sequences. This strength of spiking neurons for automatic temporal feature extraction from EEG signals was the major caveat of this study.

Such promising results allow us to apply raw EEG signals in classification tasks. Thus, this chapter uses raw EEG signals (after removing artifacts) as input to our proposed SNN model for depression detection.

Depression detection includes either interview based-assessment or automatic detection using computational tools. Using these computational frameworks and non-invasive

neuroimaging tools like EEG signals or fMRI, mental illness could be detected by the effectiveness of different brain regions' communication with each other (J. Wang et al., 2020; Al Zoubi et al., 2019; Kragel et al., 2022; Shim et al., 2018; M. L. Elliott et al., 2018), or through brain activity patterns (Stevens et al., 2021) for early intervention and better treatment outcomes. Structural connectivity refers to the anatomical organisation of different brain regions, and functional connectivity is defined as the relationships developed between brain regions over time. The configuration of structural connections formulates the functional connectivity within the brain (Stevens et al., 2021).

The magnitude and direction of the information flow between two or more connected brain regions (Ewald et al., 2013; Nolte et al., 2008) lead to pattern development over time which is the basis for understanding functional behaviours in the brain. These patterns and alterations are visible in structural and/or functional connectivities within and between brain regions of affected individuals (de Kwaasteniet et al., 2013; Du et al., 2018). Researchers have found extensive alterations in the functional connectivity of frontal-limbic network in depressed groups (Thibodeau et al., 2006; Ahmadlou et al., 2012). Irregularities in information processing that disrupt cognitive functioning are also reported as one of the symptoms (Warren et al., 2015; Roiser & Sahakian, 2017; R. Elliott et al., 2011). Analysis of information flow through inter- and intra-hemispheric connections and long- and short-range communications are of great significance for the clinical diagnosis and treatments (Thibodeau et al., 2006; Güntürkün et al., 2020).

EEG signals recorded from brain regions at timescales represent the spiking behaviour of neurons. On the other hand, SNNs model spiking neurons capable of analysing temporal information efficiently. However, applying SNNs to produce temporal-based feature extraction and classification is still poorly understood or under-explored (Khosla et al., 2021). There is no optimal design of the SNN framework that explored these traditional approaches of information flow through inter- and intra-hemispheric connections and long- and short-range communications from raw EEG signals.

This integration of AI, neuroscience, and psychology can provide a way to identify biomarkers that could possibly supplement clinical decision-making. Various EEG biomarkers have been recognised during the study of depression. Depression is linked with aberrant structural and functional connectivity observed in the orbitofrontal, the anterior cingulate, the hippocampus, the basal ganglia, and the amygdala areas of the brain (Disabato, Bauer, Soares & Sheline, 2016). Considering the Power Spectral Density (PSD) of EEG signals, different findings have been reported in the literature: Frontal alpha symmetry (FAA) (Fingelkurts & Fingelkurts, 2015; Gollan et al., 2014); functional abnormality in centro-parietal-occipital sites, and prefrontal cortex (decreased alpha oscillations) (Wan et al., 2020); inter-hemispheric asymmetry in frontal, central and occipital brain regions (Duan et al., 2020); lower power values (alpha and theta bands) in central, temporal, occipital, parietal, and frontal areas of the brain for depressed individuals as compared to a control group (Bachmann et al., 2018), differences in the left hemisphere (C3, O1, P3, T3, F7) and right hemisphere (O2) (Hosseinifard et al., 2013).

A good biomarker is simple, workable, validated thoroughly, and easily understandable by clinicians (Hahn, Nierenberg & Whitfield-Gabrieli, 2017; Gabrieli, Ghosh & Whitfield-Gabrieli, 2015; Dubois & Adolphs, 2016). In Chapter 3, we have identified a few potential biomarkers through FIN visualisation, and, in this chapter, we perform extensive analysis on identifying and validating these biomarkers by evaluating the classification performance of the SNN model using six different brain regions.

This chapter aims to achieve the following research objectives:

1. To evaluate the effectiveness of the proposed temporal-based SNN architecture for EEG classification.

2. To design an efficient SNN framework to produce temporal-based feature extraction for EEG classification.

(i) to optimise the information flow into the SNN, and

(ii) to identify prominent brain regions in depression

This chapter provides an opportunity to effectively integrate AI, neuroscience, and psychology by designing an end-to-end SNN framework that can be applied in clinical settings.

5.2 Literature Review

This section briefly overviews the existing studies using the Figshare dataset for depression detection.

The authors in this study (Mumtaz, Xia, Mohd Yasin, Azhar Ali & Malik, 2017) proposed an ML approach using an LR model for the classification task. Feature extraction methods involved wavelet techniques and a combination of wavelet, STFT, and EMD approaches. The best features were selected based on the rank-based method according to ROC criteria. One hundred iterations of the 10-fold cross-validation technique were used for training. The model trained with features extracted from the wavelet techniques achieved accuracy, sensitivity, specificity, and F-measure of 89.6% (+/-5.1), 81.7% (+/-11.3), 96.7% (+/-3.1), 0.77% (+/-2.9) respectively. On the other hand, the model trained with combined features obtained accuracy, sensitivity, specificity, and F-measure of 90.5% (+/-8.3), 91.6% (+/-5.7), 88.7% (+/-7.5), 84% (+/-3.6) respectively.

The authors (Saeedi, Saeedi & Maghsoudi, 2020) analyzed 2,000 samples (7.8 s) of 64 subjects (30 normal and 34 depressed) by frequency power of EEG signals and wavelet packet decomposition entropies. They used Welch's periodogram on every channel to extract power bands: delta (0.5–4 Hz), theta (4–8 Hz), alpha (8–13 Hz), beta (13–30 Hz), and gamma (30–50 Hz) allowing 50% overlap between segments

with a Hamming window (frequency-based features). They also used the wavelet packet decomposition technique to separate breakdown signals into certain low and high frequencies (time-frequency based features). Approximate entropy and sample entropy were applied to the wavelet packet co-efficients as non-linear features. The genetic algorithm identified the best features amongst these attributes using linear SVM, enhanced KNN, and MLP classifiers trained using a 10-fold cross-validation technique.

The statistical Student's t-test was used to test the usefulness of the features. Gamma power showed a significant difference between patients with depressive symptoms and control subjects. A significant difference was observed in the non-linear features drawn out from the signals with wavelet packet decomposition and entropies. Some of the key discoveries of this study are: gamma power is higher in depressed individuals than the control subjects, non-linear features indicate better performance than the linear features, and the genetic algorithm expressed O1, O2, Pz, T6, and Fp2 EEG channels as the highest weighted features. The authors concluded that future research should investigate the gamma band for depression-oriented studies.

Table 5.1 shows the classification accuracy of various ML models with different feature extraction methods.

Table 5.1: Results of classification accuracy
(Saeedi et al., 2020)

Methods	**Results**
1. Frequency-based features	The highest accuracy was achieved from gamma oscillations in all the classifiers. **SVM** 87.93% (+/-4.5) **E-KNN** 91.38% (+/-3.8) **KNN** 86.27% (+/- 5.2) **MLP** 82.67% (5.8) E-KNN was successful in achieving the highest accuracy of 92% when trained together with all the band powers. **SVM** 89.96%(± 5.3) **E-KNN** 92.00%(± 6.1) **KNN** 82.47%(± 6.8) **MLP** 88.33%(± 7.2)

Continued over page

Table 5.1: Results of classification accuracy... *(continued)*

Methods	Results
2. Time-Frequency based features	Best accuracy was achieved using both the non-linear features as input to the E-KNN classification algorithm. **SVM** 91.38%(± 4.5) **E-KNN** 94.28%(± 3.0) **KNN** 82.47%(± 5.3) **MLP** 90.00% (± 6.8)
3. Linear and non-linear based features	Linear SVM performed well when trained together with linear (power bands) and non-linear (entropies) features. **SVM** 93.75%(± 4.8) **E-KNN** 93.10%(± 4.4) **KNN** 87.93%(± 5.3) **MLP** 92.18%(6.6)

Continued over page

Table 5.1: Results of classification accuracy... *(continued)*

Methods	Results
4. Selected features by genetic algorithm	Proposed weighted E-KNN consisting of 14 features showed the highest accuracy, sensitivity, and specificity. **SVM** 95.31%(± 5.2) **E-KNN** 98.44%(± 3.4) **KNN** 92.18%(± 6.9) **MLP** 93.75%(± 6.8)

All of the studies mentioned above include extensive feature extraction steps that remove important information, especially sequential temporal information. Despite the high accuracy of the classification results of EEG data, none of the papers reviewed above reported the actual brain patterns that can be used to distinguish the groups. There are gaps related to applying brain features underlying depression in ML.

Next, existing studies that identified biomarkers using SNN and EEG signals for emotion recognition have been reviewed.

The authors in (Alzhrani, Doborjeh, Doborjeh & Kasabov, 2021) employed NeuCube framework (a brain-inspired SNN architecture) (N. K. Kasabov, 2014) used DREAMER's dataset (Katsigiannis & Ramzan, 2017) for emotion recognition using EEG signals. The EEG signals were recorded by presenting stimuli in the form of different pictures to the subjects – excitement, amusement, sadness, fear, anger, disgust, happiness, calmness, and surprise. EEG data consisted of 128 timepoints, 14 EEG channels (AF3, F7, F3, FC5, T7, P7, O1, O2, P8, T8, FC6, F4, F8, AF4), and 23 samples of each. The average classification accuracy of this model was 94.83%, whereas MLP

produced an accuracy of 79.69% using grid search optimisation. Further, this research concluded that positive emotions are linked with increased neuronal activation in frontal areas (F7, F3, AF4). In contrast, negative emotions caused an increase in synaptic strengths in the frontal ((F4, AF3, F7, F8)) and parietal (P7, P8) regions of the brain.

Another study (He, Li & Ju, 2021) was conducted on a public dataset, i.e., DEAP dataset (Koelstra et al., 2011) using the NeuCube (N. K. Kasabov, 2014) framework for an emotional binary valence classification task. The EEG signals were downsampled to 128 Hz from 512 Hz. The authors chose only four EEG signals with the last 30 seconds recording to achieve computational efficiency, so the dataset finally consisted of 32 subjects with 40 samples per subject. After using grid optimisation, the model achieved a classification accuracy of 68.91% with 10-fold cross-validation. Further, they found that channels F3 and F4 were more informative than Fp1 and Fp2 for this classification problem.

Both of these used the same architecture with different input characteristics. The second study's performance was relatively low compared to the first one due to the downsampling of EEG signals and four EEG channels with 30 seconds of temporal information. Also, the deSNN module used for supervised learning utilises the first order of spikes neglecting the rest of the temporal pattern for making classification decisions. These studies use 1471 spiking neurons in their architecture, increasing the computational cost. On the other hand, these studies gave us an understanding of critical brain areas involved with negative emotions (indicative of depressive symptoms) and positive emotions and showed the successful integration of SNN and EEG signals for classification purposes.

5.3 Methods

5.3.1 Dataset Description

Each subject of the proprietary dataset used for depression detection in Chapter 3 consisted of 16,383 rows (timepoints) and 61 columns (features). To have more samples for better learning and classification performance, we divided each sample into three more samples generating 66 samples altogether (30 depressed, 36 healthy) with 5,461 time points (rows) in each sample, keeping the number of columns (i.e., 61) consistent. We have used different public datasets in this chapter to test and validate the effectiveness of our proposed temporal architecture for spatiotemporal data classification.

Figshare Dataset

Wajid Mumtaz collected this dataset (Mumtaz, 2016) in 2016 at Hospital Universiti Sains Malaysia (HUSM), Kelantan, Malaysia. He recorded the EEG signals according to the international 10±20 system from various brain regions: the frontal lobe included seven electrodes: Fp1, F3, F7, Fz, Fp2, F4, and F8; the central brain region had C3, C4, and Cz; the parietal lobe included P3, Pz, and P4; the occipital involved O1, O2; and the electrodes T3, T4, T5, T6 covered left and the right temporal region of the brain – 19 EEG channels.

MDD patients met the internationally recognised diagnostic criteria for depression (DSM-IV). The participants were psychiatrically examined and then identified as depressed or healthy with BDI-II scores greater than ten and less than 10, respectively. The dataset comprised 28 healthy subjects and 28 MDD patients in eyes-closed (5 minutes) and eyes-open (5 minutes) states at a sampling frequency of 256 Hz.

PREDICT Dataset

This dataset comprises 46 patients and 75 healthy controls, 121 subjects in total (Cavanagh, Napolitano, Wu & Mueen, 2017; Cavanagh, Bismark, Frank & Allen, 2019). The depression level of all the participants was measured using BDI and the Spielberger Trait Anxiety Inventory (TAI) through the Structured Clinical Interview for the Depression process. The dataset consists of 64 EEG channels recorded at a sampling frequency of 500 Hz for 4,000 ms in resting eyes closed condition. The list of EEG channels includes FP1, FPZ, FP2, AF3, AF4, F7, F5, F3, F1, FZ, F2, F4, F6, F8, FT7, FC5, FC3, FC1, FCZ, FC2, FC4, FC6, FT8, T7, C5, C3, C1, CZ, C2, C4, C6, T8, TP7, CP5, CP3, CP1, CPZ, CP2, CP4, CP6, TP8, P7, P5, P3, P1, PZ, P2, P4, P6, P8, PO7, PO5, PO3, POZ, PO4, PO6, PO8, O1, OZ, O2. Subjects with a BDI score greater or equal to 15 were considered as the depressed group, and subjects within the healthy group had a BDI score less than 15.

The Figshare and PREDICT datasets were used for depression detection using raw EEG signals. Further, the PREDICT dataset was used to optimise our proposed architecture's end-to-end design by applying traditional psychology methods for depression detection. Since SNN is known for its small-sample learning ability (Tavanaei & Maida, 2016; Rekabdar et al., 2017, 2018), we have reduced the dataset in terms of subjects. The SNN model was trained using 22 samples (11 healthy and 11 depressed) and tested on eight samples (four healthy and four depressed) on both datasets. To the best of our knowledge, SNN frameworks have not yet been applied to these open datasets for EEG classification.

5.3.2 2-layered SNN Architecture

The proposed 2-layered temporal-based SNN architecture with RMSE metric as described in Section 4.2.2 was used to answer the research questions.

The following provides a brief overview of this framework for EEG classification:

1. The public dataset initially available in .edf (Wikipedia contributors, 2020) format is transformed to .csv format using the MNE Python library (Gramfort et al., 2013). Due to the high variability in the range of EEG values, Z-score standardisation, is used as a pre-processing step for the EEG signals.

2. The BSA algorithm encodes the EEG signals into spike trains. The parameters of the BSA algorithm are optimised using the DE algorithm to get accurate spike trains.

3. All the input nodes are connected to all the LIF neurons in the hidden layer and all the LIF neurons from the hidden layer are connected to an output LIF neuron in the output layer. The STDP learning rule is used to adapt the weights between these layers.

4. The dataset is divided into an 80%-20% ratio for training and testing purposes. Leave one out cross-validation method is applied to the 80% training data.

5. The RMSE metric calculated from the spiking neuron's membrane potential in the output layer is employed as the classification criterion. This metric is computed between all the training and the test/validation samples. The label of the training sample, which has the least RMSE value among all the pairs, is assigned as a label to the test/validation label.

6. The optimisation algorithm aimed to find the best SNN parameters. Various parameters governing the dynamics of the Leaky-Integrate-Fire neuron (the threshold and the refractory period) and STDP algorithm (the maximum and the minimum synaptic change), along with the number of spiking neurons and the range (minimum and maximum value) of the synaptic weights were optimised using the DE algorithm.

5.4 Experiments and Results

5.4.1 Experiment design

The experimental design to achieve the first research objective of this chapter to evaluate the effectiveness of our proposed temporal-based SNN architecture for EEG classification was quite straightforward. In the case of the Figshare dataset, the central 1000 time points from 76,800 time points with 19 EEG channels per sample were used for depression detection. This experiment tested the effectiveness of the proposed 2-layered SNN architecture with temporal coding techniques on complex raw EEG signals. Sensitivity was chosen as the fitness function for this experiment. It is defined as the ratio between how many participants were identified as depressed to how many were actually labelled as depressed. (Note: not having enough computing hardware to speed up the computation process was the reason to use only 1000 time points for two generations of DE. Optimisation with 76,800 time points would have been time-consuming.)

To achieve the second research objective of this chapter, to design an efficient SNN framework to produce temporal-based feature extraction for EEG classification, the PREDICT dataset was used. The input from EEG signals to the proposed was designed with different traditional approaches inspired by psychology. The following section explains in detail the different input configurations to (a) identify the best way of information flow from EEG data to SNN by comparing four input configurations and (b) identify the potential brain regions. The F1-Score (Flach & Kull, 2015) was used as the fitness function. It is defined as the harmonic mean of precision and recall measures. Recall ensures that the model is not overlooking the people with depression, while precision ensures it is not misclassifying too many people as having depression when they do not. A good model will have high true positives and negatives and fewer false positives and false negatives (Flach & Kull, 2015). In other words, a good model

is one that will not predict a person with depression as healthy and also will not predict a healthy person as depressed. Thus, a metric, i.e., F1-Score, that considers precision and recall were important to evaluate the model (Jordan, 2021).

Input Configurations: Traditional approaches Inspired by Psychology

The information flow into the brain and among different brain regions affects cognitive functioning (Warren et al., 2015; Roiser & Sahakian, 2017; R. Elliott et al., 2011), which might indicate a mental disorder. The PREDICT EEG dataset used here consists of 64 channels. Different brain regions considered important for studying depression are illustrated in Figure 5.1. The EEG electrode montage for 64 channels is shown in Figure 5.2. The EEG channels with odd numbers represent electrical information from the left hemisphere, whereas information from the right hemisphere is indicated with an even number on the EEG electrode.

Based on the prominent brain regions identified in depression, as described earlier, we have extracted a small subset of EEG channels from the original dataset. Additionally, information redundancy and computational complexity are increased with multichannel EEG signals (Shen et al., 2020).

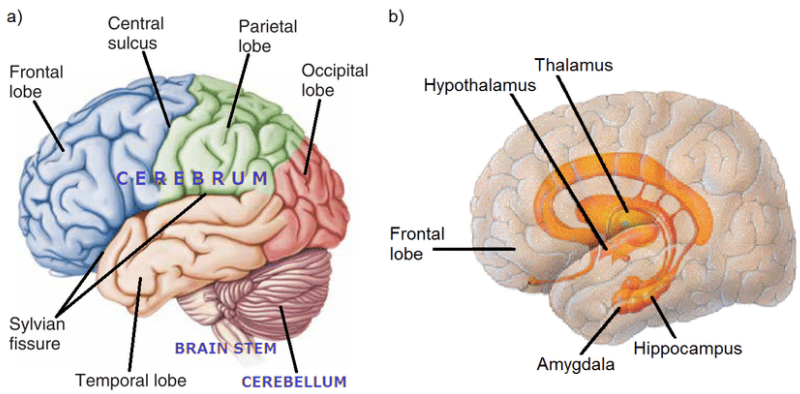

Figure 5.1: *Graphical Representation of the Major Parts of the Brain Structures from (Falcone & Villanueva, 2017)*

Input Strategy: Flow of Information to SNN

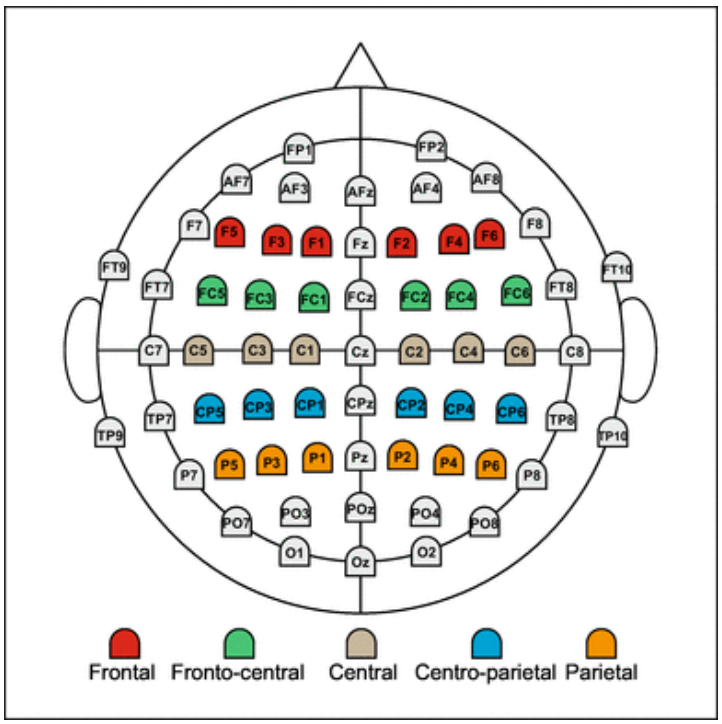

Figure 5.2: *EEG electrodes montage with 64 channels for recording EEG signals from (Behroozmand & Sangtian, 2018)*

After selecting a subset of EEG channels, the input module, i.e., the information flow of EEG signals to the proposed SNN architecture, was strategised. The most prominent and traditional approaches in psychology for clinical diagnosis and treatments include information flow through inter- and intra-hemispheric connections and long- and short-range communications (Thibodeau et al., 2006; Güntürkün et al., 2020). Inspired by these methods, four different SNN frameworks were designed to understand these functional connectivities in healthy and depressed subjects, as described below. The input strategies designed were aimed at achieving the second research objective.

1. Difference in EEG channels: Studies by (Coan & Allen, 2004; Hu et al., 2011; Deslandes et al., 2008) have found asymmetries, i.e., anatomical and functional differences in the left and right hemispheres of the human brain. Based on this, an input strategy was devised by taking the differences between different EEG pairs. EEG signal information from the left hemisphere and another EEG channel

from the right hemisphere form one EEG pair. The n^{th} discrete difference (i.e., along the column axis) between each EEG pair was calculated and then fed as input to our proposed SNN architecture. This meant that the temporal information was retained. The difference between the following EEG pairs was calculated as shown in Table 5.2. "diff" indicates the n^{th} discrete difference between those EEG pairs calculated using the Numpy library in Python (Harris et al., 2020).

Table 5.2: Brain Asymmetry: Input Strategy

EEG channel 1	**EEG channel 2**	**Input**
F1	F2	diff([F1, F2])
F3	F4	diff([F3, F4])
F7	F8	diff([F7, F8])
F5	F6	diff([F5, F6])
C1	C2	diff([C1, C2])
C3	C4	diff([C3, C4])
C5	C6	diff(C5, C6])
CP3	CP4	diff([CP3, CP4])
P1	P2	diff([P1, P2])
O1	O2	diff([O1, O2])

2. Short- and Long-distant EEG channels: As defined earlier, functional connectivity studies the temporal correlations between different brain regions. Different approaches were examined in this study to obtain the best way to examine this connectivity. The development of normal brain functional networks is characterised by a “local to distant” organization (Fair et al., 2009). Brain regions with short-range functional connections are often specialised for modular information processing and operate with lower time- and energy-cost. By contrast, long-range functional connections allow integrative information processing across distributed brain systems with higher time- and energy-cost (Sepulcre et al., 2010). The balance of long- and short-range functional connections is critical for the

efficiency of cortical information communication and energy cost. People with mental health issues often show changes in functional connectivity with decreases in short- and long-range communications (Garcia-Casares et al., 2014; Guo et al., 2016, 2017).

Table 5.3: Short-distance Electrodes: Input Strategy

EEG channel 1	EEG channel 2	Input
F1	F5	mean([F1,F5])
F2	F6	mean(F2,F6])
F3	FC3	mean([F3,FC3])
F4	FC4	mean([F4,FC4])
FT8	FC6	mean([FT8,FC6])
C3	P3	mean([C3,P3])
C4	P4	mean(C4,P4])
T8	P8	mean([T8,P8])
T7	P7	mean([T7,P7])
O1	O2	mean([O1,O2])

Electrodes with less than 10cm distance between them were considered for the classification using short-distance EEG channels as shown in 5.3. Long-distance electrode pairs have greater than 10cm between them as shown in 5.4. The average of each electrode pair was calculated (temporal information retained) which then was fed as an input to our proposed SNN architecture.

The "mean" in Tables 5.3 and 5.4 represents the computation of the mean across the EEG electrode pairs using the Numpy library (Harris et al., 2020).

3. Grouped Features: 24 EEG channels were grouped into 8 clusters and averaged over each cluster.

Out of these four input settings, using "Brain Asymmetry" as the input to the SNN model showed better classification performance, and hence it is considered as the best information flow from EEG signals into the SNN model (refer to Section 5.4.2). Brain Asymmetry or differences between the left and right sides of the brain were further

Table 5.4: Long-distance Electrodes: Input Strategy

EEG channel 1	EEG channel 2	Input
F7	F8	mean([F7,F8])
F3	O1	mean([F3,O1])
F4	O2	mean([F4,O2])
T7	T8	mean([T7,T8])
P7	P8	mean([P7,P8])
FT7	FT8	mean([FT7,FT8])
FC5	FC6	mean(FC5,FC6])
F5	P5	mean([F5,P5])
C6	P6	mean([C6,P6])
TP7	TP8	mean([TP7,TP8])

Table 5.5: Grouped Channels Electrodes: Input Strategy

EEG channels	Input
F1,F7,F3,F5	Left Frontal: mean([F1,F7,F3,F5])
F2,F4,F6,F8	Right Frontal: mean([F2,F4,F6,F8])
C5,C3,C1	Left Central: mean([C5,C3,C1])
C2,C4,C6	Right Central: mean([C2,C4,C6])
P7,P5,P3,P1	Left Parietal: mean([P7,P5,P3,P1])
P2,P4,P6,P8	Right Parietal: mean([P2,P4,P6,P8])
T7	Left Temporal
T8	Right Temporal
O1	Left Occipital
O2	Right Occipital

explored to identify the potential EEG channels that can yield functional biomarkers of depression.

Input Strategy: Identification of Biomarkers The key brain structures identified in the existing literature and in Chapter 3 were selected to recognise the biomarkers of depression. This section describes the input configuration for the design of the SNN framework to achieve the third research objective.

1. Frontal Region Asymmetry: The difference between the right and left hemispheres of the frontal area was considered as the input to the SNN.

2. Asymmetry in Central Region: EEG channels across the central region of the

Table 5.6: Frontal Region: Input

EEG channes	Input
F1, F2	diff([[F1,F2]])
F3,F4	diff([[F3,F4]])
F7, F8	diff([[F7, F8]])
F5,F6	diff([[F5,F6]])

brain were chosen as the input here.

Table 5.7: Central Region: Input

EEG channes	Input
C1,C2	diff([[C1,C2]])
C3,C4	diff([[C3,C4]])
C5,C6	diff([[C5,C6]])

3. Asymmetry in Central-Parietal-Frontal Regions: Asymmetry within brain regions "Central-Parietal-Frontal" collectively was propagated to SNN.

Table 5.8: Central Parietal Frontal Regions: Input

EEG channes	Input
FC1,FC2	diff([[FC1,FC2]])
FC3,FC4	diff([[FC3,FC4]])
FC5,FC6	diff([[FC5,FC6]])
CP1,CP2	diff([[CP1,CP2]])
CP3,CP4	diff([[CP3,CP4]])
CP5,CP6	diff([[CP5,CP6]])

4. Asymmetry in Temporal-Frontal-Parietal Regions: The difference within the "Temporal-Frontal-Parietal" across the brain hemisphere was propagated to SNN.

5. Asymmetry in Parietal Region: The difference in an individual brain region (parietal) of the left and right sides of the brain was considered as an input here.

6. Asymmetry in Parietal-Occipital Regions:

   Asymmetry in "Parietal-Occipital" was derived using the difference between the EEG channels as shown below:

Table 5.9: Temporal Frontal Parietal Regions: Input

EEG channes	Input
TP7, TP8	diff([[TP7, TP8]])
T7,T8	diff([[T7,T8]])
FT7, FT8	diff([[FT7, FT8]])

Table 5.10: Parietal Region: Input

EEG channes	Input
P1,P2	diff([[P1,P2]])
P3,P4	diff([[P3,P4]])
P5,P6	diff([[P5,P6]])
P7,P8	diff([[P7,P8]])

5.4.2 Results

The first section presents the results measuring the effectiveness of the proposed temporal-based SNN architecture for spatiotemporal classification of raw EEG signals using the Figshare dataset. Next, the results obtained by applying the traditional methodologies from psychology to design an efficient SNN framework using the PREDICT dataset are described.

EEG Classification: Figshare Dataset

Table 5.13 shows the optimised parameters for training the SNN using 1000 timepoints of EEG signals at a sampling frequency of 32 Hz. Table 5.12 shows the descriptive statistics of different SNN parameters.

Table 5.14 shows the average classification results of 30 runs using the same SNN parameters as described in Table 5.13.

Visualisation: Temporal Patterns

Spike train analysis gives the opportunity to interpret the brain activity of healthy and depressed groups through the spiking behaviour of neurons. The visualisation in

Table 5.11: Parietal Occipital Regions: Input

EEG channes	Input
O1,O2	diff([[O1,O2]])
PO3,PO4	diff([[PO3,PO4]])
PO5,PO6	diff([[PO5,PO6]])
PO7,PO8	diff([[PO7,PO8]])

Table 5.12: Descriptive Statistics on 2^{nd} generation

SNN Parameters	Minimum	Maximum	Mean	Standard Deviation
LIF threshold	0.234228688	0.557771778	0.428488858	0.061920702
Refractory time	2.165485362	10.24575179	5.690159235	2.009474988
Potentiation magnitude	0.035910446	0.050552847	0.042802421	0.003005262
Depression magnitude	0.009559305	0.03281875	0.019422209	0.005184928
Number of neurons	82	117	93	8
Minimum weight (lower limit)	-0.758657954	0.111288935	-0.227255211	0.233414785
Max weight (upper limit)	0.891598267	7.986724728	3.399135364	1.990160628
Sensitivity	0.836252703	0.936252703	0.896252703	0.018440213

Chapter 3 explained the patterns that were developed in the 3D reservoir through the interaction of neurons with each other. Based on the spike times, the connections were strengthened and weakened using the STDP rule. This chapter discusses the spiking behaviour of neurons organised in a layered structure. Interpreting the sequences of spike trains that flows from input nodes to the output layer is useful in finding temporal patterns in both groups.

1. Raster plot:

   (a) Training Data:

   Figures 5.3 and 5.4 represent the behaviour of spiking neurons before the training process for healthy and depressed groups. The encoded data was propagated through the network of spiking neurons, and their firing activity was recorded. Figures 5.5 and 5.6 show the firing activity of the spiking neurons of both the groups after training. In both figures, the x-axis represents the time duration, and the y-axis represents the neurons. The blue

Table 5.13: Optimised Parameters for Training using RMSE metric

SNN parameters	Values
LIF threshold	0.395859
Refractory time	8.97133013
Potentiation magnitude	0.022398273
Depression magnitude	0.014139193
Number of neurons	112
Minimum weight (lower limit)	-0.066688
Max weight (upper limit)	0.537678967

Table 5.14: Average Classification Results on X_central 1000

Sensitivity	Accuracy	Specificity	Precision
0.83	80 %	80 %	100 %

dot represents the spiking event, i.e., the neuron has emitted a spike at the given time.

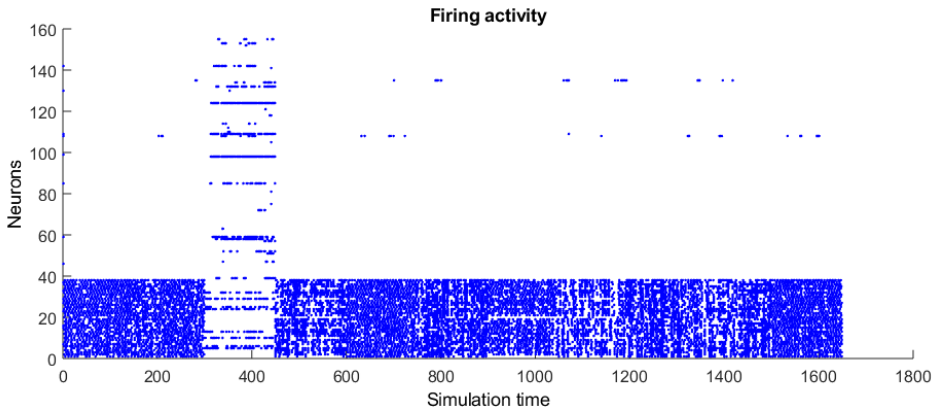

Figure 5.3: *Firing Activity of spiking neurons before training for Healthy subjects*

It is seen that for both groups, spiking neurons experienced more inhibition during the training process. The firing of spiking neurons has decreased post-STDP training. Spiking neurons show more excitation when stimulated with the MDD group samples than with those in the healthy group.

(b) Test Data:

Figures 5.7 and 5.8 were produced by propagating the test samples into the

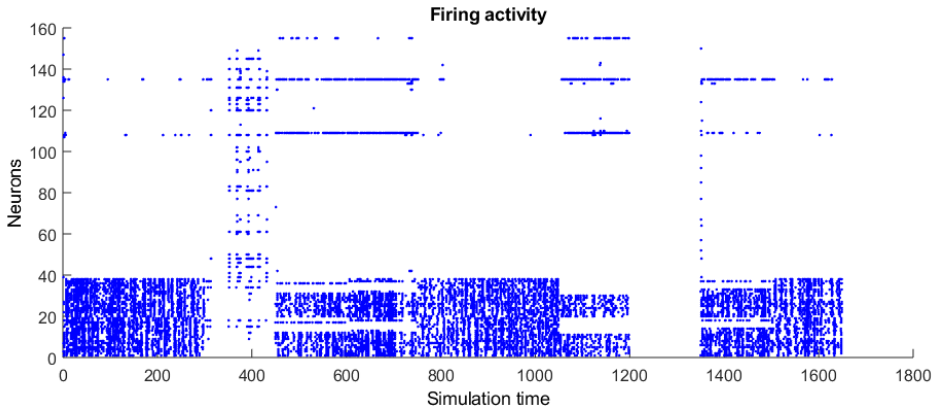

Figure 5.4: *Firing Activity of spiking neurons before training for MDD subjects*

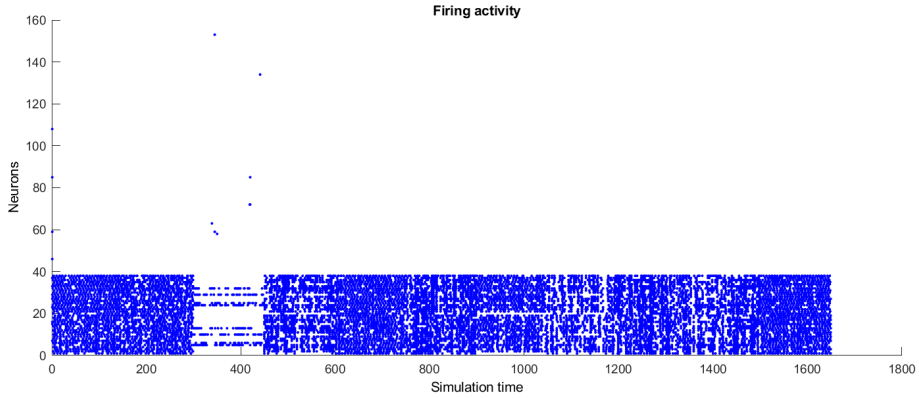

Figure 5.5: *Firing Activity of spiking neurons after training for Healthy subjects*

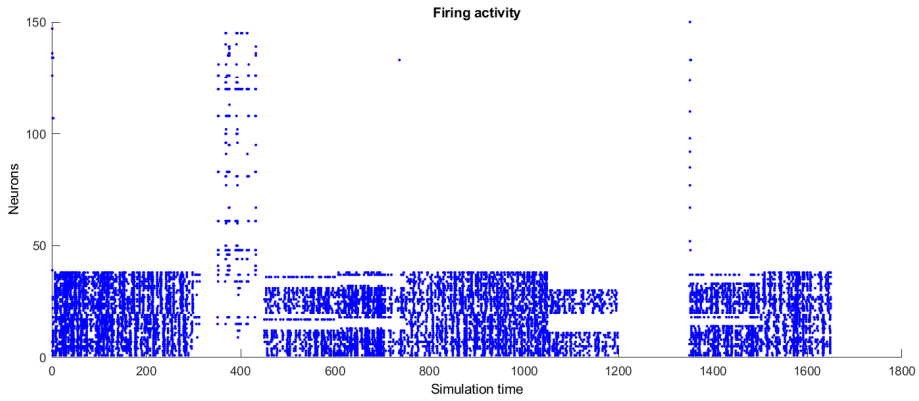

Figure 5.6: *Firing Activity of spiking neurons after training for MDD subjects*

pool of spiking neurons (the weights were not updated).

The firing activity shows a significant difference between the groups. The spiking

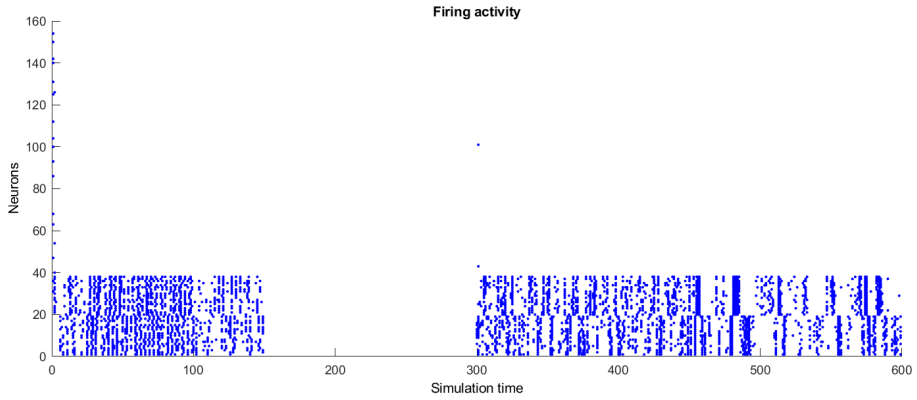

Figure 5.7: *Firing Activity of spiking neurons after training for Healthy subjects (test phase)*

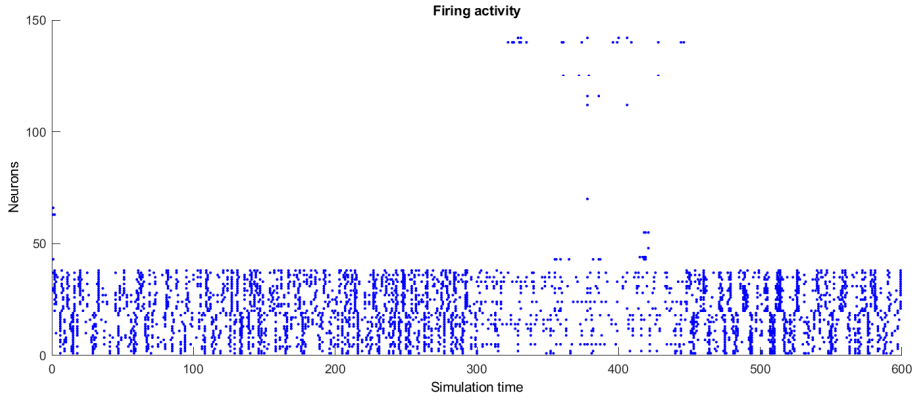

Figure 5.8: *Firing Activity of spiking neurons after training for MDD subjects (test phase)*

activity of neurons appears greater in the MDD group than in the healthy group. Thus, training the SNN model using temporal coding features separated both groups effectively.

2. Firing rate of spiking neurons: Firing rate defines the average of the number of spikes over a temporal scale. The firing rate of neurons depends on the intensity of the stimulating current and the time of stimulation.

   (a) Training Data: Figures 5.9 and 5.10 demonstrate that neurons emit more spikes (greater firing rate) within the time period of 1650 seconds when stimulated with MDD subjects. However, healthy individuals produce less fluctuation in spiking neurons' firing rate within the same time window.

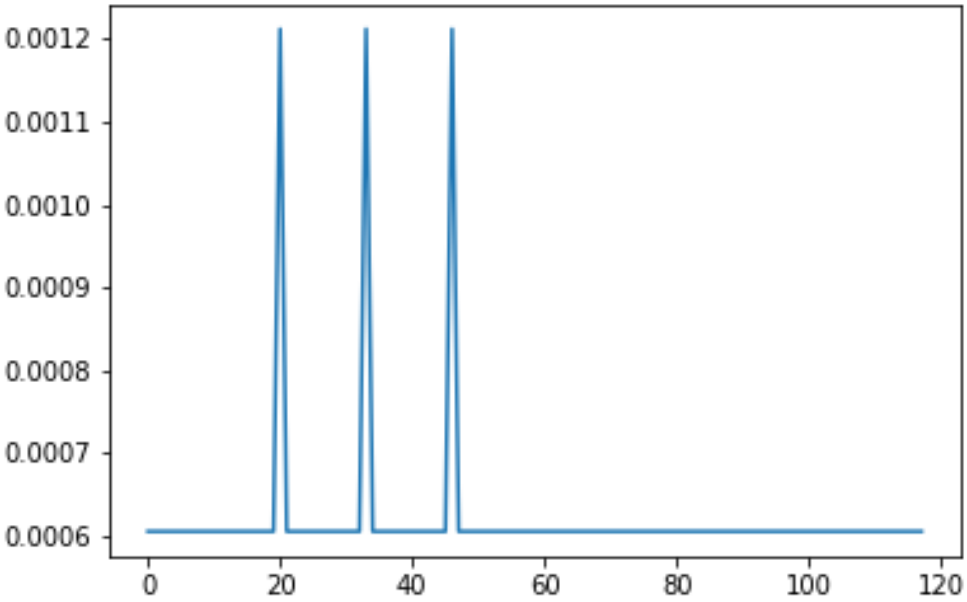

Figure 5.9: *Firing rate of spiking neurons after training for the healthy group - the x-axis represents the neuron number, and the y-axis represents the firing rate of the neuron*

(b) Test Data: Similar spiking neuron patterns were observed during test data propagation. The healthy group shows a constant firing rate, whereas the depressed group shows variability in the spiking behaviour of neurons as shown in Figures 5.11 and 5.12 respectively.

The figures illustrated here show the firing rate of all the neurons in the network. We have 38 input nodes, 116 hidden neurons, and one output neuron. In the training process, the firing rate of the hidden and output neuron in the healthy class lies within the range of 0.0006 and 0.0012. However, the firing rate for the MDD class lies between 0 and 0.014. When stimulated with the MDD samples, the neurons have fired multiple times and with higher firing frequency. The SNN learns spatiotemporal patterns from the input dataset to distinguish two classes. The learned pattern is reflected in the firing activities of the spiking neurons. In

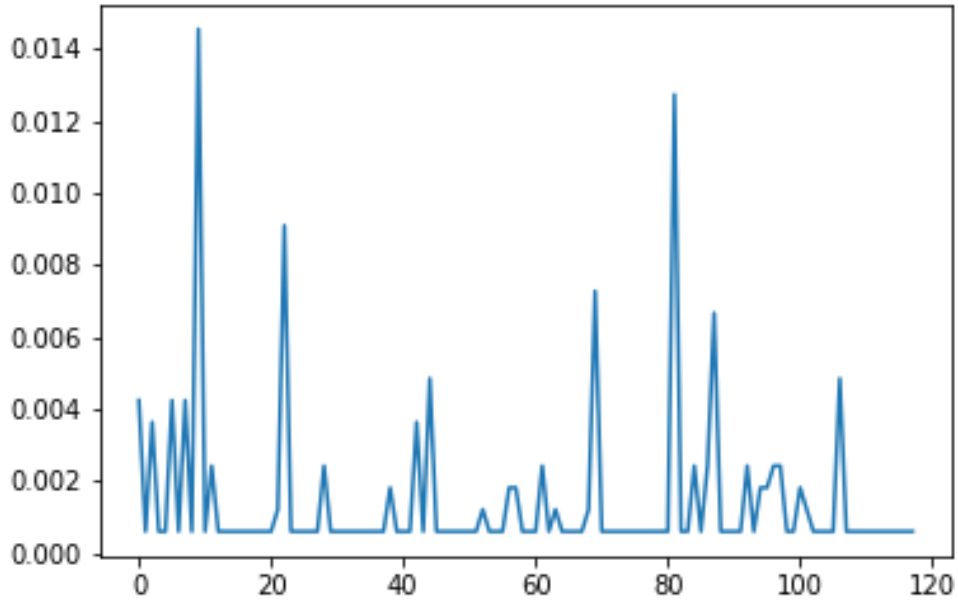

Figure 5.10: *Firing rate of spiking neurons after training for MDD group- the x-axis represents the neuron number, and the y-axis represents the firing rate of neuron*

this case, the SNN produced less firing activity (fewer spikes) when stimulated with healthy subjects and more firing (more spikes) during the stimulation of MDD subjects. Now, the trained SNN model recalls these relationships during the prediction process to predict a label to the input.

Less fluctuation in the healthy group means that, for these samples, information received by spiking neurons was separated by large time durations. Hence, they could not produce enough spikes, or these samples did not have enough information, i.e., spikes to excite spiking neurons.

3. Inter Spike Interval (ISI) distribution: ISI is the time difference between each pair of successive spike arrival times. In the figures presented below, the x-axis shows the ranges of difference in the spike arrival times (ISI) and the y-axis shows the number of spiking neurons under a given ISI distribution.

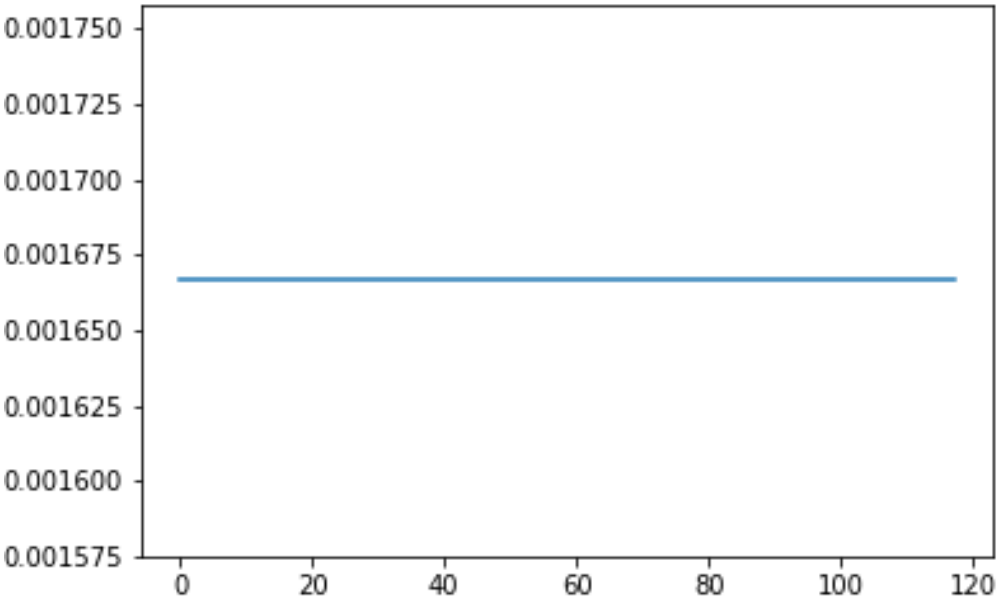

Figure 5.11: *Firing rate of spiking neurons for the healthy group- the x-axis represents the neuron number, and the y-axis represents the firing rate of neuron*

(a) Training Data: The ISI distribution amongst the spiking neurons of both the groups before and after the training process is illustrated in Figures 5.13, 5.14 and Figures 5.15, 5.16.

We can see that the time difference between the firing of few neurons is greater than 400 seconds in the healthy group during the training process and around 100 neurons have an ISI less than 100 as shown in Figure.5.15. On the other hand, the ISI distribution in the MDD group varies as shown in Figure 5.16 from 0 to 1400 seconds.

(b) Test Data: Spiking behaviour in terms of the ISI illustration shown in Figure 5.17 and Figure 5.18 clearly indicates MDD subjects have a broader range of ISI than the healthy group.

The firing rate analysis and ISI distribution of MDD show irregular spiking patterns

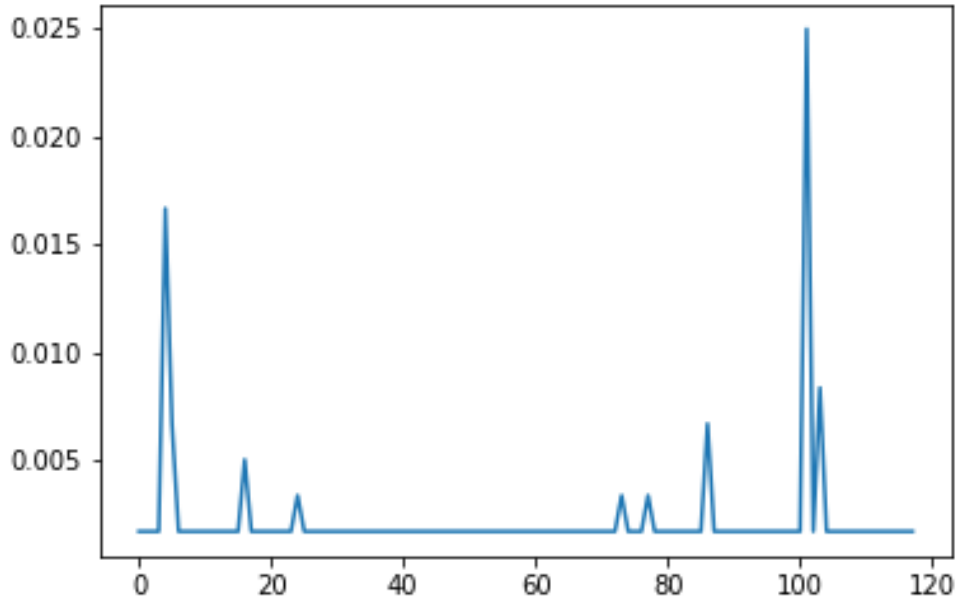

Figure 5.12: *Firing rate of spiking neurons for the MDD group- the x-axis represents the neuron number, and the y-axis represents the firing rate of the neuron*

compared to the patterns revealed by spiking neurons when stimulated by the healthy groups. This leads to the conclusion that there is increased spiking activity during the MDD stimulus.

Further, comparing the ISI before and after the training process, it is evident that the number of neurons with less than 100 seconds of ISI has reduced from 700 to 100 in the healthy group. Similarly, for the MDD group, it has dropped from 1000 to almost 200. The time difference between the two spikes is more distinguishable in pre and post-STDP training, which is one reason for the inhibition of SNN. Weight analysis can further provide details about the overall learning of the SNN model.

Overall Learning of SNN Network: Analysis of Weights

Along with the firing threshold and refractory time of the spiking neuron, the connection strength of the synapses (i.e., the synaptic current) greatly impacts the firing activity of

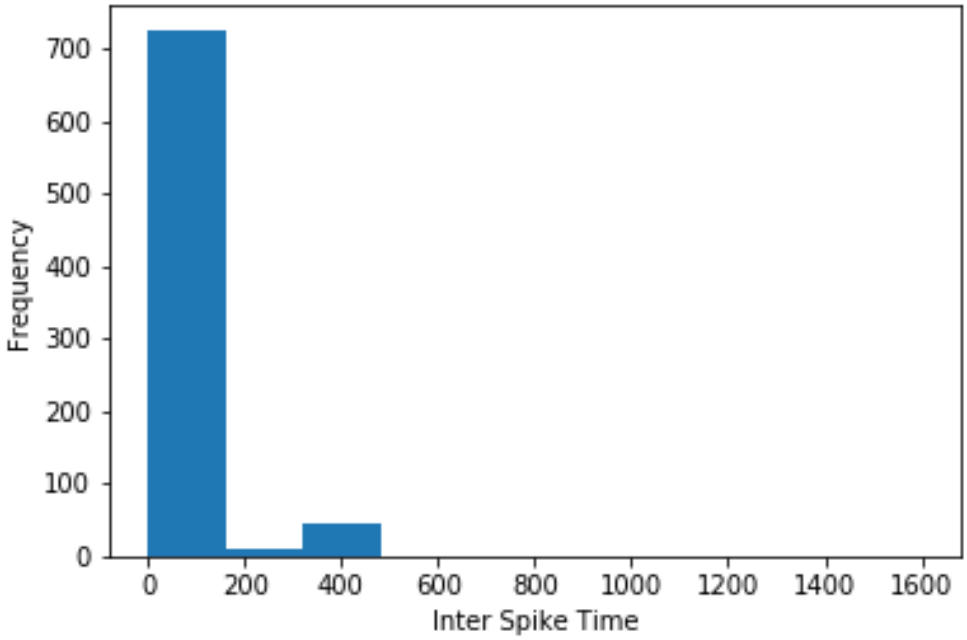

Figure 5.13: *Inter-spike intervals of spiking neurons in the hidden layer before training for the healthy group*

the spiking neurons. The polarity of the synaptic weights either causes excitation or inhibition in the SNN. A strong connection exists between weights and the number of spikes before and after the STDP training process.

Table 5.15: Spike Statistics

Groups	Pre-Training spikes	Post-Training spikes
Healthy group (training data)	785	121
MDD group (training data)	1163	279
Healthy group (test data)	-	118
MDD group (test data)	-	156

The number of spikes decreased tremendously, post-training, for both the groups, as shown in Table 5.15. On the other hand, the number of spikes is higher in the MDD group than in the healthy group. Table 5.16 shows that there were more negative weights in the SNN after the training process, and hence the SNN model experienced inhibition.

Spike train analysis using 1000 timepoints indicates significant differences in both

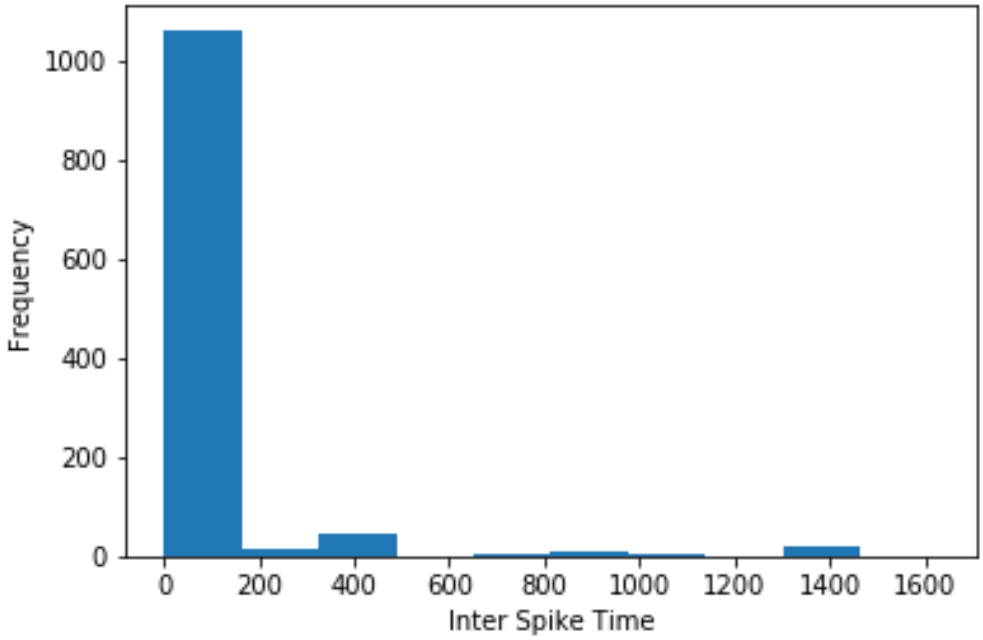

Figure 5.14: *Inter-spike intervals of spiking neurons in the hidden layer before training for the MDD group*

groups. Thus, our proposed SNN model could successfully classify both groups through temporal coding techniques.

Application of Methods from Psychology to SNN: PREDICT Dataset

To design an efficient SNN framework, four SNN models and six SNN models were implemented to achieve the research objectives: identifying the best input strategy and the biomarkers of depression. The results for each of these objectives are described in the following order a) Performance evaluation using F1 score for two generations of DE b) Comparative analysis using optimised SNN parameters using accuracy, recall, precision, recall, and F1 score c) Statistical analysis results: Student-t, Friedman and Wilcoxon tests.

All of these SNN models were evaluated using cross-validation techniques and compared against each other using their mean F1 scores. However, it is difficult to

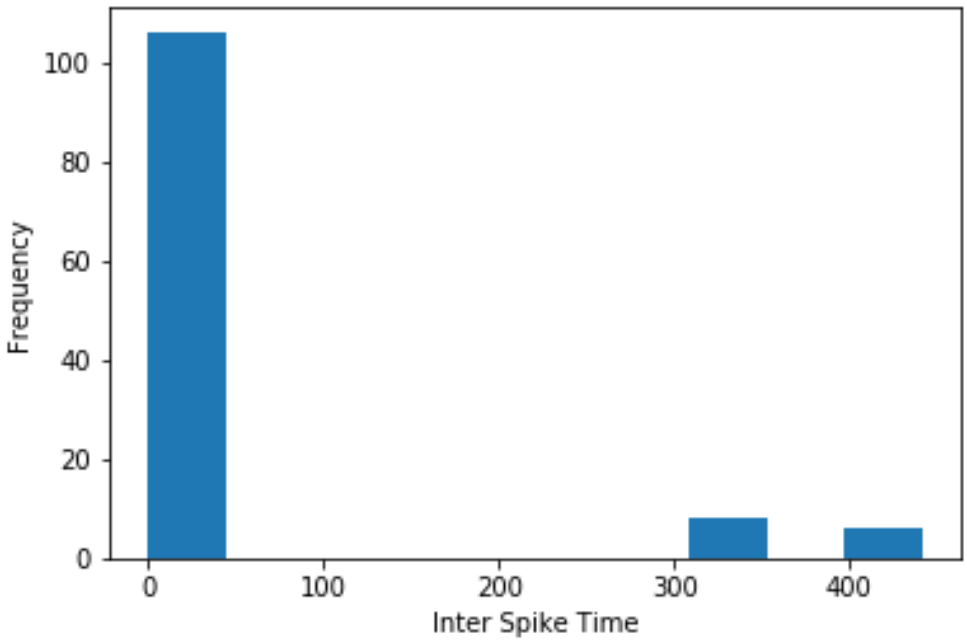

Figure 5.15: *Inter-spike intervals of spiking neurons in the hidden layer after training for the healthy group*

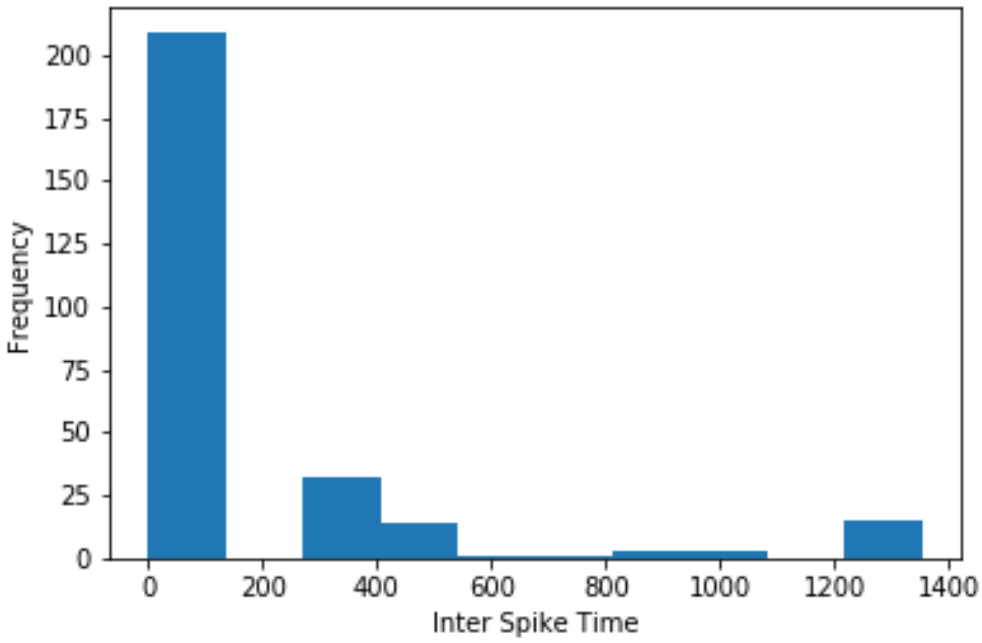

Figure 5.16: *Inter-spike intervals of spiking neurons in the hidden layer after training for the MDD group*

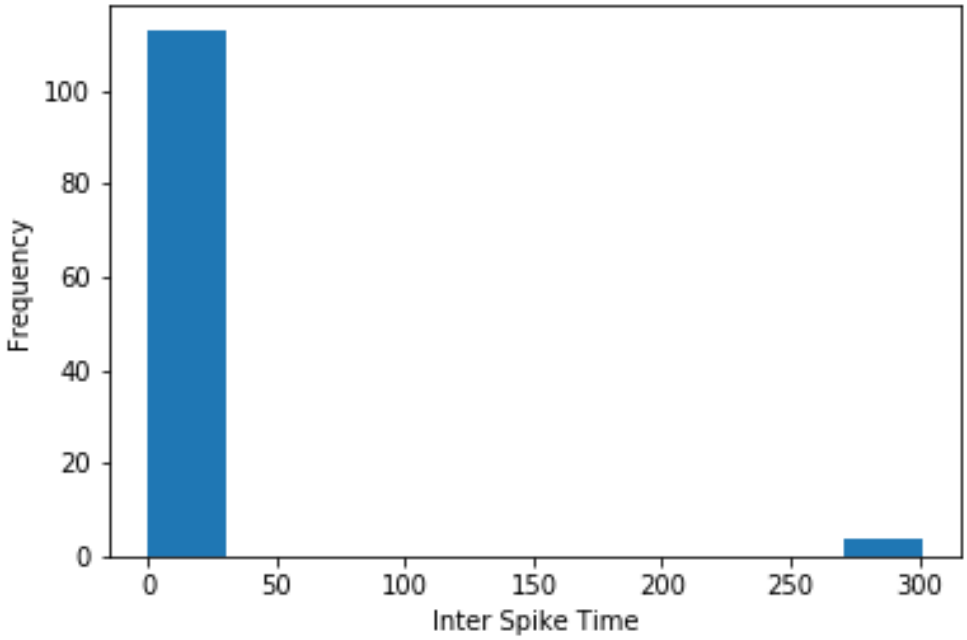

Figure 5.17: *Inter-spike intervals of spiking neurons in the hidden layer for the Healthy group (test phase)*

conclude if the differences between these models are real or if the results are a statistical fluke. Thus, these statistical tests are significant in comparing the performances of these models. All the SNN parameters in these ten models were optimised using DE. Detailed information on the statistics of optimisation and the optimised SNN parameters are added in Appendix A.

Efficient Flow of Information: Classification Performance

As mentioned earlier, seven different SNN parameters were optimised using DE with an F1 score as the fitness function. Table 5.17 presents the performance evaluation of four models on F1 score in the 2^{nd} generation of DE.

Table 5.18 shows the average classification results of 30 runs using the optimised SNN parameters. "Class 1" represents healthy individuals, whereas "Class 2" represents depressed individuals.

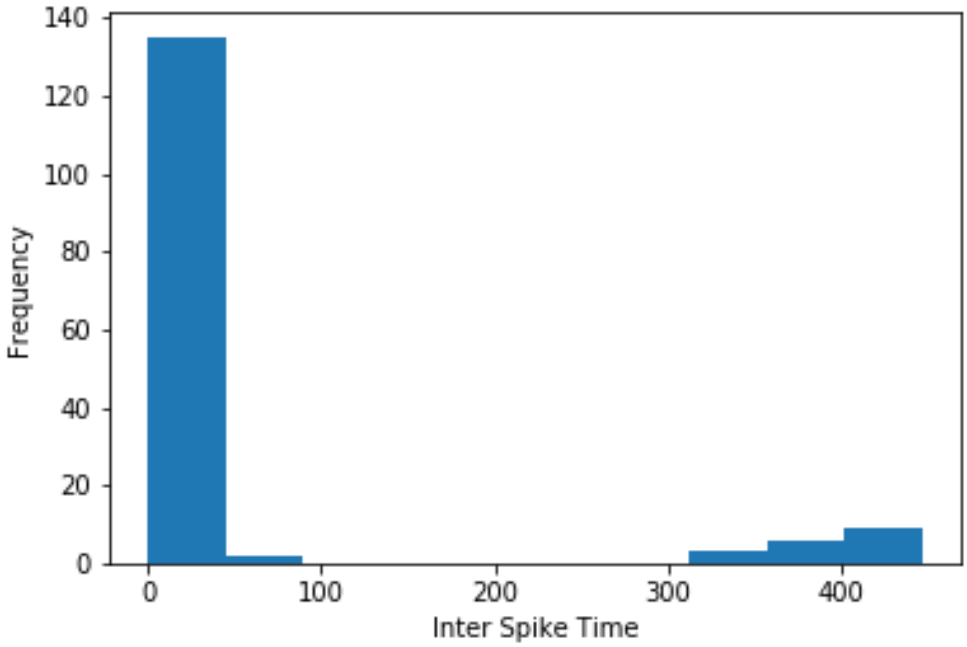

Figure 5.18: *Inter-spike intervals of spiking neurons in the hidden layer for the MDD group (test phase)*

Table 5.18: Comparative Analysis of Input Strategies

	Classification	**Accuracy**	**Precision**	**Recall**	**F-Score**
Brain Asymmetry	Class 1	86.66	0.84	0.72	0.83
	Class 2	80	0.74	0.74	0.74
Short-distance	Class 1	66	0.55	0.5	0.64
	Class 2	66	0.64	0.45	0.56
Long-distance	Class 1	80	0.76	0.62	0.78
	Class 2	76	0.64	0.64	0.64
Grouped features	Class 1	74	0.65	0.65	0.65
	Class 2	70	0.6	0.58	0.62

Further, statistical tests were conducted using the SPSS software to rank the models. The F1 score of 70 optimization process runs for four models was used here. First, the paired t-test statistical analysis was performed. The significance value, p, was set to 0.05, with the null hypothesis (H0) being, “There is statistically no significant difference between the accuracy of each paired model.”

Table 5.16: Number of positive and negative weights

Process	Total Count
Before the training process	
Number of positive synaptic weights	1353
Number of negative synaptic weights	3210
Post-training process	
Number of positive synaptic weights	1297
Number of negative synaptic weights	3266

Table 5.17: Performance Evaluation of Classifiers: Input Strategies

	Threshold	No. of neurons	Weights(min,max)	F1 Score
Brain Asymmetry	0.44	98	$-0.96, 4.94$	0.86
Short-distance	0.18	104	$-0.95, 4.13$	0.68
Long-distance	0.01	103	$-0.03, 0.26$	0.80
Grouped features	0.20	100	$-0.73, 3.92$	0.76

SNN models with four different input strategies were implemented; hence, there were six pairs of models for comparison. For all the combinations, the significance value was far less than 0.05 except for one pair, i.e., "Long-distance communication and Grouped Features," where the p-value was 0.132. Thus, the null hypothesis was rejected except for this pair and concluded that the other models' performance was significantly different.

Further, we performed the Friedman test as shown in Table 5.19 to test and rank all the implemented models. After analysing the mean rankings, the model with "Brain Asymmetry" as an input strategy was found to have a mean rank value of 3.27, the highest among all the input strategies. Thus, we could infer that "Brain Asymmetry" is the most effective and best strategy for inputting data from EEG signals to SNN.

Identification of Biomarkers: Classification Performance

Table 5.20 describes the performance of different SNN model with different EEG channels. Again, the measures represent the output of the 2^{nd} generation of the DE optimisation process.

Table 5.19: Friedman Test: Input Strategies

Input Strategies	**Mean Rank**
Brain Asymmetry	3.27
Long-Distance Communication	2.76
Short-Distance Communication	2.07
Grouped Features	1.90

Table 5.20: Performance Evaluation of Classifiers

Classifier	***Threshold***	***No. of neurons***	***Weights(min,max)***	***F1 Score***
Frontal Region	0.05	110	$-0.61, 2.45$	0.85
Central	0.15	92	$-0.4, 3.55$	0.85
Central-Parietal-Frontal Regions	0.19	95	$-0.18, 0.15$	0.83
Temporal-Frontal-Parietal Regions	0.43	85	$-0.14, 0.3$	0.75
Parietal-Occipital Regions	0.17	113	$-0.02, 4.02$	0.75
Parietal	0.19	86	$-0.05, 4.187$	0.69

Table **??** describes the average performance of 30 runs of each of six SNN models using the optimised SNN parameters.

Table 5.21: Comparative Analysis of Asymmetry in Different Brain Regions

Classifier	**Classes**	**Accuracy**	**Precision**	**Recall**	**F1 Score**
Frontal Region	Class 1	84	0.84	0.72	0.80
	Class 2	74	0.70	0.69	0.70
Central Region	Class 1	84	0.81	0.79	0.80
	Class 2	78	0.68	0.65	0.70
Central-Parietal-Frontal Regions	Class 1	74	0.65	0.62	0.70
	Class 2	70	0.65	0.67	0.66
Temporal-Frontal-Parietal Regions	Class 1	72	0.65	0.65	0.65
	Class 2	68	0.57	0.50	0.52
Parietal-Occipital Regions	Class 1	68	0.58	0.52	0.57
	Class 2	63	0.64	0.45	0.56
Parietal Region	Class 1	60	0.66	0.44	0.53
	Class 2	55	0.20	0.28	0.22

Further, we conducted statistical tests using SPSS to rank the models. The F1-score of 70 runs of the optimisation process for the four models was used here. First, we

performed the paired t-test statistical analysis. The significance value, p, was set to 0.05, with the null hypothesis (H0) being, “There is statistically no significant difference between the accuracy of each paired model.”

SNN models with six different input strategies were implemented; hence, we have 12 pairs of models for comparison. For all the combinations, the significance value was far less than 0.05 except for two pairs, i.e., "Frontal Region and Central Region," where the p-value was 0.974. And the other is "Central-Parietal-Frontal Regions and Parietal-Occipital Regions," with a p-value of 0.065. Thus, the null hypothesis was rejected except for these pairs, and it was concluded that the performance of the other models was significantly different.

Further, the Friedman test was performed to test and rank all the implemented models, as shown in Table 5.22. After analysing the mean rankings, "Asymmetry in Frontal Regions" was found to be the potential biomarker for depression. Following this was the "Central Region" and finally, the "Central-Parietal-Frontal Regions". EEG channels representing these brain regions are shown in Tables 5.6, 5.7, and 5.8, respectively.

Table 5.22: Friedman Test

Brain Regions	**Mean Rank**
Frontal	4.74
Central	4.69
Frontal-Temporal-Parietal	3.96
Central-Parietal-Frontal	3.44
Parietal-Occipital	2.89
Parietal	1.29

The performance of models with an individual brain region, i.e., Frontal and Central, are very close to each other. Next is the model with asymmetry within brain regions, i.e., "Central-Parietal-Frontal." To further rank these models with individual brain regions and collective brain regions, a post hoc analysis using the Wilcoxon test was conducted as shown in Table 5.23. Negative ranks define the number of runs out of 70, where the

performance of the first brain region is less than the second one. Positive ranks define the number of runs out of 70, where the performance of the first brain region is greater than the second one. Finally, ties represent the number of instances where each brain region produces the same F1 score. Thus, it can be inferred that brain asymmetry with individual regions – frontal (first) and central (second) are effective in differentiating healthy and depressed populations.

Table 5.23: Wilcoxon Test

Brain Regions	Negative Ranks	Positive Ranks	Ties
Central and Frontal	34	35	1
Central-Parietal-Frontal and Frontal	54	15	1
Central-Parietal-Frontal and Central	51	19	0
Frontal-Temporal-Parietal and Frontal	47	23	0
Frontal-Temporal-Parietal and Central-Parietal-Frontal	28	42	0

5.5 Conclusion and Discussion

The proposed feed-forward SNN with RMSE as the classification criterion successfully distinguished healthy and depressed individuals using raw EEG signals. The accuracy of the NeuCube model described in Chapter 3 for classifying depressed versus healthy subjects EEG data was 68.18% (EC) and 72.13% (EO). The proposed feed-forward SNN with RMSE as the classification criterion achieved an overall accuracy of 80% in the EC state. The results showed that the complete temporal pattern of spiking neurons contains more useful information than just the order of first spikes as used in the deSNN classification module of the NeuCube architecture. The attributes derived from the voltage of the output neuron proved that timely neuronal membrane potential is as important as event-based spike data. The proposed SNN framework leveraging temporal features offers a new methodology that provides high efficiency with fewer EEG channels, i.e., only 19, fewer timepoints, i.e., only 1,000, and fewer training

samples, i.e., only 22. Therefore, the hypothesis that spiking neurons can encode the rhythmic behaviour of EEG signals that will aid the classification of the depressive group separately from the healthy one was tested and accepted.

One of the challenges for AI is the discovery and interpretation of the patterns formed due to the connection between neurons. Understanding these patterns, i.e., the neural basis, is an important goal in understanding human behaviour, emotions, learning, memory, etc. Spike train analysis using time coding features was explored to gain insights into the inner workings of spiking neurons. The understanding of the rhythmic nature of these neurons through analysing neural activity gave insights into the brain activities of healthy and depressed individuals. Existing studies (Fitzgerald, Laird, Maller & Daskalakis, 2008; Fitzgerald, Srithiran et al., 2008) found that depressed individuals show increased brain activity compared to healthy individuals. Table 5.15 shows increased spiking activity in depressed individuals as compared to healthy groups.

This chapter further explored the aspects of the functional connectivities between different brain regions of healthy and depressed subjects to design an end-to-end efficient AI framework for EEG classification. Different approaches applied in psychology using EEG data in clinical settings were discussed. This helped us to identify the effective way to input data from EEG signals to SNN and to associate potential brain regions for depression detection. Brain asymmetry (intra-hemispheric communication) and long-distance communications indicated depression, which aligns with our previous results described in Section 3.4. Our results showed that depressive disorders are most efficiently characterised using the brain asymmetry in the frontal region (EEG channels: F1-F2, F3-F4, F5-F6, F7-F8). This outcome aligns with the existing studies (Kaiser et al., 2015; J. Wang et al., 2020) and with the results produced using the NeuCube architecture in Section 3.4. Apart from the frontal region, asymmetry in the central brain area and within the central-parietal-frontal brain areas also showed effective classification performance. Thus, the frontal, central, frontocentral, and central-parietal

asymmetries, i.e., F1-F2, F3-F4, F5-F6, F7-F8, C1-C2, C3-C4, C5-C6 and within FC1-FC2, FC3-FC4, FC5-FC6, CP1-CP2, CP3-CP4, CP5-CP6 are identified as potential biomarkers of depression.

Future research could allow the SNN parameters to evolve further from the 2^{nd} generation to the 100^{th}. In the proposed architecture, the threshold of all the spiking neurons is the same. However, the real neurons in the brain have different properties. The threshold of spiking neurons in the next layer could be calculated based on the firing rate or ISI of spiking neurons in the previous layer. Additionally, based on the complexity of the problem, more complex neuron models, i.e., biophysical models with neurotransmitters and neuroreceptors with reinforcement learning-based STDP should be implemented in the future.

The depression detection presented in this thesis consists of binary classification, i.e., healthy and depressed groups. The depressed group can be further classified into three subgroups: mild, moderate, and severe depression. Thus, after binary classification, future work is required to classify these sub-groups of the depressed group. There are two possible solutions to approach this problem: a multilabel classification model or a regression model predicting the depression score. SNN-based ensemble classification and regression models could potentially be the technique to resolve such problems.

Since brain asymmetry proved to be potentially successful in separating depressed and healthy individuals, synchrony among the neurons across different brain regions would provide a better understanding of brain activities in healthy and depressed individuals. This neuronal behaviour could be explored in the future.

5.6 Chapter Summary

The results from the experiments showed that the proposed architecture characterising the temporal associations within EEG signals proved efficient and successful on two

different open datasets. The importance of temporal-based spiking features for spatiotemporal classification and the crucial role of analysing neural firing patterns for interpreting brain activities is discussed. Different brain regions are investigated in this chapter to identify the functional biomarkers of depression.

The difference in the electrical activities of the left and right hemispheres, i.e., brain asymmetry, stood out as the best strategy of information flow, and the frontal lobe as the most prominent brain region. The thorough experimentation with the proposed architecture with two different public datasets proved the robustness of our architecture. The results for identifying the best input strategy and biomarkers detection correlated with the existing studies in psychology. These findings established an excellent construct validity of the proposed SNN model, and our third hypothesis that changes in the brain reflected in bioelectrical activities could produce distinguishing temporal patterns for classification is accepted.

Thus, it can be concluded that the traditional approaches in the psychology of analysing hemispheric differences across the brain regions (frontal, central, and central-parietal-frontal) should be considered as an input to a temporal-based SNN architecture for the classification of raw EEG signals. Along with music instrument recognition, this thesis has laid the foundation for using SNN models to augment clinical decisions through methods, classification performance, and insights using temporal patterns.

This chapter will be published as a journal paper.

The third phase of this research is completed with Chapter 5. The proposed 2-layered architecture was tested and validated on three different spatiotemporal datasets – music, Figshare, and PREDICT. From a 2-layered architecture, this research enters the final phase of proposing a novel deep SNN framework in Chapter 6.

Chapter 6

Design of Binary filters for Spatio-temporal Spike Feature Extraction using Hybrid Coding Techniques

Learning in the cerebral cortex involves information processing at multiple levels of neurons (Yamins & DiCarlo, 2016) with adaptive synaptic strengths (Hebb, 1949a) and is mainly responsible for high classification accuracies of DL architectures. To match the performance of the SNN model with DL architectures such as CNNs, recent studies have adopted a similar design approach to implement variations of deep SNNs. These studies have combined the convolution and pooling operation of CNNs to extract the features from the data and propagate them to the fully connected layer or recurrent reservoir of spiking neurons, forming a deep SNN. The state-of-the-art architectures use ANN-SNN conversion techniques to implement a deep SNN. The CNN to SNN conversions are challenging as they use approximation techniques for producing spikes in SNNs that may result in the loss of temporal feature information. In short, it is not

currently known how to build SNN architectures that combine the advantages of both CNNs and SNNs such that temporal features can be extracted layer by layer within a spiking neural framework.

This chapter proposes a novel deep SNN-based classification architecture in which higher layers use filters to learn spike-based features from spike trains. Inspired by the filters designed to extract shapes from the hand-written digits in CNNs, hand-engineered binary filters are proposed for spike-based feature extraction.

This chapter, presenting a new architectural model to build a deep SNN-based architecture inspired by CNN-SNN architectures, addresses the following research questions:

1. How far can we go in building deep SNN so that sufficient information is transmitted to make the neurons fire in the next layer?

    (i) What filters can be applied on the spike train to build another layer of spiking neurons by extracting spike-based features?

The proposed deep SNN in this chapter is based on the following hypothesis: Neural networks learn features from the input data. Applying filters at different layers in SNN will produce better feature representations of the input data.

6.1 Introduction

Chapter 3 demonstrated the capability of spiking neurons in classifying healthy and depressed individuals and revealed connection patterns in these individuals. The changes in neuronal connections (synaptic weights) during the learning process formed these patterns. Chapter 4 showed the capability of rich neuronal information being produced by spiking neurons. The spiking neurons in the hidden layer reveal different rhythmic patterns for music and EEG signals. The output neuron's properties (spike times and

membrane potential) successfully separated these two groups. The effectiveness of the proposed architecture was tested on two public datasets in chapter 5. This architecture consisted of one hidden layer followed by an output layer. A deep neural network is said to have more than two hidden layers (LeCun et al., 2015). Such deep architectures are mainly responsible for higher classification accuracies in deep neural networks such as CNN and CNN-LSTM networks. Thus, this chapter discusses the design of deep SNN frameworks using temporal feature extraction.

Moving from 2-layered SNN architecture, recent studies have implemented variations of deep SNNs comprising convolutional and pooling layers along with supervised/unsupervised learning algorithms as discussed in Section 2.2. Features are extracted by filters (convolution kernels) over the input, and subsequent layers combine the previous layer's filter output to learn increasingly complex and abstract features.

Understanding the behaviour of spiking neurons through spike train analysis revealed the value of information hidden in temporal coding in the previous three phases of this research. A relationship between the spike trains and neural code is required to build the next layer of spiking neurons. Hence, hand-crafted binary filters are proposed to develop these relationships using hybrid neural coding schemes. The central theme of this chapter focuses primarily on exploring the SNN's ability to classify spatiotemporal data combined with the hierarchical feature representation capability of deep CNNs.

First, the building blocks of CNNs that have inspired this deep SNN-based architecture are described. Recent ANN-SNN conversion techniques to build deep SNNs are discussed. Following that, we propose our hand-crafted filters for spike-based feature extraction with the algorithmic formalisation of our proposed deep SNN model.

6.1.1 Convolution Neural Networks

CNNs (LeCun et al., 2010) are state-of-the-art NN architectures for complex analysis of visual imagery. In multilayer perceptrons, each neuron is connected to all the neurons in the next layer. CNNs are biologically inspired in the way that the connectivity between the neurons is similar to the structure of the animal visual cortex. The visual cortex consists of millions of neurons, each carrying different information. This is called the sensory space. A receptive field is a portion of this sensory space that generates neuronal responses when excited. In the deep learning context, the receptive field is the restricted input region that produces features. In other words, CNNs can develop an association between the output feature and its input region (a portion of an entire area). Thus, CNN's features local connectivity through two important operations: convolution and pooling.

The hidden neurons are connected to the subset of input depending on the kernel size provided in the convolutional layer. Features are extracted locally and later combined to form higher-order features. Pixels become edglets, edglets become motifs, motifs become parts, parts become objects, and objects become scenes in computer vision applications. This suggests that vision recognition architectures (and those for other modalities such as audio and natural language) should have many trainable stages piled on top of each other, one for each level in the feature hierarchy. Thus, the main objective of a CNN is to build hierarchical feature representations through multiple convolutional and pooling layers, as shown in Figure 6.1.

In Figure 6.1, let us consider the input a coloured image. As a result, each feature map would be a $2D$ matrix for each colour channel of the input. Each feature map represents a particular feature extracted by convolving kernels at all locations of the input. Each feature stage consists of three steps: the convolutional (filter bank layer), the activation function that adds the non-linearity component, and finally, the pooling

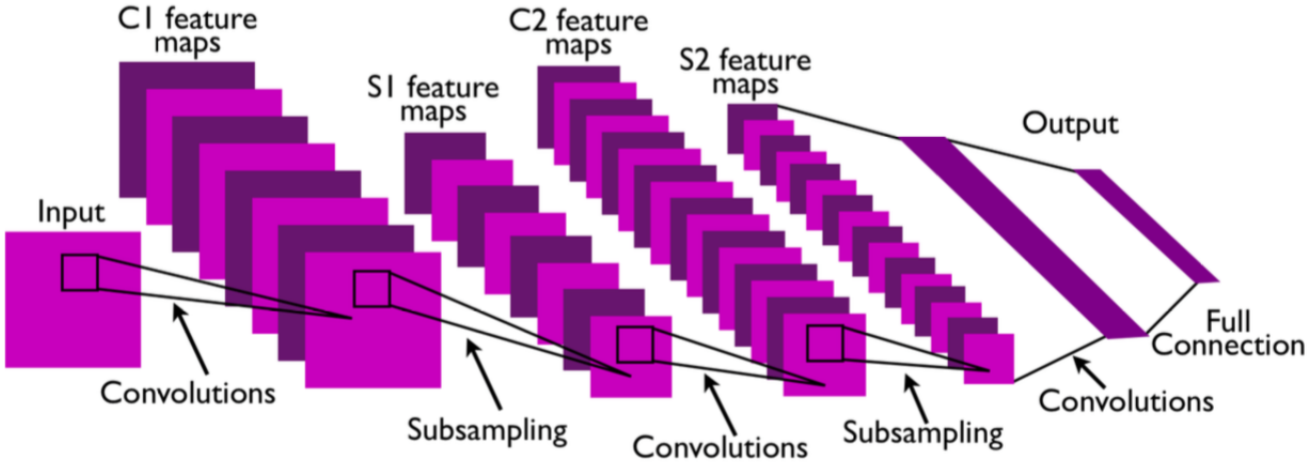

Figure 6.1: *A Convolutional NN with two levels of feature extraction from (LeCun et al., 2010)*

layer. The objective of the CNN is to reduce a high-dimensionality input object into its corresponding feature representations with lower dimensions. Each layer involved in achieving this has been described as follows:

Convolutional Layer

An input coloured image has three dimensions: height, width, and depth. The input image is divided into local receptive fields or perceptrons with n_1 feature maps of size $n_2 * n_3$. This map contains information about a feature in the image. Each layer consists of m_1 filters, and each filter detects a particular feature at every location on the input image. Let each trainable filter (kernel) be denoted as K_{ij}. The output $Y_i^{(l)}$ of layer l comprises $m_1(l)$ feature maps of size $m_2(l) * m_3(l)$. So, the i^{th} feature map represented as $Y_i(l)$ is calculated as:

$$Y_i^{(l)} = B_j(l) + \sum_{j=1}^{m_1^{(l-1)}} K_{ij}^{(l)} * Y_j^{(l-1)} \tag{6.1}$$

where $*$ represents a convolutional operation and $B_j^{(l)}$ is a bias matrix. Kernel $K_{ij}^{(l)}$ connects the local receptive field, i.e., the j^{th} feature map in layer $(l-1)$ with the i^{th}

feature map in layer (l).

This filter is shifted to the next position as determined by the stride size. The process is repeated until the filter covers all the locations of the input image. As seen in Figure 6.1 over the convolutions operation, the area surrounded by the black box is the input feature map. The size of this box is dependent on the kernel size. This box then moves horizontally and vertically, performing the convolution operation which produces the output feature map. Each filter extracts a particular feature in the input image. Also, the filter is not connected to each pixel in the image. It is connected to the receptive field, i.e., the input feature map where the filter is applied. This type of connectivity is called local connectivity.

Non-linearity Layer

In this layer, the outputs produced by the convolutional layer, i.e., the feature maps, are passed to an activation function. This layer creates activation maps as the outputs. The output size is the same as the input since this layer performs element-wise operations. In most CNNs, rectified linear units (ReLu) are used as activation functions.

In other words, the non-linearity layer l takes the output feature maps from the convolutional layer $(l-1)$ and produces activation maps or activation volumes $Y_i^{(l)}$:

$$Y_i^{(l)} = f(Y_i^{(l-1)}) \tag{6.2}$$

where f denotes an activation function. Considering ReLU as the activation function, the above equation can be written as:

$$Y_i^{(l)} = max(0, Y_i^{(l-1)}) \tag{6.3}$$

This layer can be described as enforcing local competition between adjacent features in a feature map and between features in the same spatial position.

Pooling Layer

The pooling layer treats each activation map separately and applies an aggregation function to the values of each activation map. Basically, this layer reduces the resolution of the output feature map and is also known as the downsampling or dimensionality reduction step.

A window region of size $F_1^{(l)}$ x $F_2^{(l)}$ is defined, and the pooling operation reduces this window to a single value. The window is moved by an amount defined by the stride number $S^{(l)}$. This process of reducing the spatial space is repeated until the window sweeps all the locations of the activation maps. Max and average pooling are the two popular reduction methods. In max pooling, the maximum value within the window region is selected, whereas the mean of all the values within the window region is calculated in average pooling. Studies have shown that max pooling and similar variants demonstrate faster convergence.

Therefore, the pooling operation preserves the feature in a smaller representation and discards less important data. This layer reduces the spatial size of activation maps, and hence the computational cost is also decreased progressively through the network.

Fully Connected Layer

This layer is typically a multilayer perceptron network that maps the output of the previous layers (activation volumes) into a class distribution probability. For each category of inputs, the features are extracted using convolutional and pooling layers, and the fully connected layer creates a stochastic likelihood representation of each category. At this stage, an error is calculated as the difference between the expected and actual values. The error is propagated back into the network to the neurons through the gradient descent algorithm.

Thus, the main objective of CNNs is feature extraction and a reduction in the spatial

region, preserving the significant features. This hierarchical feature learning in deep CNNs has attracted recent interest in EEG-based classifications (Sandheep, Vineeth, Poulose & Subha, 2019; Thanaraj et al., 2020; Acharya et al., 2018; Mao, Fathurrahman, Lee & Chang, 2020). The success of CNN is dependent on many hyperparameters like filter size, activation function, pooling size, learning rate, etc. In most of these studies, EEG signals were considered images, where EEG data was divided into several frames. This results in the loss of sequential spatial characteristics across multiple EEG channels and temporal characteristics across multiple brain regions of EEG data. Understanding the mental representations formed over time in the brain is the key to mental disorder issues (Kadipasaoglu et al., 2015). Also, there remains a gap in understanding the human brain's functionality and DL architectures (Cox & Dean, 2014; Churchland & Sejnowski, 1994).

Keeping in mind the governing principle of artificial neurons, research evolved in the development of SNNs, which are capable of modelling spatial-temporal information processing in the brain (Maass, 1997a) as the transfer function of neurons deals with time and could be a potential solution to handle EEG data.

Learning in SNNs can be categorised into two groups: a) spike-based learning and b) rate-based learning. STDP, as described in Section 1.1.5, plays an important role in the memory and learning of the human brain (Dan & Poo, 2004; Masquelier, Guyonneau & Thorpe, 2009). Thus, spike-based processing in combination with STDP can enable SNNs to learn input patterns. These unsupervised SNN models succeeded in various pattern recognition complex tasks with a full-connected hierarchical topology (Diehl & Cook, 2015; N. Kasabov et al., 2013; Masquelier & Thorpe, 2007; Kheradpisheh et al., 2018; Kheradpisheh, Ganjtabesh & Masquelier, 2016).

Rate-based learning techniques are indirect approaches to training that involve a complex ANN-SNN conversion. First, backpropagation is used to train an ANN, which is then converted to the equivalent SNN. This is achieved by mapping the activations of

the ANN to the spiking rates of the SNN. As discussed in Chapter 2, SNNs are behind ANNs in terms of performance. To overcome this limitation, researchers (C. Lee et al., 2018; Panda, Srinivasan & Roy, 2017; Tavanaei & Maida, 2016; Mozafari, Ganjtabesh, Nowzari-Dalini, Thorpe & Masquelier, 2019) started moving to ANN-SNN conversion techniques as described below (Rueckauer, Lungu, Hu & Pfeiffer, 2016).

6.1.2 ANN to SNN Conversions

ANN to SNN conversion techniques use a rate-based learning approach to increase the SNN's classification performance. The real continuous values obtained through the non-linearity layer (activation functions) are converted into firing rates in the SNN. Thus, the output from the activation function of a second-generation neuron acts an input to a spiking neuron.

The spiking rate of a neuron is defined as the number of spikes in a given time period. Another way to compute the spiking rate of a neuron model is by using the input current and membrane potential. The firing rate of a LIF model from Equation 1.3 is computed as follows:

$$f = \frac{1}{\tau_{ref} + \tau_m * \log(\frac{RI}{RI-\vartheta})} \tag{6.4}$$

where τ_{ref} is the refractory period, τ_m is the membrane-time constant, R is the membrane resistance, $I(t)$ is the sum of current supplied by the synapses and ϑ is the threshold voltage.

When τ_{ref}, τ_m and R are each set to a value of 1, the firing rate of the spiking neuron of the corresponding input current functions in a manner similar to the ReLU activation function in ANNs. In the ReLU function, the output is the same as the input if the input value is positive; otherwise, 0 (input value is negative or 0). This relation between the transfer function is the basis of the ANN-SNN conversion (Hunsberger & Eliasmith,

2016).

One of the implementations of the conversion of the output of an activation of an ANN at each layer as an input to a spiking neuron at the same layer is described below. The activation a_i^l of neuron i in layer l in ANN is described as follows:

$$a_i^l := max\left(0, \sum_{j=1}^{N_l-1} W_{ij}^l \cdot a_j^{l-1} + b_i^l\right) \tag{6.5}$$

where L is the number of layers in ANN with weights W_{ij}^l connecting neurons from layer $l-1$ to layer $l, \mathrm{l} \in 1, ..., L$ with bias b_i^l of neuron i in layer l. For the first layer in ANN, the activation a^0 is equal to the normalised input x.

From Equations 1.3 and 1.4, the membrane potential of LIF neuron $u(t)_i^l$ is stimulated with an input current $z(t)_i^l$

$$z_i^l = \tau * \sum_{j}^{l-1} W_{ij}^l \Theta_j^{l-1} \tag{6.6}$$

,

$$\Theta_j^{l-1} = \Theta(u(t-1)_i^l) + z(t)_i^l - \vartheta \tag{6.7}$$

The spiking neuron accumulates the current, computes the membrane potential $u(t)_i^l$ and when $u(t)_i^l$ crosses the voltage threshold ϑ, it emits a spike.

Let dt be the stimulating period of an input pattern to a spiking neuron. The firing rate of a spiking neuron is defined as the number of spikes in a given time window T. For ANN-SNN conversion, an approximation is calculated by the following correlation:

$$f_i^l(T) = \frac{a_i^l}{dt} \tag{6.8}$$

A Poisson spike train to simulates a neuron that fires for time duration T at an average rate of $f_i^l(T)$. A random number is generated for time T and if it is less than

$f_i^l(T)$, that event is considered as a spike; else no spike.

A detailed review on existing ANN-SNN conversions is provided in Chapter 2.

Training deep SNNs using an indirect rate-based approach has major drawbacks:

1. Gradient descent and BP methods are suitable for processing real-valued numbers and are not biologically plausible (Bengio et al., 2015)

2. Longer processing times

3. Encoding the input to SNNs requires many spikes that may result in the loss of temporal feature information.

4. Bias representation in SNNs is not simple and most of the existing architectures neglect the equivalent component of bias

In summary, the following factors are the drivers for designing a novel deep SNN-based architecture: the success achieved by CNNs, the capability of spiking neurons to handle time, the efficiency of STDP in learning input patterns, and a more biological implementation of convolutional spiking neural network architectures.

The next section presents kernels that are responsible for feature extraction from the previous layer (low-level features) and pass on to the next layers (high-level features).

6.1.3 Binary Filters and Spike Train Kernels

Due to CNN's capability to perform better generalisation and produce high accuracy, it has been favoured for many computer vision tasks. However, this performance was achievable only with deeper CNN architectures, leading to greater memory consumption. Network compression techniques and new architectural styles were introduced with the aim of reducing on-device memory utilisation while still maintaining performance. With efforts to attain this, binary filters have been proposed for CNNs in (Tseng et al., 2018). Orthogonal variable spreading factor (OSVF) codes (The MathWorks, 1999)

popular in wireless networks were used to generate the deterministic binary filters for convolutional layers. This architecture greatly reduced the number of parameters to be learned in the convolutional layers as they incorporated binary weights instead of floating point numbers. They employed a coefficient representing the strength of binary basic vectors. Instead of updating entire filters, this architecture updated this coefficient for the binary basic vectors responsible for filter generation. They had implemented backpropagation to train the network.

We are not going into the details of the OSVF and training processes as we have not incorporated them into our study. But the application of binary filters in CNN attracted our attention. Designing filters for a spike train to extract information after one level of spiking neurons is the central idea of this study. To this end, we examined a few studies that applied filters (especially used in image recognition) on spike trains. The spike trains are used to represent and process the neural information in spiking neurons, which can integrate many aspects of neural information, such as time, space, frequency, phase, etc. (Whalley, 2013; X. Wang, Lin, Zhao & Ma, 2016). Spike train analysis is the characterisation of neuronal activity in a specified time window to convert discrete values into continuous values.

Considering a spike train as a high dimensionality vector, experts (Haeusler & Maass, 2007; Jurjuţ et al., 2009, 2011; Nikolić, Haeusler, Singer & Maass, 2006) convolved the spikes with exponential decaying kernels to produce a signal (real continuous values). In (Jurjuţ, Gheorghiu, Singer, Nikolić & Mureşan, 2019) research, the authors applied classical spike train analysis methods to quantify and study neurons' collective and individual behaviour. They inferred that the contribution of silent neurons is as vital as that of active neurons in the expression of neuronal patterns. State vectors were produced by convolving the spike train with an exponentially decaying kernel and then clustered them using K-Means to identify the classes of state vectors. Later, analysis methods such as smoothed peri-Stimulus time histograms (PSTH), direction and orientation

tuning, and auto- and cross-correlograms were applied to the occurring patterns (binary events, i.e., the spike train). Much work on the potential of applying kernel methods on spike trains has been carried out here (I. M. Park, Seth, Paiva, Li & Principe, 2013). Experts in this field describe various positive definite kernels to characterise the spike train by mapping them into objects in reproducing kernel Hilbert space (RKHS) (Paiva, Park & Principe, 2009), i.e., feature space. By applying a point-process kernel on the spike train, which was extracted from audio signals and transformed them into RKHS, K. Li and Príncipe (K. Li & Príncipe, 2018) achieved recognition accuracy of 95.23% with fewer input channels and epochs.

Further, Ke et al. (Ke et al., 2020) performed hand gesture recognition using convolutional spiking neural networks. However, here the convolutional kernels are applied on spike trains. The first layers consist of LIF neurons which encode the input, followed by convolutional and pooling layers. Finally, the output layer again consists of fully connected LIF neurons. Two datasets (Strathclyde and CapgMyo) were used for experimentation, achieving classification accuracies of 98.76% and 98.21%, respectively. The kernels designed for computer vision applications were applied on the spike trains.

A comparative study of coding schemes was conducted by Guo et al. (Guo et al., 2021) to find the best neural coding scheme for information transmission between neurons. The pixel information was encoded into spikes using these coding schemes. Their performance was evaluated for the classification of Modified National Institute of Standards and Technology (MNIST) and Fashion-MNIST datasets. Time-to-first spike coding performed well as compared to other coding techniques, whereas burst coding transferred information between neurons quickly.

All the above-listed studies demonstrated that the utilisation of spike train kernels could allow various signal processing techniques and ML of spike trains by providing a feature space for computation. Discrete spike trains are first converted to continuous

functions through the convolution calculation of the specific kernel function, and then the supervised learning algorithm is constructed for SNNs. ANN-SNN conversion techniques are a popular design for deep SNNs, and, in this area, Kim et al.(Kim et al., 2018) is the relevant study that proposed a deep SNN by incorporating the temporal information of spike trains. Further, S. Park et al. (S. Park et al., 2019) used burst spikes and hybrid coding schemes at different layers of deep SNNs. In both of these studies, the weights of a trained DNN were transferred to SNNs. This conversion adds complexity to the architecture and also underestimates the capability of spiking neurons and STDP. The primary objective of this research has been to build a pure SNN-based architecture.

Most of the works in the literature reviewed above suggested the concept of deep learning in SNNs by combining convolutional layers with SNNs or converting the output of the activation function from a CNN into the firing rate for spiking neurons. There is no method that can demonstrate deep learning of input patterns in an SNN as part of its internal learning mechanism instead of embedding convolutional layers or borrowing the concept of spiking neurons in the CNN structure.

Taking inspiration from these studies and the spike train analysis in Section 4.3.2, we started focusing on ways to utilise temporal information in the spike trains to transmit information between different layers of an SNN. After observing the significant information coded in firing spiking patterns for musical instrument recognition and depression detection in chapters 4 and 5, respectively, and reviewing the existing articles, we found that currently, it is not known on how to build SNN architectures that combine the advantages of both CNNs and SNNs such that temporal features can be extracted layer by layer within a spiking neural framework. Hence, we formulated our research question: "What filters can be applied on the spike train to build another layer of spiking neurons by extracting features?" and decided to build a deep SNN based on hybrid neural coding schemes, as discussed in the next section.

6.2 Proposed Hand Crafted Filters

One of the novelties of this research study lies in the evolved implementation of deep SNN architecture – multiple levels of deep spiking neurons. This research presents a new architectural model to build a deep spiking neural-based architecture inspired by CNN-SNN architecture and kernel methods. In this section, first, we propose the hand-crafted filters, and then we will describe how they can fit into our architecture for classifying spatiotemporal data.

We have two options for spike feature extraction: a) using kernels, as mentioned in section 6.1.3, and b) transforming the spike train into a different feature space or designing hand-crafted filters. We designed simple hand-crafted 3D and 5D filters for the initial investigations to extract features such as time-to-first-spike and time-to-last-spike and frequency coding in a given time window and across the spiking neurons. The proposed filters are convolved with the spike trains extracting spatial and temporal features.

These filters count the spikes every 3 and 5 seconds of the time window. Thus, we are utilising temporal information within a small spatial region. Considering the spike train of all the neurons in a matrix structure, the row represents the time dimension $(t_1, t_2, .., t_n)$, and the column represents the number of hidden neurons $(n_1, n_2, .., n_n)$ and the cell value indicates the status of the spike $(1 : spike$ or $0 : nospike)$. The following filters are convolved with the spike train to extract the spatiotemporal information.

In SNNs, information is transmitted and processed only when the neuron emits a spike, i.e., when the neuron's membrane potential crosses the threshold. Spikes are considered event-based data; they might contain little information themselves. At the same time, the amount of information transmitted ahead should be enough to make inferences and should not cause energy inefficiency. Maintaining this balance of

exciting the neurons in the higher layers and implementing computationally efficient deep SNNs is a great challenge. Spike-based strategies, i.e., different neural coding schemes (Gerstner & Kistler, 2002) are key factors that allow the amount of information to be transmitted.

As the stimulus information reaches the brain, the information is processed and transmitted to the neurons of the next stage. Numerous types of neurons are located at different human brain locations and perform different functions (Mochizuki et al., 2016). Spike trains generated from external stimuli can be regular, irregular, or depict some intricate temporal patterns dependent on the type of brain cell, brain area, and stimulus. We have seen different temporal patterns in Chapter 4 for violin and piano signals and in Chapter 5 for healthy and depressed individuals. Based on this theory that neurons use different coding schemes at different locations and our experiments in the previous chapters, we have proposed layer-wise neural coding schemes for building deep SNNs.

6.2.1 Neural Coding

Information representation in the brain by neurons is termed neural coding. The main objective of neural coding is to describe the relationship between a stimulus and a single neuron or a group of neurons. This research aims to study neural encoding, i.e., mapping from stimulus to neuronal responses. On a higher level, neural coding can be divided into the rate and temporal coding. Rate coding is defined as the number of spikes per unit of time. It is assumed that the information about stimulus lies in the firing rate of neurons. When the information is encoded in spike timings or the time difference between two spikes (inter-spike interval), the coding technique is defined as temporal coding.

How information is processed at different levels will eventually affect the memory

of the network. F. I. Craik and Lockhart (F. I. Craik & Lockhart, 1972) defined depth as "the meaningfulness extracted from the stimulus rather than in terms of the number of analyses performed upon it (p.48)." Shallow processing is when the information is encoded based on its structure or physical qualities. In contrast, deep processing is when we go deeper to understand the meaning of a context, word, etc. For example, when starting this Ph.D. journey, I read everything related to SNNs, EEG signals, and depression, but in the later stages of my research, I narrowed down this scope. I did not read all the research papers but applied a layer of filtering and actually read very specific papers deeply associated with my research objectives. Based on this approach, all the information about spikes is transmitted through layer 1; for the later stages, specific information about spikes is transmitted.

1. Layer 1: Frequency Coding – This filter calculates the number of spikes in 3s and 5s window time.

Table 6.1: Layer 1: Frequency Coding

	n_1	n_2	n_3
t_1	1	1	1
t_2	1	1	1
t_3	1	1	1

	n_1	n_2	n_3	n_4	n_5
t_1	1	1	1	1	1
t_2	1	1	1	1	1
t_3	1	1	1	1	1
t_4	1	1	1	1	1
t_5	1	1	1	1	1

2. Layer 2: Time-to-First Spike and Time-to-Last Spike – Number of spikes during the first and last seconds within the window time.

Table 6.2: Layer 2: Time-to-First Spike and Time-to-Last Spike

1	1	1
0	0	0
1	1	1

1	1	1	1	1
0	0	0	0	0
0	0	0	0	0
0	0	0	0	0
1	1	1	1	1

3. Layer 3: Time-to-First Spike or Time-to-Last Spike – The number of spikes in the first second of 3s and 5s time duration.

Table 6.3: Layer 3: Time-to-First or Time-to-Last spikes

1	1	1
0	0	0
0	0	0

1	1	1	1	1
0	0	0	0	0
0	0	0	0	0
0	0	0	0	0
0	0	0	0	0

With these filters, the flow of information is controlled at each stage, which controls the firing of neurons in the subsequent layers. This phenomenon will ultimately lead to feature extraction of input patterns encoded in the spatiotemporal spikes. Finally, these patterns are fed to the output spiking neuron. Similar to the previous architectures, the classification decision is made using the combination of RMSE and Gamma factors.

The primary objective of adding these binary filters for the convolutional operation is to preserve the relationship between the input patterns and the spatiotemporal spike trains. The sparsity of spikes at each layer leads to a unique temporal pattern for each group for better classification.

6.3 Proposed Deep SNN Using Hybrid Neural Coding Schemes

This research presents a new architectural model to build a deep spiking neural-based architecture inspired by CNN-SNN architecture, as shown in Figure 6.2. In this architecture, a spatiotemporal dataset is first converted into spike trains using a Spike Encoding algorithm, where the input value is considered as a current to spiking neurons. Based on the firing threshold, the network of spiking neurons will produce spatiotemporal firing patterns (0: no spike and 1:spikes). From this step, we propose three layers of

feature extraction using the three kernels mentioned in section 6.2.1. For each layer, convolution and max pooling operations are performed. Spike coding features are extracted and transmitted using these binary filters to the next layer of spiking neurons. This process will produce unique spatiotemporal firing patterns for each input class.

Spike train analysis described in sections 4.3.2 and 5.4.2 reveals the spatiotemporal patterns produced by spiking neurons. Additionally, the classification accuracies achieved by incorporating time dimension through the implementation of Gamma and RMSE metrics demonstrated the capability of spiking neurons in separating two classes. With these two caveats, a deep SNN framework is proposed to learn unique patterns from the spatiotemporal inputs for classification purposes.

The proposed framework is as follows:

(i) Input layer consists of spatiotemporal signals.

(ii) Spike encoding: The input signals are encoded into spike trains using LIF neurons. During the encoding process, the real values of the input signals acting as input currents will be multiplied by the synaptic weights, and the neuronal membrane potential is calculated. Spike is emitted if the voltage crosses the threshold value; else, no spikes are emitted in the network. Algorithm 8 provides the pseudocode for implementation purposes.

(iii) Spike trains are propagated to the hidden layer, producing the first layer of spike trains.

(iv) Layer 1 kernel, i.e., frequency coding, is convolved with the spike trains.

(v) Max pooling operation is applied. This step reduces the dimensionality of spike trains. Also, here the output consists of real values.

(vi) Spike encoding converts the output from the max pooling operation into spike trains.

(vii) These steps (convolution, pooling, encoding) are repeated for the next two layers.

(viii) The spike trains produced from the max pooling operation at layer three are propagated to the output layer.

(ix) The output layer consists of the LIF spiking neuron. The classification criteria used in this architecture are the same as those used in the previous two architectures.

(x) Weights from the input layer to the hidden layer and the hidden layer to the output layer are trained using STDP.

Algorithm 8 Spike Encoding Algorithm

procedure SPIKE ENCODING($features, threshold$)
  Set firing threshold, refractory period, random weights {-1,1} of size $(numofchannels, numoftimepoints)$
  for each input pattern **do**
    for each signal in input pattern **do**
      Initialise LIF neuron
      for i <= signal duration (timepoints) **do**
        Compute membrane potential according to LIF neuron where current is calculated as the multiplication of each signal value (s_i) and weight (w_i)
      end for
    end for
  end for
  Spike train of size $(numberofchannels, numberoftimepoints)$ is produced for each sample
end procedure

Thus, we have proposed a pure deep SNN architecture where encoding uses spiking neurons, spatiotemporal features are extracted from spike trains using neural code

schemes, and weights are trained using STDP. Classification is performed using the spatiotemporal pattern produced by the output spiking neuron.

6.3.1 Algorithmic Design

Algorithm 9 Deep SNN for Spike-based Spatio-Temporal Feature Extraction using Binary Filters

procedure SPIKE-BASED FEATURE EXTRACTION

Encode spatiotemporal data into spike trains using Spike Encoding Algorithm. The number of spiking neurons is the same as the number of features in the dataset. The number of time points in spike trains will be equal to the number of time points in the data.

Create a set of positive and negative input neurons

Create network connectivity by establishing synaptic connections between input neurons and hidden neurons (full connectivity). Negative input neurons have the same weight value as the positive but multiplied by -1

Assign random weights between hidden layer neurons and output neuron between {-1,1}

Create connections from the hidden layer to the output layer (full connectivity)

Assign random weights between hidden layer neurons and output neuron between {-1,1}

Set neuron threshold, refractory time for all the LIF neurons

Set $time\_window = number of samples in data$ and $max\_iteration value$ (for e.g. 100)

Create training set 80% and test set 20%

while $iteration <= max\_iteration$ **do**

    for each training input pattern **do**

        for each input neuron **do**

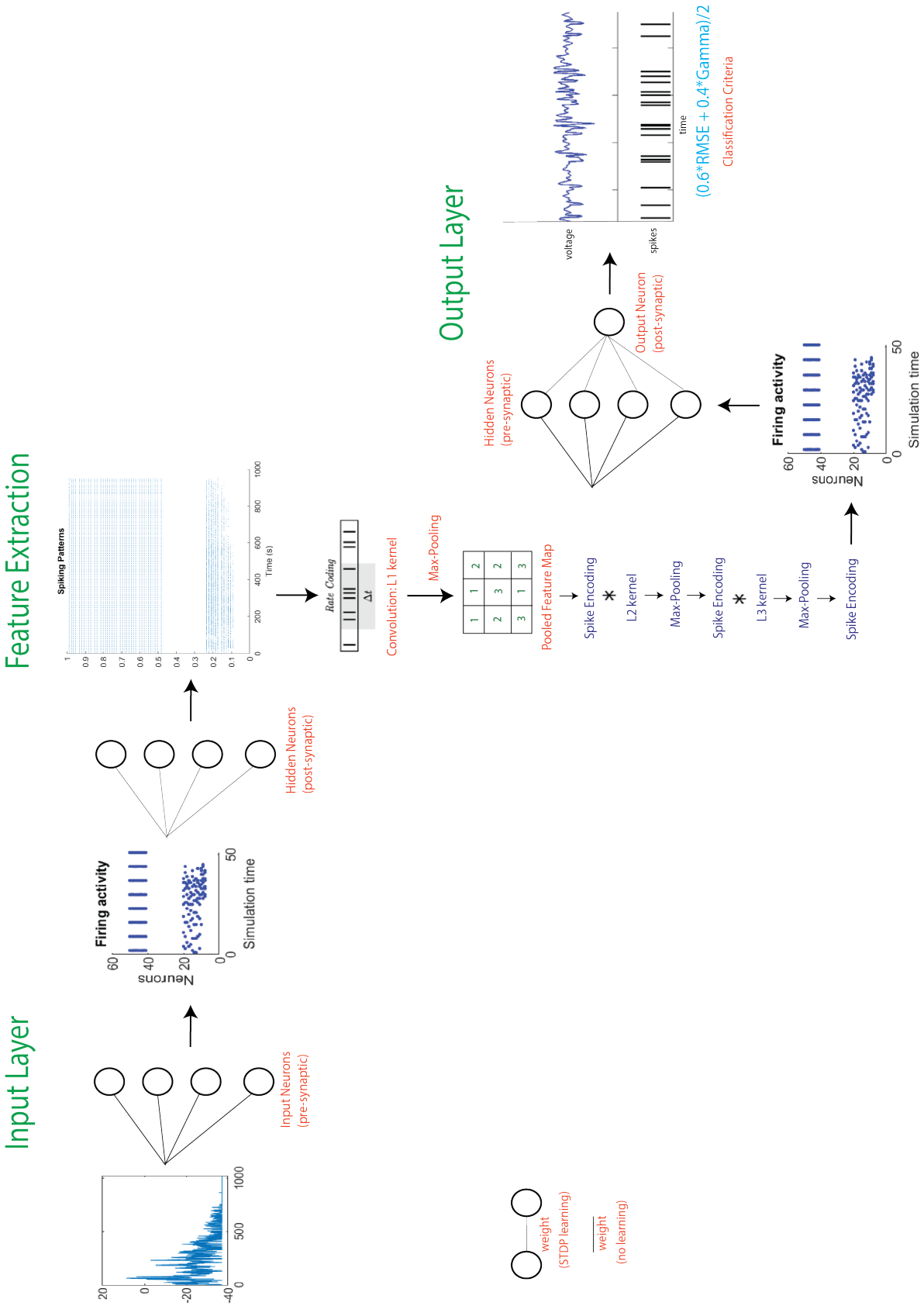

Figure 6.2: *Proposed deep SNN architecture using conv-pooling layers*

14: Propagate input spikes to hidden neurons using LIF neuron
15: **end for**
16: Adapt synaptic weights between input neurons and 1st layer of hidden neurons according to STDP rule
17: Apply layer one kernel on spike trains
18: Perform max-pooling
19: Perform spike encoding
20: Propagate spikes to the next layer of spiking neurons
21: Apply layer two kernel on spike trains
22: Perform max-pooling
23: Perform Spike Encoding
24: Apply layer 3 kernel on spike trains
25: Perform max-pooling
26: Perform spike encoding
27: Adapt synaptic weights according to STDP rule
28: Propagate spikes to the output LIF neuron
29: Store the firing times and membrane potential of the output neuron
30: Adapt synaptic weights according to STDP rule
31: **end for**
32: **for** each test pattern **do**
33: **for** each input neuron **do**
34: Propagate input spikes to hidden neurons using LIF neuron
35: **end for**
36: Adapt synaptic weights between input neurons and 1st layer of hidden neurons according to the STDP rule
37: Apply layer one kernel on spike trains
38: Perform max-pooling

Perform spike encoding

Propagate spikes to the next layer of spiking neurons

Apply layer two kernels on spike trains

Perform max-pooling

Perform spike encoding

Apply layer three kernels on spike trains

Perform max-pooling

Perform spike encoding

Propagate spikes to the output LIF neuron

Store the firing times and membrane potential of the output neuron

Compute similarity metric, i.e., Gamma factor and RMSE using spike times and voltage of output neuron of test and all train samples. Compute the classification metric as $(0.6RMSE * 0.4Gamma)$ / 2.

Assign the label of the training sample which is closest to the test sample

Calculate the fitness function: $F1 - Score$

Create the next population using the DE algorithm: neuron's threshold, refractory time, STDP parameters, number of neurons in all hidden layers, range of weights

end for

end while

end procedure

A deep SNN architecture with three layers of convolution and pooling can be built using the proposed architecture. Some spiking information is lost at each layer, but this will restrict the firing of neurons in the next layer. In this way, the proposed architecture is capable of extracting important input patterns in the shape of spiking information, i.e., spike trains. As a result, the patterns of spike trains in the hidden layers and output layer will vary according to different groups. The size of filters, the pooling operation,

and the order of convolution and pooling layers can be fine-tuned based on the results of optimisation using Differential Evolution. Thus, this research has evolved based on the various hypotheses and experimentation discussed in previous chapters and has finally been successful in proposing a framework for a deep SNN architecture with a hierarchical feature extraction process. The proposed architecture is simple and a pure SNN-based architecture without any conversions from deep learning models to SNN and the application of signal processing techniques. Thus, the proposed architecture could reduce the complexities involved in these conversions and is capable of extracting information from spatiotemporal signals, encoding them to spatiotemporal spiking patterns.

6.4 Conclusion and Discussion

In this chapter, we proposed binary filters to leverage information, i.e., spatiotemporal features from spike trains. The proposed binary filters convolve with the spike trains, and the pooling operation summarises the feature information in the features maps. The output values from the max pooling operation are used as an input current to the spike encoding algorithm. These features are employed to build the succeeding layer of spiking neurons. The proposed deep SNN architecture best utilises all the capabilities of spiking neurons and STDP to perform classification tasks and reduces the complexity involved in ANN-SNN conversions. Using the DE algorithm to find the optimal SNN parameters makes this architecture effective for analysing and classifying spatiotemporal data.

To the best of our knowledge, hand-engineered spike-based filters have been applied to build a deep SNN model for the first time. Thus, this research investigated and proposed a novel feature learning and classification approach by processing spatiotemporal information amongst neural spikes using STDP. Thus, our fourth hypothesis is

conceptually valid and accepted. Thorough experimentation is required in the future to evaluate the performance of the proposed methodology.

In the current design, the threshold of spiking neurons at each layer is fixed. In the future, a dynamic threshold could be adapted. The threshold of the spiking neurons could be adjusted in multiple ways. First, calculate the maximum and minimum value of membrane potential at each layer and compare it with the current fixed threshold. If the current voltage value is more than the maximum weighted voltages at that timestep, the threshold value can be scaled up by a certain factor. If the current membrane potential is less than the minimum voltage of the previous layer, the threshold could be scaled down. Repeating this dynamical adjustment of the neuron's threshold at each layer will enable information transfer from one layer to the next. This will produce a unique temporal firing pattern at the output layer, increasing the classification performance.

A second way to implement dynamic threshold adaption is to use ISI. The time difference between two spikes in the previous layer affects the membrane potential of the next layer. A relationship could be built between the ISI of input spike trains and the membrane potentials of neurons in the next layer. In the future, attempts can be made to model this behaviour mathematically.

With these potential approaches to adapt the threshold at each layer and optimise using DE, the decision-making process of the proposed deep SNN could be effective. Future experimentation is required to evaluate this concept and the proposed SNN architecture.

6.5 Chapter Summary

This chapter proposed a hybrid coding technique to build a deep feed-forward SNN-based architecture. The proposed hand-crafted filters can theoretically extract spatial and temporal features from spike trains. This is the first time that hand-engineered

spike-based filters are applied to build a deep SNN model. Apart from this, introducing a new spike encoding module in the proposed architecture makes this architecture a pure SNN-based temporal framework.

Thus, this research investigated and proposed a novel feature learning and classification approach by processing spatiotemporal information amongst neural spikes using STDP. The deep SNN architecture with hierarchical feature extraction using rate-coding and time-coding neural schemes provides a basis for a different way of analysing spatiotemporal data.

With this chapter, we complete the final phase of this research study.

Chapter 7

Conclusion and Future Directions

This chapter summarises the main contributions of this thesis along with the limitations and possibilities for future research.

7.1 Main Contributions of this Thesis

This thesis explored the techniques of building deep SNNs for classifying spatiotemporal data. Starting from a brain-inspired 3D SNN model in chapter 3 and progressing to a deep feed-forward SNN-based architecture in chapter 6, the efficiency of the proposed architectures have been successful in analysing music and EEG signals in chapters 4 and 5 . An end-to-end SNN framework for improved psychiatric healthcare by incorporating the traditional EEG approaches of psychology has been proposed. Further, a deep SNN analytic framework has been designed by extracting spike-based features through proposed hand-crafted binary filters.

The major contributions of this research are summarised below:

1. Neucube-based SNN architecture was applied for depression detection, which revealed unique patterns in the brain activity of healthy and depressed subjects. This contribution is related to RQ1.

2. A novel 2-layered feed-forward architecture was proposed for classifying spatiotemporal data. This contribution is related to RQ2.

3. An end-to-end SNN design was proposed for EEG classification. This contribution is related to RQ3.

4. Binary filters were proposed to leverage the patterns produced by spiking neurons. This contribution is related to RQ4.

5. A novel deep SNN with a hierarchical feature extraction approach was presented. This contribution is related to RQ4.

In summary, this research has contributed to the fields of AI and psychology. Using EEG signals representing the aggregation of neuronal spiking information underneath the scalp surface with a computational model accumulating the spiking information provides a new way to identify brain disorders. DNNs require thousands of training samples to perform classification tasks. The proposed temporal-based SNN architecture with the LOOCV technique and DE showed the capability of SNN with 10 and 22 training samples for music-instrument recognition and depression detection, respectively. Thus, utilising temporal-based computational procedures for treating sequential temporal data proved a viable potential approach. Along with spike timings, this research showed the applicability of utilising neuron voltage information for increased classification performance. This is significant as, in biological neurons, membrane potentials inside and outside the cell direct the movement of ions allowing information to flow between different neurons. This enables learning in the human brain. Thus, the timely neuronal voltage information used as a classification criterion enables the SNN model to learn from the input data better.

Further, AI techniques learn internal data representations during training by mapping the input to the output. Analysis of these representations through spike train analysis

provides better interpretability of brain activities. This explainability can assist clinicians in their decision-making process. The classification performance of the SNN model using brain asymmetry as the input proved more successful in depression detection and more computationally efficient than the standard feature extraction processes. Instead of using many EEG channels to improve classification performance, the proposed architecture demonstrated that asymmetry in frontal brain regions with eight frontal EEG channels could indicate depression disorders. In the future, the proposed SNN architectures could be utilised to analyze and classify spatiotemporal data.

In the following, a brief overview of my Ph.D. study contributions, along with their future prospects, is provided.

7.1.1 Chapter 3 Contributions and Future Directions

In this chapter, the capability of spiking neurons and STDP in distinguishing two groups, healthy and depressed, were explored. A brain-inspired NeuCube architecture was proposed for processing and classifying EEG signals. This framework had three core modules.

1. Encoding layer – This module uses a threshold-based representation (TBR) algorithm for encoding the EEG signals into spike trains.

2. 3D SNN reservoir – The SNNr module maps the EEG signals into a 3D space using the Talairach brain template. The encoded spike trains called input neurons are mapped to their corresponding physical location in the reservoir. LIF neurons with recurrent connections are implemented here. The initial structural connectivity between the neurons in the network and the initial weights of the neuronal connections (synapses) are implemented using the small-world connectivity property. The synaptic weights are then adapted using the unsupervised learning algorithm, STDP.

3. Output layer – The output layer implements deSNN and KNN models to classify the input samples.

The NeuCube framework was compared with MLP and LSTM networks for depression detection. It outperformed both MLP and LSTM networks demonstrating the small-sample learning capability of SNNs. Applying SNNs to process and temporal data is more effective as the computational model of spiking neurons incorporates temporal dimension in their design. Along with the classification of healthy and depressed groups, the research reported in this chapter investigated the brain connectivity of depressed and healthy individuals in eyes-closed and eyes-open states. These methodologies were tested on a real EEG recording dataset for healthy and depressed groups. The unsupervised learning revealed distinguishable patterns in the models related to the frontal, central, and parietal areas of the depressed versus the control subjects that suggest potential markers for early depression prediction.

The encoding algorithm of the NeuCube framework is one that needs to be investigated further. Currently, the simplest model, i.e., threshold-based encoding, was implemented. However, in the future, different encoding techniques must be established according to the nature of the input data. One such encoding method is introduced in this research – spike-based encoding, where spiking neurons produce the spike trains. The raw values of EEG signals would then be considered as the input current or energy to the spiking neurons. Experiments could be conducted in the future to test this particular module.

Another aspect that should be explored further is the classifier module, i.e., deSNN, algorithm. Currently, deSNN develops the spatiotemporal pattern for each input sample using rank-order learning. The order of the first spikes of each output neuron is stored along with its class sample during the training phase. This module considers only the order of first spikes and ignores the patterns generated later during training. This

algorithm is very powerful as it utilises both the information contained in the order of the first input spikes and the information contained in the timing of the subsequent spikes, which is used to adapt weights between SNNr and the output layer. There is a potential possibility that more information would be encoded in the spatiotemporal pattern of output neurons in the later simulation periods rather than only the first spikes. Hence, this aspect could be further explored to investigate the whole spatiotemporal pattern during the entire stimulation time of output neurons. The topology and classification module in the NeuCube framework has been modified in our proposed architecture introduced in Chapter 4.

Chapter 3 has been published as a conference paper (Shah et al., 2019).

7.1.2 Chapter 4 Contributions and Future Directions

In this chapter, the structural connectivity and the classification modules of the NeuCube framework are modified to build a temporal-based SNN architecture. Next, the rhythmic behaviour of music signals encoded in the spiking activities of computational spiking neurons is investigated through spike train analysis. A novel classification criterion is proposed using all the available information from the spiking neuron, i.e., the firing times and the membrane potential characterised by the time domain. This chapter gave a different and interesting perspective to our research by looking at depression detection from a musical perspective. The approach from a musical perspective provided us with a fundamental understanding of how SNNs could be utilised in the processing of spatiotemporal data. The findings about the behaviour of the spiking neurons from the musical perspective were utlised as the foundation for further research on EEG signals for depression detection using SNN. Considering the above mentioned factors, the contributions from a musical perspective may not have been major contributions; however, they played a substantial role in concluding the applicability of SNNs for

spatiotemporal data. Thus, this chapter offers a simple and effective 2-layered feed-forward SNN architecture by fully utilising spike timings and membrane potential for classifying music and violin signals. A comparative analysis between rate-coding and temporal-coding techniques has been conducted in this chapter. The proposed classifier is compared with traditional ML methods like DT, KNN, and SVM. The architecture showed better classification accuracy with fewer samples and spiking neurons in the hidden layer.

A feed-forward SNN architecture proposed for processing and classifying music signals consisted of three core modules.

1. Encoding layer – This module uses the BSA algorithm for encoding the EEG signals into spike trains.

2. Hidden layer – The single hidden layer consists of LIF neurons where all the input neurons are connected to all the neurons in this layer. The synaptic weights are then adapted using the unsupervised learning algorithm, STDP.

3. Output layer – The output layer implements Gamma and RMSE metrics to classify the input samples. All the neurons in the hidden layer are connected to the single output LIF neuron, and the synapses are modified using STDP.

The Gamma metric, i.e., the spike train similarity measure, should be further explored and improvised to make classification decisions. Coincidence for an individual spike is established if its firing time is within 2ms of the firing time of the corresponding spike in the reference spike train. Also, there is a chance that varying currents can produce similar spike trains. Hence, a metric with a fusion of coincidence factor, ISI, and membrane potential should be further explored.

Chapter 4 has been published as a journal paper (Shah et al., 2022).

7.1.3 Chapter 5 Contributions and Future Directions

This chapter applied the proposed 2-layered SNN-based architecture to EEG signals for depression detection. The RMSE metric calculated with the temporal information as the classification criterion proved successful. This SNN-based research is the first study on the application of depression detection. Hence, to ensure the reliability and effectiveness of the proposed temporal-based SNN architecture, it was applied to two publicly available datasets – Figshare and PREDICT.

The proposed architecture showed the small-sample learning ability to spike neurons and STDP in classifying these two groups. An interesting fact that depressed people tend to have more spiking activities in their brains as compared to healthy groups was observed. Further, this chapter explored the different strategies of information flow from EEG signals to SNN – brain asymmetry, short- and long-distant communications, and clusters of grouped EEG signals from similar brain regions. Additionally, this chapter investigated the different brain regions to identify the functional biomarkers of depression. The difference in the electrical activities of the left and right hemispheres, i.e., brain asymmetry, stood out as the best strategy of information flow. More specifically, the asymmetry within frontal and central individual brain regions, followed by asymmetry within frontal, central, and parietal brain regions, were identified as the potential biomarkers of depression. Developments in this chapter offered the potential to greatly enhance our understanding of brain connectivity abnormalities through temporal-based SNN architecture in depression detection.

In the current implementation, the threshold of all the spiking neurons is the same; however, neurons demonstrate different properties in the brain. The threshold of spiking neurons in the next layer could be calculated based on the firing rate or ISI of spiking neurons in the previous layer. Additionally, based on the complexity of the problem, more complex neuron models, i.e., biophysical models with neurotransmitters and

neuroreceptors with reinforcement learning-based STDP, should be implemented in the future.

Further, considering the nature of the problem in the real world, there would exist individuals who are experiencing mild, moderate, or severe depression. In the future, a voting or ensemble approach should be considered to distinguish these depressed groups. Post-binary classification of healthy and depressed groups, an ensemble approach, could be employed for further separating the three subgroups of depression: mild, moderate, and severe depression. Two possible solutions to this problem exist; a multilabel classification model or a regression model predicting the depression score. SNN-based ensemble classification and regression models could potentially be the technique to resolve such problems.

Chapter 5 will be published in a journal.

7.1.4 Chapter 6 Contributions and Future Directions

This chapter proposed a hybrid coding technique to build a deep feed-forward SNN-based architecture. The architectural model proposed binary filters for feature extraction from the spike trains of lower levels. The proposed hand-crafted filters can theoretically extract spatial and temporal features from spike trains. This architectural design enabling hierarchical feature extraction from spike trains is the first research work to build a deep SNN using spike-based filters to the best of our knowledge. Apart from this, a new spike encoding module consisting of LIF neurons is introduced in the proposed architecture, which makes this architecture a pure SNN-based temporal framework. Conceptually, the proposed deep SNN can extract temporal features at each layer. This will enable the development of unique temporal patterns with distinguishable spiking activities at the output layer. The hybrid classification criterion-based temporal coding features, i.e., the RMSE and Gamma metrics, will enhance the performance of the proposed deep

temporal-SNN framework capable of classifying any spatiotemporal datasets.

However, this architecture can have a trade-off where the neuron's membrane potential may take longer to exceed the threshold if the distance between two spikes is greater or if it receives fewer spikes from the previous layer. The reason is that the threshold of spiking neurons at each layer is fixed in the current design. To overcome this challenge, a dynamic threshold could be adapted. The threshold of the spiking neurons could be adjusted in multiple ways. First, calculate each layer's maximum and minimum membrane potential value and compare it with the current fixed threshold. If the current voltage value exceeds the maximum weighted voltages at that timestep, the threshold value can be scaled up by a certain factor. If the current membrane potential is less than the minimum voltage of the previous layer, the threshold could be scaled down. Repeating this dynamical adjustment of the neuron's threshold at each layer will enable information transfer from one layer to the next. This will produce a unique temporal firing pattern at the output layer, increasing the classification performance.

A second way to implement dynamic threshold adaption is to use the ISI. The time difference between two spikes in the previous layer affects the membrane potential of the next layer. In other words, ISI is inversely proportional to the firing of spiking neurons. Thus, to regulate the firing of spiking neurons, a relationship could be built between the ISI of input spike trains and the membrane potentials of neurons in the next layer. In the future, attempts can be made to model this behavior mathematically.

With these potential approaches to adapt the threshold at each layer along with the optimisation of different SNN parameters, the decision-making process of the proposed deep SNN could be effective. The proposed architecture needs to be tested and evaluated on different spatiotemporal datasets. The configuration of filters, i.e., the size, needs to be explored and optimised using the DE algorithm.

Furthermore, this research has implemented the simplest yet most efficient of all the spiking neuron models, i.e., the LIF neuron model. Izhikevich neuron model (Izhikevich,

2004) could be adapted in this research because of its capability to produce different behaviours of cortical neurons.

To conclude, this thesis has employed the NeuCube-based SNN architecture for depression detection with classification accuracy from 68% to 72% and 54% to 58% with 66 and 22 samples, respectively. Further, the proposed temporal-based architecture has been applied to three datasets: Music signals (10 samples), Figshare (22 samples), and the PREDICT depression datasets (22 samples), producing classification accuracy between 80% to 93%. Finally, a framework to build a deep SNN through hierarchical feature extraction from spike trains is introduced. With these various contributions achieved and improvements suggested as part of future work, the SNN architecture shows the capability to be utilised for other spatiotemporal data classification. For example, the SNNs could be utilised for natural language processing (NLP) applications like text classification using social media for depression detection. The linguistic data has a sequential structure that shows a unique advantage for the utilisation of SNNs. The large language models (LLMs) like Generative Pre-trained Transformers (GPT-3) (Brown et al., 2020) used in NLP applications are pre-trained models for generating human-like text and other NLP tasks like sentiment classification, question-answering, text summarisation, etc. They have achieved impressive performance but have come with serious computation and energy consumption during the training and inference stages. GPT-3 is trained on large text datasets with 175 billion parameters consisting of recurrent, feedforward, embedding, and attention layers. These layers work together to process the input text and generate output predictions. They provide pre-trained embeddings that capture words' semantic and syntactic meaning as they are trained on large datasets. For SNNs to be in NLP applications, binary events could be created from the pre-trained embeddings to convert continuous values into spikes. With 0's and 1's in the spiking data, lots of multiplicative operations would be replaced by additive operations. After the embedding layer, bi-directional SNNs, attention, and learning

mechanisms need to be implemented to allow SNNs to learn a sentence's forward and backward contexts. Further, massive hyperparameter tuning would be required to train the model on large datasets. With powerful hardware available like TrueNorth chip (Merolla et al., 2014), SNNs in the future will become effective for NLP tasks as well (Xiao et al., 2022).

To summarise, this research, with its integration of biological principles, neuroscience, and psychology, has opened new research avenues in processing spatiotemporal information with the layered organisation of spiking neurons.

References

Abásolo, D., Escudero, J., Hornero, R., Gómez, C. & Espino, P. (2008). Approximate entropy and auto mutual information analysis of the electroencephalogram in alzheimer's disease patients. *Medical & biological engineering & computing*, *46*(10), 1019–1028.

Abásolo, D., Hornero, R., Escudero, J. & Espino, P. (2008). A study on the possible usefulness of detrended fluctuation analysis of the electroencephalogram background activity in alzheimer's disease. *IEEE transactions on Biomedical Engineering*, *55*(9), 2171–2179.

Abdar, M. (2015). Using decision trees in data mining for predicting factors influencing of heart disease. *Carpathian Journal of Electronic and Computer Engineering*, *8*(2), 31.

Abdar, M., Zomorodi-Moghadam, M., Zhou, X., Gururajan, R., Tao, X., Barua, P. D. & Gururajan, R. (2020). A new nested ensemble technique for automated diagnosis of breast cancer. *Pattern Recognition Letters*, *132*, 123–131.

Abhang, P. A., Gawali, B. & Mehrotra, S. (2016). *Introduction to eeg-and speech-based emotion recognition*. Academic Press.

Acharya, U. R., Oh, S. L., Hagiwara, Y., Tan, J. H., Adeli, H. & Subha, D. P. (2018). Automated eeg-based screening of depression using deep convolutional neural network. *Computer methods and programs in biomedicine*, *161*, 103–113.

Acharya, U. R., Sudarshan, V. K., Adeli, H., Santhosh, J., Koh, J. E., Puthankatti, S. D. & Adeli, A. (2015). A novel depression diagnosis index using nonlinear features in eeg signals. *European neurology*, *74*(1-2), 79–83.

Ahmadlou, M., Adeli, H. & Adeli, A. (2012). Fractality analysis of frontal brain in major depressive disorder. *International Journal of Psychophysiology*, *85*(2), 206–211.

Akbari, H., Sadiq, M. T., Payan, M., Esmaili, S. S., Baghri, H. & Bagheri, H. (2021). Depression detection based on geometrical features extracted from sodp shape of eeg signals and binary pso. *Traitement du Signal*, *38*(1).

Aldworth, Z. N., Dimitrov, A. G., Cummins, G. I., Gedeon, T. & Miller, J. P. (2011). Temporal encoding in a nervous system. *PLoS computational biology*, *7*(5), e1002041.

Allen, J. J., Urry, H. L., Hitt, S. K. & Coan, J. A. (2004). The stability of resting frontal electroencephalographic asymmetry in depression. *Psychophysiology*, *41*(2), 269–280.

Alzhrani, W., Doborjeh, M., Doborjeh, Z. & Kasabov, N. (2021). Emotion recognition and understanding using eeg data in a brain-inspired spiking neural network architecture. In *2021 international joint conference on neural networks (ijcnn)* (pp. 1–9).

Al Zoubi, O., Mayeli, A., Tsuchiyagaito, A., Misaki, M., Zotev, V., Refai, H., ... others (2019). Eeg microstates temporal dynamics differentiate individuals with mood and anxiety disorders from healthy subjects. *Frontiers in human neuroscience*, *13*, 56.

Alzubaidi, L., Zhang, J., Humaidi, A. J., Al-Dujaili, A., Duan, Y., Al-Shamma, O., ... Farhan, L. (2021). Review of deep learning: Concepts, cnn architectures, challenges, applications, future directions. *Journal of big Data*, *8*, 1–74.

Antelis, J. M., Falcón, L. E. et al. (2020). Spiking neural networks applied to the classification of motor tasks in eeg signals. *Neural Networks*, *122*, 130–143.

Antoniades, A., Spyrou, L., Martin-Lopez, D., Valentin, A., Alarcon, G., Sanei, S. & Took, C. C. (2018). Deep neural architectures for mapping scalp to intracranial eeg. *International journal of neural systems*, *28*(08), 1850009.

Ay, B., Yildirim, O., Talo, M., Baloglu, U. B., Aydin, G., Puthankattil, S. D. & Acharya, U. R. (2019). Automated depression detection using deep representation and sequence learning with eeg signals. *Journal of medical systems*, *43*(7), 1–12.

Bachmann, M., Päeske, L., Kalev, K., Aarma, K., Lehtmets, A., Ööpik, P., ... Hinrikus, H. (2018). Methods for classifying depression in single channel eeg using linear and nonlinear signal analysis. *Computer methods and programs in biomedicine*, *155*, 11–17.

Bairy, G. M., Lih, O. S., Hagiwara, Y., Puthankattil, S. D., Faust, O., Niranjan, U. & Acharya, U. R. (2017). Automated diagnosis of depression electroencephalograph signals using linear prediction coding and higher order spectra features. *Journal of Medical Imaging and Health Informatics*, *7*(8), 1857–1862.

Bashivan, P., Rish, I., Yeasin, M. & Codella, N. (2015). Learning representations from eeg with deep recurrent-convolutional neural networks. *arXiv preprint arXiv:1511.06448*.

Behroozmand, R. & Sangtian, S. (2018). Neural bases of sensorimotor adaptation in the vocal motor system. *Experimental Brain Research*, *236*(7), 1881–1895.

Bengio, Y., Lee, D.-H., Bornschein, J., Mesnard, T. & Lin, Z. (2015). Towards biologically plausible deep learning. *arXiv preprint arXiv:1502.04156*.

Berlin, S. J. & John, M. (2020). Light weight convolutional models with spiking neural network based human action recognition. *Journal of Intelligent & Fuzzy Systems*, *39*(1), 961–973.

Blackhart, G. C., Minnix, J. A. & Kline, J. P. (2006). Can eeg asymmetry patterns predict future development of anxiety and depression?: A preliminary study. *Biological psychology*, *72*(1), 46–50.

Bohte, S. M., Kok, J. N. & La Poutré, J. A. (2000). Spikeprop: backpropagation for networks of spiking neurons. In *Esann* (Vol. 48, pp. 419–424).

Brette, R. (2015). Philosophy of the spike: rate-based vs. spike-based theories of the brain. *Frontiers in systems neuroscience*, 151.

Brown, T., Mann, B., Ryder, N., Subbiah, M., Kaplan, J. D., Dhariwal, P., ... others (2020). Language models are few-shot learners. *Advances in neural information processing systems*, *33*, 1877–1901.

Bullmore, E. & Sporns, O. (2009). Complex brain networks: graph theoretical analysis of structural and functional systems. *Nature reviews neuroscience*, *10*(3), 186–198.

Butts, D. A., Weng, C., Jin, J., Yeh, C.-I., Lesica, N. A., Alonso, J.-M. & Stanley, G. B. (2007). Temporal precision in the neural code and the timescales of natural vision. *Nature*, *449*(7158), 92–95.

Cao, Y., Chen, Y. & Khosla, D. (2015). Spiking deep convolutional neural networks for energy-efficient object recognition. *International Journal of Computer Vision*, *113*(1), 54–66.

Cao, Y. & Grossberg, S. (2012). Stereopsis and 3d surface perception by spiking neurons in laminar cortical circuits: A method for converting neural rate models into spiking models. *Neural Networks*, *26*, 75–98.

Cao, Y., Grossberg, S. & Markowitz, J. (2011). How does the brain rapidly learn and reorganize view-invariant and position-invariant object representations in the inferotemporal cortex? *Neural Networks*, *24*(10), 1050–1061.

Capecci, E., Kasabov, N. & Wang, G. Y. (2015). Analysis of connectivity in neucube spiking neural network models trained on eeg data for the understanding of functional changes in the brain: A case study on opiate dependence treatment. *Neural Networks*, *68*, 62–77.

Carstensen, A.-K. & Bernhard, J. (2019). Design science research–a powerful tool for improving methods in engineering education research. *European Journal of Engineering Education*, *44*(1-2), 85–102.

Cavanagh, J. F., Bismark, A. W., Frank, M. J. & Allen, J. J. (2019). Multiple dissociations between comorbid depression and anxiety on reward and punishment processing: Evidence from computationally informed eeg. *Computational Psychiatry (Cambridge, Mass.)*, *3*, 1.

Cavanagh, J. F., Napolitano, A., Wu, C. & Mueen, A. (2017). The patient repository for eeg data+ computational tools (pred+ ct). *Frontiers in neuroinformatics*, *11*, 67.

Chan, V., Liu, S.-C. & van Schaik, A. (2007). Aer ear: A matched silicon cochlea pair with address event representation interface. *IEEE Transactions on Circuits and Systems I: Regular Papers*, *54*(1), 48–59.

Chemin, B., Huang, G., Mulders, D. & Mouraux, A. (2018). Eeg time-warping to study non-strictly-periodic eeg signals related to the production of rhythmic movements. *Journal of neuroscience methods*, *308*, 106–115.

Chen, R., Ma, H., Xie, S., Guo, P., Li, P. & Wang, D. (2018). Fast and efficient deep sparse multi-strength spiking neural networks with dynamic pruning. In *2018 international joint conference on neural networks (ijcnn)* (pp. 1–8).

Chen, Y., Mai, Y., Feng, R. & Xiao, J. (2022). An adaptive threshold mechanism for accurate and efficient deep spiking convolutional neural networks. *Neurocomputing*, *469*, 189–197.

Churchland, P. S. & Sejnowski, T. J. (1994). *The computational brain*. MIT press.

Coan, J. A. & Allen, J. J. (2004). Frontal eeg asymmetry as a moderator and mediator of emotion. *Biological psychology*, *67*(1-2), 7–50.

Cooper, R. (2018). *Diagnosing the diagnostic and statistical manual of mental disorders*. Routledge.

Cox, D. D. & Dean, T. (2014). Neural networks and neuroscience-inspired computer vision. *Current Biology*, *24*(18), R921–R929.

Craik, A., He, Y. & Contreras-Vidal, J. L. (2019). Deep learning for electroencephalogram (eeg) classification tasks: a review. *Journal of neural engineering*, *16*(3), 031001.

Craik, F. I. & Lockhart, R. S. (1972). Levels of processing: A framework for memory research. *Journal of verbal learning and verbal behavior*, *11*(6), 671–684.

Crick, F. et al. (1989). The recent excitement about neural networks. *Nature*, *337*(6203), 129–132.

Dan, Y. & Poo, M.-m. (2004). Spike timing-dependent plasticity of neural circuits. *Neuron*, *44*(1), 23–30.

Davidson, R. J. (1992). *Emotion and affective style: Hemispheric substrates.* SAGE Publications Sage CA: Los Angeles, CA.

Davidson, R. J. (1998). Anterior electrophysiological asymmetries, emotion, and depression: Conceptual and methodological conundrums. *Psychophysiology*, *35*(5), 607–614.

Debener, S., Beauducel, A., Nessler, D., Brocke, B., Heilemann, H. & Kayser, J. (2000). Is resting anterior eeg alpha asymmetry a trait marker for depression? *Neuropsychobiology*, *41*(1), 31–37.

de Kwaasteniet, B., Ruhe, E., Caan, M., Rive, M., Olabarriaga, S., Groefsema, M., ... Denys, D. (2013). Relation between structural and functional connectivity in major depressive disorder. *Biological psychiatry*, *74*(1), 40–47.

Deng, L. (2012). The mnist database of handwritten digit images for machine learning research [best of the web]. *IEEE Signal Processing Magazine*, *29*(6), 141–142.

Dervin, J. (1990). Co-planar stereotaxic atlas of the human brain 3-dimensional proportional system: An approach to cerebral imaging 1988j. talairich and p. tournoux mark rayport georg thieme verlag. stuttgart, new york 3 13 711 701 1 price dm 268. pp. 122. illustrations 130. *The Journal of Laryngology & Otology*, *104*(1), 72–72.

Deslandes, A. C., De Moraes, H., Pompeu, F. A., Ribeiro, P., Cagy, M., Capitão, C., ... Laks, J. (2008). Electroencephalographic frontal asymmetry and depressive symptoms in the elderly. *Biological psychology*, *79*(3), 317–322.

Diehl, P. U. & Cook, M. (2015). Unsupervised learning of digit recognition using spike-timing-dependent plasticity. *Frontiers in computational neuroscience*, *9*, 99.

Diehl, P. U., Neil, D., Binas, J., Cook, M., Liu, S.-C. & Pfeiffer, M. (2015). Fast-classifying, high-accuracy spiking deep networks through weight and threshold balancing. In *2015 international joint conference on neural networks (ijcnn)* (pp. 1–8).

Disabato, B., Bauer, I. E., Soares, J. C. & Sheline, Y. (2016). Neural structure and organization of mood pathology. In *The oxford handbook of mood disorders.*

Doborjeh, M. G., Wang, G. Y., Kasabov, N. K., Kydd, R. & Russell, B. (2015). A spiking neural network methodology and system for learning and comparative analysis of eeg data from healthy versus addiction treated versus addiction not treated subjects. *IEEE transactions on biomedical engineering*, *63*(9), 1830–1841.

Doborjeh, Z., Doborjeh, M., Taylor, T., Kasabov, N., Wang, G. Y., Siegert, R. & Sumich, A. (2019). Spiking neural network modelling approach reveals how mindfulness training rewires the brain. *Scientific reports*, *9*(1), 1–15.

Drevets, W. C. (2000). Neuroimaging studies of mood disorders. *Biological psychiatry*, *48*(8), 813–829.

DSM-IV., A. P. A. T. F. o. (1993).
In *Dsm-iv draft criteria: Amer psychiatric pub incorporated.*

Du, L., Liu, H., Du, W., Chao, F., Zhang, L., Wang, K., ... Tang, Y. (2018). Stimulated left dlpfc-nucleus accumbens functional connectivity predicts the anti-depression and anti-anxiety effects of rtms for depression. *Translational psychiatry*, *7*(11), 1–10.

Duan, L., Duan, H., Qiao, Y., Sha, S., Qi, S., Zhang, X., ... Wang, C. (2020). Machine learning approaches for mdd detection and emotion decoding using eeg signals. *Frontiers in Human Neuroscience*, *14*, 284.

Dubois, J. & Adolphs, R. (2016). Building a science of individual differences from fmri. *Trends in cognitive sciences*, *20*(6), 425–443.

Elliott, M. L., Romer, A., Knodt, A. R. & Hariri, A. R. (2018). A connectome-wide functional signature of transdiagnostic risk for mental illness. *Biological psychiatry*, *84*(6), 452–459.

Elliott, R., Zahn, R., Deakin, J. & Anderson, I. M. (2011). Affective cognition and its disruption in mood disorders. *Neuropsychopharmacology*, *36*(1), 153–182.

Ewald, A., Avarvand, F. S. & Nolte, G. (2013). Identifying causal networks of neuronal sources from eeg/meg data with the phase slope index: a simulation study. *Biomedizinische Technik/Biomedical Engineering*, *58*(2), 165–178.

Fair, D. A., Cohen, A. L., Power, J. D., Dosenbach, N. U., Church, J. A., Miezin, F. M., ... Petersen, S. E. (2009). Functional brain networks develop from a "local to distributed" organization. *PLoS computational biology*, *5*(5), e1000381.

Falcone, C. M. & Villanueva, M. A. M. (2017). *Methods for noninvasive localization of focal epileptic activity with magnetoencephalography* (Unpublished doctoral dissertation). Universitat Politècnica de Catalunya (UPC).

Fan, Y., Yu, R., Li, J., Zhu, J. & Li, X. (2020). Eeg-based mild depression recognition using multi-kernel convolutional and spatial-temporal feature. In *2020 ieee international conference on bioinformatics and biomedicine (bibm)* (pp. 1777–1784).

Faust, O., Ang, P. C. A., Puthankattil, S. D. & Joseph, P. K. (2014). Depression diagnosis support system based on eeg signal entropies. *Journal of mechanics in medicine and biology*, *14*(03), 1450035.

Ferrari, C., Ciricugno, A. & Cattaneo, Z. (2022). Cerebellar contribution to emotional

body language perception. In *The emotional cerebellum* (pp. 141–153). Springer.

Fingelkurts, A. A. & Fingelkurts, A. A. (2015). Altered structure of dynamic electroencephalogram oscillatory pattern in major depression. *Biological Psychiatry*, *77*(12), 1050–1060.

Fingelkurts, A. A., Fingelkurts, A. A., Rytsälä, H., Suominen, K., Isometsä, E. & Kähkönen, S. (2006). Composition of brain oscillations in ongoing eeg during major depression disorder. *Neuroscience research*, *56*(2), 133–144.

Fitzgerald, P. B., Laird, A. R., Maller, J. & Daskalakis, Z. J. (2008). A meta-analytic study of changes in brain activation in depression. *Human brain mapping*, *29*(6), 683–695.

Fitzgerald, P. B., Srithiran, A., Benitez, J., Daskalakis, Z. Z., Oxley, T. J., Kulkarni, J. & Egan, G. F. (2008). An fmri study of prefrontal brain activation during multiple tasks in patients with major depressive disorder. *Human Brain Mapping*, *29*(4), 490–501.

Flach, P. & Kull, M. (2015). Precision-recall-gain curves: Pr analysis done right. *Advances in neural information processing systems*, *28*.

Flor-Henry, P., Lind, J. C. & Koles, Z. J. (2004). A source-imaging (low-resolution electromagnetic tomography) study of the eegs from unmedicated males with depression. *Psychiatry Research: Neuroimaging*, *130*(2), 191–207.

Friedman, M. (1937). The use of ranks to avoid the assumption of normality implicit in the analysis of variance. *Journal of the american statistical association*, *32*(200), 675–701.

Fukushima, K. & Miyake, S. (1982). Neocognitron: A self-organizing neural network model for a mechanism of visual pattern recognition. In *Competition and cooperation in neural nets* (pp. 267–285). Springer.

Fukushima, M., Rauske, P. L. & Margoliash, D. (2015). Temporal and rate code analysis of responses to low-frequency components in the bird's own song by song system neurons. *Journal of Comparative Physiology A*, *201*(12), 1103–1114.

Fusi, S., Annunziato, M., Badoni, D., Salamon, A. & Amit, D. J. (2000). Spike-driven synaptic plasticity: theory, simulation, vlsi implementation. *Neural computation*, *12*(10), 2227–2258.

Gabrieli, J. D., Ghosh, S. S. & Whitfield-Gabrieli, S. (2015). Prediction as a humanitarian and pragmatic contribution from human cognitive neuroscience. *Neuron*, *85*(1), 11–26.

Garcia-Casares, N., Jorge, R. E., Garcia-Arnes, J. A., Acion, L., Berthier, M. L., Gonzalez-Alegre, P., ... others (2014). Cognitive dysfunctions in middle-aged type 2 diabetic patients and neuroimaging correlations: a cross-sectional study. *Journal of Alzheimer's Disease*, *42*(4), 1337–1346.

Garner, S. R. et al. (1995). Weka: The waikato environment for knowledge analysis. In *Proceedings of the new zealand computer science research students conference* (Vol. 1995, pp. 57–64).

Gerstner, W. & Kistler, W. M. (2002). *Spiking neuron models: Single neurons, populations, plasticity*. Cambridge university press.

Gerstner, W., Ritz, R. & Van Hemmen, J. L. (1993). Why spikes? hebbian learning

and retrieval of time-resolved excitation patterns. *Biological cybernetics*, *69*(5), 503–515.

Ghassemzadeh, H., Mojtabai, R., Karamghadiri, N. & Ebrahimkhani, N. (2005). Psychometric properties of a persian-language version of the beck depression inventory-second edition: Bdi-ii-persian. *Depression and anxiety*, *21*(4), 185–192.

Ghosh-Dastidar, S. & Adeli, H. (2009). Spiking neural networks. *International journal of neural systems*, *19*(04), 295–308.

GI, K. F. (1989). A hierarchical neural network capable of visual pattern recognition. *Neural Network*, *1*.

Gollan, J. K., Hoxha, D., Chihade, D., Pflieger, M. E., Rosebrock, L. & Cacioppo, J. (2014). Frontal alpha eeg asymmetry before and after behavioral activation treatment for depression. *Biological psychology*, *99*, 198–208.

Gollisch, T. & Meister, M. (2008). Rapid neural coding in the retina with relative spike latencies. *science*, *319*(5866), 1108–1111.

Gotlib, I. H. (1998). Eeg alpha asymmetry, depression, and cognitive functioning. *Cognition & Emotion*, *12*(3), 449–478.

Goulden, N., McKie, S., Thomas, E. J., Downey, D., Juhasz, G., Williams, S. R., ... Elliott, R. (2012). Reversed frontotemporal connectivity during emotional face processing in remitted depression. *Biological Psychiatry*, *72*(7), 604–611.

Gramfort, A., Luessi, M., Larson, E., Engemann, D. A., Strohmeier, D., Brodbeck, C., ... others (2013). Meg and eeg data analysis with mne-python. *Frontiers in neuroscience*, *7*, 267.

Grin-Yatsenko, V. A., Baas, I., Ponomarev, V. A. & Kropotov, J. D. (2010). Independent component approach to the analysis of eeg recordings at early stages of depressive disorders. *Clinical Neurophysiology*, *121*(3), 281–289.

Grossberg, S. (1987). Competitive learning: From interactive activation to adaptive resonance. *Cognitive science*, *11*(1), 23–63.

Grossberg, S., Markowitz, J. & Cao, Y. (2011). On the road to invariant recognition: Explaining tradeoff and morph properties of cells in inferotemporal cortex using multiple-scale task-sensitive attentive learning. *Neural Networks*, *24*(10), 1036–1049.

Güntürkün, O., Ströckens, F. & Ocklenburg, S. (2020). Brain lateralization: a comparative perspective. *Physiological reviews*, *100*(3), 1019–1063.

Guo, W., Fouda, M. E., Eltawil, A. M. & Salama, K. N. (2021). Neural coding in spiking neural networks: A comparative study for robust neuromorphic systems. *Frontiers in Neuroscience*, *15*, 212.

Guo, W., Liu, F., Chen, J., Wu, R., Li, L., Zhang, Z., ... Zhao, J. (2017). Using short-range and long-range functional connectivity to identify schizophrenia with a family-based case-control design. *Psychiatry Research: Neuroimaging*, *264*, 60–67.

Guo, W., Liu, F., Chen, J., Wu, R., Zhang, Z., Yu, M., ... Zhao, J. (2016). Decreased long-and short-range functional connectivity at rest in drug-naive major depressive disorder. *Australian & New Zealand Journal of Psychiatry*, *50*(8), 763–769.

Haeusler, S. & Maass, W. (2007). A statistical analysis of information-processing properties of lamina-specific cortical microcircuit models. *Cerebral cortex*, *17*(1), 149–162.

Hahn, T., Nierenberg, A. A. & Whitfield-Gabrieli, S. (2017). Predictive analytics in mental health: applications, guidelines, challenges and perspectives. *Molecular psychiatry*, *22*(1), 37–43.

Harris, C. R., Millman, K. J., van der Walt, S. J., Gommers, R., Virtanen, P., Cournapeau, D., ... Oliphant, T. E. (2020, September). Array programming with NumPy. *Nature*, *585*(7825), 357–362. Retrieved from `https://doi.org/10.1038/s41586-020-2649-2` doi: 10.1038/s41586-020-2649-2

Hastie, T., Tibshirani, R., Friedman, J. H. & Friedman, J. H. (2009). *The elements of statistical learning: data mining, inference, and prediction* (Vol. 2). Springer.

He, Y., Li, C. & Ju, X. (2021). Emotion classification using eeg data in a brain-inspired spiking neural network. In *2021 11th international conference on intelligent control and information processing (icicip)* (pp. 433–437).

Hebb, D. O. (1949a). The first stage of perception: growth of the assembly. *The Organization of Behavior*, *4*, 60–78.

Hebb, D. O. (1949b). *The organization of behavior: a neuropsychological theory*. J. Wiley; Chapman & Hall.

Henriques, J. B. & Davidson, R. J. (1991). Left frontal hypoactivation in depression. *Journal of abnormal psychology*, *100*(4), 535.

Heo, H., Sung, D. & Lee, K. (2013). Note onset detection based on harmonic cepstrum regularity. In *2013 ieee international conference on multimedia and expo (icme)* (pp. 1–6).

Hinrikus, H., Suhhova, A., Bachmann, M., Aadamsoo, K., Võhma, Ü., Lass, J. & Tuulik, V. (2009). Electroencephalographic spectral asymmetry index for detection of depression. *Medical & biological engineering & computing*, *47*(12), 1291–1299.

Hinrikus, H., Suhhova, A., Bachmann, M., Aadamsoo, K., Võhma, Ü., Pehlak, H. & Lass, J. (2010). Spectral features of eeg in depression.

Hinton, G., Deng, L., Yu, D., Dahl, G. E., Mohamed, A.-r., Jaitly, N., ... others (2012). Deep neural networks for acoustic modeling in speech recognition: The shared views of four research groups. *IEEE Signal processing magazine*, *29*(6), 82–97.

Hochreiter, S. & Schmidhuber, J. (1997). Long short-term memory. *Neural computation*, *9*(8), 1735–1780.

Home, G. R. (2016). *Free conservative christian music.* Retrieved from `https://gospelriver.com/music`

Hosseinifard, B., Moradi, M. H. & Rostami, R. (2013). Classifying depression patients and normal subjects using machine learning techniques and nonlinear features from eeg signal. *Computer methods and programs in biomedicine*, *109*(3), 339–345.

Howard, G., Gale, E., Bull, L., de Lacy Costello, B. & Adamatzky, A. (2012). Evolution of plastic learning in spiking networks via memristive connections. *IEEE Transactions on Evolutionary Computation*, *16*(5), 711–729.

Hu, B., Majoe, D., Ratcliffe, M., Qi, Y., Zhao, Q., Peng, H., ... Moore, P. (2011).

Eeg-based cognitive interfaces for ubiquitous applications: Developments and challenges. *IEEE Intelligent Systems*, *26*(5), 46–53.

Hubel, D. H. & Wiesel, T. N. (1959). Receptive fields of single neurones in the cat's striate cortex. *The Journal of physiology*, *148*(3), 574–591.

Hubel, D. H. & Wiesel, T. N. (1962). Receptive fields, binocular interaction and functional architecture in the cat's visual cortex. *The Journal of physiology*, *160*(1), 106–154.

Hunsberger, E. & Eliasmith, C. (2016). Training spiking deep networks for neuromorphic hardware. *arXiv preprint arXiv:1611.05141*.

Illing, B., Gerstner, W. & Brea, J. (2019). Biologically plausible deep learning—but how far can we go with shallow networks? *Neural Networks*, *118*, 90–101.

Iosifescu, D. V., Greenwald, S., Devlin, P., Mischoulon, D., Denninger, J. W., Alpert, J. E. & Fava, M. (2009). Frontal eeg predictors of treatment outcome in major depressive disorder. *European Neuropsychopharmacology*, *19*(11), 772–777.

Izhikevich, E. M. (2003). Simple model of spiking neurons. *IEEE Transactions on neural networks*, *14*(6), 1569–1572.

Izhikevich, E. M. (2004). Which model to use for cortical spiking neurons? *IEEE transactions on neural networks*, *15*(5), 1063–1070.

Jin, Y., Zhang, W. & Li, P. (2018). Hybrid macro/micro level backpropagation for training deep spiking neural networks. *arXiv preprint arXiv:1805.07866*.

Jirayucharoensak, S., Pan-Ngum, S. & Israsena, P. (2014). Eeg-based emotion recognition using deep learning network with principal component based covariate shift adaptation. *The Scientific World Journal*, *2014*.

Johansson, R. S. & Flanagan, J. R. (2009). Coding and use of tactile signals from the fingertips in object manipulation tasks. *Nature Reviews Neuroscience*, *10*(5), 345–359.

Jolivet, R., Rauch, A., Lüscher, H.-R. & Gerstner, W. (2006). Predicting spike timing of neocortical pyramidal neurons by simple threshold models. *Journal of computational neuroscience*, *21*(1), 35–49.

Jordan, J. (2021). *Evaluating a machine learning model.* Retrieved 2022-01-30, from `https://www.jeremyjordan.me/evaluating-a-machine-learning-model/`

Jurjuţ, O. F., Gheorghiu, M., Singer, W., Nikolić, D. & Mureşan, R. C. (2019). Hold your methods! how multineuronal firing ensembles can be studied using classical spike-train analysis techniques. *Frontiers in systems neuroscience*, *13*, 21.

Jurjuţ, O. F., Nikolić, D., Pipa, G., Singer, W., Metzler, D. & Mureşan, R. C. (2009). A color-based visualization technique for multielectrode spike trains. *Journal of neurophysiology*, *102*(6), 3766–3778.

Jurjuţ, O. F., Nikolić, D., Singer, W., Yu, S., Havenith, M. N. & Mureşan, R. C. (2011). Timescales of multineuronal activity patterns reflect temporal structure of visual stimuli. *PLoS One*, *6*(2), e16758.

Kadipasaoglu, C. M., Forseth, K., Whaley, M., Conner, C. R., Rollo, M. J., Baboyan, V. G. & Tandon, N. (2015). Development of grouped iceeg for the study of cognitive processing. *Frontiers in psychology*, *6*, 1008.

Kaiser, R. H., Andrews-Hanna, J. R., Wager, T. D. & Pizzagalli, D. A. (2015). Large-scale network dysfunction in major depressive disorder: a meta-analysis of resting-state functional connectivity. *JAMA psychiatry*, *72*(6), 603–611.

Kapoor, A. (2019). *Hands-on artificial intelligence for iot: Expert machine learning and deep learning techniques for developing smarter iot systems*. Packt Publishing Ltd.

Kasabov, N. (2018). Time-space, spiking neural networks and brain-inspired artificial intelligence, springer.

Kasabov, N., Dhoble, K., Nuntalid, N. & Indiveri, G. (2013). Dynamic evolving spiking neural networks for on-line spatio-and spectro-temporal pattern recognition. *Neural Networks*, *41*, 188–201.

Kasabov, N. K. (2014). Neucube: A spiking neural network architecture for mapping, learning and understanding of spatio-temporal brain data. *Neural Networks*, *52*, 62–76.

Katsigiannis, S. & Ramzan, N. (2017). Dreamer: A database for emotion recognition through eeg and ecg signals from wireless low-cost off-the-shelf devices. *IEEE journal of biomedical and health informatics*, *22*(1), 98–107.

Kaur, C., Bisht, A., Singh, P. & Joshi, G. (2021). Eeg signal denoising using hybrid approach of variational mode decomposition and wavelets for depression. *Biomedical Signal Processing and Control*, *65*, 102337.

Ke, W., Xing, Y., Di Caterina, G., Petropoulakis, L. & Soraghan, J. (2020). Deep convolutional spiking neural network based hand gesture recognition. In *2020 international joint conference on neural networks (ijcnn)* (pp. 1–7).

Kheradpisheh, S. R., Ganjtabesh, M. & Masquelier, T. (2016). Bio-inspired unsupervised learning of visual features leads to robust invariant object recognition. *Neurocomputing*, *205*, 382–392.

Kheradpisheh, S. R., Ganjtabesh, M., Thorpe, S. J. & Masquelier, T. (2018). Stdp-based spiking deep convolutional neural networks for object recognition. *Neural Networks*, *99*, 56–67.

Khosla, A., Khandnor, P. & Chand, T. (2021). Automated diagnosis of depression from eeg signals using traditional and deep learning approaches: A comparative analysis. *Biocybernetics and Biomedical Engineering*.

Kim, J., Kim, H., Huh, S., Lee, J. & Choi, K. (2018). Deep neural networks with weighted spikes. *Neurocomputing*, *311*, 373–386.

King, J.-R. & Dehaene, S. (2014). Characterizing the dynamics of mental representations: the temporal generalization method. *Trends in cognitive sciences*, *18*(4), 203-210.

Kingma, D. P. & Ba, J. (2014). Adam: A method for stochastic optimization. *arXiv preprint arXiv:1412.6980*.

Kistler, W. M., Gerstner, W. & Hemmen, J. L. v. (1997). Reduction of the hodgkin-huxley equations to a single-variable threshold model. *Neural computation*, *9*(5), 1015–1045.

Knott, V., Mahoney, C., Kennedy, S. & Evans, K. (2001). Eeg power, frequency, asymmetry and coherence in male depression. *Psychiatry Research: Neuroimaging*,

106(2), 123–140.

Koelstra, S., Muhl, C., Soleymani, M., Lee, J.-S., Yazdani, A., Ebrahimi, T., ... Patras, I. (2011). Deap: A database for emotion analysis; using physiological signals. *IEEE transactions on affective computing*, *3*(1), 18–31.

Koessler, L., Maillard, L., Benhadid, A., Vignal, J. P., Felblinger, J., Vespignani, H. & Braun, M. (2009). Automated cortical projection of eeg sensors: anatomical correlation via the international 10–10 system. *Neuroimage*, *46*(1), 64–72.

Koo, P., Berger, C., Bartz, J., Wybitul, P. & Höppner, J. (2015). P124. qeeg and csd power analysis in depression. *Clinical Neurophysiology*, *126*(8), e151–e152.

Kragel, P. A., Hariri, A. R. & LaBar, K. S. (2022). The temporal dynamics of spontaneous emotional brain states and their implications for mental health. *Journal of cognitive neuroscience*, *34*(5), 715–728.

Krizhevsky, A., Sutskever, I. & Hinton, G. E. (2012). Imagenet classification with deep convolutional neural networks. *Advances in neural information processing systems*, *25*, 1097–1105.

Książek, W., Abdar, M., Acharya, U. R. & Pławiak, P. (2019). A novel machine learning approach for early detection of hepatocellular carcinoma patients. *Cognitive Systems Research*, *54*, 116–127.

Lagorce, X., Orchard, G., Galluppi, F., Shi, B. E. & Benosman, R. B. (2016). Hots: a hierarchy of event-based time-surfaces for pattern recognition. *IEEE transactions on pattern analysis and machine intelligence*, *39*(7), 1346–1359.

LeCun, Y., Bengio, Y., Hinton, G. et al. (2015). Deep learning. nature, 521 (7553), 436-444. *Google Scholar Google Scholar Cross Ref Cross Ref*.

LeCun, Y., Boser, B., Denker, J. S., Henderson, D., Howard, R. E., Hubbard, W. & Jackel, L. D. (1989). Backpropagation applied to handwritten zip code recognition. *Neural computation*, *1*(4), 541–551.

LeCun, Y., Kavukcuoglu, K. & Farabet, C. (2010). Convolutional networks and applications in vision. In *Proceedings of 2010 ieee international symposium on circuits and systems* (pp. 253–256).

Lee, C., Srinivasan, G., Panda, P. & Roy, K. (2018). Deep spiking convolutional neural network trained with unsupervised spike-timing-dependent plasticity. *IEEE Transactions on Cognitive and Developmental Systems*, *11*(3), 384–394.

Lee, J. H., Delbruck, T. & Pfeiffer, M. (2016). Training deep spiking neural networks using backpropagation. *Frontiers in neuroscience*, *10*, 508.

Leuchter, A. F., Cook, I. A., Hunter, A. M., Cai, C. & Horvath, S. (2012). Resting-state quantitative electroencephalography reveals increased neurophysiologic connectivity in depression. *PloS one*, *7*(2), e32508.

Li, D., Tang, J., Deng, Y. & Yang, L. (2021). Classification of resting state eeg data in patients with depression. In *2020 ieee international conference on e-health networking, application & services (healthcom)* (pp. 1–2).

Li, J., Duan, X., Cui, Q., Chen, H. & Liao, W. (2019). More than just statics: temporal dynamics of intrinsic brain activity predicts the suicidal ideation in depressed patients. *Psychological medicine*, *49*(5), 852–860.

Li, K. & Príncipe, J. C. (2018). Biologically-inspired spike-based automatic speech

recognition of isolated digits over a reproducing kernel hilbert space. *Frontiers in neuroscience*, *12*, 194.

Li, L., Jamieson, K., DeSalvo, G., Rostamizadeh, A. & Talwalkar, A. (2017). Hyperband: A novel bandit-based approach to hyperparameter optimization. *The Journal of Machine Learning Research*, *18*(1), 6765–6816.

Li, X., Hu, B., Sun, S. & Cai, H. (2016). Eeg-based mild depressive detection using feature selection methods and classifiers. *Computer methods and programs in biomedicine*, *136*, 151–161.

Li, X., Hu, B., Xu, T., Shen, J. & Ratcliffe, M. (2015). A study on eeg-based brain electrical source of mild depressed subjects. *Computer methods and programs in biomedicine*, *120*(3), 135–141.

LLC, D. A. G. (2010). *Fir filters by windowing.* Retrieved 2010-10-40, from `http://www.labbookpages.co.uk/audio/firWindowing.html#code`

Logiaco, L., Quilodran, R., Procyk, E. & Arleo, A. (2015). Spatiotemporal spike coding of behavioral adaptation in the dorsal anterior cingulate cortex. *PLoS biology*, *13*(8), e1002222.

Maass, W. (1997a). Networks of spiking neurons: The third generation of neural network models. *Neural Networks*, *10*(9), 1659-1671. Retrieved from `https://www.sciencedirect.com/science/article/pii/S0893608097000117` doi: https://doi.org/10.1016/S0893-6080(97)00011-7

Maass, W. (1997b). Networks of spiking neurons: the third generation of neural network models. *Neural networks*, *10*(9), 1659–1671.

Maass, W. & Bishop, C. M. (2001). *Pulsed neural networks*. MIT press.

Machens, C. K., Prinz, P., Stemmler, M. B., Ronacher, B. & Herz, A. V. (2001). Discrimination of behaviorally relevant signals by auditory receptor neurons. *Neurocomputing*, *38*, 263–268.

Mamoshina, P., Vieira, A., Putin, E. & Zhavoronkov, A. (2016). Applications of deep learning in biomedicine. *Molecular pharmaceutics*, *13*(5), 1445–1454.

Mao, W., Fathurrahman, H., Lee, Y. & Chang, T. (2020). Eeg dataset classification using cnn method. In *Journal of physics: conference series* (Vol. 1456, p. 012017).

Maratos, A., Gold, C., Wang, X. & Crawford, M. (2008). Music therapy for depression. *Cochrane database of systematic reviews*(1).

Marblestone, A. H., Wayne, G. & Kording, K. P. (2016). Toward an integration of deep learning and neuroscience. *Frontiers in computational neuroscience*, 94.

Martinez-Murcia, F. J., Górriz, J. M., Ramírez, J. & Ortiz, A. (2018). Convolutional neural networks for neuroimaging in parkinson's disease: is preprocessing needed? *International journal of neural systems*, *28*(10), 1850035.

Masquelier, T., Guyonneau, R. & Thorpe, S. J. (2009). Competitive stdp-based spike pattern learning. *Neural computation*, *21*(5), 1259–1276.

Masquelier, T. & Thorpe, S. J. (2007). Unsupervised learning of visual features through spike timing dependent plasticity. *PLoS computational biology*, *3*(2), e31.

Mathers, C. D. & Loncar, D. (2006). Projections of global mortality and burden of disease from 2002 to 2030. *PLoS medicine*, *3*(11), e442.

McFee, B., Raffel, C., Liang, D., Ellis, D. P., McVicar, M., Battenberg, E. & Nieto, O. (2015). librosa: Audio and music signal analysis in python. In *Proceedings of the 14th python in science conference* (Vol. 8, pp. 18–25).

Mechler, F., Victor, J. D., Purpura, K. P. & Shapley, R. (1998). Robust temporal coding of contrast by v1 neurons for transient but not for steady-state stimuli. *Journal of Neuroscience*, *18*(16), 6583–6598.

Mehlhorn, H. & Schreiber, F. (2013). Small-world property. In W. Dubitzky, O. Wolkenhauer, K.-H. Cho & H. Yokota (Eds.), *Encyclopedia of systems biology* (pp. 1957–1959). New York, NY: Springer New York. Retrieved from https://doi.org/10.1007/978-1-4419-9863-7_2 doi: 10.1007/978-1-4419-9863-7_2

Merolla, P. A., Arthur, J. V., Alvarez-Icaza, R., Cassidy, A. S., Sawada, J., Akopyan, F., ... others (2014). A million spiking-neuron integrated circuit with a scalable communication network and interface. *Science*, *345*(6197), 668–673.

Min, S., Lee, B. & Yoon, S. (2017). Deep learning in bioinformatics. *Briefings in bioinformatics*, *18*(5), 851–869.

Mitchell, A. J., Vaze, A. & Rao, S. (2009). Clinical diagnosis of depression in primary care: a meta-analysis. *The Lancet*, *374*(9690), 609–619.

Mochizuki, Y., Onaga, T., Shimazaki, H., Shimokawa, T., Tsubo, Y., Kimura, R., ... others (2016). Similarity in neuronal firing regimes across mammalian species. *Journal of Neuroscience*, *36*(21), 5736–5747.

Mohammadi, M., Al-Azab, F., Raahemi, B., Richards, G., Jaworska, N., Smith, D., ... Knott, V. (2015). Data mining eeg signals in depression for their diagnostic value. *BMC medical informatics and decision making*, *15*(1), 1–14.

Mohanty, R., Priyadarshini, A., Desai, V. S. & Sirisha, G. (2018). Applications of spiking neural network to predict software reliability. In *Intelligent engineering informatics* (pp. 149–157). Springer.

Moon, S.-E., Jang, S. & Lee, J.-S. (2018). Convolutional neural network approach for eeg-based emotion recognition using brain connectivity and its spatial information. In *2018 ieee international conference on acoustics, speech and signal processing (icassp)* (pp. 2556–2560).

Moroney, L. (2020). *Ai and machine learning for coders*. O'Reilly Media.

Mozafari, M., Ganjtabesh, M., Nowzari-Dalini, A., Thorpe, S. J. & Masquelier, T. (2019). Bio-inspired digit recognition using reward-modulated spike-timing-dependent plasticity in deep convolutional networks. *Pattern recognition*, *94*, 87–95.

Mumtaz, W. (2016, 11). *Eeg data new.* Retrieved from https://figshare.com/articles/dataset/EEG_Data_New/4244171 doi: 10.6084/m9.figshare.4244171.v1

Mumtaz, W., Xia, L., Mohd Yasin, M. A., Azhar Ali, S. S. & Malik, A. S. (2017). A wavelet-based technique to predict treatment outcome for major depressive disorder. *PloS one*, *12*(2), e0171409.

Nandrino, J.-L., Pezard, L., Martinerie, J., El Massioui, F., Renault, B., Jouvent, R., ... Widlöcher, D. (1994). Decrease of complexity in eeg as a symptom of depression.

Neuroreport: An International Journal for the Rapid Communication of Research in Neuroscience.

Narayan, R., Grana, G. & Sen, K. (2006). Distinct time scales in cortical discrimination of natural sounds in songbirds. *Journal of neurophysiology*, *96*(1), 252–258.

Neftci, E. O., Augustine, C., Paul, S. & Detorakis, G. (2017). Event-driven random back-propagation: Enabling neuromorphic deep learning machines. *Frontiers in neuroscience*, *11*, 324.

Newson, J. J. (2018). The challenges of mental health diagnosis. , *25*. Retrieved from `https://sapienlabs.org/the-challenges-of-mental-health-diagnosis/`

Nguyen, A., Yosinski, J. & Clune, J. (2015). Deep neural networks are easily fooled: High confidence predictions for unrecognizable images. In *Proceedings of the ieee conference on computer vision and pattern recognition* (pp. 427–436).

Nguyen, D.-A., Tran, X.-T., Dang, K. N. & Iacopi, F. (2020). A lightweight max-pooling method and architecture for deep spiking convolutional neural networks. In *2020 ieee asia pacific conference on circuits and systems (apccas)* (pp. 209–212).

Nikolić, D., Haeusler, S., Singer, W. & Maass, W. (2006). Temporal dynamics of information content carried by neurons in the primary visual cortex. *Advances in neural information processing systems*, *19*.

Nissen, C., Feige, B., König, A., Voderholzer, U., Berger, M. & Riemann, D. (2001). Delta sleep ratio as a predictor of sleep deprivation response in major depression. *Journal of psychiatric research*, *35*(3), 155–163.

Nissen, C., Feige, B., Nofzinger, E. A., Voderholzer, U., Berger, M. & Riemann, D. (2006). Eeg slow wave activity regulation in major depression. *Somnologie-Schlafforschung und Schlafmedizin*, *10*(2), 36–42.

Nolte, G., Ziehe, A., Nikulin, V. V., Schlögl, A., Krämer, N., Brismar, T. & Müller, K.-R. (2008). Robustly estimating the flow direction of information in complex physical systems. *Physical review letters*, *100*(23), 234101.

O'Connor, P., Neil, D., Liu, S.-C., Delbruck, T. & Pfeiffer, M. (2013). Real-time classification and sensor fusion with a spiking deep belief network. *Frontiers in neuroscience*, *7*, 178.

Oh, S. L., Ng, E. Y., San Tan, R. & Acharya, U. R. (2018). Automated diagnosis of arrhythmia using combination of cnn and lstm techniques with variable length heart beats. *Computers in biology and medicine*, *102*, 278–287.

Olah, C. (2015). Understanding lstm networks.

O'Malley, T., Bursztein, E., Long, J., Chollet, F., Jin, H., Invernizzi, L. et al. (2019). *Keras Tuner*. `https://github.com/keras-team/keras-tuner`.

Omel'Chenko, V. & Zaika, V. (2002). Changes in the eeg-rhythms in endogenous depressive disorders and the effect of pharmacotherapy. *Human Physiology*, *28*(3), 275–281.

Paiva, A. R., Park, I. & Principe, J. C. (2009). A reproducing kernel hilbert space framework for spike train signal processing. *Neural computation*, *21*(2), 424–449.

Palmer, S. M., Crewther, S. G., Carey, L. M. et al. (2015). A meta-analysis of changes

in brain activity in clinical depression. *Frontiers in human neuroscience*, *8*, 1045.

Panda, P., Srinivasan, G. & Roy, K. (2017). Convolutional spike timing dependent plasticity based feature learning in spiking neural networks. *arXiv preprint arXiv:1703.03854*.

Pandya, M., Altinay, M., Malone, D. A. & Anand, A. (2012). Where in the brain is depression? *Current psychiatry reports*, *14*(6), 634–642.

Pang, B., Nijkamp, E. & Wu, Y. N. (2020). Deep learning with tensorflow: A review. *Journal of Educational and Behavioral Statistics*, *45*(2), 227–248.

Park, I. M., Seth, S., Paiva, A. R., Li, L. & Principe, J. C. (2013). Kernel methods on spike train space for neuroscience: a tutorial. *IEEE Signal Processing Magazine*, *30*(4), 149–160.

Park, S., Kim, S., Choe, H. & Yoon, S. (2019). Fast and efficient information transmission with burst spikes in deep spiking neural networks. In *2019 56th acm/ieee design automation conference (dac)* (pp. 1–6).

Pérez-Carrasco, J. A., Zhao, B., Serrano, C., Acha, B., Serrano-Gotarredona, T., Chen, S. & Linares-Barranco, B. (2013). Mapping from frame-driven to frame-free event-driven vision systems by low-rate rate coding and coincidence processing–application to feedforward convnets. *IEEE transactions on pattern analysis and machine intelligence*, *35*(11), 2706–2719.

Petro, B., Kasabov, N. & Kiss, R. M. (2019). Selection and optimization of temporal spike encoding methods for spiking neural networks. *IEEE transactions on neural networks and learning systems*, *31*(2), 358–370.

Pezard, L., Nandrino, J.-L., Renault, B., El Massioui, F., Allilaire, J.-F., Müller, J., ... Martinerie, J. (1996). Depression as a dynamical disease. *Biological Psychiatry*, *39*(12), 991–999.

Pfeiffer, M. & Pfeil, T. (2018). Deep learning with spiking neurons: opportunities and challenges. *Frontiers in neuroscience*, 774.

Pierce, J. E., Thomasson, M., Voruz, P., Selosse, G. & Péron, J. (2022). Explicit and implicit emotion processing in the cerebellum: a meta-analysis and systematic review. *The Cerebellum*, 1–13.

Puthankattil, S. D. & Joseph, P. K. (2012). Classification of eeg signals in normal and depression conditions by ann using rwe and signal entropy. *Journal of Mechanics in Medicine and biology*, *12*(04), 1240019.

Ramirez, A. & Arbuckle, M. R. (2016). Synaptic plasticity: The role of learning and unlearning in addiction and beyond. *Biological psychiatry*, *80*(9), e73–e75.

Rekabdar, B., Fraser, L., Nicolescu, M. & Nicolescu, M. (2018). A real-time spike-timing classifier of spatio-temporal patterns. *Neurocomputing*, *311*, 183-196.

Rekabdar, B., Nicolescu, M., Nicolescu, M. & Louis, S. (2017). Using patterns of firing neurons in spiking neural networks for learning and early recognition of spatio-temporal patterns. *Neural Computing and Applications*, *28*(5), 881-897.

Riesenhuber, M. & Poggio, T. (1999). Hierarchical models of object recognition in cortex. *Nature neuroscience*, *2*(11), 1019–1025.

Roiser, J. P. & Sahakian, B. J. (2017). 16 information processing in mood disorders. *The Oxford handbook of mood disorders*, 179.

Roy, Y., Banville, H., Albuquerque, I., Gramfort, A., Falk, T. H. & Faubert, J. (2019). Deep learning-based electroencephalography analysis: a systematic review. *Journal of neural engineering*, *16*(5), 051001.

Rubin, R., Monasson, R. & Sompolinsky, H. (2010). Theory of spike timing-based neural classifiers. *Physical review letters*, *105*(21), 218102.

Rueckauer, B. & Liu, S.-C. (2018). Conversion of analog to spiking neural networks using sparse temporal coding. In *2018 ieee international symposium on circuits and systems (iscas)* (pp. 1–5).

Rueckauer, B., Lungu, I.-A., Hu, Y. & Pfeiffer, M. (2016). Theory and tools for the conversion of analog to spiking convolutional neural networks. *arXiv preprint arXiv:1612.04052*.

Rueckauer, B., Lungu, I.-A., Hu, Y., Pfeiffer, M. & Liu, S.-C. (2017). Conversion of continuous-valued deep networks to efficient event-driven networks for image classification. *Frontiers in neuroscience*, *11*, 682.

Saeedi, M., Saeedi, A. & Maghsoudi, A. (2020). Major depressive disorder assessment via enhanced k-nearest neighbor method and eeg signals. *Physical and Engineering Sciences in Medicine*, *43*(3), 1007–1018.

Salustri, C., Tecchio, F., Zappasodi, F., Bevacqua, G., Fontana, M., Ercolani, M., ... Rossini, P. M. (2007). Cortical excitability and rest activity properties in patients with depression. *Journal of Psychiatry and Neuroscience*, *32*(4), 259–266.

Sandheep, P., Vineeth, S., Poulose, M. & Subha, D. (2019). Performance analysis of deep learning cnn in classification of depression eeg signals. In *Tencon 2019-2019 ieee region 10 conference (tencon)* (pp. 1339–1344).

Sarangdhar, M. & Kambhampati, C. (2008). Spiking neurons: Is coincidence-factor enough for comparing responses with fluctuating membrane voltage? In *Proceedings of the world congress on engineering* (Vol. 2, pp. 2–4).

Sartorius, N. (2001). The economic and social burden of depression. *Journal of Clinical Psychiatry*, *62*, 8–11.

Satuvuori, E. & Kreuz, T. (2018). Which spike train distance is most suitable for distinguishing rate and temporal coding? *Journal of neuroscience methods*, *299*, 22–33.

Satuvuori, E., Mulansky, M., Bozanic, N., Malvestio, I., Zeldenrust, F., Lenk, K. & Kreuz, T. (2017). Measures of spike train synchrony for data with multiple time scales. *Journal of neuroscience methods*, *287*, 25–38.

Schaffer, C. (1993). Selecting a classification method by cross-validation. *Machine learning*, *13*, 135–143.

Schirrmeister, R. T., Springenberg, J. T., Fiederer, L. D. J., Glasstetter, M., Eggensperger, K., Tangermann, M., ... Ball, T. (2017). Deep learning with convolutional neural networks for brain mapping and decoding of movement-related information from the human eeg. arxiv. *arXiv preprint arXiv:1703.05051*.

Schliebs, S. & Kasabov, N. (2013). Evolving spiking neural networks: A survey. *Evolving Systems*, *4*, 12. Retrieved from `https://doi.org/10.1007/s12530-013-9074-9`

Schrauwen, B. & Van Campenhout, J. (2003a). Bsa, a fast and accurate spike train

encoding scheme. In *Proceedings of the international joint conference on neural networks, 2003.* (Vol. 4, p. 2825-2830 vol.4). doi: 10.1109/IJCNN.2003.1224019

Schrauwen, B. & Van Campenhout, J. (2003b). Bsa, a fast and accurate spike train encoding scheme. In *Proceedings of the international joint conference on neural networks, 2003.* (Vol. 4, pp. 2825–2830).

Seal, A., Bajpai, R., Agnihotri, J., Yazidi, A., Herrera-Viedma, E. & Krejcar, O. (2021). Deprnet: A deep convolution neural network framework for detecting depression using eeg. *IEEE Transactions on Instrumentation and Measurement*, *70*, 1–13.

Sengupta, A., Ye, Y., Wang, R., Liu, C. & Roy, K. (2019). Going deeper in spiking neural networks: Vgg and residual architectures. *Frontiers in neuroscience*, *13*, 95.

Sepulcre, J., Liu, H., Talukdar, T., Martincorena, I., Yeo, B. T. & Buckner, R. L. (2010). The organization of local and distant functional connectivity in the human brain. *PLoS computational biology*, *6*(6), e1000808.

Shah, D., Narayanan, A. & Espinosa-Ramos, J. I. (2022). Utilizing the neuronal behavior of spiking neurons to recognize music signals based on time coding features. *IEEE Access*, *10*, 37317–37329.

Shah, D., Wang, G. Y., Doborjeh, M., Doborjeh, Z. & Kasabov, N. (2019). Deep learning of eeg data in the neucube brain-inspired spiking neural network architecture for a better understanding of depression. In *International conference on neural information processing* (pp. 195–206).

Sharma, G., Parashar, A. & Joshi, A. M. (2021). Dephnn: A novel hybrid neural network for electroencephalogram (eeg)-based screening of depression. *Biomedical Signal Processing and Control*, *66*, 102393.

Sharma, M., Achuth, P., Deb, D., Puthankattil, S. D. & Acharya, U. R. (2018). An automated diagnosis of depression using three-channel bandwidth-duration localized wavelet filter bank with eeg signals. *Cognitive Systems Research*, *52*, 508–520.

Shen, J., Zhang, X., Huang, X., Wu, M., Gao, J., Lu, D., ... Hu, B. (2020). An optimal channel selection for eeg-based depression detection via kernel-target alignment. *IEEE Journal of Biomedical and Health Informatics*.

Shim, M., Im, C.-H., Kim, Y.-W. & Lee, S.-H. (2018). Altered cortical functional network in major depressive disorder: A resting-state electroencephalogram study. *NeuroImage: Clinical*, *19*, 1000–1007.

Sihn, D. & Kim, S.-P. (2019). A spike train distance robust to firing rate changes based on the earth mover's distance. *Frontiers in Computational Neuroscience*, *13*, 82.

Sironi, A., Brambilla, M., Bourdis, N., Lagorce, X. & Benosman, R. (2018). Hats: Histograms of averaged time surfaces for robust event-based object classification. In *Proceedings of the ieee conference on computer vision and pattern recognition* (pp. 1731–1740).

Smit, D., Posthuma, D., Boomsma, D. & De Geus, E. (2007). The relation between frontal eeg asymmetry and the risk for anxiety and depression. *Biological psychology*, *74*(1), 26–33.

Smith, K. (2014). Mental health: a world of depression. *Nature News*, *515*(7526), 180.

Smith, K. M., Renshaw, P. F. & Bilello, J. (2013). The diagnosis of depression: current and emerging methods. *Comprehensive psychiatry*, *54*(1), 1–6.

Song, S., Miller, K. D. & Abbott, L. F. (2000). Competitive hebbian learning through spike-timing-dependent synaptic plasticity. *Nature neuroscience*, *3*(9), 919–926.

Sporea, I. & Grüning, A. (2013). Supervised learning in multilayer spiking neural networks. *Neural computation*, *25*(2), 473–509.

Spyrou, I.-M., Frantzidis, C., Bratsas, C., Antoniou, I. & Bamidis, P. D. (2016). Geriatric depression symptoms coexisting with cognitive decline: A comparison of classification methodologies. *Biomedical Signal Processing and Control*, *25*, 118–129.

Stam, C. J. (2005). Nonlinear dynamical analysis of eeg and meg: review of an emerging field. *Clinical neurophysiology*, *116*(10), 2266–2301.

Stevens, J. S., Harnett, N. G., Lebois, L. A., van Rooij, S. J., Ely, T. D., Roeckner, A., ... others (2021). Brain-based biotypes of psychiatric vulnerability in the acute aftermath of trauma. *American journal of psychiatry*, *178*(11), 1037–1049.

Stewart, J. L., Bismark, A. W., Towers, D. N., Coan, J. A. & Allen, J. J. (2010). Resting frontal eeg asymmetry as an endophenotype for depression risk: sex-specific patterns of frontal brain asymmetry. *Journal of abnormal psychology*, *119*(3), 502.

Stewart, J. L., Towers, D. N., Coan, J. A. & Allen, J. J. (2011). The oft-neglected role of parietal eeg asymmetry and risk for major depressive disorder. *Psychophysiology*, *48*(1), 82–95.

Storn, R. & Price, K. (1997). Differential evolution–a simple and efficient heuristic for global optimization over continuous spaces. *Journal of global optimization*, *11*(4), 341–359.

Stromatias, E., Soto, M., Serrano-Gotarredona, T. & Linares-Barranco, B. (2017). An event-driven classifier for spiking neural networks fed with synthetic or dynamic vision sensor data. *Frontiers in neuroscience*, *11*, 350.

Sun, D., Yang, X., Liu, M.-Y. & Kautz, J. (2018). Pwc-net: Cnns for optical flow using pyramid, warping, and cost volume. In *Proceedings of the ieee conference on computer vision and pattern recognition* (pp. 8934–8943).

Tabuchi, M., Monaco, J. D., Duan, G., Bell, B., Liu, S., Liu, Q., ... Wu, M. N. (2018). Clock-generated temporal codes determine synaptic plasticity to control sleep. *Cell*, *175*(5), 1213–1227.

Takano, T., Funahashi, Y. & Kaibuchi, K. (2019). Neuronal polarity: positive and negative feedback signals. *Frontiers in cell and developmental biology*, *7*, 69.

Tamaazousti, Y. (2018). *On the universality of visual and multimodal representations* (Unpublished doctoral dissertation).

Tavanaei, A., Kirby, Z. & Maida, A. S. (2018). Training spiking convnets by stdp and gradient descent. In *2018 international joint conference on neural networks (ijcnn)* (pp. 1–8).

Tavanaei, A. & Maida, A. (2019). Bp-stdp: Approximating backpropagation using spike timing dependent plasticity. *Neurocomputing*, *330*, 39–47.

Tavanaei, A. & Maida, A. S. (2016). Bio-inspired spiking convolutional neural

network using layer-wise sparse coding and stdp learning. *arXiv preprint arXiv:1611.03000*.

Tavanaei, A. & Maida, A. S. (2017). Multi-layer unsupervised learning in a spiking convolutional neural network. In *2017 international joint conference on neural networks (ijcnn)* (p. 2023-2030). doi: 10.1109/IJCNN.2017.7966099

Thanaraj, K. P., Parvathavarthini, B., Tanik, U. J., Rajinikanth, V., Kadry, S. & Kamalanand, K. (2020). Implementation of deep neural networks to classify eeg signals using gramian angular summation field for epilepsy diagnosis. *arXiv preprint arXiv:2003.04534*.

The MathWorks, I. (1999). *Ovsf code generator.* Retrieved 2022-04-06, from `https://au.mathworks.com/help/comm/ref/ovsfcodegenerator.html`

Thibodeau, R., Jorgensen, R. S. & Kim, S. (2006). Depression, anxiety, and resting frontal eeg asymmetry: a meta-analytic review. *Journal of abnormal psychology*, *115*(4), 715.

Thiele, J., Bichler, O. & Dupret, A. (2018). *Event-based, timescale invariant unsupervised online deep learning with stdp. front. comput. neurosci. 12, 46 (2018).*

Thorpe, S. & Gautrais, J. (1998). Rank order coding. In *Computational neuroscience* (pp. 113–118). Springer.

Thorpe, S. J. & Imbert, M. (1989). Biological constraints on connectionist modelling. *Connectionism in perspective*, 63–92.

Trimble, M. & Hesdorffer, D. (2017). Music and the brain: the neuroscience of music and musical appreciation. *BJPsych international*, *14*(2), 28–31.

Tseng, V.-S., Bhattachara, S., Fernández-Marqués, J., Alizadeh, M., Tong, C. & Lane, N. D. (2018). Deterministic binary filters for convolutional neural networks..

Turkson, R. E., Qu, H., Mawuli, C. B. & Eghan, M. J. (2021). Classification of alzheimer's disease using deep convolutional spiking neural network. *Neural Processing Letters*, *53*(4), 2649–2663.

Ullah, A., Muhammad, K., Del Ser, J., Baik, S. W. & de Albuquerque, V. H. C. (2018). Activity recognition using temporal optical flow convolutional features and multilayer lstm. *IEEE Transactions on Industrial Electronics*, *66*(12), 9692–9702.

van Rossum, M. C. (2001). A novel spike distance. *Neural computation*, *13*(4), 751–763.

Venna, S. R., Tavanaei, A., Gottumukkala, R. N., Raghavan, V. V., Maida, A. S. & Nichols, S. (2018). A novel data-driven model for real-time influenza forecasting. *IEEE Access*, *7*, 7691–7701.

Victor, J. D. & Purpura, K. P. (1996). Nature and precision of temporal coding in visual cortex: a metric-space analysis. *Journal of neurophysiology*, *76*(2), 1310–1326.

Vreeken, J. (2003). *Spiking neural networks, an introduction.* Utrecht University: Information and Computing Sciences.

Wan, Z., Huang, J., Zhang, H., Zhou, H., Yang, J. & Zhong, N. (2020). Hybrideegnet: A convolutional neural network for eeg feature learning and depression discrimination. *IEEE Access*, *8*, 30332–30342.

Wang, J., Wang, X., Wang, X., Zhang, H., Zhou, Y., Chen, L., ... Wu, L. (2020). Increased eeg coherence in long-distance and short-distance connectivity in children with autism spectrum disorders. *Brain and Behavior*, *10*(10), e01796.

Wang, X., Lin, X., Zhao, J. & Ma, H. (2016). Supervised learning algorithm for spiking neurons based on nonlinear inner products of spike trains. In *International conference on intelligent computing* (pp. 95–104).

Warren, M. B., Pringle, A. & Harmer, C. J. (2015). A neurocognitive model for understanding treatment action in depression. *Philosophical Transactions of the Royal Society B: Biological Sciences*, *370*(1677), 20140213.

Watts, D. J. & Strogatz, S. H. (1998). Collective dynamics of 'small-world'networks. *nature*, *393*(6684), 440–442.

Waugh, C. E., Shing, E. Z. & Avery, B. M. (2015). Temporal dynamics of emotional processing in the brain. *Emotion Review*, *7*(4), 323–329.

Whalley, K. (2013). Timing is key in the olfactory system. *Nature Reviews Neuroscience*, *14*(7), 458–458.

Whiteford, H. A., Degenhardt, L., Rehm, J., Baxter, A. J., Ferrari, A. J., Erskine, H. E., ... others (2013). Global burden of disease attributable to mental and substance use disorders: findings from the global burden of disease study 2010. *The lancet*, *382*(9904), 1575–1586.

Whittington, J. C. & Bogacz, R. (2019). Theories of error back-propagation in the brain. *Trends in cognitive sciences*, *23*(3), 235–250.

Wikipedia contributors. (2020). *European data format — Wikipedia, the free encyclopedia*. `https://en.wikipedia.org/w/index.php?title=European_Data_Format&oldid=978635468`. ([Online; accessed 8-January-2021])

Wilcoxon, F. (1992). *Individual comparisons by ranking methods*. Springer.

Williams, J. B. (1988). A structured interview guide for the hamilton depression rating scale. *Archives of general psychiatry*, *45*(8), 742–747.

Williams, S. Z., Chung, G. S. & Muennig, P. A. (2017). Undiagnosed depression: A community diagnosis. *SSM-population health*, *3*, 633–638.

Wu, Y., Deng, L., Li, G., Zhu, J. & Shi, L. (2018). Spatio-temporal backpropagation for training high-performance spiking neural networks. *Frontiers in neuroscience*, *12*, 331.

Xiao, R., Wan, Y., Yang, B., Zhang, H., Tang, H., Wong, D. F. & Chen, B. (2022). Towards energy-preserving natural language understanding with spiking neural networks. *IEEE/ACM Transactions on Audio, Speech, and Language Processing*, *31*, 439–447.

Xu, Y., Zeng, X. & Zhong, S. (2013). A new supervised learning algorithm for spiking neurons. *Neural computation*, *25*(6), 1472–1511.

Yamazaki, K., Vo-Ho, V.-K., Bulsara, D. & Le, N. (2022). Spiking neural networks and their applications: A review. *Brain Sciences*, *12*(7), 863.

Yamins, D. L. & DiCarlo, J. J. (2016). Using goal-driven deep learning models to understand sensory cortex. *Nature neuroscience*, *19*(3), 356–365.

Yang, X., Lin, J., Zheng, W., Zhao, J., Ji, M., Lei, Y. & Chai, Z. (2020). Research on

learning mechanism designing for equilibrated bipolar spiking neural networks. *Artificial Intelligence Review*, *53*(7), 5189–5215.

Yildirim, Ö. (2018). A novel wavelet sequence based on deep bidirectional lstm network model for ecg signal classification. *Computers in biology and medicine*, *96*, 189–202.

Yıldırım, Ö., Pławiak, P., Tan, R.-S. & Acharya, U. R. (2018). Arrhythmia detection using deep convolutional neural network with long duration ecg signals. *Computers in biology and medicine*, *102*, 411–420.

Yildirim, O., San Tan, R. & Acharya, U. R. (2018). An efficient compression of ecg signals using deep convolutional autoencoders. *Cognitive Systems Research*, *52*, 198–211.

Zenke, F. & Ganguli, S. (2018). Superspike: Supervised learning in multilayer spiking neural networks. *Neural computation*, *30*(6), 1514–1541.

Zhang, A., Lipton, Z. C., Li, M. & Smola, A. J. (2021). Dive into deep learning. *arXiv preprint arXiv:2106.11342*.

Zhang, M., Qu, H., Belatreche, A., Chen, Y. & Yi, Z. (2018). A highly effective and robust membrane potential-driven supervised learning method for spiking neurons. *IEEE transactions on neural networks and learning systems*, *30*(1), 123–137.

Zhang, X., Li, J., Hou, K., Hu, B., Shen, J. & Pan, J. (2020). Eeg-based depression detection using convolutional neural network with demographic attention mechanism. In *2020 42nd annual international conference of the ieee engineering in medicine & biology society (embc)* (pp. 128–133).

Appendix A

Additional information here

The additional information about the results of Chapters 5 is described here. The first section shows the descriptive statistics of different SNN parameters during the DE optimisation process. Further, it illustrates the optimised SNN parameters used to identify optimal input strategy and biomarkers for depression detection as described in Chapter 5.

A.1 Input Strategy: Optimal Flow of Information

Brain Asymmetry :

Table A.1: Descriptive Statistics on 2^{nd} generation

SNN Parameters	Minimum	Maximum	Mean	Standard Deviation
LIF threshold	0.011297207	0.488162912	0.257159578	0.14377902
Refractory time	1.659897964	10.0236973	5.748894859	2.16525917
Potentiation magnitude	0.001176168	0.051414163	0.024416052	0.013934081
Depression magnitude	0.001426848	0.048710208	0.025069832	0.013201878
Number of neurons	47 122	100	13	
Minimum weight (lower limit)	-0.983375165	-0.076994026	-0.554446725	0.286856151
Max weight (upper limit)	0.152487873	4.943841966	2.178376832	1.381505189
F1-score	0.63769231	0.863333333	0.785769792	0.098945847

Table A.2: Optimised Parameters for Training using RMSE metric

SNN parameters	Values
LIF threshold	0.449266884
Refractory time	2.732306579
Potentiation magnitude	0.043628343
Depression magnitude	0.038595924
Number of neurons	98
Minimum weight (lower limit)	-0.962375495
Max weight (upper limit)	4.943841966

Short-distant Communication :

Table A.3: Descriptive Statistics on 2^{nd} generation

SNN Parameters	**Minimum**	**Maximum**	**Mean**	**Standard Deviation**
LIF threshold	0.017871714	0.48539972	0.279005296	0.130395591
Refractory time	2.460650281	9.996234897	5.868856109	2.272412518
Potentiation magnitude	-0.000252204	0.050960556	0.02454511	0.013017462
Depression magnitude	-0.000357819	0.049036247	0.028448498	0.014137481
Number of neurons	54	149	119	20
Minimum weight (lower limit)	-0.990052819	0.02180323	-0.488100957	0.300663529
Max weight (upper limit)	0.09554071 5.109356223	2.609619819	1.612771519	
F1-Score	0.507902242	0.682999623	0.591566544	0.038649724

Table A.4: Optimised Parameters for Training using RMSE metric

SNN parameters	**Values**
LIF threshold	0.189995301
Refractory time	5.630197857
Potentiation magnitude	0.002007237
Depression magnitude	0.034523588
Number of neurons	104
Minimum weight (lower limit)	-0.945612717
Max weight (upper limit)	4.131858731

Long-distant Communication :

Table A.5: Descriptive Statistics on 2^{nd} generation

SNN Parameters	**Minimum**	**Maximum**	**Mean**	**Standard Deviation**
LIF threshold	-0.01887696	0.521442779	0.240160104	0.154604663
Refractory time	1.884595232	9.888483857	6.095093682	2.519578591
Potentiation magnitude	0.005	0.048968809	0.027752836	0.011463896
Depression magnitude	0.002339196	0.049956055	0.026482852	0.012566925
Number of neurons	50 122	101	11	
Minimum weight (lower limit)	-0.984367493	-0.007820374	-0.544799149	0.269404024
Max weight (upper limit)	0.1	4.940319892	2.703738021	1.421569861
F1-Score	0.459454206	0.803643791	0.607038157	0.068294151

Table A.6: Optimised Parameters for Training using RMSE metric

SNN parameters	**Values**
LIF threshold	-0.01887696
Refractory time	8.655213678
Potentiation magnitude	0.030907118
Depression magnitude	0.039100724
Number of neurons	103
Minimum weight (lower limit)	-0.305681532
Max weight (upper limit)	2.685397476

Grouped Features :

Table A.7: Descriptive Statistics on 2^{nd} generation

SNN Parameters	**Minimum**	**Maximum**	**Mean**	**Standard Deviation**
LIF threshold	-0.010525729	0.568038541	0.232002501	0.158321532
Refractory time	1.998501742	10.56565126	6.288016255	2.409968236
Potentiation magnitude	-0.001908237	0.050331289	0.025215437	0.014045126
Depression magnitude	0.001429001	0.049654914	0.027589727	0.012438958
Number of neurons	49	119	98	14
Minimum weight (lower limit)	-1.063754976	0.018759835	-0.512609875	0.261142993
Max weight (upper limit)	0.057370056	5.170692298	2.819511149	1.485312998
F1-Score	0.518910256	0.764761905	0.640253103	0.055399834

Table A.8: Optimised Parameters for Training using RMSE metric

SNN parameters	**Values**
LIF threshold	0.202643962
Refractory time	2.092227908
Potentiation magnitude	0.015323299
Depression magnitude	0.031334039
Number of neurons	100
Minimum weight (lower limit)	-0.737232904
Max weight (upper limit)	3.916496139

A.2 Identification of Depression Biomarkers

Frontal Region :

Table A.9: Descriptive Statistics on 2^{nd} generation

SNN Parameters	Minimum	Maximum	Mean	Standard Deviation
LIF threshold	0.022636481	0.470408204	0.140236554	0.099870102
Refractory time	2.47508711	10.1637724	5.750664195	1.989448108
Potentiation magnitude	-0.002590687	0.052242426	0.018417071	0.015576822
Depression magnitude	0.00707333	0.049355051	0.030403408	0.012561417
Number of neurons	84 117	105	8	
Minimum weight (lower limit)	-0.96709706	0.08579757	-0.490930045	0.275327179
Max weight (upper limit)	0.147646491 4.036113113	2.260177316	1.026355227	
F1-Score	0.575	0.857142857	0.701803408	0.05289173

Table A.10: Optimised Parameters for Training using RMSE metric

SNN parameters	Values
LIF threshold	0.0593169829
Refractory time	4.901399028
Potentiation magnitude	0.003491231
Depression magnitude	0.012346415
Number of neurons	110
Minimum weight (lower limit)	-0.60639291
Max weight (upper limit)	2.459480723

Temporal-Frontal-Parietal Region :

Table A.11: Descriptive Statistics on 2^{nd} generation

SNN Parameters	Minimum	Maximum	Mean	Standard Deviation
LIF threshold	0.006049855 0.509290664	0.25384464	0.155656175	
Refractory time	1.587300413 9.750577549	5.944682325	2.465047271	
Potentiation magnitude	0.003877074 0.050168807	0.030985007	0.014430506	
Depression magnitude	-0.001669073 0.043959257	0.018403861	0.013086242	
Number of neurons	50 118	99	13	
Minimum weight (lower limit)	-0.993315539 0.012220539	-0.553715277	0.269622736	
Max weight (upper limit)	-0.02604934	4.942754622	2.447728689	1.276054021
F1-Score	0.547619048	0.742296919	0.669410718	0.043700396

Table A.12: Optimised Parameters for Training using RMSE metric

SNN parameters	Values
LIF threshold	0.432112137
Refractory time	7.479974449
Potentiation magnitude	0.046558587
Depression magnitude	0.027704171
Number of neurons	85
Minimum weight (lower limit)	-0.14347762
Max weight (upper limit)	2.872988269

Parietal Region :

Table A.13: Descriptive Statistics on 2^{nd} generation

SNN Parameters	**Minimum**	**Maximum**	**Mean**	**Standard Deviation**
LIF threshold	0.010084168	0.503700271	0.251505881	0.144483676
Refractory time	2.525332774 9.628594705	6.14986261	1.914780246	
Potentiation magnitude	-0.000749987	0.053888844	0.024500325	0.015599007
Depression magnitude	0.000688748	0.049749311	0.027245024	0.013408906
Number of neurons	80	120	99	12
Minimum weight (lower limit)	-1.003273008	-0.053446048	-0.548170154	0.257741503
Max weight (upper limit)	0.127965994	5.053889874	2.343521208	1.566332697
F1-Score	0.083916084	0.692857143	0.449116164	0.141898327

Table A.14: Optimised Parameters for Training using RMSE metric

SNN parameters	**Values**
LIF threshold	0.193758939
Refractory time	3.858512096
Potentiation magnitude	0.012088184
Depression magnitude	0.019132255
Number of neurons	86
Minimum weight (lower limit)	-0.053446048
Max weight (upper limit)	4.187087817

Central Region :

Table A.15: Descriptive Statistics on 2^{nd} generation

SNN Parameters	**Minimum**	**Maximum**	**Mean**	**Standard Deviation**
LIF threshold	0.04055374	0.541125634	0.243757945	0.114621523
Refractory time	2.354801269	10.03707681	5.586797227	2.016075609
Potentiation magnitude	-0.002859544	0.045859308	0.011742367	0.009032573
Depression magnitude	0.016448691	0.047798306	0.034508442	0.008081906
Number of neurons	82.59656408	116	100	9
Minimum weight (lower limit)	-0.997966317	-0.221860298	-0.66017322	0.233584606
Max weight (upper limit)	0.439124721	5.266229326	2.088881884	1.355573388
F1-Score	0.553846154	0.857142857	0.701516314	0.051554887

Table A.16: Optimised Parameters for Training using RMSE metric

SNN parameters	**Values**
LIF threshold	0.156108403
Refractory time	3.259093533
Potentiation magnitude	-0.001432446
Depression magnitude	0.029684723
Number of neurons	92
Minimum weight (lower limit)	-0.499884062
Max weight (upper limit)	3.55172681

Central-Parietal-Frontal Region :

Table A.17: Descriptive Statistics on 2^{nd} generation

SNN Parameters	**Minimum**	**Maximum**	**Mean**	**Standard Deviation**
LIF threshold	0.011037049	0.4970811	0.183018423	0.121543224
Refractory time	2.419768841	9.926534941	6.367431815	2.11473659
Potentiation magnitude	0.00158153	0.049899109	0.021425732	0.012062338
Depression magnitude	0.001806133	0.04473561	0.026001191	0.011532283
Number of neurons	50	119	97	14
Minimum weight (lower limit)	-0.99821291	0.016994315	-0.483143494	0.273674847
Max weight (upper limit)	0.00966029	4.809755319	2.663796696	1.40128103
F1-Score	0.401960784	0.833333333	0.632244091	0.087756701

Table A.18: Optimised Parameters for Training using RMSE metric

SNN parameters	**Values**
LIF threshold	0.195271999
Refractory time	8.586723002
Potentiation magnitude	0.023163212
Depression magnitude	0.03701195
Number of neurons	95
Minimum weight (lower limit)	-0.179345201
Max weight (upper limit)	0.15932723

Parietal-Occipital Regions :

Table A.19: Descriptive Statistics on 2^{nd} generation

SNN Parameters	**Minimum**	**Maximum**	**Mean**	**Standard Deviation**
LIF threshold	0.014318115	0.510861227	0.293097776	0.145838098
Refractory time	2.07008111	9.844469016	5.488347347	2.268364562
Potentiation magnitude	0.005256471	0.052733559	0.029592685	0.014827461
Depression magnitude	0.002094776	0.049371076	0.024924802	0.013886318
Number of neurons	80	117	101	10
Minimum weight (lower limit)	-0.996411098	-0.00606013	-0.484844219	0.264070078
Max weight (upper limit)	0.092115089 5.141700464	2.664433927	1.532859575	
F1-Score	0.309134615	0.75952381	0.602039344	0.094088183

Table A.20: Optimised Parameters for Training using RMSE metric

SNN parameters	**Values**
LIF threshold	0.17553567
Refractory time	9.421021372
Potentiation magnitude	0.006392921
Depression magnitude	0.011459683
Number of neurons	113
Minimum weight (lower limit)	-0.02576943
Max weight (upper limit)	4.026641304